SYNTHESIS, PHYSICAL CHARACTERIZATION, AND CHROMATOGRAPHIC PERFORMANCE OF 1.7 μm AND 1.1 μm SUPERFICIALLY POROUS PARTICLES PACKED IN CAPILLARY COLUMNS FOR LIQUID CHROMATOGRAPHY

Laura E. Blue

A dissertation submitted to the faculty of the University of North Carolina at Chapel Hill in partial fulfillment of the requirements for the degree of Doctor of Philosophy in the department of Chemistry (Analytical Chemistry).

Chapel Hill
2012

Approved by:

Dr. James W. Jorgenson

Dr. Mark H. Schoenfisch

Dr. Royce W. Murray

Dr. Michel Gagne

Dr. Joseph L. Templeton

ABSTRACT

LAURA E. BLUE: Synthesis, Physical Characterization, and Chromatographic Performance of 1.7 μm and 1.1 μm Superficially Porous Particles Packed in Capillary Columns for Liquid Chromatography
(Under the direction of James W. Jorgenson)

The predicted advantages of superficially porous particles over totally porous particles are decreased eddy dispersion, longitudinal diffusion, and resistance to mass transfer contributions to the theoretical plate height. These potential advantages arise from the effect of the inherently narrow particle size distribution on column packing and reduced diffusion volume due to the thin porous layer. While superficially porous particles are commercially available, further improvements in performance are predicted by decreasing the particle diameter, increasing the pore diameter, and decreasing the porous layer thickness. Both 1.7 μm and 1.1 μm superficially porous particles with a ρ value greater than 0.83 have been synthesized using a layer-by-layer method tuned for production of smaller diameter particles of varying pore diameter. Example synthesis parameters include type of polyelectrolyte, drying method, and sintering temperature. Using the revised synthesis conditions, monodisperse, uniformly coated superficially porous particles were produced. Following synthesis, these particles were packed into 30 μm i.d. capillary columns and their chromatographic performance evaluated using electrochemical detection. Based on the initial studies, the column efficiency was not as good as predicted, but was similar to that for commercially available products.

It is believed that the column packing process plays a critical role in the sub-par column performance. To determine if column performance could be predicted by solvent-particle interactions, in-solution microscopy, sedimentation velocity, and dynamic light scattering of particles in various slurry solvents were investigated and compared to column performance. Aggregating slurry solvents and high slurry concentrations were found to produce columns with increased efficiency but still have not reached theoretical values.

Due to the predicted advantages of superficially porous particles for slowly diffusing analytes, particles of varying pore diameter were synthesized by altering the diameter of the colloidal silica used to produce the porous layer. Particles with pores ranging from 87 Å to 248 Å were produced. The performance of these particles was assessed using small molecules, peptides, and proteins. The performance of the larger analytes by LC/MS was found to improve as the pore diameter was increased, but was less efficient than that found for 1.9 μm Acquity BEH.

ACKNOWLEDGEMENTS

There are many people that have contributed to where I am and who I am today. First and foremost, I would like to thank my family for their unconditional support and words of encouragement. Even when I thought I could not succeed they motivated me to push harder and to never give up. Specifically I would like to thank Eric for always being there for me, being my calm and collected half, and for supporting me in every decision I have made along the way.

The research presented here would not have been possible without my advisor, Dr. Jorgenson. Thank you for giving me the opportunity to work in your lab and for helping me grow as a scientist. I also would like to thank all of the Jorgenson group members past and present for their insight and making life in the lab enjoyable. Specifically, I would like to thank Rachel Leiberman for her guidance when I first joined the lab, Christine Hebling for inspiring me to always be better and for all of her support and guidance throughout the years, Kaitie Fague and Jordan Stobaugh for their help with generating LC/MS data and figures, and Ed Franklin for reviewing my dissertation. I would also like to thank Angie Proctor and Emily Oblath for helping me make it through graduate school with a smile on my face. This research was made possible through collaboration with Waters Corporation. I would like to thank Dr. Kevin Wyndham, Nicole Lawrence, and Dr. Geoff Gerhardt for all of their support and Nicole for carrying out physical characterization of the particles produced in-house.

TABLE OF CONTENTS

LIST OF TABLES

LIST OF FIGURES

LIST OF ABBREVIATIONS

ACN	Acetonitrile
BEH	Ethylene Bridged Hybrid
BET	Brunauer, Emmett, and. Teller
BSA	Bovine Serum Albumin
C	Catechol
C_m	Resistance to mass transfer in the mobile phase
C4	n-butyl
C8	n-octyl
C18	n-octadecyl
DI	Deionized
DLS	Dynamic Light Scattering
DLS PDI	Dynamic Light Scattering Polydispersity Index
ESI	Electrospray ionization
F_{CS}	Colloidal silica footprint
HMW PAH	High Molecular Weight Poly(allylamine hydrochloride)
HMW PDDA	High Molecular Weight Poly(diallydimethyl ammonium chloride)
HPLC	High Pressure Liquid Chromatography
HQ	Hydroquinone
IPA	Isopropanol
IT	Short-range interchannel
LMW PAH	Low Molecular Weight Poly(allylamine hydrochloride)

LMW PDDA	Low Molecular Weight Poly(diallydimethyl ammonium chloride)
LC	Liquid Chromatography
MeOH	Methanol
MW	Molecular Weight
m/z	mass-to-charge ratio
NPS	Non-Porous Silica
PDI	Polydispersity Index
PEI	Poly(ethylamine)
PTFE	Polytetrafluoroethylene
Q-TOF	Quadrupole-Time of Flight
R	Resorcinol
RSD	Relative Standard Deviation
SEM	Scanning Electron Microscope
SPP	Superficially Porous Particle
SSA	Specific Surface Area
StDef Filter	Standard Definition Filter
TC	Trans-column
TEAP	triethylammonium phosphate
TEOS	tetraethyl-orthosilicate
TFA	trifluoroacetic acid
THF	Tetrahydrofuran
TS	Trans-channel
UHPLC	Ultrahigh Pressure Liquid Chromatography

UHPLC-MS^{E}	Ultrahigh Pressure Liquid Chromatography-Mass Spectrometry^{E}
4MC	4-Methyl Catechol

LIST OF SYMBOLS

A	Eddy dispersion van Deemter coefficient
a	Reduced eddy dispersion van Deemter coefficient
A_{IT}	Short-range interchannel contribution to the *A*-term
A_{LRI}	Long-range interchannel contribution to the *A*-term
A_{TC}	Trans-column contribution to the *A*-term
A_{TP}	Trans-particle contribution to the *A*-term
A_{TS}	Trans-channel contribution to the *A*-term
α	Degree of aggregation
B	Longitudinal diffusion van Deemter coefficient
b	Reduced longitudinal diffusion van Deemter coefficient
β	Diffusion coefficient scalar parameter to account for varying particle porous layer thickness
X	Packing structure parameter
χ	Bonded phase surface coverage
C	Resistance to mass transfer van Deemter coefficient
C_{AT}	Aris-Taylor coefficient
C_f	External (eluent) film resistance to mass transfer for superficially porous particles
C_M	Resistance to mass transfer in the mobile phase van Deemter coefficient
C_{MSt}	Resistance to mass transfer in the stagnant mobile phase van Deemter coefficient
Cp	Trans-particle solid-liquid mass transfer coeeficient

C_S	Resistance to mass transfer in the stationary phase van Deemter coefficient
c	Reduced resistance to mass transfer van Deemter coefficient
%C	Percent carbon (w/w%)
D	Diffusion coefficient
d_{cs}	Colloidal silica diameter
d_{core}	Diameter of core particle
d_c/d_p	Diameter of core to total diameter of particle, aspect ratio
D_{eff}	Effective diffusion coefficient
d_{eff}	Effective particle diameter
d_f	Liquid stationary phase thickness
D_m	Diffusion of analyte in the mobile phase
D_p	Particle diffusivity across the porous stationary phase
d_p	Total particle diameter
$d_{p,i}$	Individual particle diameter
$d_{p,n}$	Number average particle diameter
d_{pore}	Pore diameter
$d_{p,v}$	Volume average particle diameter
D_S	Diffusion coefficient in the stationary phase
d_s	Stationary phase file thickness
ε	Intraparticle porosity
ε_f	Particle porosity filled with solvent
ε_i	Interparticle porosity
ε_e	External column porosity

ε_p	Particle porosity
ε_T	Total column porosity
g	Gravitational constant
γ'	Tortuosity factor
γ_m	Obstruction factor in the mobile phase
γ_r	Coefficient related to the contribution of eluent convection to the radial dispersion of the sample
γ_S	Obstruction factor in the stationary phase
η	Viscosity
H	Height equivalent to a theoretical plate
H_A	Height equivalent to a theoretical plate due to eddy dispersion
H_B	Height equivalent to a theoretical plate due to longitudinal diffusion
H_C	Height equivalent to a theoretical plate due to resistance to mass transfer
$H_{diffusion}$	Diffusion contribution to the coupled *A*-term
H_{flow}	Flow contribution to the coupled A-term
H_{heat}	Heat of friction contribution to the theoretical plate height
H_{min}	Minimum theoretical plate height
h_{min}	Reduced theoretical plate height
h	Reduced theoretical plate height
K	Henry's constant
K_2	particle-solvent dependant constant
k	Boltzmann's constant
k'	Relative retention factor, capacity factor

k_f	External film mass transfer coefficient
k_1	Zone retention factor
L	Column length
λ	Scaling factor for the A-term contribution based on the van Deemter equation
λ_i	Structural parameter for the A-term based on the Giddings equation
λ_{IT}	Short-range interchannel structural parameter
λ_{TC}	Trans-column structural parameter
m_l	Column length/column inner diameter
m_r	Column inner radiusr/particle diameter
MW	Molecular weight
N	Number of theoretical plates
N_C	Number of coating steps
nC	Number of carbons in the bonding ligand
n_i	Number of particles with a specific particle diameter
N_p	Number of particle in column
Ω	Effective diffusivity of the analyte in the porous shell to the bulk diffusion coefficient
P_c	Peak capacity
ΔP	Change in pressure
ΔP_{opt}	Pressure required to obtain the optimum flow rate
p_1/q_1	Factor to account for the concentration of the sample in the stationary phase as compared to the total column
Φ	Flow resistance

ϕ	Fraction of mobile phase stagnant in the particle pores
ϕ_p	Volume fraction of the particles
φ	Intraparticle tortuosity
r	Layer thickness growth rate
R_{cs}	Ratio of pore diameter to colloidal silica diameter
Re	Reynolds number
r_H	Hydrodynamic radius
R_s	Resolution
ρ	Core diameter/total particle diameter
ρ_{skel}	Density of the particle skeleton
ρ_l	Density of the solvent
SA_{CS}	Surface area of colloidal silica particle
SA_{NPS}	Surface area of NPS particle
SA_V	Surface area per column volume
SA_{total}	Total surface area of a superficially porous particle
Sc	Schmidt number
Sh	Sherwood number
SSA	Specific surface area
T	Temperature
T_f	Tailing factor
t_o	Void time (dead time)
T_p	Porous layer thickness
TPV	Total pore volume (from BET measurements)

t_r	Retention time
Δt	Length of gradient in time units
Δt_R	Retention time difference between critical pair
u	Linear velocity
u_0	Superficial linear velocity
u_{opt}	Optimum linear velocity
V	Total particle volume
v	Reduced linear velocity
V_c	Total column volume
$v_{experimental}$	Experimentally obtained sedimentation velocity
$v_{extreme}$	Linear velocity of mobile phase a higher or lower value than the mean linear velocity
v_{mean}	Mean mobile phase linear velocity
V_{MP}	Volume of mobile phase per column volume
V_p	Volume of column occupied by particles
V_{pore}	Pore volume per particle
v_S	Sedimentation velocity
V_{SP}	Volume of stationary phase per column volume
$\%V_{core}$	Percent of the total particle volume that is occupied by the solid core
$\%V_{porous}$	Percent of the total particle volume that is porous
$v_{theoretical}$	Theoretically obtained sedimentation velocity
$W_{C,p}$	Weight of carbon per particle
$W_{C,v}$	Weight of carbon per column volume
$w_{full,5\%}$	Peak width at the base

$w_{front,5\%}$	Front half peak width
W_p	Weight of one particle
$w_{t,i}$	4σ peak width
ω_α	Ratio of the exchange distance to the particle diameter between velocity extremes
ω_β	Fractional departure of the velocity extreme from the mean value
ω_i	Structural parameter for the A-term based on the Giddings equation
ω_{IT}	Short-range interchannel structural parameter
ω_λ	Structural parameter typically near unity
ω_{TC}	Trans-column structural parameter
$\omega_{\beta,c}$*	Relative velocity difference between the center and the wall of the column
ξ_2	Three-point parameter based on the Garnett-Torquato model

CHAPTER 1: INTRODUCTION

1.1 SUPERFICIALLY POROUS PARTICLES

1.1.1 Historical Background

Pellicular particles were introduced by Horvath *et. al.* to carry out highly efficient separations with lower pressure requirements for fast analyses.[1,2] Following this initial development, Dupont, Merck, and Waters Inc. developed similar materials for use with liquid chromatography.[3-5] The products were commercialized as Zipax, Perisorb, and Corasil, respectively, which had particle diameters around 40 μm.[4,6] Initially, superficially porous particles showed significant advantages over similarly sized totally porous particles, but in the mid-1970's these materials became overshadowed by development of smaller diameter, spherical, totally porous particles.[7,8] Not until recently have superficially porous particles again attracted attention.

The development of superficially porous particles was advanced by the application of the layer-by-layer process which alternates layers of positively charged polyelectrolyte and negatively charged colloidal silica. The alternating layer deposition on a solid surface was proposed by R. K. Iler for assembly of different types of molecules in each layer.[9] In 1970, J.J. Kirkland applied this concept to build a multi-layer coating of colloidal silica on a solid silica core for the synthesis of 5 μm superficially porous particles.[3] This process was more recently applied to the synthesis of smaller diameter particles and was commercialized as

Halo, which has a particle diameter of 2.7 μm and a pore diameter of 80Å.[10] Following the introduction of Halo particles, similarly sized particles such as Kinetex, Ascentis Express, Poroshell, and Accucore were introduced by Phenomenex, Supelco, Agilent Technologies, and Thermo Fisher, respectively. Based on earlier work, Agilent Technologies varied this procedure to produce 5.0 μm Poroshell particles with 300 Å pores.[3] Others followed with the production of particles suitable for proteins, such as Halo-ES and Aeris WIDEPORE by Advanced Materials Technology and Phenomenex, respectively.

1.1.2 Synthesis Methods

Since the initial development of superficially porous particles by Horvath, several production methods have been employed. One improvement was to modify the layer-by-layer method developed by Kirkland to include spray-drying to produce highly uniform particles.[11] Alternatively, the method employed by Büchel *et. al.* forms superficially porous particles by adding a tetraethyl-orthosilicate (TEOS)/porogen mixture to a suspension of non-porous silica (NPS) cores. The porogen, n-octadecyltrimethoxysilane, is removed by calcination forming a porous structure. The particles produced by this method have a 0.42 μm core and 75 nm porous shell, composed of pores in the range of 17-38 Å.[12] The particles produced by this method are much smaller in diameter and pore size than is typically useful for chromatographic supports. Another method for preparation introduced by Chen and Wei is based on coacervation, which forms spherical particles held together by hydrophobic forces due to the surrounding liquid. NPS cores in an aqueous solution are combined with colloidal silica particles and urea to which an acidic formaldehyde solution is added. Upon addition of the formaldehyde, a urea/formaldehyde polymer is formed. The colloidal silica and polymer then form a layer around the NPS core due to hydrophobic

repulsion. Following coacervation, the polymer can be removed by heating, leaving pores between the colloidal silica particles. The resulting particles can vary in size from 0.1 to 100 μm with the porous layer ranging from 1% to 80% of the total particle diameter. This method also allows for formation of larger pores, in the range of 15 to 1000 Å.[13] The most recent method, based on a sol-gel process, has been developed by Omamogho and Glennon. With this method, a porous shell is grown on the non-porous silica core by dispersement of NPS in a mixed surfactant solution. The surfactant acts to sterically stabilize the silica sol particles allowing formation of pores and inhibiting coagulation of the suspension. The surfactant is believed to cover the NPS surface with loops extending into solution. These loops allow for the formation of pores between the colloidal silica particles. The pores initially formed are too small to be chromatographically useful, but can be expanded up to 300 Å through hydrothermal heating in an oil-in-water emulsion system. These particles have diameters up to 2 μm and the porous layer thickness varies from 0.1 to 0.5 μm.[14] Each of these synthesis methods offer different favorable product features, but to date none offer monodispersity, ease of preparation, suitable particle diameter, pore size, and porous layer thickness in combination.

1.1.3 Commercially Available Products

After the initial development and release of Halo particles, the majority of the other column manufacturers quickly came out with similar products, Table 1-1.[15] Most of these particles are best suited for small molecule analysis due to the thickness of the porous layer, $\rho < 0.73$ ($\rho = d_{core}/d_p$), and having roughly 90 Å pores. The particles focused on peptide separations, Halo-ES, Poroshell 120, Aeris, and Ascentis Express Peptide-ES have a suitable pore diameter, but may have too thick of a porous layer to achieve the full efficiency gains of

using superficially porous particles ($0.63 \leq \rho \leq 0.73$). Based on studies by Horvath *et. al*. the ρ value for peptides should be greater than 0.87.[35] Lastly, there are only two products on the market, Poroshell 300 and Aeris WIDEPORE, targeting proteins, which is the class of molecules predicted to see the greatest benefit in using superficially porous particles over totally porous particles. While Poroshell 300 and Aeris WIDEPORE have a suitable pore diameter and porous layer thickness, the particle diameter is much larger than what would be desired for high efficiency separations.

While these products show that there have been significant advances in the development of superficially porous particles in recent years, there are still areas where improvement is possible. To date, the smallest superficially porous particles available have a particle diameter of 1.7 μm (Kinetex and Aeris by Phenomenex). Further improvements to chromatographic performance, however, can be expected by moving to even smaller diameter particles. Based on the dependence of the *A*-term and *C*-term on the particle diameter, reduction in the particle diameter should lead to greater efficiency.[16] This improvement in efficiency has been made possible by the advent of ultrahigh pressure liquid chromatography.[17] Another area with potential for improving efficiency is the porous layer thickness of the particle. It has been proposed by Horvath *et. al.* that a porous layer volume less than 35% of the total particle volume will be most beneficial.[35] Based on the diffusion rate of macromolecules, it is predicted that the thinner the porous layer the more efficient the mass transfer, and therefore the better the chromatographic performance of the column.[18,19] While efficiency is improved with a very thin porous layer, the drawback of this is the possible decrease in sample loading capacity. A balance between these two variables must be achieved to give the most desirable performance characteristics.

1.2 VAN DEEMTER EQUATION

The chromatographic separation mechanisms for a well packed column are typically described by the simplified van Deemter equation

$$H = A + \frac{B}{u} + Cu \tag{1-1}$$

where the overall height equivalent to a theoretical plate (H) of a chromatographic column is the sum of the contributions from eddy dispersion (A), longitudinal diffusion (B), and resistance to mass transfer (C) at a specified mobile phase linear velocity (u). Figure 1-1 illustrates how these three contributions to the theoretical plate height as described by the van Deemter equation are related. For an efficient column, the minimum plate height (H_{min}) for a packed bed should be approximately twice that of the column packing particle diameter.[20] An additional contribution to H at high flow rates, for highly retained analytes, or for eluents with low thermal conductivity is due to the heat of friction (H_{heat}) of the eluent percolating through the column bed. For the work to be presented here, this contribution can be ignored due to the use of weakly retained analytes, relative retention factors, k', less than two and due to the use of capillary columns that efficiently transfer heat.[18]

In order to compare columns packed with different sized particles or analytes with different diffusion coefficients, the van Deemter equation is presented in the reduced form.

$$h = a + \frac{b}{v} + cv \tag{1-2}$$

The reduced parameters a-, b-, and c-terms are dimensionless parameters which allow comparison of column performance between any packed columns. It is predicted that a well packed column will have the following reduced terms: $a = 1.5$, $b = 1$, and $c = 0.17$.[20]

The reduction of the plate height is achieved by removing the dependence on the particle diameter,d_p. Therefore the reduced plate height, h, is defined as:

$$h \equiv \frac{H}{d_p} \tag{1-3}$$

Accordingly, the reduced linear velocity, v, is defined as:

$$v \equiv \frac{ud_p}{D_m} \tag{1-4}$$

where D_m is the analyte diffusion coefficient in the mobile phase. A well packed column will typically have a minimum reduced plate height (h_{min}) of approximately two and an optimum reduced linear velocity (v_{opt}) of approximately three.

1.2.1 A-term Comparison

The eddy dispersion term is a function of the size and distribution of the interparticle channels in a packed bed and based on van Deemter theory is velocity independent. The channel distribution has been predicted to be independent of the type of particle.

$$H_A = \lambda d_p \tag{1-5}$$

Where λ is between 1.5 and 2 for a well packed column and a value greater than 2 is an indication of a poorly packed bed. This form of the A-term assumes that broadening is only due to the interstitial volume. Giddings found that there is a contribution to the A-term from diffusion between streams leading to a coupled equation.[21]

$$H_{A,i} = \frac{1}{\frac{1}{H_{flow}} + \frac{1}{H_{diffusion}}} = \frac{1}{\frac{1}{2\lambda_i d_p} + \frac{D_m}{\omega_i d_p^2 u}} \tag{1-6}$$

The contribution from flow to the coupled A-term is scaled by how many different flow velocities are present (λ_i). This diffusion contribution is scaled to the distance and span over

which velocity variations are considered (ω_i). The packed bed structural parameters for spherical particles λ_i and ω_i are defined as follows:[21]

$$\lambda_i = \frac{\omega_\beta^2 \omega_\lambda}{2} \tag{1-7}$$

$$\omega_i = \frac{\omega_\alpha^2 \omega_\beta^2}{2} \tag{1-8}$$

Where ω_β is the fractional difference between the deviation of the velocity extreme from the mean value to the mean velocity ($\omega_\beta = ((v_{extreme}-v_{mean})/v_{mean})$, ω_λ is a structural parameter typically near unity, and ω_α is the fraction or number of particle diameters traveled to get from one velocity extreme to another over the distance dictated by the type of *A*-term contribution (to be discussed below) being considered (ω_α = diffusion distance/d_p). ω_λ is a structural parameter accounting for the differences in the persistence of velocity length for beds packed with polydisperse particles. The persistence to velocity length is considered to be proportional to the particle diameter because for a given change in particle diameter, the relative packing structure remains unchanged but the length of each interparticle channel will change by the same fraction as the particle diameter. Therefore, independent of the distance over which velocity inequalities are being determined (differing *A*-term contribution), the persistence of velocity length will directly scale with the particle diameter. To clarify the difference between ω_λ and ω_α, ω_λ depends on the length of the interparticle channels and ω_α describes behavior on a wider scale as dictated by the contribution under investigation. The coupling shown in equation 1-6 accounts for the interaction between flow and diffusive exchange mechanisms acting to reduce the velocity persistence distance, thus decreasing the plate height. From equation 1-6, it is observed that $H_{A,i}$ will be less than either H_{flow} or

$H_{diffusion}$ alone. As the linear velocity increases, $H_{A,i}$ increases gradually as a function of the diffusion controlled portion until approaching the value of H_{flow}.[21]

The contributions to the height equivalent to a theoretical plate based on Giddings theory are the trans-channel (A_{TS}), short-range interchannel (A_{IT}), long-range interchannel (A_{LRI}), trans-column (A_{TC}), and trans-particle (A_{TP}) effects, Figure 1-2.

$$H_A = H_{A,TS} + H_{A,IT} + H_{A,TC} + H_{A,LRI} + H_{A,TP} \tag{1-9}$$

Based on experimentation by Khirevich *et. al.*, the long-range interchannel (A_{LRI}) contribution was found to be negligible.[22] Furthermore, trans-particle contributions (A_{TP}) are considered negligible since there is no convective contribution to movement of the molecules through the particle.[22, 23]

The trans-channel (TS) eddy dispersion is due to the velocity differences existing within the interparticle channel. The local velocity in the center of the interparticle space is approximately twice the average velocity in the channel, leading to band spreading of the analyte. The distance over which exchange occurs is over the distance of one interparticle channel.[24, 25]

$$H_{A,TS} = \frac{1}{\frac{1}{0.9d_p} + \frac{D_m}{0.0045d_p^2 u}} \tag{1-10}$$

The values for λ_{TS} and ω_{TS} were theoretically determined for spherical particles with an interparticle porosity value of 0.40 with an S-type packing structure. An S-type packing was theoretically generated by dividing a simulation box into *n* equal cubic cells and each particle center was placed randomly in the cell. This produced a random, dense bed structure.[22]

The short-range interchannel (IT) eddy dispersion accounts for differences in the local packing density over a distance of a few particles diameters, which produce differences

in the flow velocities between neighboring channels. Small channels produced by regions of high packing density have lower flow velocities than for large channels produced by low packing density regions.[26]

$$H_{A,IT} = \frac{1}{\frac{1}{0.5d_p} + \frac{D_m}{0.13d_p^2 u}} \tag{1-11}$$

As was the case for the trans-channel values, λ_{IT} and ω_{IT} were obtained at an interparticle porosity value of 0.40 for an S-type packing structure.[22] The sample diffusivity through porous particles may relax the concentration gradient between close interparticle channels, reducing the short-range interparticle eddy dispersion contribution.

The last contribution to the eddy dispersion, trans-column (TC), is due to radial inhomogeneities in the packed bed leading to radial variations in the flow velocity over the distance of the column inner diameter. This is the only A-term contribution that is directly affected by the porosity of the packing material.[24]

$$H_{A,TC} = \frac{1}{\frac{1}{2\lambda_{TC} d_p} + \frac{D_m}{\omega_{TC} d_p^2 u}} \tag{1-12}$$

The structural parameter, λ_{TC}, accounts for the number of differing flow velocities across the diameter of the column over the number of particles per column length.

$$\lambda_{TC} = \frac{p_1}{q_1} m_l \omega_{\beta,c}^{*\,2} \tag{1-13}$$

The p_1/q_1 ratio is the ratio of two integers dependent on the polynomial order, n, of the radial flow profile in the absence of diffusion, where n has been found previously to be equal to eight.[24] This predicts a p_1/q_1 ratio of 8/225, which accounts for the time an analyte spends in the center of the column versus near the column wall. The m_l value represents the number

of particles per column length. For calculations described here, m_l = 150,000 (column length/particle diameter, 15 cm/1 μm). $\omega^*_{\beta,c}$ is the relative velocity difference between the center of the column and at the wall, $\omega^*_{\beta,c}$ = 1.5%. Therefore, the contribution from flow to the coupled A_{TC}-term is scaled by the amount of time an analyte spends in the fast moving center region (p_1/q_1), the variance in the flow velocities across the column ($\omega^{*2}_{\beta,c}$), and the number of particles per column length (m_l).[24]

The structural parameter, ω_{TC}, accounts for the span of velocities which is reduced by analyte retention.

$$\omega_{TC} = \frac{\varepsilon_i C_{AT} m_r^2}{\varepsilon_T (1 + k')} \tag{1-14}$$

ε_i is the interparticle porosity, typically equal to 0.40 and ε_T is the total column porosity, ε_T = 0.65, which includes both the interparticle and intraparticle porosity. The dispersion due to laminar flow is described by the Aris-Taylor coefficient, C_{AT}, which was set equal to 1.1 x 10^{-7} based on previous studies performed by Gritti *et. al*.[24] The m_r ratio is the ratio of the inner column radius to the particle diameter, which represents one-half of the number of particles across the diameter of the column, m_r = 15 (15 μm/1 μm). The dispersion due to flow (C_{AT}) within the interparticle space is reduced due to retention, as represented by (1+k'), k' = 2. The diffusion contribution to the coupled A_{TC}-term is scaled by the dispersion due to laminar flow within the interparticle space, which is reduced by increased analyte retention due to no diffusion in the mobile phase occurring when an analyte is retained.

For the molecular diffusion contribution to the A_{TC}-term, D_m is replaced with the summation of the effective diffusion (see equation 1-20), D_{eff}, and diffusion due to convention in the interparticle volume.[24]

$$D_m = D_{eff} + 0.5\varepsilon_i \gamma_r d_p u \tag{1-15}$$

The effective diffusivity accounts for the diffusivity through a packed bed immersed in eluent composed of particles with a solid core and an outer porous layer. The diffusion contribution to D_{eff} is due to the interparticle porosity, ε_i, allowing for dispersion due to convection, γ_r ($\gamma_r = 0.3$).

$$H_{A,TC} = \frac{1}{\frac{q_2}{2p_1 d_p m_l \omega_{\beta,c}^{*2}} + \frac{\varepsilon_T (D_{eff} + 0.5\varepsilon_i \gamma_r d_p u)(1+k')}{\varepsilon_i C_{AT} m_r^2 d_p^2 u}} \tag{1-16}$$

This contribution, $H_{A,TC}$, has been found to theoretically decrease as the porous layer thickness of the particle is decreased due to the decrease in the diffusion distance, Figure 1-3.[26] While the contribution from the trans-column eddy dispersion decreases with decreasing porous layer thickness, the contribution to the total eddy dispersion is small, Figure 1-4. Due to the magnitude of the A_{IT}-term (10^{-1}) and the A_{TS}-term (10^{-2}), the variation in A_{total} as a function of porous layer thickness is slight. This slight improvement does not contribute to the improved performance of the 2.7 μm Halo and 1.7 μm Kinetex particles because they are found to be in the constant h_A region. Therefore, the experimentally observed improved *A*-term performance must be due to the improvement in the packing structure which is not accounted for in the theoretical calculations.

Based on recent experiments, it has been seen that the *A*-term varies between columns packed with totally porous and superficially porous particles of the same diameter. This difference may be due to the improved radial homogeneity of superficially porous particle packed beds due to decreased polydispersity and increased surface roughness, leading to a reduction in the trans-column contribution than predicted.[26]

1.2.2 B-term Comparison

The longitudinal diffusion term describes molecular diffusion in the axial direction and is inversely proportional to the linear velocity. It is defined as the variance arising from analyte diffusion.[28]

$$H_B = \frac{2\gamma_m D_m}{u} \tag{1-17}$$

The obstruction factor, γ_m, refers to the amount of obstruction that is in the way of free movement of the analyte in the mobile phase. This value varies between 0.5 and 1, but is typically used as 0.5. From work by Gritti and Guiochon, it was proposed that the *B*-term not only depends on the molecular diffusion, D_m, but is also affected by the equilibrium between the stationary phase and mobile phase. This distinction has previously been made by expanding the B-term into a mobile phase and stationary phase contribution.[27]

$$H_B = \frac{2\gamma_m D_m}{u} + \frac{2k'\gamma_s D_s}{u} \tag{1-18}$$

The additive nature of these two contributions to the B-term was found unsatisfactory by Gritti and Guiochon because recent studies of diffusion have found that the distinction between the mobile phase and stationary phase diffusion coefficients cannot be made and relies on the variation in the volume of the particles occupied by the porous layer and the volume occupied by the solid core. This requires the use of the effective diffusion coefficient, D_{eff}, in the *B*-term equation [24]

$$H_B = \frac{2(1+k_1)D_{eff}}{u} \tag{1-19}$$

where k_1 is the zone retention factor, which will be discussed below.

Numerous models have been used to describe the diffusion within the packed bed for totally porous, superficially porous, and non-porous packing materials. Currently, the most reliable model for prediction of the effective diffusion for particles of varying porous layer thickness is the Garnett-Torquato model. This model combines the Garnett diffusion model for a spherical non-porous core surrounded by a concentric shell and the Torquato diffusion model for a random dispersion of contacting spheres in a matrix. The effective diffusion defined by this combined model is as follows:[26]

$$D_{eff} = \frac{1}{\varepsilon_i (1+k_1)} \left[\frac{1+2(1-\varepsilon_i)\beta - 2\varepsilon_i \xi_2 \beta^2}{1-(1-\varepsilon_i)\beta - 2\varepsilon_i \xi_2 \beta^2} \right] D_m \tag{1-20}$$

where ε_i is the interparticle porosity, typically equal to 0.40, ξ_2 is the three-point parameter for the random dispersion of spherical particles, equal to 0.3277 for the Garnett-Torquato model with particles in contact with each other, and β is a diffusion coefficient scalar parameter to account for particles of varying porous layer thickness. The three-point parameter (ξ_2) defines the probability of finding an analyte molecule in the porous layer of the particle. The ξ_2 value of 0.3277 is representative of particles packed in an arrangement that occupies 60% of the volume, but varies as the interparticle porosity changes.[28, 29] The diffusion coefficient scalar parameter, β, is defined as:

$$\beta = \frac{\left[\left(\frac{1-\rho^3}{1+\frac{\rho^3}{2}} \right) \Omega \right] - 1}{\left[\left(\frac{1-\rho^3}{1+\frac{\rho^3}{2}} \right) \Omega \right] + 2} \tag{1-21}$$

Where Ω is the ratio of effective diffusivity of the analyte in the porous shell to the bulk diffusion coefficient, where for a totally porous particle, ρ becomes zero which eliminates the contribution from the solid core and β reduces to:

$$\beta = \frac{\Omega - 1}{\Omega + 2} \tag{1-22}$$

Since in this case the particle is completely porous, the entire contribution of the porous shell effective diffusivity is used for the calculation of the *B*-term due to β going to zero when Ω equals 1, as is the case for a lightly retained analyte. For a non-porous particle ρ is equal to one, which reduces the value of β to a numerical constant equal to -0.5 indicating the absence of porous shell effective diffusivity.

The zone retention factor, k_1, in the H_B equation replaces the obstruction factor for totally porous particles to account for the varying porosity of superficially porous particles, but still refers to the amount of time spent in the stationary phase relative to the mobile phase[30]

$$k_1 = \frac{1 - \varepsilon_i}{\varepsilon_i}[\varepsilon_p + (1 - \varepsilon_p)K](1 - \rho^3) \tag{1-23}$$

where *K* is the Henry's constant between the solid phase and the bulk phase and ρ is the ratio of the solid non-porous core diameter to the total particle diameter ($\rho = d_{core}/d_p$).

The zone retention factor replaces the conventional retention factor k' because the distinction between the percolating eluent (analyte not retained) and the stagnant eluent (analyte retained) is made in the general rate model.[28]

$$k' = \frac{t_r - t_0}{t_0} \tag{1-24}$$

Therefore, the capacity factor is the time an analyte spends in the stationary phase versus the time in the mobile phase and the zone retention factor is the time the analyte remains stationary in the pores versus the time spent in the interparticle mobile phase.

Assesing the effective diffusion coefficient as a whole finds it to represent the molecular diffusion coefficient scaled by the fraction of the column volume occupied by the porous layer and the fraction of the analyte that is retained on the particles.

Taking all of these variable into account the *B*-term for particles of varying porous layer thickness is defined as:[26]

$$H_B = \frac{2}{\varepsilon_i}\left[\frac{1+2(1-\varepsilon_i)\beta-2\varepsilon_i\xi_2\beta^2}{1-(1-\varepsilon_i)\beta-2\varepsilon_i\xi_2\beta^2}\right]\frac{D_m}{u} \tag{1-25}$$

The *B*-term magnitude dependence on porous layer thickness is shown in Figure 1-5. The *B*-term is relatively independent of porous layer thickness at values of ρ less than 0.4. Above this value you see the efficiency gains achievable with the reduction of the porous layer thickness due to the decrease in the available intraparticle volume for diffusion.

1.2.3 C-term Comparison

The *C*-term is directly proportional to the linear velocity and is composed of various resistance to mass transfer contributions to the theoretical plate height including: stationary phase partitioning (C_{SP}), interparticle mobile phase (C_M), and the stagnant intraparticle mobile phase (C_{MSt}). The C_{SP} component is the resistance to mass transfer due to the analyte partitioning in the stationary phase. The greater the stationary phase thickness (d_f) and the slower the diffusion of the analyte in the stationary phase (D_S), the greater contribution partitioning has on the *C*-term.[31]

$$H_{C,SP} = \frac{2k'd_f^2u}{3(1+k')^2D_S} \tag{1-26}$$

This contribution becomes zero for an unretained analyte due to the dependence on the capacity factor (k') and again approaches zero for a highly retained analyte after going through a maximum value.

A contribution to the resistance to mass transfer in the mobile phase is the C_{MSt}-term, which accounts for the time an analyte spends in the stagnant intraparticle mobile phase, such as within the pores of the column packing material. This contribution depends on the fraction of the mobile phase that is stagnant within the pores of the particles, ϕ, which is typically 0.5 for a totally porous particle. Also, since the stagnant mobile phase is dependent on the pore structure of the particle, a tortuosity factor (γ') is included to account for this variation. The greater the intraparticle tortuosity factor the less the stagnant mobile phase contributes to the *C*-term.[31]

$$H_{C,MSt} = \frac{(1-\phi+k')^2 d_p^2 u}{30(1-\phi)(1+k')^2 \gamma' D_m} \tag{1-27}$$

Due to the dependence of the stationary phase mass transfer and the amount of stagnant mobile phase on the particle porosity, the $H_{C,SP}$ and $H_{C,MST}$ equations have been combined to account for the variable porous layer thickness of superficially porous particles. This combined contribution, $H_{C,P}$, relates to all the trans-particle mass transfer processes. The Laplace transformation of the general rate model was used to determine the series of moments related to the effect the sold core has on the trans-particle mass transfer resistance.[26, 32, 33]

$$H_{C,p} = \frac{1}{30}\frac{k_1^2}{(1+k_1)^2}\frac{\varepsilon_i}{(1-\varepsilon_i)}\frac{1+2\rho+3\rho^2-\rho^3-5\rho^4}{(1+\rho+\rho^2)^2}\frac{d_p^2 u}{D_p} \tag{1-28}$$

D_p is the diffusion coefficient of the analyte within the stationary phase and is related to both the molecular diffusion, D_m, and the analyte diffusion coefficient in the stationary phase, D_S.[24]

$$D_p = \varepsilon_p \gamma' \gamma_m D_m + (1-\varepsilon_p) K D_S \tag{1-29}$$

The $H_{C,P}$-term has the greatest variation as a function of porous layer thickness. A decrease in the reduced plate height of 45% is achieved in decreasing the porous layer thickness from a ρ value of 0.73 to 0.83, Figure 1-6.

The interparticle mobile phase mass transfer term, C_M, in a packed bed relates to the time needed for an analyte molecule to diffuse in the mobile phase to the particle surface.

$$H_{C,M} = \frac{(1+6k'+11k'^2)d_p^2 u}{24(1+k')^2 D_m} \tag{1-30}$$

This has been modified, C_f, to account for the decrease in particle porosity due to the solid core and the increased surface roughness that forms a variable, stationary eluent film layer on superficially porous particles. Based on the Laplace transformation of the general rate model to produce a series of moments the external film mass transfer resistance can be determined.[26, 32, 33] The term "film" represents the layer of stationary eluent surrounding the particle surface and is not referring to the stationary phase layer.

$$H_{C,f} = \frac{1}{3}\frac{k_1^2}{(1+k_1)^2}\frac{\varepsilon_i}{(1-\varepsilon_i)}\frac{d_p u}{k_f} \tag{1-31}$$

The k_1 term accounts for the varying porosity of the particles and k_f is the external (eluent) film mass transfer coefficient defined as follows:

$$k_f = \frac{(Sh)(D_m)}{d_p} \tag{1-32}$$

The Sherwood number, *Sh*, is the ratio of the particle diameter to the thickness of the eluent film layer, which represents the convective mass transport with respect to diffusive mass transport and is typically in the range of 5-15 in packed columns based on the Wilson-Geankoplos equation.[34-36]

$$Sh = \frac{1.09}{\varepsilon_i} Sc^{1/3} \mathrm{Re}^{1/3} \tag{1-33}$$

The Schmidt number, *Sc*, and Reynolds number, *Re*, are related to mobile phase diffusion and linear velocity, respectively. The Schmidt number physically relates to the relative thickness of the hydrodynamic layer and the mass transfer boundary layer, which account for the momentum (viscosity) diffusion and the mass diffusion convection processes,

$$Sc = \frac{\eta}{\rho_l D_m} \tag{1-34}$$

whereas the Reynolds number is the ratio of the inertial forces to the viscous forces.[37] When the viscous forces are dominating the flow, as is the case for our purposes, the flow will have smooth, constant motion (laminar flow).

$$\mathrm{Re} = \frac{u_o d_p \rho_l}{\eta(1-\varepsilon_i)} \tag{1-35}$$

The inverse relationship of the density and viscosity of the mobile phase in equations 1-33 and 1-34 lead to the independence of the Sherwood number on the specific mobile phase.

$$Sh = \frac{1.09 u_o d_p}{\varepsilon_i D_m (1-\varepsilon_i)} \tag{1-36}$$

As seen in Figure 1-7, the magnitude of the H_{Cf}-term is relatively independent of the porous layer thickness until ρ values of 0.9 are achieved. Therefore, most superficially porous particles will show no improvement due to improved eluent film mass transfer.

When all of the contributions to the theoretical plate height are taken into account at varying ρ values, the improvements from superficially porous particle are visible, Figure 1-8, but not sizable. The reduced plate height for particles with a ρ value of 0.63 compared to 0.73 show a 10% decrease. The plot of the height equivalent to a theoretical plate (for small molecules) as a function of linear velocity for non-porous, superficially porous, and totally porous particles further indicate the improvements found when decreasing porous layer thickness, Figure 1-9. While an increase in efficiency is seen for small molecules, the efficiency improvements from superficially porous particles are most readily seen for more slowly diffusing analytes, Figure 1-10.

1.3 POROUS LAYER THICKNESS CONSIDERATIONS

Based on the modified contributions to the theoretical plate height, it is evident that decreasing the porous layer thickness of the particle will lead to more efficient separations. Not only is the stagnant mobile phase term reduced (as contained within C_p), but there are also reductions in the *A*- and *B*- terms. The *C*-term decreases the most from a reduction in the trans-particle resistance to mass transfer contributions such as the amount of stagnant mobile phase present.[38] Additionally, based on studies by Omamogho *et. al*., as the porous layer thickness was decreased the *A*-term was found to decrease accordingly.[20]. The direct cause for this reduction has not been established, but has been consistently observed. Lastly, the thinner porous layer produces less volume for analyte diffusion, thus decreasing the *B*-term contribution to the theoretical plate height. Due to all of these contributions, the efficiency of superficially porous particles improves as the porous layer thickness is decreased.

1.3.1 Theoretical Porous Layer Thickness Based on Analyte Molecular Weight

Currently, the majority of commercially available particles have a core diameter to particle diameter ratio (ρ) in the range of 0.63 to 0.73. While this ratio is useful for analytes with fast diffusion rates, such as small molecules, this porous layer thickness is predicted to be too high for more slowly diffusing analytes, such as peptides and proteins. Independent of analyte size, the efficiency is predicted to increase as the porous layer thickness decreases and the height equivalent to a theoretical plate decreases until a minimum is reached for non-porous particles, as seen in Figure 1-10.[38] From this comparison it is evident that the improvement in efficiency is more pronounced as the analyte molecular weight is increased due to slower diffusion. Particularly at linear velocities greater than the optimum which is the typical range of operation for macromolecular separations.

While theoretical plates are a common measure of efficiency a more robust measure of separation power is resolution between different analytes. The resolution between two analytes depends on the peak widths, described by the height equivalent to a theoretical plate, and the difference between their residence time in the stationary phase. Figure 1-11 shows the resolution of two analytes as a function of porous layer thickness. At the optimum linear velocity for each of the analytes differing in molecular weight, the resolution gain is not found to be significant, Figure 1-11(a). As the operating linear velocity is increased to four times the optimum, Figure 1-11(b), the resolution gains for superficially porous particles are found to be evident predominantly due to the reduced *C*-term contribution.[39] This is particularly important for the separation of proteins which are usually run well above the optimum linear velocity. Based on the resolution improvement of superficially porous particles, the predicted optimum ρ values for a small molecule (MW < 500 Da), small

peptide (MW ≈ 1000 Da), medium peptide (MW ≈ 6000 Da), and a protein (MW ≈ 60,000 Da) are 0.50, 0.73, 0.87, and 0.95, respectively.[36]

Based on theoretical plate height and resolution, it is evident that the porous layer thickness of commercially available products is suitable for small molecules and small peptides although the greatest efficiency gains for superficially porous particles is predicted for macromolecules which require a thinner porous layer to achieve the improved separation efficiency. Commercial products such as Poroshell 300 and Aeris WIDEPORE have a suitable porous layer thickness, but the particle diameter is greater than desired. To address this, sub-2 micron particles with ρ values between 0.82 and 0.92 were synthesized as will be discussed in the following chapters.

1.3.2 Chromatographic Considerations

While the separation efficiency for large molecular weight compounds is predicted to increase with decreasing porous layer thickness, the loading capacity and retention are greatly reduced. To compensate for this loss in retention, typically the mobile phase strength is decreased to maintain adequate resolution. Although, the loss of loading capacity should be less than expected due to the catch-and-release nature of protein adsorption and desorption. Typically it is believed that proteins interact minimally with the interior of totally porous particles, therefore the solid core of superficially porous particles should not significantly affect the loading capacity. When the organic concentration of the mobile phase is low, the majority of the proteins will be completely retained on the stationary phase and have no predisposition to enter the pores of the particle. As the organic concentration in the mobile phase is increased minuscule amounts, a protein goes from being fully retained to completely unretained. Therefore the analyte has little interaction with the stationary phase in

the interior of a porous particle, which would reduce the expected decrease in loading capacity when decreasing the porous layer thickness.

Further consideration must be placed on the extra-column volume of the system. As the column efficiency improves the band broadening effects of extra-column volume have a greater effect on the resulting chromatographic efficiency. To maintain the efficiency gains of superficially porous particles, the volumes of connectors and the detector must be reduced and the injection time adjusted.

1.4 PARTICLE DIAMETER CONSIDERATIONS

1.4.1 Theoretical Advantages of Decreasing Particle Diameter

Based on the expansion of the *A*-term and *C*-term, the height equivalent to a theoretical plate is shown to be dependent on the particle diameter.

$$A \propto d_p \tag{1-37}$$

$$C \propto d_p^2 \tag{1-38}$$

The proportionalities show decreasing the particle diameter correlates to an increase in separation efficiency through a reduction in the height equivalent to a theoretical plate. The decrease in the *C*-term produces further gains by decreasing the slope in the high linear velocity region. This allows operation at higher linear velocities with less loss of separation efficiency, leading to faster analyses and increased sample throughput. The effect of particle size reduction on separation efficiency is shown in Figure 1-12. At the optimum linear velocity, 1 μm particles are predicted to decrease the theoretical plate height by 67% over 3 μm particles.

1.4.2 Instrument Considerations

While there are proven advantages to smaller diameter particles, the pressure requirements of the instrument increase to compensate for the increased flow resistance through the column. This can be explained by the pressure drop across a column, ΔP, necessary to obtain a mobile phase linear velocity, u, given below.[40]

$$\Delta P = \frac{\Phi \eta L u}{d_p^2} \tag{1-39}$$

Where Φ is the flow resistance factor, η is the viscosity of the solvent, and L is the length of the packed bed. Furthermore, the optimum linear velocity (u_{opt}) is inversely proportional to the particle diameter.

$$u_{opt} = \frac{3D_m}{d_p} \tag{1-40}$$

Taking both relationships into consideration, the pressure required to obtain the optimum flow rate is dictated as follows:

$$\Delta P_{opt} = \frac{3\Phi \eta L D_m}{d_p^3} \tag{1-41}$$

To accommodate the high pressure requirement of sub-2 micron particles, conventional HPLC equipment with a typical pressure limit of ~400 bar (6000 psi) had to be modified with ultra-high pressure pumps to perform high resolution separations of complex mixtures.[17] This technology allows the separation efficiency gains predicted by decreasing the particle diameter.

1.5 PORE DIAMETER CONSIDERATIONS

The majority of commercial particles have a pore diameter of approximately 90Å. The Poroshell 300 particles have 300 Å pores but are only available in a 5 μm particle

diameter and Aeris WIDEPORE particles have 200 Å pores but have a 3.6 μm particle diameter. Particles useful for peptides include the Halo-Peptide ES, Aeris, and the Poroshell 120, which have approximately 120 Å pores. Based on the efficiency predictions for superficially porous particle, the greatest advantages are to be seen for large molecular weight compounds requiring larger pore diameters.

1.5.1 Relationship Between Pore Size and Molecular Weight

Based on traditional experimental guidelines, analysis of small molecule analytes (MW < 1000 Da) are performed with particles having a pore diameter of approximately 90 Å. Therefore, all commercially available superficially porous particles are suitable for small molecule separations. As the size of the analyte is increased, such as for peptides, the typical pore size used is 120 Å. Analytes larger in size than this require even larger pores such as 300 Å, but even this size is too small for very large analytes such as monoclonal antibodies. The use of small pores for proteins have been found to lead to the loss of biological activity, reduced recovery, and produce peak multiplets.[41-43] Therefore, to harness the improved efficiency predicted for macromolecules by superficially porous particles, the pore size must be increased. Furthermore, the ability to easily modify the pore size for different applications is desirable.

1.6 THESIS OVERVIEW

The work presented in this thesis is focused on improving separation efficiency through the development of smaller diameter superficially porous particles with a thin porous shell with various pore sizes. Chapters 2 and 3 discuss the synthesis development and preliminary performance characterization of 1.7 μm and 1.1 μm superficially porous particles, respectively. In this work the layer-by-layer method for synthesis was modified for

use with smaller diameter particles. Chapter 4 compares the performance of 1.1 μm superficially porous particles with different pore sizes. The efficiency for small molecules, peptides, and proteins were assessed at each pore diameter value. Chapter 5 investigates the role of slurry solvent and slurry concentration on the column packing process and performance. A general method for determining relatively better slurry solvents is presented here.

1.7 REFERENCES

[1] Horvath, C.; Lipsky, S.R. *J. Chrom. Science* 7 (1969) 109-116.

[2] Horvath, C.G.; Preiss, B.A.; Lipsky, S.R. *Anal. Chem.* 39 (1967) 1422-1428.

[3] Kirkland, J.J. *US Patent 3505785* 1970.

[4] Parris, N.A. *Instrumental LC: a practical manual on high performance liquid chromatographic methods*, Elsevier Scientific Publishing Company, New York, 1976.

[5] Little, J.N.; Horgan, D.F.; Bombaugh, K.J. *J. Chrom. Science* 8 (1970) 625-629.

[6] Kaczmarski, K.; Guiochon, G. *Anal. Chem.* 79 (2007) 4648-4656.

[7] Kirkland, J.J. *Anal. Chem.* 64 (1992) 1239-1245.

[8] Snyder, L.; Kirkland, J.J.; Glajch, J.L. *Practical HPLC Method Development*, Wiley, New York, 2nd. ed. 1997.

[9] Iler, R.K. *US Patent 3485658* 1969.

[10] Kirkland, J.J.; Langlois, T.J. *US Patent 0189944 A1* 2007.

[11] Kirkland, J.J. *US Patent 4070283* 1978.

[12] Buchel, G.; Unger, K.K.; Matsumoto, A.; Tsutsumi, K. *Adv. Mater.* 10 (1998) 1036-1038.

[13] Chen, W.; Wei, T-C. *Eu. Patent EP2218500 A2* 2010.

[14] Glennon, J.D.; Omamogho, J. *US Patent W02010/061367 A2* 2010.

[15] Gritti, F.; Leonardis, I.; Abia, J.; Guiochon, G. *J. Chrom. A* 1217 (2010) 3819-3843.

[16] Gritti, F.; Cavazzini, A.; Marchetti, N.; Guiochon, G. *J. Chrom. A* 1157 (2007) 289-303.

[17] MacNair, J.E.; Lewis, K.C.; Jorgenson, J.W. *Anal. Chem.* 69 (1997) 983-989.

[18] Gritti,F.; Guiochon, G. *J. Chrom. A* 1176 (2007) 107-122.

[19] Snyder, L.; Kirkland, J.J.; Dolan, J.W. *Introduction to Modern Liquid Chromatography*, Wiley, New York, 3rd ed., 2010.

[20] Omamogho, J.O.; Hanrahan, J.P.; Tobin, J.; Glennon, J.D. *J. Chrom. A* 1218 (2011) 1942-1953.

[21] Giddings, J.C. *Dynamics of Chromatography: Principles and Theory*, Marcel Dekker Inc., New York, 1965.

[22] Khirevich, S.; Holtzel, A.; Seidel-Morgenstern, A.; Tallarek, U. *Anal. Chem.* 81 (2009) 7057-7066.

[23] Tallarek, U.; Bayer, E.; Guiochon, G. *J. Am. Chem. Soc.* 120 (1998) 1494-1505.

[24] Gritti, F.; Guiochon, G. *J. Chrom. A* 1221 (2012) 2-40.

[25] Khirevich, S.; Daneyko, A.; Holtzel, A.; Seidel-Morgenstern, A.; Tallarek, U. *J. Chrom. A* 1217 (2010) 4713-4722.

[26] Gritti, F.; Guiochon, G. *Chem. Eng. Science* 66 (2011) 3773-3782

[27] Desmet, G.; Broeckhoven, K.; De Smet, J.; Deridder, S.; Baron, G.V.; Gzil, P. *J. Chrom. A* 1188 (2008) 171-181.

[28] Torquato, S.; Lado, F. *Phys. Review* 33 (1986) 6428-6435.

[29] Mikdam, A.; Makradi, A.; Ahzi, S.; Garmestani, H.; Li, D.S.; Remond, Y. *Intl. J. Sol. Surf.* 46 (2009) 3782-3787.

[30] Kaczmarski, K.; Guiochon, G. *Anal. Chem.* 79 (2007) 4648-4656.

[31] Neue, U. *HPLC Columns: Theory, Technology, and Practice*, Wiley-VCH,. New York, 1997.

[32] Gritti, F.; Guiochon, G. *J. Chrom. A* 1218 (2011) 907-921.

[33] Cavazzini, A.; Griti, F.; Kaczmarski, K.; Marchetti, N.; Guiochon, G. *Anal. Chem.* 79 (2007) 5972-5979.

[34] Miyabe, K.; Kawaguchi, Y.; Guiochon, G. *J. Chrom. A* 1217 (2010) 3053-3062.

[35] Unger, K.K.; Skudas, R.; Shulte, M.M. *J. Chrom. A* 1184 (2008) 393-415.

[36] Gritti, F.; Guiochon, G. *Chem. Eng. Science* 72 (2012) 108-114.

[37] Incropera, F.P.; DeWitt, D.P. *Fundamentals of Heat and Mass Transfer*, 3rd ed.. John Wiley & Sons, New York, 1990.

[38] Horvath, K.; Gritti, F.; Fairchild, J.N.; Guiochon, G. *J. Chrom. A* 1217 (2010) 6373-6381.

[39] Gritti, F.; Guiochon, G. *J. Chrom. A* 1217 (2010) 6350-6365.

[40] MacNair, J.; Patel, K.D.; Jorgenson, J.W. Anal. Chem 71 (1999) 700-708.

[41] Dillon, T.M.; Bohdarenko, P.V.; Rehder, D.S.; Pipes, G.D.; Kleemann, G.R.; Ricci, M. *J. Chrom. A* 1120 (2006) 112-120.

[42] Tanaka, N.; Kimata, K.; Mikawa, Y.; Hosoya, K.; Araki, T.; Ohtsu, Y.; Shiojma, Y.; Tsuboi, R.; Tsuchuya, H. *J. Chromatogr. 535* (1990) 13-31.

[43] Guan-Sajonz, H.; Guiochon, G.; Davis, E.; Gulakowski, K.; Smith, D.W. *J. Chrom. A* 773 (1997) 33-51.

1.8 TABLES

Name	Manufacturer	Particle Diameter (μm)	ρ	Pore Diameter (Å)
Halo	Advanced Materials Technology	2.7	0.63	90
Halo-ES	Advanced Materials Technology	2.7	0.63	160
Poroshell 120	Agilent Technologies	2.7	0.63	120
Poroshell 300	Agilent Technologies	5.0	0.80	300
Kinetex	Phenomenex	2.6	0.73	100
Kinetex	Phenomenex	1.7	0.73	100
Aeris PEPTIDE	Phenomenex	3.6	0.72	100
Aeris PEPTIDE	Phenomenex	1.7	0.74	100
Aeris WIDEPORE	Phenomenex	3.6	0.89	200
Ascentis Express	Supelco	2.7	0.63	90
Ascentis Express Peptide-ES	Supelco	2.7	0.63	160
Accucore	Thermo Fisher	2.6	0.58	80
Nucleoshell	Macherey-Nagel	2.7	0.63	90

Table 1-1: Summary of commercially available particles from manufacturers literature

1.9 FIGURES

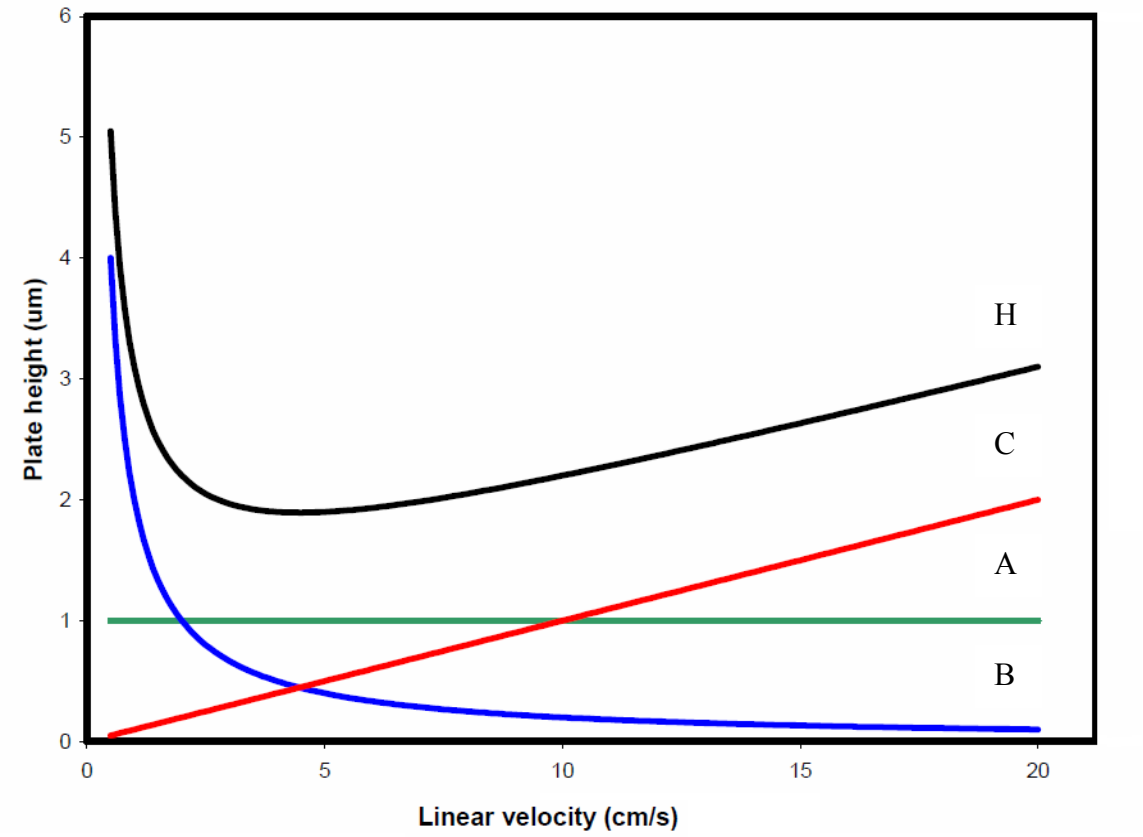

Figure 1-1: Theoretical relationship between the *A*-, *B*-, and *C*-term of the van Deemter equation.

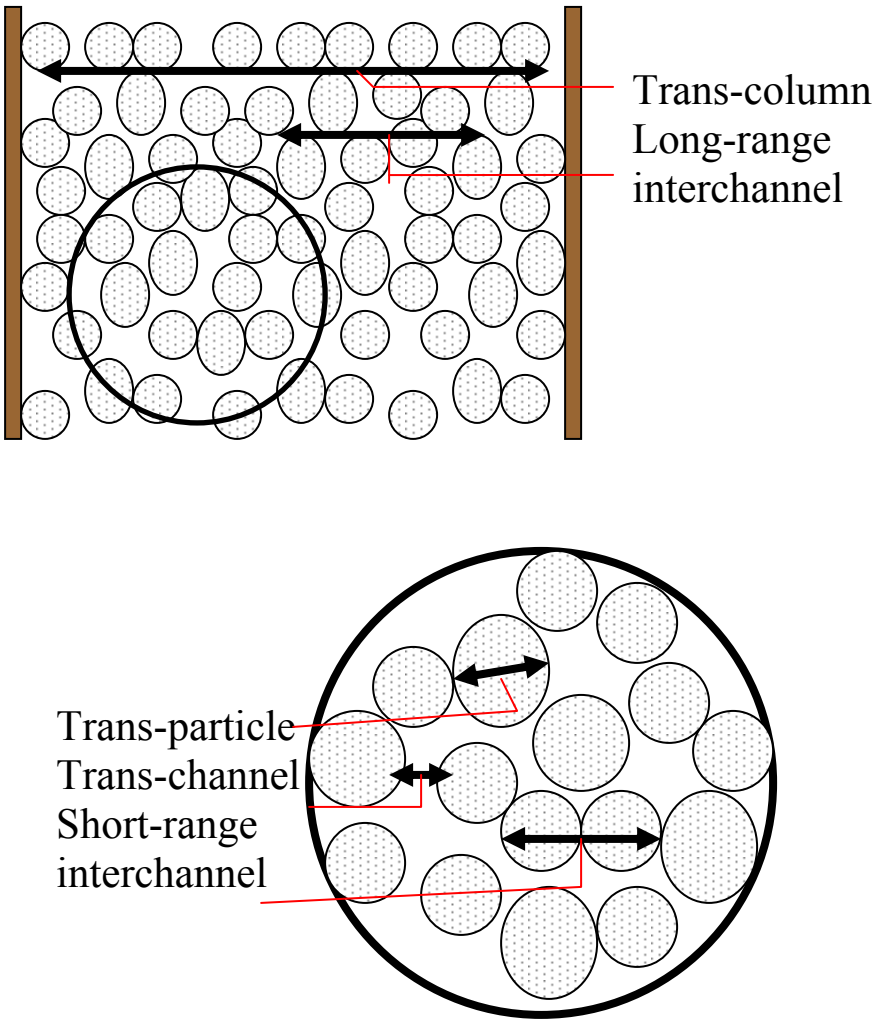

Figure 1-2: Diagram of the location and distance of the different contributions to eddy dispersion in a packed column. Reproduction from [21].

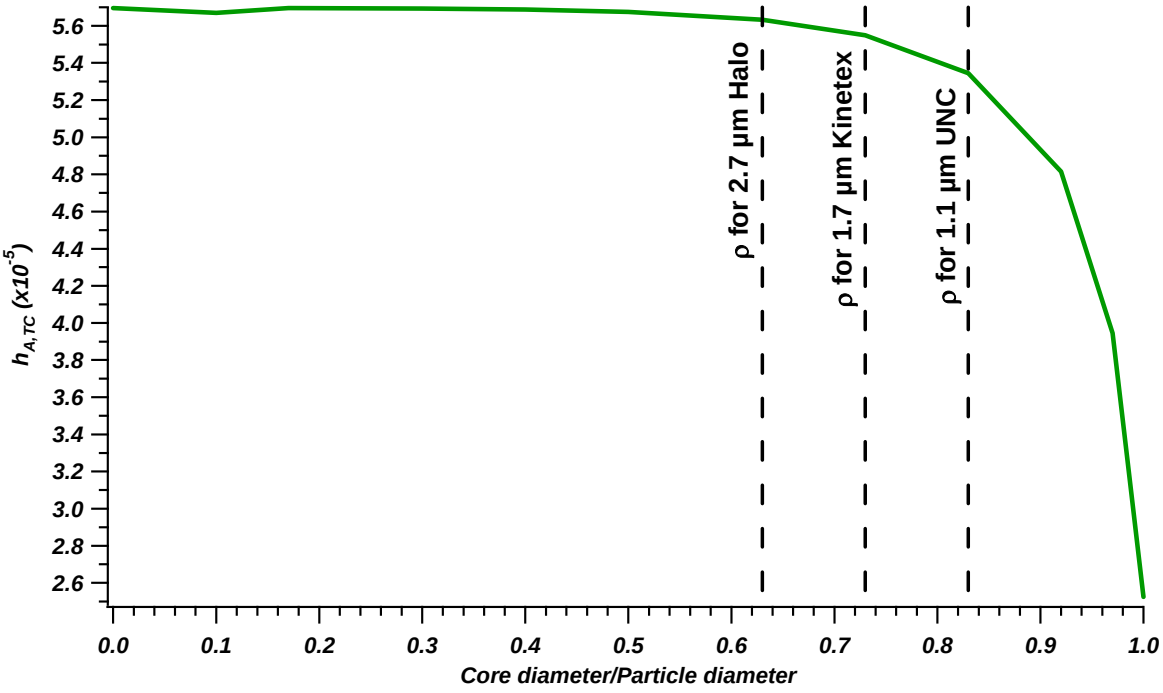

Figure 1-3: Theoretical relationship between the porous layer thickness and the $h_{A,TC}$-term. $p_l/q_l = 8/225$, $m_l = 150{,}000$, $m_r = 15$, $\omega^*_{\beta,c} = 1.5\%$, $\varepsilon_T = 0.65$, $\varepsilon_i = 0.40$, $k' = 2$, $\gamma_r = 0.3$, $v = 3$

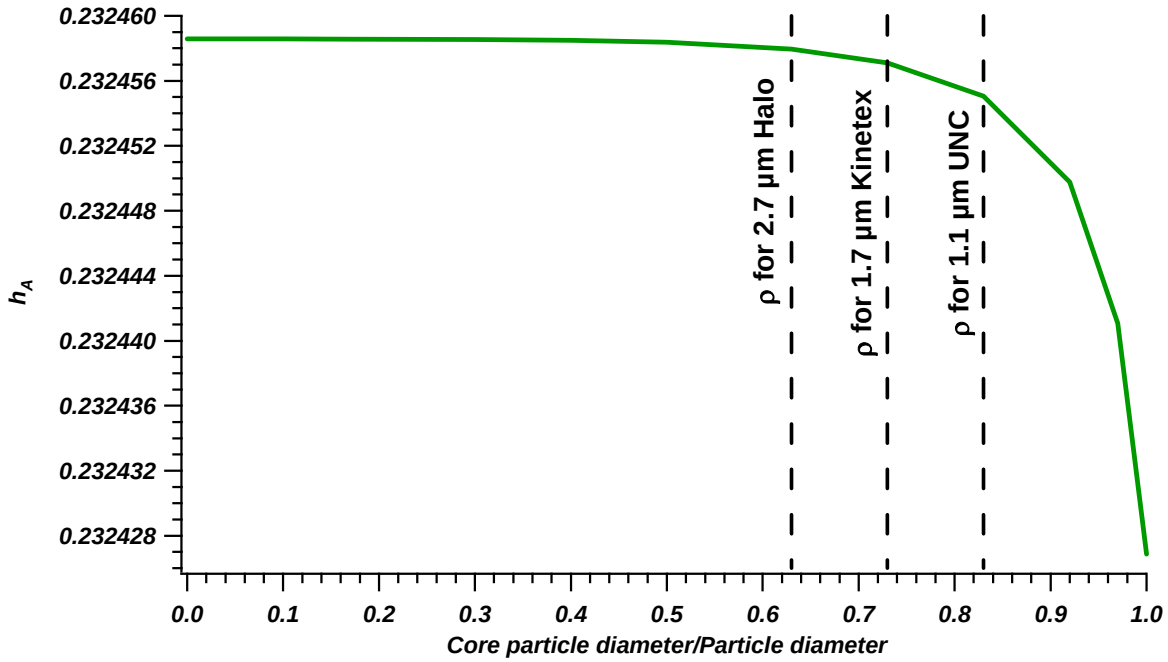

Figure 1-4 Theoretical relationship between h_A (total) and the porous layer thickness. p_l/q_l = 8/225, m_l = 150,000, m_r = 15, $\omega^*_{\beta,c}$ = 1.5%, ε_T = 0.65, ε_i = 0.40, k' = 2, γ_r = 0.3, v = 3

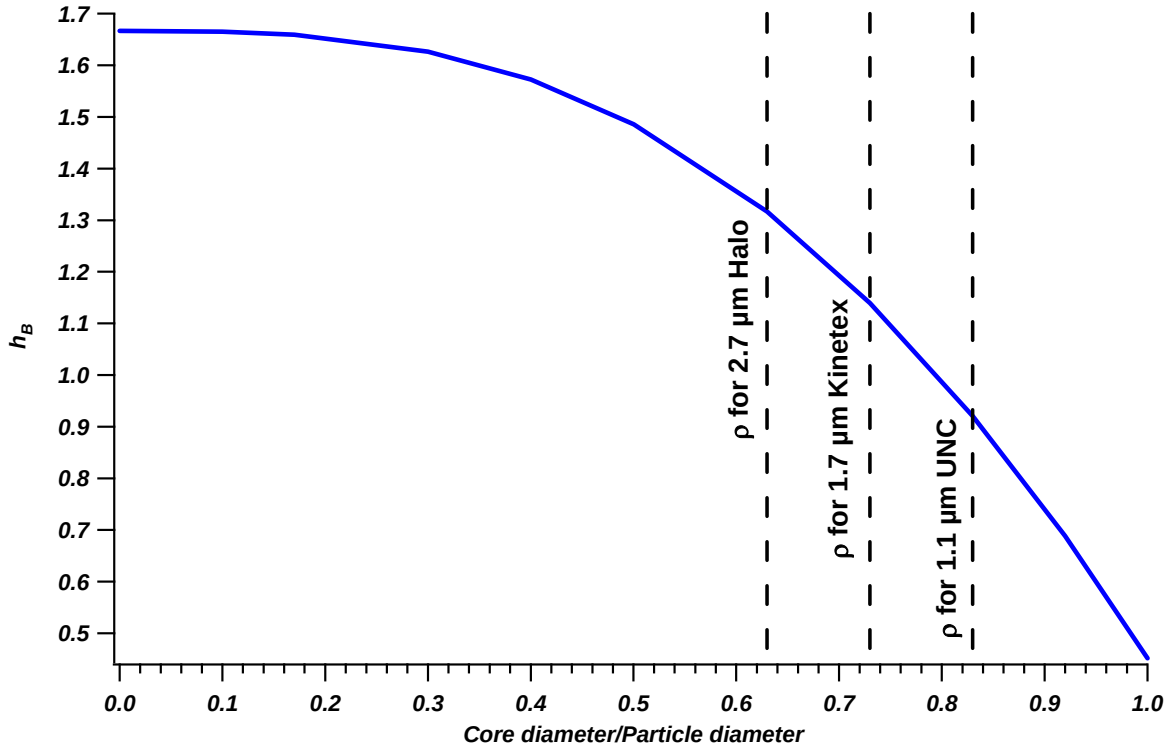

Figure 1-5: Theoretical relationship between the porous layer thickness and the h_B-term. ε_i = 0.40, ξ_2 = 0.3277, Ω = 1, and v = 3

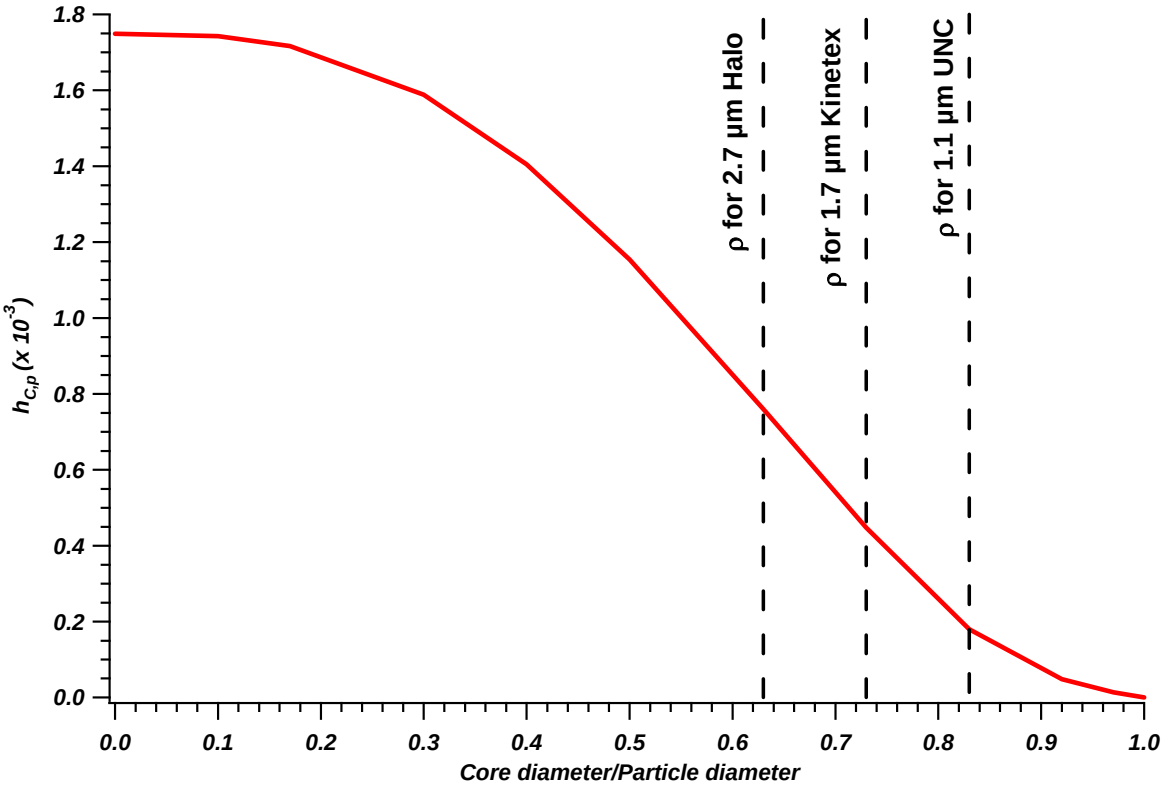

Figure 1-6: Theoretical relationship between the trans-particle (porous layer thickness and the liquid stationary phase and stagnant mobile phase) resistance to mass transfer ($h_{C,p}$). K = 0.5, Sh = 10, ε_i= 0.40, k_1 varies as a function of ρ

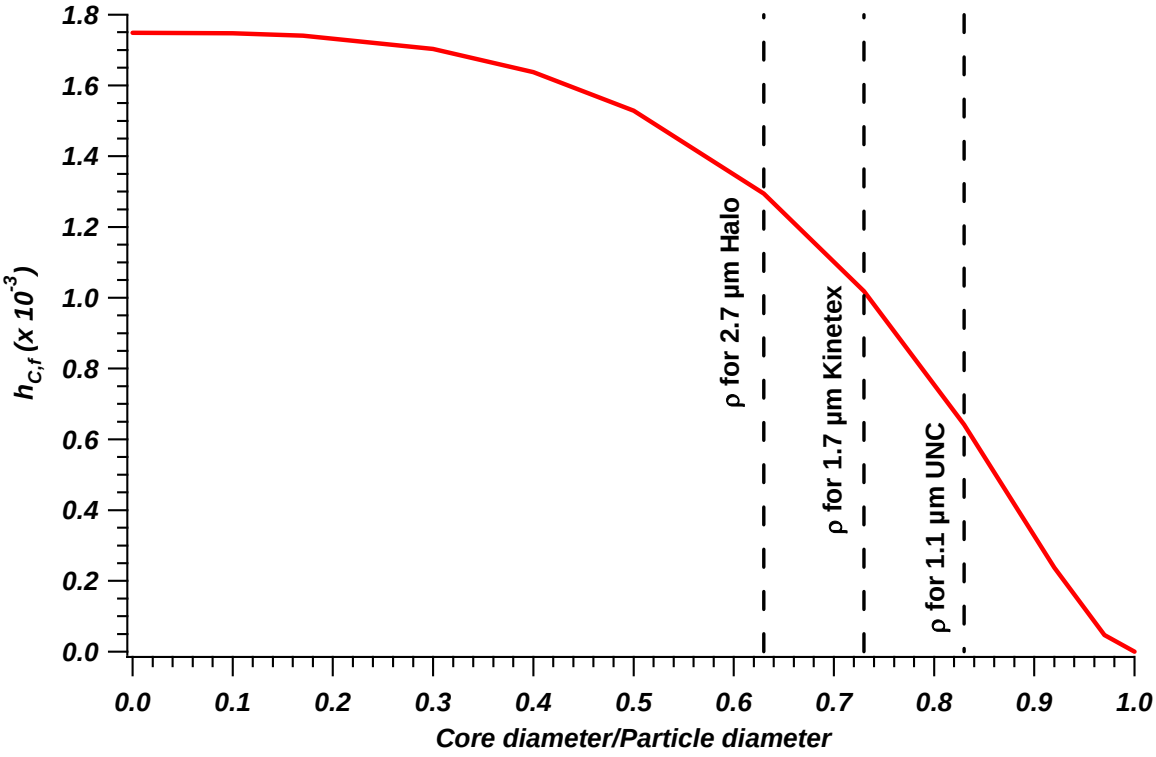

Figure 1-7: Theoretical relationship between the porous layer thickness and the mobile phase resistance to mass transfer ($h_{C,f}$). $\varepsilon_i = 0.40$ and k_1 varies with porous layer thickness

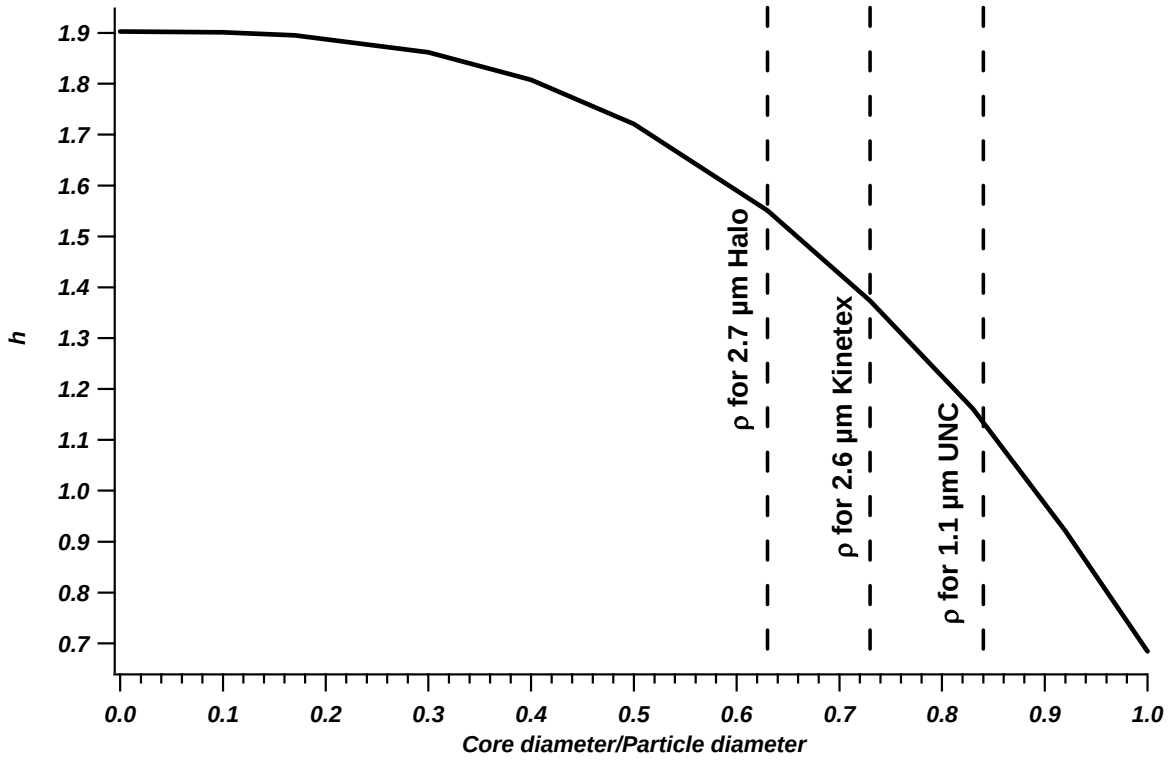

Figure 1-8: Theoretical relationship between the porous layer thickness and the theoretical plate height at $v = 3$.

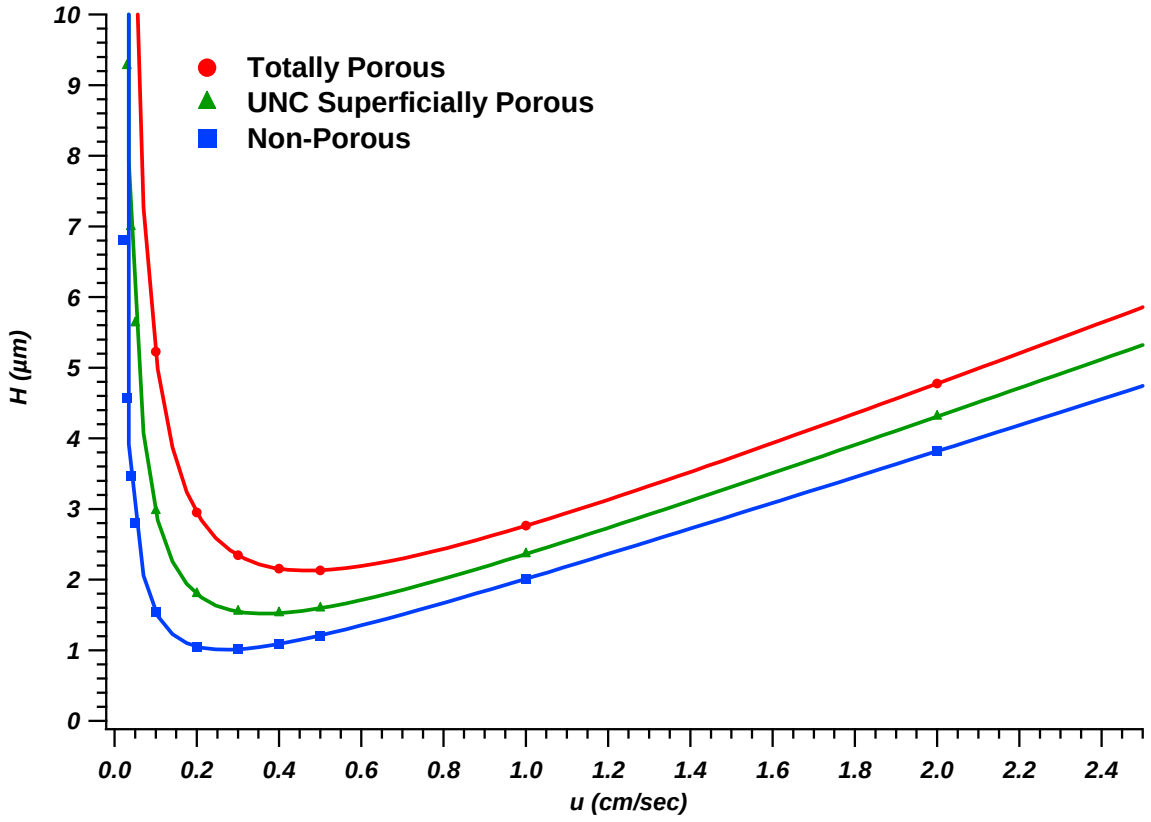

Figure 1-9: Theoretical relationship between the theoretical plate height and linear velocity at varying porous layer thickness for a small molecules analyte (D_M = 1 x 10^{-5}). d_p =1.0 µm

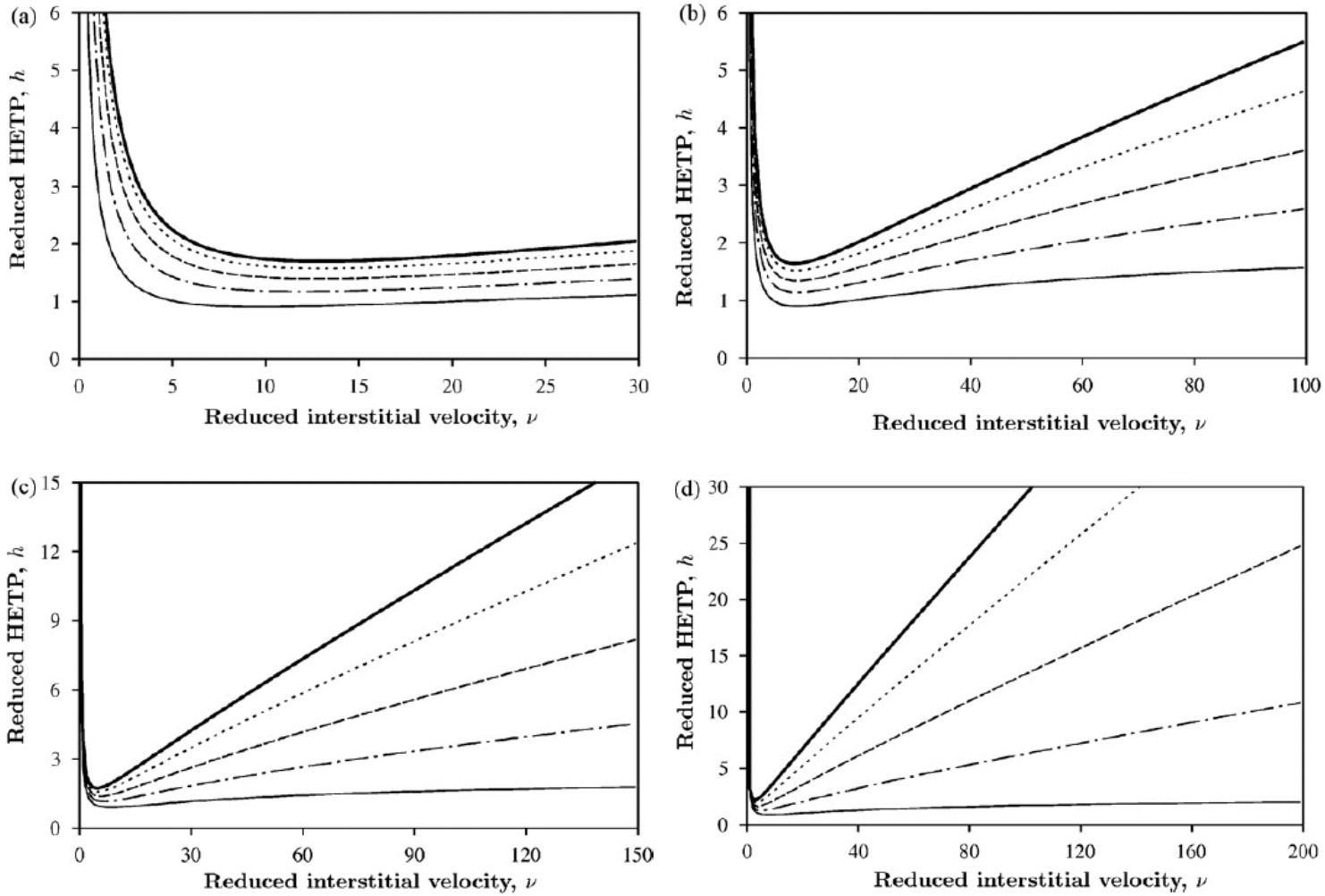

Figure 1-10: Reduced plate heights of compounds having different molecular sizes as a function of reduced velocity, for different porous layer thickness. ρ = 1: solid line, ρ = 0.85: dot-dashed line, ρ = 0.7: dashed line, ρ = 0.5: dotted line, ρ = 0: thick solid line. (a) small molecule; (b) medium-sized peptide; (c) large peptide; (d) protein.[35]

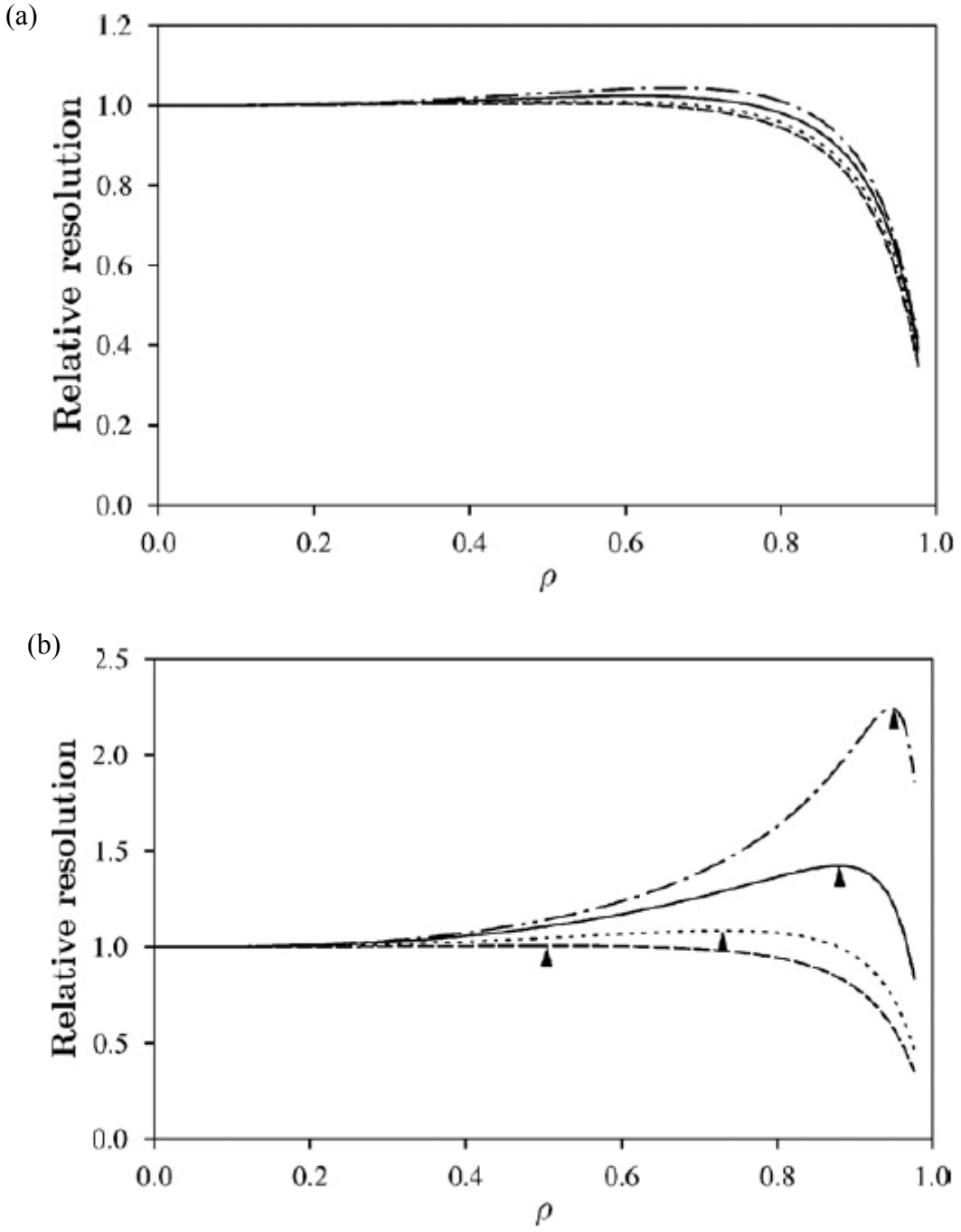

Figure 1-11: Resolution of pairs of compounds having different molecular sizes. Dashed line: small molecule; dotted line: medium-sized peptide; solid line: large peptide; dot-dashed line: protein. Plots of the resolution on a column packed with superficially porous particles relative to the resolution on a column packed with fully porous particles. (a) Resolution calculated at the optimum linear velocity for the analyte of interest (b) Resolution calculated at the optimum linear velocity for small molecules.[35]

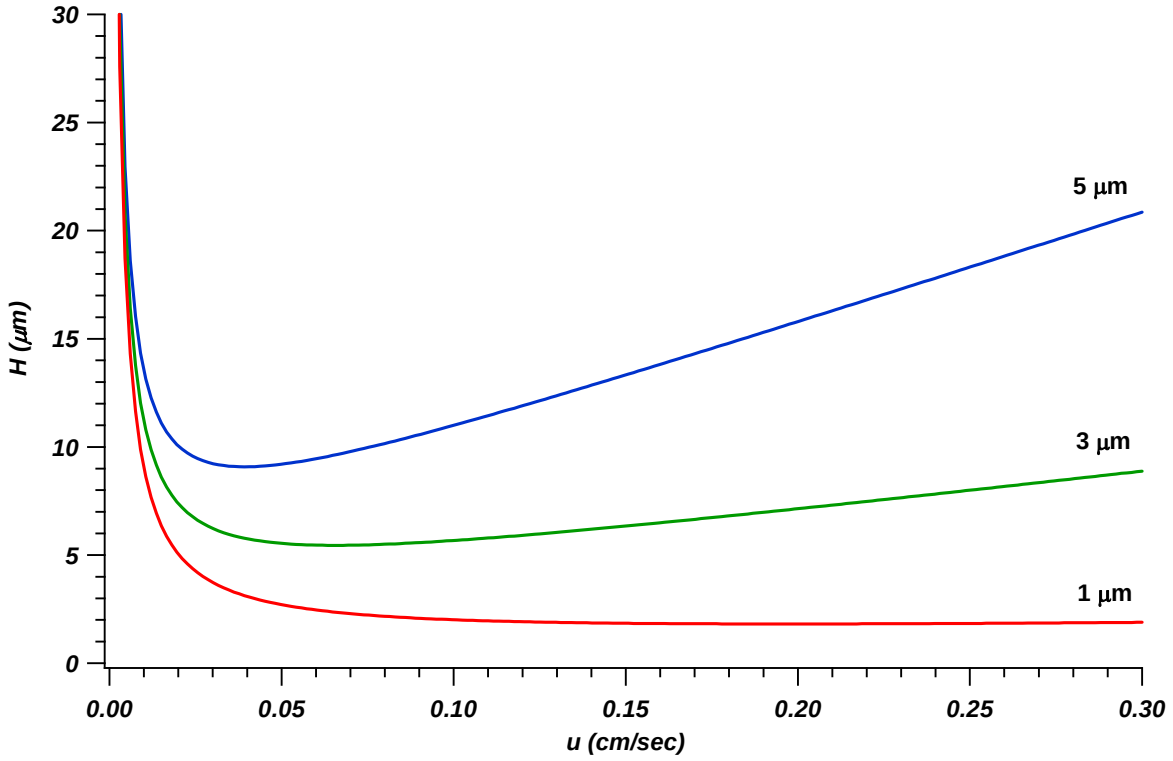

Figure 1-12: Effect of decreasing particle diameter on efficiency. $D_m = 1.0 \times 10^{-5}$ cm^2/sec and $d_p = 1.0$ μm

CHAPTER 2: SYNTHESIS AND CHROMATOGRAPHIC EVALUATION OF 1.7 μm SUPERFICIALLY POROUS PARTICLES

2.1 INTRODUCTION

2.1.1 Previous Developments

While superficially porous or pellicular particles have been around since the 1970s, they have been overshadowed by the use of totally porous particles until recent years.[1-8] The developments by Kirkland led to the production of small diameter, spherical, monodisperse superficially porous particles which has brought their use back into popularity. Upon development of the product, Halo (Advanced Materials Technology), most other column manufacturers have released similar products. The majority of the commercial products mirror the Halo particle dimensions with a 2.7 μm total particle diameter and 90 Å pores. Deviations from this include 1.7 μm particles produced by Phenomenex and 5 μm, 300 Å pore particles produced by Agilent Technologies.

Independent of the dimensions of superficially porous particles, they have been found to show chromatographic efficiency gains over the more widely used totally porous particles. The predominant improvements in efficiency arise from decreases in the *A*-term and *C*-term contributions to the theoretical plate height. The *A*-term decrease arises from improvements in column packing due to the monodispersity of superficially porous particles, and the *C*-term improves as the porous layer thickness is decreased. [6, 7, 9-13] Improvement of these terms

leads to a decrease in the theoretical plate height, which provides a more efficient separation.

2.1.2 Desirable Particle Characteristics

Desirable characteristics for liquid chromatographic (LC) column packing materials are inertness, mechanical robustness, broad pH stability, and compatibility with mobile phase solvents.[14] Today the breadth of LC applications necessitate the ability to run analyses at extreme pH values and to allow for shorter analysis times by running at higher flow rates. Furthermore, the material should allow the use of high water content mobile phases for analysis of pharmaceutical and biological compounds.

In addition to chemical and system compatibility aspects of the packing material, there are also a number of physical characteristics that allow for improvement of the chromatographic performance of the support. These include particle shape, particle size distribution, carbon load, absence of metal impurities, and surface roughness.[15-17] The support most commonly used today is spherical silica particles. The particle shape has been found to influence the packing density of the column and the geometry of the interstitial spaces.[18] The use of spherical, monodisperse particles allows for the production of a more homogeneous and dense packing structure than that of a column packed with irregularly shaped particles, and leads to a more efficient separation.[18] The column bed homogeneity achieved with spherical particles produces a more efficient chromatographic separation due to the reduction of the *A*-term contribution to the theoretical plate height.

Additionally, the particle size distribution affects the efficiency of the column packing process which in turn affects the chromatographic efficiency. The deleterious effects of a broad particle size distribution on column packing produce columns with

chromatographic performance worse than predicted from computational analysis. [12, 19-20] Particle polydispersity has been found to produce columns with radial particle size segregation and variations in packing density, which lead to a reduction in column efficiency.[12,21, 22] Therefore, a monodisperse support is desirable.

Further variations in column efficiency arise from the functionalization of the chromatographic support. The most common functional group in use for reversed phase separations is octadecyl (C18), but the amount of surface coverage between manufacturers of C18 bonded phases varies. The resulting surface coverage produced by the bonding procedure is typically quantified by the carbon load of the column packing material. Packing materials with higher carbon load have greater loading capacity and resolving power, but are also more retentive, making fast separations more difficult.[23] The analysis of interest must be considered when determining what carbon load will be most useful. Further variation can occur due to the presence of free silanol groups on the support surface, which can act as adsorption sites for analytes, particularly bases, leading to peak broadening.[8,13] To reduce these affects, a support should be adequately endcapped to reduce the amount of free silanols available for secondary interaction.

Additional surface interactions can arise from the presence of trace metal impurities within the particle structure. The presence of these impurities typically arise from the type of silica used, but can also arise from sources in the synthesis process. To reduce the presence of metal impurities, Type B silica has become the standard support material. Type B silica is synthesized from an organic sol rather than the older Type A silica synthesized from an inorganic sol. Type B material is synthesized in a manner which minimizes the amount of trace metals, particularly aluminum, in the lattice.[8] This high purity material reduces

interactions with basic compounds and reduces the variations in silanol acidity leading to more efficient separations.[24, 25]

Lastly is the affect of the particle surface roughness on the column packing structure and the resulting column efficiency. It has been proposed by Gritti and Guiochon that particles with a rough external surface exhibit greater friction between particles during packing which leads to a more open packing structure. [20, 26, 27] While contradictory to initial findings in the literature that a dense bed leads to a more efficient separation, this open bed structure is thought to contribute to the increased efficiency seen with superficially porous particles over totally porous particles. Further effects of surface roughness arise from the role it is thought to play in altering the film mass transfer kinetics of the sample to the stationary phase.[9, 26, 28] The surface roughness has been predicted to cause a higher than predicted *C*-term value for superficially porous particles leading to less efficient separations at higher linear velocities, but is similar to the *C*-term seen for totally porous particles.[26] While the experimentally observed *C*-term is greater than predicted, the decrease in the *A*-term allows for an overall more efficient separation with superficially porous particles over totally porous particles.

2.1.3 Historical Challenges

Throughout time there have been challenges in the ability to make LC packing materials with the desired properties. One challenge in the development of efficient packing materials has been the production of material with a sufficiently narrow particle size distribution. Particles with high polydisersity have been found to be difficult to pack, which produces columns with inferior chromatographic efficiency.[19,20, 29] Initial porous liquid chromatography supports had particle size diameters greater than 100 μm and were

irregularly-shaped materials with broad particle size distributions.[30] As the synthetic process was improved, the polydispersity of the materials was also decreased. Today, totally porous packing materials have particle size relative standard deviations (RSDs) in the range of 15-20%, greatly improved over the initial materials, but still leaving room for improvement.[10, 31] Further advances have been achieved through the development of superficially porous particles which have particle size RSD values under 5%. [10]

Challenges also arise in the development of packing materials with smaller particle diameters. While it is evident that decreasing the particle diameter of the packing material leads to improved chromatographic efficiency, there are challenges due to the increased backpressure required to run such columns.[8, 13, 32] This is not only a concern for the pumping system, but also for the mechanical strength required of the packing material.[33] While silica is considered a mechanically strong material, the material becomes weaker as pores of increasing diameter and volume are introduced.[18, 34] This is a concern for totally porous particles and continues to be problematic for superficially porous particles. While the solid core of superficially porous particles should increase the mechanical strength over totally porous particles, the boundary between the non-porous and porous layer introduces a point of weakness. Therefore, moving to smaller diameter superficially porous particles to improve efficiency requires increased mechanical strength of the support.

A further challenge when using smaller particle diameters is developing column frits that will contain the particles within the column without clogging. In order to retain particles within the bed, a frit should have a pore size no larger than one half that of the average particle diameter.[35] Therefore, for 1 μm particles, the frit pore size can be no larger than 0.5 μm. Moving to frits with these smaller pore sizes has been found to lead to clogging due

to the mobile phase, instrument, and sample.[35-37] To allow for the efficiency gains of smaller diameter particles, sample and solvent clean-up measures must be improved.

Additional challenges arise in the development of superficially porous particles in terms of porous layer uniformity. The initial developments of pellicular particles by Horvath led to very uniform coatings, but this was expected due to the large non-porous core diameter and the application of a single porous layer.[1-2] As further developments of these materials were carried out it was found that as the porous layer thickness was increased to improve loading capacity, the surface uniformity degraded.[38] Several attempts to overcome this have been investigated, such a using spray-drying and sol-gel chemistry rather than a layer-by-layer method, but problems still arise with thicker porous layers.[37, 20] Therefore to produce particles with smaller diameters and thicker porous layers, further synthesis modifications are required.

2.1.4 Particle Characterization

The term particle size is ambiguous unless the means of calculation is specified. Typically, the particle size refers to the number average particle diameter ($d_{p,n}$). [13]

$$d_{p,n} = \frac{\Sigma d_{p,i} n_i}{\Sigma n_i} \tag{2-1}$$

Where $d_{p,i}$ is each individual particle diameter and n_i is the number of particles with that specific particle diameter. This particle diameter is most applicable when comparing the flow resistances between columns packed with different sized particles. The number average particle diameter is used for all comparisons and calculations except for reduced parameter calculations which use the volume average particle diameter. The volume average particle diameter ($d_{p,v}$) is more applicable in cases when assessing the chromatographic efficiency. [13]

$$d_{p,v} = \frac{\Sigma d_{p,i} d_{p,i}^3 n_i}{\Sigma d_{p,i} d_{p,i}^2 n_i} \tag{2-2}$$

For a monodisperse batch of particles the number average and the volume average particle sizes are identical, but this is rarely the case for real particles. For a non-monodisperse sample the volume average particle size will be greater than the number average particle size. The greater the difference between the two particle sizes, the greater the polydispersity of the batch.

Additionally, to assess the performance of a chromatographic column, the viscosity of the mobile phase must be known to allow for approximation of the linear flow velocity through the use of the Kozeny-Carmen equation.[13]

$$u = \frac{\Delta P \Phi^2 d_{p,n}^2 \varepsilon_i^{\,2}}{180 \eta L (1 - \varepsilon_i)^2} \tag{2-3}$$

Where the linear flow velocity, u, is related to the pressure drop across the length of the column, ΔP, flow resistance, Φ, the number average particle diameter, $d_{p,n}$, interparticle porosity, ε_i, column length, L, and viscosity, η. The solvent viscosity has have been found to change significantly and non-linearly with varying pressure.[39-41] To accurately determine the linear flow velocity for our system at specified pressures, the viscosity values for water/acetonitrile mixtures as reported by Thompson have been used.[42]

The need to accurately determine the viscosity is also important for the determination of the diffusion coefficient, D, by the Stokes-Einstein equation[43]

$$D = \frac{kT}{6\pi\eta r_H} \tag{2-4}$$

where the Boltzmann's constant, k, temperature, T, viscosity, η, and the hydrodynamic radius, r_H contribute to the diffusion coefficient. The diffusion coefficient of the test analyte

is required for calculating the reduced plate height and reduced linear velocity. While variation of the diffusion coefficient as a function of pressure is small at conventional HPLC pressures, the variation becomes significant at UHPLC pressures.[44] To accurately determine the diffusion coefficient, the diffusion coefficient in the desired mobile phase must be calculated for each test analyte. The work carried out by Kaiser *et.al*. determined diffusion coefficient values over the full range of water/acetonitrile mixtures with varying pressure. Diffusion coefficient values at 70/30 water/acetonitrile were extracted from this work. At a viscosity of 1.00 cP, the diffusion coefficient for ascorbic acid, hydroquinone, resorcinol, catechol, and 4-methyl catechol are 6.22 x 10^{-6}, 7.67 x 10^{-6}, 7.64 x 10^{-6}, 8.07 x 10^{-6}, and 7.45 x 10^{-6} cm^2/second, respectively.[44] These values were used for all reduced parameter calculations for analyses carried out in 70/30 water/acetonitrile.

Further particle characterization in terms of packing structure can be evaluated based on the capacity factor, k'.

$$k' = \frac{t_r - t_o}{t_o} \tag{2-5}$$

Where t_r is the analyte retention time and t_o is the void time. Through determination of the k' values for a column, the relative packing density can be determined.[45, 46] The greater the capacity factor, the more stationary phase present for retention which indicates a higher packing density. While this comparison is useful, it is only accurate for comparing columns packed with identical particles: same dimensions, pore characteristics, and functionalization.

2.1.5 Chromatographic Performance Assessment

Typically the van Deemter equation is used to describe the performance of a chromatographic column. For a well-packed column, the van Deemter equation is a suitable fit, but as the packing uniformity varies, the fit is no longer applicable due to deviations at

higher linear velocities. Giddings argued that the origin of the problem with the van Deemter equation is the assumption that the different contributions to the theoretical plate height are independent of each other.[13] To correct for this, the Giddings equation harmonically couples the packed bed dispersion (A) and the mobile phase resistance to mass transfer terms (C_M).[47]

$$H = \frac{B}{u} + C_s u + C_{MSt} + \frac{1}{\frac{1}{A} + \frac{1}{C_M u}} \tag{2-6}$$

The A-term traditionally accounts for the band broadening due to the variation of the size of the interparticle spaces. It is assumed that an analyte molecule will only travel in a single flow path, but Giddings suggests that in practice, this is not the case. When an analyte molecule can only travel in one flow path the band spreading will be extensive. But when the analyte is allowed to diffuse, then the analyte is capable of sampling slower and faster flow paths, thus reducing the A-term band spreading due to diffusional averaging. The C_M-term accounts for the resistance to mass transfer in the mobile phase. It is traditionally assumed that analyte molecules only move by diffusion in the mobile phase to the stationary phase surface. In the case of a packed bed, however, flow is another mechanism of mass transfer in the mobile phase. Due to the presence of flow, analyte molecules can be brought directly to the surface of the particle. Through these mechanisms, the traditionally proposed effects of band broadening due to the C_M-term are reduced by the presence of flow. In looking at these two effects, both the A-term and the C_M-term assist each other to reduce the individual contributions to band broadening.[48]

While the van Deemter equation may be incorrect in assuming all contributions to the theoretical plate height act independently, it nevertheless describes without difficulty the

results for a well-packed column, with minimal curvature in the *C*-term dominated region.[13]

2.2 MATERIALS AND METHODS

Modifications to the Kirkland protocol were made to provide a more suitable synthesis method for smaller diameter superficially porous particles that met the criteria of monodisperse particle size and robust particle structure.[49] The particles were synthesized by alternating a layer of positively charged polyelectrolyte and negatively charged colloidal silica on a non-porous silica (NPS) core until the desired porous layer thickness was achieved.

2.2.1 Initial Synthesis

Following the conditions specified in the 2007 Kirkland patent, two batches of particles were synthesized. For both batches, 0.5% (w/w%) high molecular weight poly(diallyldimethylammomiun chloride) (HMW PDDA) (Sigma Aldrich; St. Louis, MO) and Nalco 1034A (20 nm) colloidal silica (Nalco; Chicago, IL) were used. The first batch was prepared by alternating 10 layers of HMW PDDA and colloidal silica. The second batch was prepared by alternating 5 layers. Both batches were sized based on SEM images and packed into columns for chromatographic evaluation.

2.2.2 Polyelectrolyte Layer

To determine the effect of varying the molecular weight of polyelectrolyte, a 0.5% (w/w%) aqueous solution of polyelectrolyte was prepared. The polyelectrolytes investigated (Figure 2-1) were low molecular weight poly(diallydimethylammonium chloride), 100-200 kDa, (LMW PDDA) and high molecular weight poly(diallyldimethylammonium chloride), 400-500 kDa (HMW PDDA). Both polyelectrolytes used were purchased from Sigma-Aldrich (St. Louis, MO). NPS particles, 1.5 μm, purchased from Eprogen (Darien, IL) were

heated at 1000°C for 24 hours in a Thermo Scientific Lindberg Blue M Furnance (Waltham, MA) to produce 1.4 μm particles with a particle diameter RSD of 3.3%. The calcined NPS core particles were then re-hydroxylated in 10% (v/v%) aqueous nitric acid (Fisher Scientific; Waltham, MA) under reflux conditions for sixteen hours. The NPS core particles were washed with deionized water until the pH was neutral and then dried under heated vacuum at 80°C for sixteen hours. The polyelectrolyte solution was then added to a 10% (w/w%) aqueous suspension of 1.4 μm NPS core particles at the ratio of 5:1 (w:w) and shaken by hand for ten minutes. The suspension was washed in triplicate by adding 30 mL deionized water for every 100 mg of particles to a centrifuge tube, shaken thoroughly, and particles pelleted by centrifugation. The particles were then coated with a 10% (w/w%) aqueous solution of Nalco 1034A (20 nm) colloidal silica (Nalco; Chicago, IL) and washed in triplicate as stated above. Three full coating layers for each polyelectrolyte were prepared. The growth rate, colloidal silica surface coverage, and particle size distribution were determined for each type of polyelectrolyte based on scanning electron microscope (SEM) images.

The effect of polyelectrolyte solution concentration was investigated using LMW PDDA solution concentrations of 0.5%, 0.1%, 0.25%, and 0.05% (w/w%). Both, Nalco 1034A (Nalco; Chicago, IL) and Ludox AS-30 (Sigma Aldrich; St. Louis, MO) were used to determine if the type of colloidal silica affects the required concentration of polyelectrolyte used in the synthesis. Three full coating layers for each concentration and type of colloidal silica were prepared. The growth rate, colloidal silica surface coverage, and particle size distribution were determined at each concentration based on SEM images.

For the investigation of the effect of the increased number of washing steps between coating polyelectrolyte and colloidal silica, 1.5 μm NPS (Eprogen; Darian, IL), 0.5% (w/w%) LMW PDDA Sigma Aldrich; St. Louis, MO), and 10% AS-30 (12 nm) colloidal silica (Sigma Aldrich; St. Louis, MO) were used. Two batches were prepared side-by-side, one batch was washed 2 times after each coating step and the other was washed 5 times. The particles were washed by adding 30 mL deionized water for every 100 mg particle to a centrifuge tube, shaken thoroughly, and particles pelleted by centrifugation.

2.2.3 Colloidal Silica Layer

The colloidal silica solutions used were Nyacol NexSil8 (8 nm), Nyacol NexSil85 (85 nm), Nyacol NexSil125 (125 nm) (Nyacol Nano Technologies Inc.; Ashland, MA), Nalco 1030 (13 nm), Nalco 1034A (20 nm) (Nalco; Chicago, IL), and Ludox AS-30 (12 nm) (Sigma Aldrich; St. Louis, MO). A 10% (w/w%) aqueous solution of colloidal silica, pH adjusted to 3.5 with 10% nitric acid (v/v%), was combined with LMW PDDA coated NPS cores at a ratio of 1:1 (w:w) and shaken by hand for 15 minutes. The solution was then washed in triplicate by adding 30 mL deionized water for every 100 mg of particles to a centrifuge tube, shaken thoroughly, and particles pelleted by centrifugation. For each colloidal silica size, two full coating layers was prepared. Visual examination of surface uniformity and colloidal silica monodispersity were assessed by SEM. The particle size was determined with Image J software (National Institute of Health; Bethesda, MD).

2.2.4 Solution Mixing Method

The effect of the solution mixing method was assessed by comparing particles prepared by adding either polyelectrolyte or colloidal silica to an aqueous suspension of NPS particles in a centrifuge tube to those prepared by adding polyelectrolyte or colloidal silica to

an aqueous suspension of particles stirring in a glass beaker. The solution prepared in a centrifuge tube was shaken by hand while the solution prepared in the beaker was mixed using a stir bar. The particle monodispersity and surface uniformity were assessed by SEM.

2.2.5 Drying Method

Particles were dried at 25°C, 50°C, 80°C, 105°C, and by vacuum lyophilization. After drying, a portion of each sample was placed on an aluminum SEM stub and images collected. Particles dried under each condition were visually inspected for surface uniformity and agglomeration.

2.2.6 Sintering Temperature

Following drying, the polyelectrolyte was removed by heating at 540°C for sixteen hours. A batch of particles was sintered at various temperatures to determine the effect on particle strength and surface melting. The particles were heated in a Thermo Scientific Lindberg Blue M Furnace (Waltham, MA) at 825°C, 855°C, 900°C, 950°C, 980°C, and 990°C in atmosphere for eighteen hours. The particles were visually inspected for signs of melting by SEM.

2.2.7 Particle Mechanical Strength Study

A portion of the sample at each sintering temperature was used to make a 3 mg/mL slurry solution in distilled water. Each solution was sonicated for 5, 10, 30, 60, 90, and 120 minutes using a Cole Parmer 8891 Sonic Bath (Vernon Hills, IL) to evaluate particle stability. At each temperature and time point, a portion of the sample was removed and placed on an aluminum SEM stub for imaging. At each temperature and timepoint 100 particles were counted. If a particle showed any sign of colloidal silica loss, the particle was classified as a “bare particle.”

2.2.8 Particle Characterization

Particle size distribution, growth rate, and surface coverage were evaluated by placing a sample aliquot on an aluminum SEM stub for imaging using a through-the-lens (TTL) detector on a Hitachi S-4700 cold cathode field emission SEM (Tokyo, Japan). Using these images, Image J software produced by the National Institute of Health (Bethesda, MD) was used to measure the diameter of 250 particles.

The layer thickness growth rate, r, was calculated based on the number of coating steps, N, by:

$$r = \frac{d_{p,n} - d_{core}}{2} \times \frac{1}{N_C} \tag{2-7}$$

Where $d_{p,n}$ is the number average total particle diameter and d_{core} is the number average diameter of the core particle.

Elemental analysis was performed using a Perkin Elmer CHN/S O elemental analyzer Series 2400 instrument (Waltham, MA). The zeta potential of 10% (w/w%) aqueous solutions of Ludox AS-30 colloidal silica were tested at the pH values of 2, 3, 4, 6, 8 and 9 using a Malvern Zetasizer Nano ZS instrument (Worcestershire, UK). The pH was adjusted with 10% nitric acid (v/v%) for pH values below nine.

The surface area, pore volume, and pore diameter measurements were carried out by Waters Corporation (Milford, MA) using a Micromeritics ASAP2420 (Norcross, GA) for Brunauer, Emmet, Teller (BET) analysis. Pore size and volume measurements by mercury intrusion were carried out by Waters Corporation (Milford, MA) using a Micrometrics AutoPore IV 9500 series pore size analyzer (Norcross, GA).

2.2.9 Particle Bonding and Endcapping

Particles were functionalized according to U.S. patent 20020070168.[50] They were bonded with n-octadecyltrichlorosilane (Gelest; Morrisville, PA) in toluene with pyridine as the base activator. Both toluene and pyridine were purchased from Sigma-Aldrich (St. Louis, MO). The particles were then refluxed in a 4.5/1 (v/v) solution of acetone/0.12 M aqueous ammonium acetate to remove any excess polymerized bonding ligand. Acetone and ammonium acetate were purchased from Thermo Fisher Scientific Inc. (Waltham, MA). The particles were then endcapped with trimethylchlorosilane (Gelest; Morrisville, PA) in toluene with pyridine as the base activator. Excess endcapping ligand was removed by refluxing the particles in a 4.5/1 (v/v) solution of acetone/0.12 M aqueous ammonium acetate. For the particles that were doubly endcapped the endcapping step was repeated.

2.2.10 Particle Sizing

The reversible flow particle sieving apparatus designed by Mellors, Figure 2-2, was used to reduce the polydispersity of the 10 layer superficially porous particle sample.[51] A set of three filters were used to form four enclosed compartments allowing different sized particles to pass into each chamber. The two filters on the ends, F1 and F3, were 2 μm polycarbonate membrane filters (spi Supplies; West Chester, PA) and the middle filter, F2, was a 3 μm polycarbonate membrane filter (spi Supplies; West Chester, PA). A 3 mg/mL slurry solution of the 10 layer particles in hexane was introduced into the inlet chamber (region 2). Hexane was selected due to the compatibility with the particle sieving apparatus. The seiveing apparatus was placed in a sonicator bath (Fisher Scientific; Waltham, MA) and hexane was pumped towards region 4. After 15 seconds, the flow direction was reversed. This flow reversal was continued for a total of 30 minutes. At the end of this time the entire

volume of each chamber was collected and SEM images were used to determine the particle size distribution of the particles in each chamber.

Alternative sizing was carried out using a top loaded filtration apparatus. A 3 mg/mL slurry of particles in acetone was allowed to flow through a membrane filter by gravity. A 2.0 μm polycarbonate and a 5.0 μm polycarbonate membrane filter were used to remove particles smaller and larger than the desired particle size. The cake and filtrate of each filtration were collected and SEM images were used to determine the particle size distribution.

2.2.11 Column Packing

Fused silica capillary tubing (Polymicro Technologies, Inc., Pheonix, AZ) with an inner diameter (i.d.) of 30 μm and an outer diameter of 360 μm was used to pack three different particle batches. Two columns for each batch were analyzed. The columns were prepared with outlet frits using 2.5 μm bare NPS particles (Bangs Laboratories; Fishers, IN). A 1-2 mm plug of these particles was pushed approximately 0.5 mm into the capillary using a tungsten wire to create room for insertion of a microelectrode for electrochemical detection. The plug of particles was then sintered in place using an in-house electric arc device. The procedure for packing capillary columns has be previously described.[13, 39, 52, 53] Briefly, the particles were suspended in acetone at a concentration of 3 mg/mL. The slurry was sonicated for 10 minutes using a Cole Parmer Ultrasonic Cleaner 8891 (Vernon Hills, IL). A packing reservoir was then filled with the slurry solution and acetone was used as the pushing solvent. The capillary column was placed in a UHPLC fitting and secured in the column packing apparatus. Column packing was initiated at 3000 psi and as the bed began to form the pressure was gradually increased to 30,000 psi at a rate of 3000 psi per centimeter

of bed growth. The packing process was stopped when the desired column length was reached by slowly releasing the pressure.

After the desired column length was reached, the column was pressurized to ~55,000 psi and flushed with several column volumes of 50/50 water/ACN with 0.1% trifluoroacetic acid (TFA) mobile phase (Fisher Scientific; Waltham, MA). The pressure was slowly released and re-pressurized to ~10,000 psi. A temporary inlet frit was put in place using a heated wire stripper (Teledyne Interconnect Devices, San Diego; CA). The column was then clipped to the desired final length. The permanent inlet frit was prepared by generating a small gap at the column inlet using an electric arc device. The column outlet was placed slightly below the electrode tip and the electric arc device was pulsed several times to cause a small amount of particles to be removed from the column. 2.5 μm NPS particles were then tapped into the gap and sintered in place using the electric arc device.

2.2.12 Column Evaluation

The detailed experimental set-up used to perform isocratic UHPLC has been previously described.[38, 52-54] Amperometric detection was accomplished by amplifying the current from a 8 μm diameter (150 – 300 μm in length) carbon fiber microelectrode that was inserted into the end of the packed capillary and held at +1.1 V vs. Ag/AgCl reference electrode. The oxidation current was converted to a voltage using a model SR750 current amplifer (Standford Research Systems; Sunnyvale, CA) with a gain of 10^9 V/A and a low pass bandwidth (3 dB) filter at 15 Hz. The signal was digitized at a data acquisition rate of 21 Hz using a 16-bit A/D converter connected to an Intel Core 2 Duo desktop computer. The data was collected using the StripChart recorder program written with LabView 6.0 (National Instruments; Austin, TX).

The mobile phase used for chromatographic evaluation was 70/30 water/ACN with 0.1% trifluoroacetic acid (TFA). The isocratic test mixture contained L-ascorbic acid, which served as the dead time marker, hydroquinone (HQ), resorcinol (R), catechol (C), and 4-methyl catechol (4MC). The concentration of each sample in the test mixture was ~200 μM.

The columns prepared for this experiment were evaluated on the basis of chromatographic performance and retentivity. Reduced parameter plots were generated by analyzing the test mixture at a variety mobile phase velocities. The chromatograms were digitally frequency filtered to remove high frequency noise and background subtracted to remove low frequency baseline drift. Theoretical plates (N) and retention time (t_r) for each analyte were determined using Igor Pro 6.0 (Wavemetrics Inc., Lake Oswego, OR) using the iterative statistical moments algorithm. Reduced parameter plots for each column were generated in order to analyze chromatographic performance. The volume average particle size for each batch of particles and the pressure dependent diffusion coefficient for each analyte were used to determine the reduced parameters for each column.

The peak asymmetry was assessed by determining the tailing factor, T_f, for each test analyte.

$$T_f = \frac{w_{full,5\%}}{2w_{front,5\%}} \tag{2-8}$$

Where the peak width at 5% of the maximum height, $w_{full,5\%}$, and the front half width at 5% of the maximum height, $w_{front,5\%}$, are used to determine the extent of the asymmetry.

The column retentivity was evaluated by plotting the k' of each analyte versus the applied pressure. A line of best fit was made through the data points giving the y-intercept, k' at atmospheric pressure. The k' at atmospheric pressure for 4MC was used to compare the retentivity and packing density of different columns. The retentivity of a column can be used

to compare the relative density of packing, assuming the same particles and stationary phase coverage, because it is directly related to the phase ratio.

2.3 RESULTS AND DISCUSSION

2.3.1 SYNTHESIS

Using the parameters suggested by Kirkland [49] as starting conditions for the synthesis of smaller diameter superficially porous particles, problems related to non-uniform surface coverage, particle agglomeration, and porous layer degradation were encountered. To overcome these difficulties, many of the synthesis parameters required alteration, as will be discussed.

2.3.1.1 Effect of the Number of Coating Steps

To increase the porous layer thickness, alternating layers of polyelectrolyte and colloidal silica were adhered to NPS core particles. The thicker the porous layer, the greater the sample loading capacity of the packing material, but as this porous layer thickness increases the separation efficiency of the material is predicted to be reduced. The initial synthesis was carried out according to the 2007 Kirkland patent.[49] A 1.4 μm NPS core particle solution was coated with ten alternating layers of HMW PDDA and Nalco 1034A, 20 nm colloidal silica. As shown in Figure 2-3, as the number of layers increases the surface coverage was found to increase, but the surface became less uniform and particle agglomeration was seen. The wide particle size distribution, Figure 2-4, arises from the presence of bare or partially bare particles as well as particles with colloidal silica aggregates/agglomerates adhered to the NPS particle surface. The colloidal silica aggregates/agglomerates may be due to the inherent characteristics of the colloidal silica solution or to the incomplete removal of polyelectrolyte. Incomplete removal of

polyelectrolyte allows for colloidal silica to form free agglomerates that can then adhere to the superficially porous particles (SPP).

A second batch of particles was synthesized using the same method, but with only five alternating layers of HMW PDDA and Nalco 1034A, 20 nm colloidal silica. In comparison to the particles with 10 full layers, the surface uniformity and monodispersity were greatly improved, as shown in Figures 2-5 and 2-6. The particle size RSD for those coated with 10 coating steps, 31.9%, was much higher than that for 5 coating steps, 6.0%. The reduction in the number of coating steps has produced particles similar in polydispersity to the Kinetex 1.7 μm particles with a particle size RSD of 4.0%.[10, 27, 31] This improved uniformity is not batch dependant, but dependant on the number of coating steps, as indicated by the RSD for the 10 coating step particles after only 5 layers, Table 2-1. Furthermore, the growth rate shown in Figure 2-7 is the same for both the 5 and 10 coating step particles. This further indicates that the non-uniformity and therefore the increased particle size RSD arises from increasing the number of coating steps. This finding also indicates that the growth rate is reproducible for the same size colloidal silica with a porous layer thickness growth of 30 nm per coating step. Based on the colloidal silica diameter it would be expected that for one layer, the particle diameter would grow by 40 nm per coating step (layer thickness grows by 20 nm). It is seen that we are producing roughly one and a half layers per coating step. This difference in growth rate correlates with the non-uniform characteristics that were observed in the SEM images. In comparison to what was seen by Kirkland when using HMW PDDA, 15 layers of particles were adhered per coating step.[49] We have consistently seen a much thinner layer applied per step. As indicated in the 2007 Kirkland patent, it is suggested that

the thicker layer is achievable due to increasing the ionic strength of the polyelectrolyte solution, but we have not found this to be the case (see section 3.3.1.5).

2.3.1.2 Effect of Particle Sizing

The particle size distribution for the 10 layer particles is much broader than desired due to bare or partially bare particles and particle agglomerates. To size classify these particles, the bonded and endcapped particles with 10 coating layers were submitted to a reversible flow particle sieving device, shown in Figure 2-2, and to a top loading filtration apparatus. With the reversible flow sieving device, particles greater than 2 μm, but smaller than 3 μm should be trapped in region 3, particles greater than 3 μm should be trapped in region 2, and particles less than 2 μm should be in regions 1 and 4. The flow direction was continuously reversed to reduce any clogging of the filter membranes and to allow for the particles to be size classified by passing through the filters with differing pore sizes. In Figure 2-8, it is seen that most of the larger agglomerates were unable to pass into region 3 and were a larger component in region 2 as predicted. In regions 2 and 3, a large number of small, bald particles were found to be present, particle diameter around 1.5 μm. This could have been due to inadequate sieving time or to partial clogging of the membrane filter, which did not allow for adequate flow of the smaller particles to the outside chambers. Since the flow direction was continuously reversed, filter clogging should not have occurred. Therefore, the presence of individual particles in both regions should be able to be remedied by running the sieving apparatus for a longer duration. It was also seen that there were some agglomerates larger than 3 μm present in region 3 (2-3 μm), Figure 2-9. Agglomerates of this size should not have been able to pass through the filter, indicating that agglomeration is occurring once passing through the filter. Visible unattached, colloidal silica agglomerates

were seen, which most likely came from particles falling apart due to the continuous sonication. While these particles have been sintered, this is an indication that the mechanical stability may not be great enough to withstand the sieving procedure. This is in agreement with what was seen in previous studies with this apparatus with use with hexane for totally porous BEH particles, but we saw more severe degradation for the superficially porous particles most likely due to the nature of the particle synthesis.[51] Regardless of the observed particle degradation, the particle size distribution in region 3 was found to improve over the starting material, Table 2-2-A.

To eliminate possible particle damage due to sonication, top loaded filtration was carried out as a comparison to the reversible flow sieving device. The particles were run through a 5.0 μm membrane filter and the filtrate was collected. The filtrate was found to have a smaller particle size RSD, 20.3%, than the initial particle slurry, 31.9% (Table 2-2-B) and the number average particle size was reduced. Furthermore, when inspecting the filtrate by SEM there were no signs of larger agglomerates or debris as was seen with the particle sieving device, Figure 2-10. This lack of debris indicates that the sonication used with the particle sieving apparatus led to the particle degradation seen previously. To remove any partially coated or bare particles the filtrate was then run through a 2.0 μm membrane filter and the cake on the filter membrane was collected. The collected particles were found to have an increased number average particle size of 2.3 μm and a slightly improved particle size RSD, 19.1%. While these values indicate that the smaller particles were removed, by looking at SEM images there were still some bare particles present. This occurred due to the top loading filteration mechanism. The particle slurry was added to the top loaded filter and as the solution passed through the membrane a particle cake formed on the membrane. This

cake acted to block the pores in the membrane, not allowing the smaller particles to pass. Potentially, multiple passes through the membrane filter would allow for complete removal of the bare particles, but would also lead to reduced recovery since particles are lost in each filtration step.

While both particle sizing methods were found to improve the particle size distribution of the batch, the top loading filtration apparatus gave more desirable results. This method produced a higher yield, took less time, and produced a narrower particle size distribution than the reversible flow sieving method. To achieve the desired particle size distribution, the top loading filtration method would need to be further revised to allow for the complete removal of bare or partially bare particles.

2.3.1.3 Effect of Polyelectrolyte Molecular Weight

Initial synthesis was carried out using HMW PDDA. Based on experimentation by Kirkland, a greater porous layer growth per coating step was achieved through the use of a higher molecular weight polyelectrolyte. Preliminarily, it was believed that the polyelectrolyte adhesion would occur in a perpendicular orientation relative to the NPS surface, Figure 2-11-A, therefore leading to greater colloidal silica adhesion per coating step as the polyelectrolyte molecular weight is increased. Experimental comparison of the number average particle diameter achieved using HMW PDDA and LMW PDDA was found to be equivalent, Table 2-3, which indicates that the polyelectrolyte adheres to the NPS surface in a parallel conformation, Figure 2-11-B. This indicates the self-limiting nature of polyelectrolyte adhesion; once the negative surface charge on the NPS particle has been neutralized by the positive charge on the polyelectrolyte no more adhesion occurs.[55]

While the particle diameter was not found to vary with polyelectrolyte molecular weight, the surface uniformity was found to be affected. As shown in Figure 2-12, after one coating step, the NPS particles coated with HMW PDDA were found to have bare regions not seen on particles coated with LMW PDDA. According to studies by Yu, it has been indicated that as the molecular weight of the polyelectrolyte is increased the likelihood of formation of polyelectrolyte globules is increased.[56] If globules, rather than extended chains, are attached to the NPS particle surface, the local surface charge would be neutralized, which would not allow colloidal silica adhesion, Figure 2-13-A. Therefore, the size of the bare region would be proportional to the size of the globule.

While both types of polyelectrolyte coated particles became less uniform as more coating steps were carried out, the particles coated with HMW PDDA were found to have a greater number of partially bare particles, consistent with what was observed for the single layer particles. Also, the HMW PDDA coated particles were found to have a larger number of colloidal silica aggregates present on the surface, Figure 2-12. From colloidal silica studies, to be discussed in section 2.3.1.5, it was found that the type of colloidal silica used can lead to the presence of colloidal silica aggregates, but a contribution from the PDDA molecular weight was still found. It is believed that the majority of the colloidal silica aggregates form from excess polyelectrolyte remaining in solution after washing, which then electrostatically attract colloidal silica. Since there is excess colloidal silica added to the solution, there would be ample present to adhere to both the NPS coated particles and any remaining excess free polyelectrolyte. The higher frequency of colloidal silica aggregates found with HMW PDDA may indicate that it is more difficult to remove excess polyelectrolyte as the molecular weight is increased.

When the number of washing steps for the HMW PDDA coated particles was varied, it was found to slightly affect the amount of webbing between particles, but increased washing did not eliminate this behavior, Figure 2-14. After the first coating step there was webbing between particles present when only two washes were carried out, but was not present for the batch that underwent five washes. Therefore, increased washing may reduce the presence of the webbing between particles. From the images collected for particles coated with multiple layers, webbing is present independent of the number of washes. Furthermore, neither case was found to have colloidal silica aggregates present on the surface of the particle. For this study, fresh stock colloidal silica solution was purchased which was found to be thinner and less cloudy than the solution used in the initial study. Therefore, the presence of colloidal silica aggregates seen previously was due to the formation of the aggregates prior to coating the superficially porous particle and not directly dependant on the type of polyelectrolyte of the number of polyelectrolyte washes.

This non-uniformity in surface coverage for HMW PDDA coated particles produced particles with a slightly greater particle size distribution than that seen for LMW PDDA coated particles, Table 2-3. These results correlate well with previous observations that as the molecular weight of the polyelectrolyte is increased, aggregates begin to form and in variable amounts, Figure 2-12-D.[56] Further comparison shows that the particle size growth rate between the two PDDA molecular weights are very similar, with the growth rate for the HMW PDDA being slightly lower due to the presence of some bare particles. This gives further evidence to support the belief that the polyelectrolyte adheres to the surface in a parallel orientation, leading to the same growth per step independent of polyelectrolyte

molecular weight. Based on the increased surface uniformity, further synthesis modifications were carried out using LMW PDDA.

2.3.1.4 Effect of Polyelectrolyte Concentration

Initial particle synthesis showed the presence of agglomeration as the non-porous core particle size and the resulting total particle diameter were decreased. The initial concentration of the polyelectrolyte may be too high to allow for adequate removal of the free polyelectrolyte leading to particle agglomeration. This was investigated by varying the polyelectrolyte concentration for two different types of colloidal silica. Shown in Figure 2-15 is the variation of LMW PDDA concentration with the use of Nalco 1034A , 20 nm colloidal silica. As the polyelectrolyte concentration was decreased, the presence of colloidal silica aggregates on the particles was found to slightly decrease, but the particle agglomeration and webbing between particles remained constant. Further examination was carried out with Ludox AS-30, 12 nm colloidal silica, to determine if the type of colloidal silica contributes to the particle agglomeration and colloidal silica aggregation. When the polyelectrolyte concentration was decreased with Ludox AS-30, Figure 2-16, it was found that at concentrations below 0.25% (w/w%) there was a higher occurrence of bare or partially bare particles. Both 0.5% (w/w%) and 0.25% (w/w%) LMW PDDA were found to give complete surface coverage, but 0.5% (w/w%) led to a slightly greater growth rate, Table 2-4. These results indicate that the type of colloidal silica does affect the extent to which the concentration of polyelectrolyte affects the surface uniformity. The Nalco 1034A colloidal silica led to a much less uniform surface which masked the effects of varying the polyelectrolyte concentration. While in the case of AS-30 colloidal silica, the colloidal silica was less aggregating which allowed the non-uniform surface affects of the polyelectrolyte

concentration to be more pronounced. For further studies, the concentration of 0.5% (w/w%) was used to produce the greatest growth per coating step and maintain complete, uniform colloidal silica surface coverage.

2.3.1.5 Effect of Colloidal Silica Type

From the studies investigating the polyelectrolyte molecular weight and concentration it has been indicated that the colloidal silica type has an effect on the surface uniformity in terms of surface coverage and the presence of colloidal silica aggregates. Initial studies were carried out with Nalco 1034A colloidal silica based on availability. This colloidal silica solution is acid stabilized at a pH of 2.8 and has a sodium counterion. When working with this material it was found that the stock solution became cloudy and thickened over time. There was no change in the volume in the bottle indicating that the solution thickening was not due to evaporation of water. Based on studies by Iler and further experimentation in our lab it was found that at lower pH, colloidal silica is more likely to form aggregates in solution leading to gel formation.[24] At low pH, the negative surface charge on colloidal silica is reduced as indicated by zeta potential measurements of AS-30 colloidal silica at varying pH, Table 2-5 This in turn reduces the repulsion between the particles, which allows the colloidal silica particles to be within closer contact of each other.

When a colloidal silica solution, Nalco 1030, stabilized at a pH of 10.2 and with an ammonium counterion was used, the stock solution was found to be stable indefinitely. As the colloidal silica solution pH was adjusted to a pH of 3.5 as recommended by U.S. patent 0189944, the solution was found to become cloudy indicating formation of colloidal silica aggregates. This is in agreement with what was seen with the acid stabilized colloidal silica solution. While signs of colloidal silica aggregation were seen, when the base stabilized

colloidal silica was used to coat the NPS particle, the surface coverage was much more uniform than that seen with the acid stabilized colloidal silica solution, Figure 2-17. Furthermore, there was no indication of larger colloidal silica aggregates attached to the NPS particles and the superficially porous particles had a visibly smoother surface. Further improvements were seen with the reduction of webbing between particles, which is seen when using acid stabilized colloidal silica. To achieve more uniform particles, only base stabilized solutions were used in subsequent studies.

Another variation in colloidal silica that was studied was the particle diameter. Independent of the colloidal silica diameter, the surface coverage was found to be uniform and complete, Figure 2-18. As the colloidal silica diameter was increased the growth rate increased and the number average particle size remained relatively constant, Table 2-6. A drawback of the larger diameter colloidal silica was an increase in the sol polydispersity. In the case of the NexSil125 solution, no colloidal silica particles with a diameter of 125 nm were found to be present. The majority were much smaller (70 nm) than the stated value (125 nm) and the largest seen were 100 nm. For the 8 nm and 13 nm colloidal silica, the particle sizes were less polydisperse based on comparing SEM images. While increasing the colloidal silica diameter to increase the pore size of the material is something we are interested in, the decreased polydispersity of the smaller diameter colloidal silica was found to be more important in our initial studies.

2.3.1.6 Effect of Solution Mixing

To allow for the reaction of the polyelectrolyte or colloidal silica with the NPS particles, the reagents needed to be introduced and then mixed for an extended duration. Initial studies were carried out by adding either polyelectrolyte or colloidal silica solution to

an aqueous NPS particle solution in a centrifuge tube. The centrifuge tube was then continuously inverted by hand for the duration of the required mixing time. Mixing and subsequent washes were also carried out in the same centrifuge tube. Particles prepared in this manner were found to have regions that were less densely coated and showed signs of mechanical deformation, Figure 2-19-A. By adding the reagents to the NPS particle solution in a centrifuge tube, upon reagent introduction there is the formation of a reagent concentration gradient. For example, when colloidal silica is added, initially the colloidal silica concentration is very high near the surface and zero at points closer to the bottom of the tube. This would create a charge differential that would promote the attraction between a colloidal silica coated NPS particle and a polyelectrolyte coated NPS particle, leading to the formation of doublets and multiplets in solution. These multiplets may remain in solution indefinitely or later break apart leading to bare crater-shaped regions as seen in Figure 2-19-A.

To reduce this phenomenon, the reagent addition and mixing method was altered to try to reduce the interaction of neighboring NPS particles. The NPS particle solution was placed in a glass beaker with continuous stirring and reagents were added slowly to the center of the vortex. This was believed to more quickly eliminate the concentration gradient of the added reagent and to reduce the amount of NPS particle interaction due to continuous solution stirring. This method was found to eliminate the presence of the bare crater-shaped regions that were seen when using a centrifuge tube, Figure 2-19-B. While there were some doublets observed it is believed that these are due to the presence of doublets in the NPS particle starting material and not due to the solution mixing method, as indicated from SEM

images of the starting material, Figure 2-20. Based on these findings all further studies were carried out by adding and mixing solutions in a stirred beaker.

2.3.1.7 Effect of Drying Temperature

After the desired porous layer thickness is achieved, the particles must then be dried before polyelectrolyte removal and particle sintering can occur. The initial condition used was to dry the particles at 105°C until visibly dry. When the particles were dried at this temperature, Figure 2-21-D, a large number of bare or partially bare particles were found to be present. At this temperature, the water inside the pores may be evaporating quickly and causing the porous layer to be pulled off by the force of the escaping water vapor. Studies have indicated that heat drying causes surface deformities and leads to a loss in surface area and pore volume for silica materials.[57] To reduce these deleterious effects, the drying temperature was decreased to 80°C, 50°C, and 25°C. At all temperatures, partially bare particles were found to be present, but the number of bare particles was slightly reduced. Therefore, fast evaporation may be contributing to the particle degradation, but other factors must play a role since bare particles were also seen when dried at 25°C.

With evaporative drying, the particles are in relatively close contact with each other. Furthermore, as the water is evaporated the particle slurry concentration continually climbs leaving less space between neighboring particles. This contact may lead to neighboring particles pulling the porous shell from their nearest neighbor as the drying front progresses through the solution. As an alternative, lyophilization should maintain separation between neighboring particles by freezing the particles within solvent shells. Additionally, the process of lyophilization has been found to preserve the structure of materials without any shrinkage in contrast to the deformity found due to the rapid removal of water by evaporative

drying.[58, 59] Using lyophilization, the dry particles were found to be very uniform, have no signs of particle degradation, and be predominately single particles, Figure 2-21-E. This supports the idea that the interaction between neighboring particles leads the particle balding. For subsequent syntheses, lyophilization was used as the drying method.

2.3.1.8 Effect of Sintering Temperature on Mechanical Stability

One of the initial difficulties seen with these particles was the degradation of the porous shell upon bonding and endcapping. This indicated that the recommended sintering temperature, 825°C, was not high enough to sinter the porous shell together and to the NPS particle. To improve the mechanical stability of these particles the sintering temperature was increased, Figure 2-22. At temperatures at or below 980°C, no visible signs of reduced porosity were present, but above this temperature porosity loss was seen, Figure 2-22-E. Based on visual inspection, the highest viable sintering temperature was found to be 980°C in order to increase mechanical stability without significant loss of porosity due to melting.

To better assess the mechanical stability, a sonication study was carried out with particles sintered at each temperatures. At each temperature, the number of particles with bare regions was found to increase as the sonication time was increased, but the number of bare particles present at the higher sintering temperatures was lower, Figure 2-23. A drop-off in the number of bare particles present in comparing sintering at 950°C versus at 980°C was seen. Since there was no visible sign of melting at 980°C, and there was an increase in mechanical stability as measured by sonication, this was the temperature deemed most useful.

Upon production of successive batches of particles, variability in the melting temperature was found. While the previous batch of particles showed no visible loss of

porosity at 980°C, the next batch produced was found to show a loss of porosity, Figure 2-24. From previous studies, the presence of impurities such as sodium from the synthesis process has been found to affect surface properties and, in turn, lower the melting point.[60, 61] Therefore, varying amounts of sodium present in the synthesis may be leading to the variation in the observed melting temperature between batches. Initially we were using a colloidal silica solution that is sodium stabilized; therefore we were adding this "impurity" to our reaction mixture. To eliminate the addition of sodium, the counter ion of the colloidal silica solution was changed to ammonium. Upon changing the colloidal silica counter ion, the sintering temperature was found to be consistent between batches, Figure 2-25.

2.3.2 COLUMN PERFORMANCE

2.3.2.1 Initial Performance and Particle Degradation

To assess the performance of synthesized particles the peak width, reduced van Deemter parameters, and the tailing factors were determined and compared to theoretical values for superficially porous particles and experimental values for totally porous particles. From theoretical calculations, it is expected that superficially porous particles should produce an *a*-, *b*-, and, *c*-term of 1.0, 1.0, and 0.10, respectively. From previous and current studies it has been found that the *b*-term typically has little variation when comparing the same type of particles, independent of the overall performance of the packing material.[13] The *B*-term is related to analyte diffusion in the longitudinal direction. Variations in this term arise when changes in the mobile phase viscosity, analysis temperature, analyte molecular weight, or the diffusion volume are found. Since the first three parameters listed are typically held constant for comparison purposes, no variation in the *B*-term should be observed, but variations in the *B*-term have been found due to the varying porous volume of the particles.[25, 61]

The 10 coating layer particles collected from top loading filtration were tested for their chromatographic performance. As seen in Figure 2-26, the test analytes are well resolved and the peak shape is symmetrical for the less retained analytes. As the analyte retention is increased, the asymmetry was also found to increase, Table 2-7. This behavior is consistent for packing materials that have incomplete bonded phase coverage which allows for free silanols to interact with the test analyte.[8] The more retained an analyte, the greater time the free silanols have for analyte adsorption/interaction. While peak asymmetry increased for more retained analytes, the tailing factor for all analytes was less than values know to cause deleterious effects on the separation. When the tailing factor is less than 2.0 it is typically considered to have negligible effects on the separation.[11]

Based on this separation, a reduced parameters plot was generated to better assess the contributions to band broadening, Figure 2-27. For hydroquinone, the h_{min} was found to be approximately 3.0. This is higher than the theoretical value, ~2.0, but was still reasonable based on the particle size polydispersity.[13, 63] This high *a*-term was expected due to the wide particle size distribution of this batch of particles, Figure 2-4. While this has been shown to not directly increase the *a*-term, it does cause non-uniformities in the formation of the packed bed due to the packing process, leading to a greater variation in the flow paths.[20, 26, 27] Lastly is the *c*-term, which again is higher than predicted, but within the same range as what has been seen for totally porous particles, Figure 2-28. This high value may be due to the non-uniform layering of the porous portion of the particle. The regions of varying porous layer thickness are due to colloidal silica aggregation, which prevent uniform mass transfer throughout the particle due to variation in the amount of stagnant mobile phase. Overall, the performance of these particles was better than expected based on the visual non-

uniformities, but are not performing as well as theory would predict for uniform superficially porous particles.

Since the particle size distribution and the particle surface uniformity were found to improve for the 5 coating layer particles, their performance was assessed. The peak width for each analyte was improved, but the more retained analytes were found to have more pronounced tailing, Figure 2-29. For hydroquinone at the optimum linear velocity, the peak width at half height was found to be 0.08 minutes and 0.03 minutes for the 10 coating layer particles and 5 coating layer particles, respectively. This improved performance was confirmed by the reduced parameters plot of the test analytes, Figure 2-30. The h_{min} for hydroquinone was found to be 1.6, which is slightly lower than theoretically predicted. Furthermore, all of the reduced parameters were found to improve over those for the 10 coating layer particles. The improvements in the a-term and *c*-term can be attributed to the narrower particle size distribution and the improved uniformity of the porous layer, respectively. While the performance for hydroquinone was better than predicted, the more retained analytes were found to deviate from this improved performance. Since the number of theoretical plates are calculated based on statistical moments rather than half height peak width, the presence of tailing for the more retained analytes decreased the number of theoretical plates. Therefore, it would be expected to see a decrease in efficiency since the more retained analytes were found to have increased tailing.

To reduce the tailing of the more retained analytes, the 5 coating layer particles were treated with a second endcapping step to reduce the number of free silanols. While the peaks for the more retained analytes were found to have decreased tailing, Table 2-7, this chromatographic feature may have been an artifact of the increased peak width, Figure 2-31.

Based on the reduced parameters plot, the performance was found to be significantly degraded upon carrying out the second endcapping step, Figure 2-32. Multiple columns were packed with these particles and similar results were achieved. The h_{min} for hydroquinone was approximately 4.0 compared to the value of 1.6 for the particles prior to the second endcapping step. The greatest performance degradation was seen in the higher linear velocity region where curvature was found to be present. Due to this, the data no longer would fit to the van Deemter equation, requiring a fit to the Giddings equation. This curvature is an indication that there is coupling between the *a*- and *c*-terms, but more importantly indicates that the packing structure of the column is no longer suitable.[13] Since multiple columns were packed with this material, producing the same results, this would indicate the there was an inherent problem with the particles and not an individual column packing.

The particles were extruded from the column bed to assess the bed structure, Figure 2-33. From these images it was seen that the majority of the particles were no longer intact. There were a large number of partially or completely bare particles, indicating that the particles were not mechanically strong enough to withstand the packing procedure. SEM images of the particle slurry before packing were taken, Figure 2-33-C and a large number of partially or completely bare particles we found to be present before column packing. Therefore, the decrease in performance was due to the degradation of the particle structure upon carrying out the second endcapping step.

2.3.2.2 Relationship Between Porous Layer Thickness and Capacity Factor

As the porous layer thickness is varied for a particle of the same diameter, it would be expected to see a similar change in analyte retention due to differences in the amount of stationary phase per unit column volume. The carbon load (%C), capacity factor, and amount

of carbon per column volume (calculation in Appendix 1) for the particles synthesized in-house as well as Kinetex particles (Phenomenex) are shown in Table 2-8-A.[13] When comparing the amount of carbon per column volume for the in-house particles, the retention of the 10 layer particles should be approximately 1.4 times greater than for the 5 layer particles due to the reduction in the amount of stationary phase present per column volume for the 5 layer particles, Table 2-8-B. This value, 1.4, is equivalent to the observed change in capacity factor, for these two columns, 1.3. The comparison between the two sizes of Kinetex particles with a capacity factor ratio of 1.3 and an amount of carbon per column volume ratio of 1.0 were found to more significantly differ. Based on this comparison, the 2.6 μm Kinetex particles are more densely packed than the 1.7 μm Kinetex particles. When comparing particles synthesized by different methods there is inconsistency in the k' ratio and the amount of carbon per column volume ratio. The two ratios for 10 layer particles compared to the 2.6 μm Kinetex particles were in agreement, but not for the 10 layer particles compared to the 1.7 μm Kinetex particles. The two ratios for the 5 layer particles compared to either size of the Kinetex particles did not agree. In all cases where a disagreement between the fold-change of the two ratios was present, the amount of carbon per column volume fold-change was higher than the k' fold-change, except for the 2.6 μm Kinetex to 1.7 μm Kinetex comparison.

Since the amount of carbon per column volume ratios were higher than predicted by the k' ratios for the Kinetex particles compared to the UNC particles, this would indicate that the Kinetex columns are less densely packed than columns packed with particles synthesized in-house. Based on work by Gritti and Guiochon, it has been suggested that a rougher particle surface causes increased friction between the particles in the packing process which

does not allow for the particles to slip by each other as easily leading to a more open packing structure.[26] In comparing the surface roughness between these two types of particles, Figure 2-34, it can be seen that the Kinetex particles have a much smoother surface than particles synthesized in-house. The smoother Kinetex particles would therefore be predicted to have a more dense packing structure than the in-house particles, but this is not the case based on the k' ratios relative to the amount of carbon per column volume ratios. The trends in flow resistance for each column is further evidence that the smoother, Kinetex particles are less densely packed than the rougher, in-house particles, Table 2-8-A. Independent of surface roughness it has been found that as the aspect ratio decreases, the packing density decreases accordingly which is in agreement with the 2.6 μm Kinetex having the lowest flow resistance.[64]

Another cause for the lower packing density of the Kinetex particles may have be due to the packing rate. When comparing the packing process between these two types of material, the Kinetex particles were found to pack more quickly. This increased rate of column packing does not allow time for reorganization and leads to a more open packing structure.[65]

Between particles synthesized in a similar manner, the predicted retention correlates with the amount of stationary phase present based on the porous layer volume and the carbon load. Therefore, for particles produced in a similar manner the retention can be predicted based on the porous layer thickness. On the other hand, the lack of correlation between the capacity factor ratio and the amount of carbon per column volume ratio for different types of particles indicates inherent differences in the porous structure of the particles.

2.3.3 OPTIMIZED SYNTHESIS PARTICLES

Particles were synthesized by alternating three layers of 0.5% (w/w%) LMW PDDA and 10% (w/w%) AS-30 colloidal silica, pH = 3.5. The reagents were added to an aqueous suspension of particles in a stirring glass beaker and then washed in triplicate in 50 mL centrifuge tubes. The particles were then dried by lyophilization and sintered at 980°C.

2.3.3.1 Particle Structure Characterization

Based on the revised synthesis conditions contained within this chapter, a batch of 1.7 μm superficially porous particles were produced. As seen in Figure 2-35, the revised conditions produced uniformly coated particles free from colloidal silica aggregates and particle agglomeration with a narrow particle size distribution, Figure 2-36. This improved uniformity was confirmed by comparing the particle size RSD for particles synthesized using the initial synthesis conditions, 6.0%, and the revised synthesis method, 2.6%. The revised method has produced particles with greater monodispersity than 1.7 μm Kinetex particles, RSD = 4.0%. [27] Furthermore, these synthesized particles were found to have a dp90/dp10 ratio equal to 1.06, which is much better than that seen for commercially available totally porous particles and similar to that seen for commercial superficially porous particles. The dp90/dp10 for 1.7 μm Acquity particles and for 1.7 μm Kinetex particles are 1.50 and 1.13, respectively.[66, 27] It is generally accepted that the spread of particle sizes has a minor affect on separation efficiency as long as the dp90/dp10 ratio is not above 1.5 to 2.0.[67] While most commercial products are within this range, the improved monodispersity is predicted to improve efficiency by allowing more uniform column packing.[29] Therefore reducing the *A*-term contribution to the theoretical plate height.

Further physical characterization of these particles was performed. The specific surface area was found to be 47 m^2/g, Table 2-9. In comparison to 1.7μm Kinetex particles with a specific surface area of 110 m^2/g, this is a significant decrease in surface area.[26] A decrease in the surface area was expected due to the thinner porous layer on the particles made in-house. Based on porous layer volume, it is predicted that the surface area would be approximately 45% lower for the in-house particles when compared to the values stated for 1.7 μm Kinetex particles, but experimentally the surface area was 57% lower. This loss of surface area may partially be due to the difference in the porous layering process of the Kinetex particles, which produce the rings visible on cross-section images, Figure 2-37. The presence of these distinct layers has previously been suggested to decrease the surface area by approximately 23%.[27] Another source may be the presence of internal loss of porosity due to melting of the in-house particles leading to a decrease in surface area as was seen with particles to be described in Chapter 3 (section 3.3.1.9).

In addition to surface area, the pore size for the in-house particles were slightly smaller, 68 Å, than that for the 1.7 μm Kinetex particles, 84 Å.[27] Typically 90 Å pores are considered suitable for small molecule analysis, but the pore size for the in-house particles was less than this. Based on the test analytes which are approximately 8 Å, the 68 Å pore size is acceptable since the pore size is much larger than the analyte size. Never the less, the pore diameter is slightly less than desirable to allow use with a variety of test analytes.

Comparing the pore size results obtained from BET N_2 adsorption and mercury intrusion porosimetry, the value obtained by mercury intrusion is slightly lower. From all the results obtained for these two techniques, the mercury intrusion pore size is consistently

smaller. In studies by Brown and Lard, it was found that discrepancies between the two techniques for silica materials was common.[68, 69]

Based on this characterization, it was found that a uniformly coated, monodisperse batch of particles was produced. While the pore size was smaller than desired, it is suitable for the analysis of small molecule test analytes.

2.3.3.2 Chromatographic Performance

While the appearance of the particles produced by the revised synthesis process appear to be more monodisperse and uniformly coated, the performance was worse than that seen with the 5 layer particles. As shown in Table 2-10, both the *a*-term and *c*-term were much higher than that for the 5 layer particles. The increase in the *a*-term indicates that there is greater variation in the interparticle bed structure of the revised synthesis particles. When comparing the k' for the columns of each particle type, little variation was observed. The k' values were 0.50 and 0.54 for the 5 layer particles and the column packed with the revised synthesis particles, respectively. This would indicate that the packing density is similar for both columns. To further investigate the cause for the *a*-term increase, the peak width of ascorbic acid, the dead time marker, for each column was measured. The peak width of ascorbic acid should be directly related to the variation in the interparticle space since no retention is present. The ascorbic acid peak width at the same dead time for the 5 layer particles and the revised synthesis particles was 0.03 minutes and 0.06 minutes, respectively. This indicates that the interparticle space of the revised synthesis column is more variable than the column packed with the 5 layer particles. This increased peak width correlates with the approximate doubling of the *a*-term for the revised synthesis particles. Therefore the increase in the *a*-term is due to the physical structure of the interparticle space.

In previous studies with superficially porous particles it has been suggested that the surface roughness produces a more open packing network due to friction between particles during column packing.[26, 27] In comparing the 5 layer particles to that of the revised synthesis particles the surface roughness was greatly diminished with the revisions. This would predict that the 5 layer particles would have a more open particle network, but this was not found to be the case based on the capacity factors. Rather it may be possible that based on the relative position of the particle cores there was a slightly more open packing network, but the presence of the irregular porous protrusions found on the 5 layer particles reduced the open volume by filling the space. This would correlate with the slightly higher retention but less band broadening of ascorbic acid.

In addition to the *a*-term, the *c*-term was also found to increase for the revised synthesis particles. While the average porous layer thickness for each type of particle is the same, some regions of varying thickness were present on the 5 layer particles as indicated by the higher RSD values, Table 2-11. This would suggest that the resistance to mass transfer for these particles would be greater, which is not found to be the case. Furthermore, it has been suggested that the greater the surface roughness of the particles the greater the mass transfer resistance of the packing material, further indicating that the *c*-term for the revised synthesis particles should be lower than that for the 5 layer particles.[26] A higher sintering temperature was used for the revised synthesis particles which may have lead to ink-bottle shaped pores leading to a greater amount of stagnant volume.[70] Without further speculation the explanation of these results is unexpected and contradictory to theoretical expectations.

The contributions from both the *a*-term and *c*-term led to a dramatic increase in the minimum theoretical plate height for the revised synthesis particles, Figure 2-38. As previously mentioned the degraded performance of the revised synthesis particles was unexpected and contradictory to previous findings. Of note was the difference in the packing rate of these two types of particles. The 5 layer particles were found to pack roughly 5 times as fast as the revised synthesis particles and packed as individual particles. Other work within our lab has suggested that the packing rate greatly dictates the performance of the column. This increased packing rate may reduce size segregation producing a more uniform size distribution across the column cross-section.[22, 71] Furthermore, a faster packing rate has been found to lead to a more open particle network within the column bed.[72] Therefore, while the appearance of the 5 layer particles was found to be inferior to that of the revised synthesis particles, the fast packing rate for the 5 layer particles may have led to their superior performance. Further studies investigating the column packing process will be discussed in Chapter 5.

2.4 CONCLUSIONS

The synthesis of 1.7 μm superficially porous particles based on the conditions specified by Kirkland produced particles with a narrower particle size distribution than totally porous particles, but were found to have regions of non-uniform colloidal silica coating. The chromatographic performance of these particles were found to be close to the predicted values, but were found to have decreasing performance for the more retained analytes. Upon revising the synthesis conditions particles were produced without visual surface imperfections, but were found to not improve the chromatographic performance. This

poor performance is believed to be due to the column packing process, which produced a more heterogeneous bed structure.

2.5 REFERENCES

[1] Horvath, C.; Lipsky, S.R. *J. Chrom. Science* 7 (1969) 109-116.

[2] Horvath, C.G.; Preiss, B.A.; Lipsky, S.R. *Anal. Chem.* 39 (1967) 1422-1428.

[3] Kirkland, J.J. *U.S. Patent 3505785* 1970.

[4] Parris, N.A. *Instrumental LC: a practical manual on high performance liquid chromatographic methods*, Elsevier Scientific Publishing Company, New York, 1976, page 28.

[5] Little, J.N.; Horgan, D.F.; Bombaugh, K.J. *J. Chrom. Science* 8 (1970) 625-629.

[6] Kaczmarski, K.; Guiochon, G. *Anal. Chem.* 79 (2007) 4648-4656.

[7] Kirkland, J.J. *Anal. Chem.* 64 (1992) 1239-1245.

[8] Snyder, L.; Kirkland, J. J.; Glajch, J.L. *Practical HPLC Method Development*, Wiley, New York, 2nd ed., 1997.

[9] Gritti, F.; Cavazzini, A.; Marchetti, N.; Guiochon, G. *J. Chrom. A* 1157 (2007) 289-303.

[10] Kirkland, J.J.; Langlois, T.J.; DeStefano, J.J. *Amer. Lab.* 39 (2007) 18-21.

[11] Snyder, L.; Kirkland, J. J.; Dolan, J.W. *Introduction to Modern Liquid Chromatography*, Wiley, New York, 3rd ed., 2010.

[12] Daneyko, A.; Holtzel, A.; Khirevich, S.; Tallarek, U. *Anal. Chem.* 83 (2011) 3903-3910.

[13] Neue, U.D. *HPLC Columns: Theory, Technology, and Practice*, Wiley-VCH, New York, 1997.

[14] Sychov, C.S.; Ilyin, M.M.; Davankov, V.A.; Sochilina, K.O. *J. Chrom. A* 1030 (2003) 17-24.

[15] Verzele, M.; DeWaele, C. *Chromatographia* 18 (1984) 84-86.

[16] Okamoto, M.; Kato, M.; Nobuhara, K.; Satoh, K.; Yamamoto, Y.; Ihara, H. *J. Chrom. A* 845 (1999) 409-415.

[17] Bereznitski, Y.; Jaroniec, M. *J. Chrom. A* 828 (1998) 51-58.

[18] Unger, K.K. *Porous silica, its properties and uses as support in column liquid chromatography*, Elsivier Scientific Publishing Company, New York, 1979.

[19] Liekens, A.; Billen, J.; Sherant, R.; Ritchie, H.; Denayer, J.; Desment, G. *J. Chrom. A* 1218 (2011) 6654-6662.

[20] Omamogho, J.O.; Glennon, J.D. *Anal. Chem.* 83 (2011) 1547-1556.

[21] Farkas, T.; Guiochon, G. *Anal. Chem.* 69 (1997) 4592-4600.

[22] Bruns, S.; Grinias, J.P.; Blue, L.E.; Jorgenson, J.W.; Tallarek, U. *Anal. Chem*. 84 (2012) 4496-4503.

[23] Zarzycki, P.K.; Kulhanek, K.M.; Smith, R. *J. Chrom. A* 955 (2002) 71-78.

[24] Iler, R.K. *The Chemistry of Silica: Solubility, Polymerization, Colloid and Surface Propertics, and Biochemistry*, Wiley-Interscience, New York, 1979.

[25] Cox, G.B. *J. Chrom. A* 656 (1993) 353-367.

[26] Gritti, F.; Guiochon, G. *J. Chrom. A* 1166 (2007) 30-46.

[27] Gritti,F.; Leonardis, I.; Abia, J.; Guiochon, G. *J. Chrom. A* 1217 (2010) 3819-3843.

[28] Marchetti, N.; Cavazzini, A.; Gritti, F.; Guiochon, G. *J. Chrom. A* 1163 (2007) 203-211.

[29] Gritti, F.; Farkas, T.; Heng, J.; Guiochon, G. *J. Chrom. A* 1218 (2011) 8209-8221.

[30] Majors, R.E. *LCGC North America* 28 (2010) 1014-1020.

[31] DeStefano, J.J.; Langlois, T.J.; Kirkland, J.J. *J. Chrom. Sci.* 46 (2008) 254-260.

[32] Jerkovich, A.; Mellors, J.S.; Jorgenson, J.W. *LCGC North America* 6 (2003) 8-12.

[33] Majors, R.E. *LCGC North America* 24 (2006) 742-753.

[34] Bogush, G.H.; Tracy, M.A.; Zukoski, C.F.I. *J. Non-Cryst. Solids* 104 (1988) 95-106.

[35] Huber, J.F.K. *Instrumentation for high-performance liquid chromatography* Elseveir Scientific Publishing Comapany, New York, 1978.

[36] Swartz, M.E. *LCGC North America Supplement* 2005.

[37] McMaster, M.C. *LC/MS: a practical users guide*, John Wiley & Sons, Inc. New Jersey, 2005.

[38] Bergna, H.E. Kirkland, J.J. *US Patent 4,477,492* 1984.

[39] Martin, M.; Blu, G.; Guiochon, G. *J. Chrom. Science* 11 (1973) 641-654.

[40] Mellors, J.S.; Jorgenson, J.W. *Anal. Chem.* 76 (2004) 5441-5450.

[41] Martin, M; Guiochon, G. *J. Chrom. A* 1090 (2005) 16-38.

[42] Thompson, J.W.; Kaiser, T.J.; Jorgenson, J.W. J. Chrom. A 1134 (2006) 201-209.

[43] Edward, J.T. *J. Chem. Educ.* 47 (1970) 261-270.

[44] Kaiser, T.J.; Thompson, J.W.; Mellors, J.S.; Jorgenson, J.W. *Anal. Chem*. 81 (2009) 2860-2868.

[45] Kennedy, R.T.; Jorgenson, J.W. *Anal. Chem.* 61 (1989) 1128-1135.

[46] Stanley, B.J.; Foster, C.R.; Guiochon, G. *J. Chrom. A* 761 (1997) 41-51.

[47] Billen, J.; Gzil, P.; de Smet, J.; Vervoot, N.; Desmet, G. *Analytica Chimica Acta* 557 (2006) 11-18.

[48] Knox, J.H. *J. Chrom. A* 831 (1999) 3-15.

[49] Kirkland, J.J.; Langlois, T.J. *US Patent 0189944 A1* 2007.

[50] Zhiping, J.; Fisk, R.P.;O'Gara, J.; Walter, T.H.; Wyndham, K.D. *US Patent 20020070168* 2002.

[51] Mellors, J.S. *UNC Doctoral Dissertation* 2005.

[52] MacNair, J.E.; Patel, K.D.; Jorgenson, J.W. *Anal. Chem*. 71 (1999) 700-708.

[53] MacNair, J.E.; Lewis, K.C.; Jorgenson, J.W. *Anal. Chem.* 69 (1997) 983-989.

[54] Jerkovich, A.D.; Mellors, J.S.; Jorgenson, J.W. LCGC North America 21 (2003) 600-610.

[55] Jayant, K.; Singh, N.H.; MacDiamond, A.G.; Sukant, T. *Handbook of Polyelectrolytes and Their Applications: Polyelectrolyte-Based Multilayers, Self-Assemblies, and Nanostructures*, American Scientific Publishers, California, Volume 1, 2002.

[56] Yu, J.; Wang, Z.; Chu, B. *Macromolecules* 25 (1992) 1618.

[57] Jafarzadeh, M.; Rahman, I.A.; Sipaut, C.S. *J. Sol-Gel Sci. Technol.* 50 (2009) 328.

[58] Brinker, C.J.; Scherer, G.W. *Sol-Gel Science: The Physics and Chemistry of Sol-Gel Processing*, Academic Press, New York, 1st ed., 1990.

[59] Wang, B.; Zhang, W.; Zhang, W.; Mujumdar, A.S.; Huang, L. *Drying Technology* 23 (2005) 7-32.

[60] Unger, K.K. *Porous Silica, its properties and uses as support in column liquid chromatography*, Elsevier Scientific Publishing, New York, 1979.

[61] DeStefano, J.J.; Langlois, T.J.; Kirkland, J.J. *J. Chrom. Sci.* 46 (2008) 254-260.

[62] Cabooter, D.; Fanigliulo, A.; Bellazzi, G.; Allieri, B.; Rottigni, A.; Desmet, G. *J. Chrom. A* 1217 (2007) 7074-7081.

[63] Kucera, P. *Microcolumn high performance liquid chromatography*, Elsevier Scientific Publishing, New York, 1984.

[64] Ehlert, S.; Rosler, T.; Tallarek, U. *J. Sep. Sci.* 31 (2008) 1719-1728.

[65] Vissers, J.P.C.; Hoeben, M.A.; Laven, J.; Claessens, H.A.; Cramers, C.A. *J. Chrom. A* 883 (2000) 11-25.

[66] *Acquity UPLC Columns* product literature.

[67] Unger, K.K.; Skudas, R.; Schulte, M.M. *J. Chrom. A* 1184 (2008) 393-415.

[68] Brown, S.M.; Lard, E.W. *Powder Technology* 9 (1974) 187-190.

[69] Kissa, E. *Dispersions: Characterization, Testing, and Measurement*, CRC Press, New York, 1999. Chapter 3.

[70] Giddings, J.C. *Dynamics of Chromatography: Principles and Theory*, Marcel Dekker Inc., New York, 1965.

[71] Khirevich, S.; Daneyko, A.; Holtzel, A.; Seidel-Morgenstem, A.; Tallarek, U. *J. Chrom. A* 1217 (2010) 4713-4722.

[72] Gluckman, J.C.; Hirose, A.; McGuffin, V.L.; Novotny, M. *Chromatographia* 17 (1983) 303-309.

[73] Kinetex product literature. Phenomenex website.

2.6 TABLES

Sample	Number Average Particle Size (μm)	RSD (%)
10 Coating Steps	1.9	39.1
Step 5 of 10 Coating Steps	1.7	6.8
5 Coating Steps	1.7	6.0

Table 2-1: Particle Size and Relative Standard Deviation of 1.4 μm core particles. 1.4 μm NPS core (Eprogen), coated with 0.5% (w/w%) HMW PDDA and 10% (w/w%) Nalco 1034A (20 nm) colloidal silica

A.

Sample	Number Average Particle Size (μm)	RSD (%)
Before Filtering	1.9	31.9
2-3 μm apparatus region	1.7	22.2
Greater than 3 μm apparatus region	2.1	35.8

B.

Sample	Number Average Particle Size (μm)	RSD (%)
Before Filtering	1.9	31.9
Less than 2.0 μm removed	2.3	19.1
Greater than 5 μm removed	1.8	20.3

Table 2-2: Size and particle size distribution A) after sizing particles with reversible flow sieving apparatus. B) after top loading filtration apparatus. 1.4 μm NPS core (Eprogen), 10 alternating layers of 0.5% (w/w%) HMW PDDA and 10% (w/w%) Nalco 1034A colloidal silica

Polyelectrolyte Type	Number Average Particle Diameter (μm)	RSD (%)	Growth Rate (nm/step)
LMW PDDA	1.7	3.3	48
HMW PDDA	1.6	4.3	40

Table 2-3: Comparison of particle diameter, particle size distribution and growth rate dependence on polyelectrolyte molecular weight.

LMW PDDA Concentration (w/w%)	Number Average Particle Size (μm)	RSD (%)	Growth Rate (nm/coating step)
0.5	1.71	3.0	50
0.25	1.65	3.1	40
0.1	1.67	3.1	48
0.05	1.58	2.8	25

Table 2-4: Effect of polyelectrolyte concentration on particle size, particle size distribution, and growth rate. 1.4 μm NPS (Eprogen), coated with three alternating layers of LMWPDDA and Ludox AS-30 (20 nm) colloidal silica.

pH	Zeta Potential (mV)
9.0	-76
8.0	-60
6.0	-29
4.0	-9.0
3.0	-5.4
2.0	-0.83

Table 2-5: Effect of pH on the zeta potential for 10% (w/w%) aqueous Ludox AS-30 (13 nm) colloidal silica.

Particle	Number Average Particle Diameter (μm)	Growth Rate (nm/coating step)
NPS before coating	1.4	N/A
NexSil8 Coated (8 nm)	1.5	15
Nalco 1030 Coated (13 nm)	1.5	20
NexSil85 Coated (85 nm)	1.6	80
NexSil125 Coated (125 nm)	1.6	80

Table 2-6: Effect of colloidal silica diameter on particle size and growth rate

	Tailing Factor		
Analyte	10 Layer Particles, Single Endcapping	5 Layer Particles, Single Endcapping	5 Layer Particles, Double Endcapping
Hydroquinone	0.93	1.0	1.1
Resorcinol	1.1	0.99	1.0
Catechol	1.2	1.2	1.1
4-Methyl Catechol	1.2	1.5	1.2

Table 2-7: Comparison of the tailing factors for the 10 layer particles and 5 layer particles packed in 30 μm i.d. capillary columns.

A.

Particle Type	%C (w/w%)	k’	Amount carbon per column volume (g/cm^3)**	Flow Resistance (g/cm^3 x sec)
5 layer particles	3.4	0.50	7.6×10^{-6}	2.3×10^{8}
10 layer particles	5.8	0.63	1.1×10^{-5}	5.3×10^{8}
1.7 μm Kinetex	12*	1.08	2.6×10^{-5}	1.5×10^{8}
2.6 μm Kinetex	12*	1.36	2.7×10^{-5}	1.2×10^{8}

B.

Comparison Particles	k’ ratio	Amount carbon per column volume ratio
10 layer/5 layer	1.3	1.4
2.6 μm Kinetex/1.7 μm Kinetex	1.3	1.0
2.6 μm Kinetex/10 layer	2.2	2.5
2.6 μm Kinetex/5 layer	2.7	3.6
1.7 μm Kinetex/10 layer	1.6	2.4
1.7 μm Kinetex/5 layer	2.2	3.4

Table 2-8: Comparison of capacity factor between different packing materials. A) capacity factors and amount of carbon per column volume (30 μm i.d. x 25 cm) B) Fold change comparison for the different packing materials. All columns run in 70/30 water/ACN with 0.1% TFA. (**) See Appendix 1 for example calculation.*[73]

A.

Specific Surface Area (m^2/g)	47
Total Pore Volume (cm^3/g)	0.09
BJD Desorption Average Pore Diameter (Å)	68

B.

Meso Pore Volume (mL/g)	0.07
Meso Mean Pore Diameter (Å)	60

Table 2-9: Physical Characteristics of 1.4 μm core particles after 3 coating steps with revised synthesis parameters determined within this chapter. A) BET analysis B) Hg intrusion analysis

	5 Layer Particles	Revised Synthesis Particles
a	0.56	1.45
b	1.18	0.83
c	0.27	0.85

Table 2-10: Reduced parameters for hydroquinone for columns packed with either 5 layer particles or revised synthesis particles. Mobile phase: 70/30 water/ACN with 0.1% TFA

	5 Layer Particles	Revised Synthesis Particles
Total Particle Diameter (μm)	1.7	1.7
Core Diameter (μm)	1.4	1.4
Porous Layer Thickness (μm)	0.15	0.15
RSD (%)	6.0	2.6

Table 2-11 Comparison of the 5 layer particles and particles synthesized by the revised synthesis conditions.

2.7 FIGURES

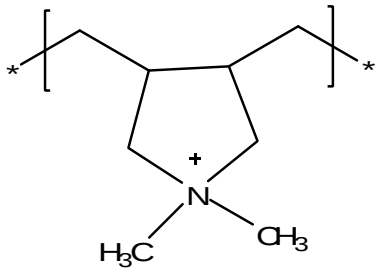

Figure 2-1: Structure of poly(diallydimethylammonium chloride)

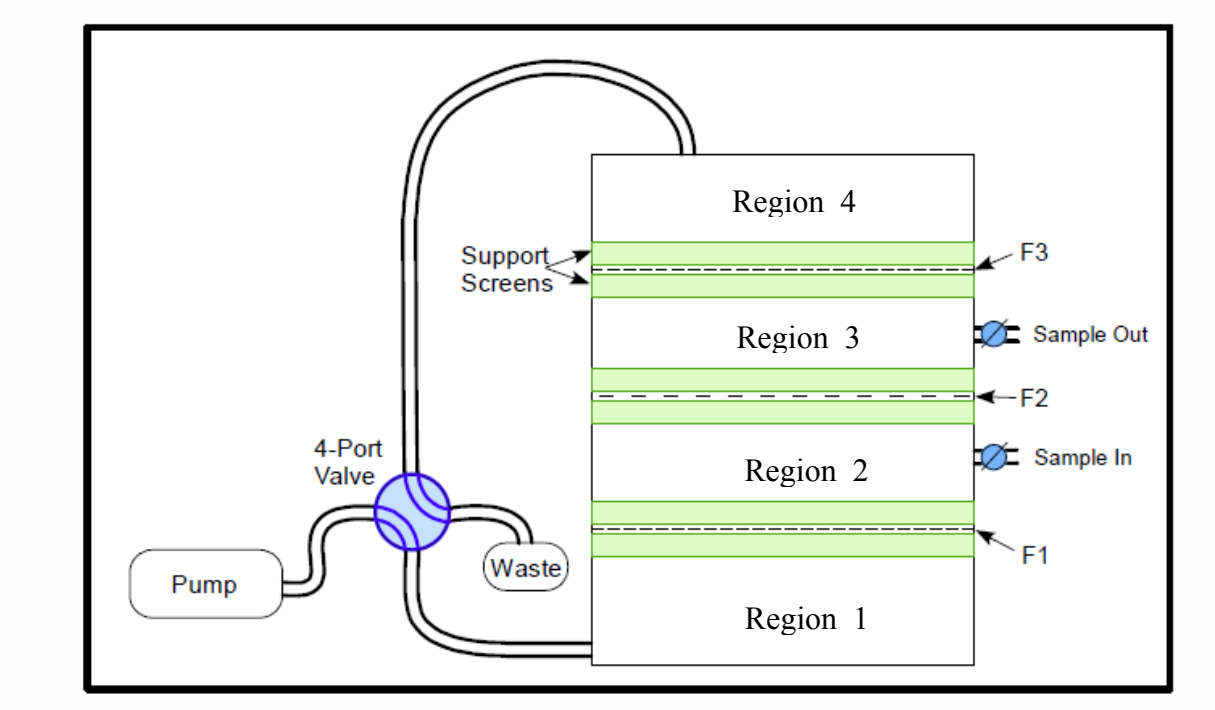

Figure 2-2: Diagram of particle sieving device. F1 and F3 are 2 μm polycarbonate membrane filters and F2 is a 3 μm polycarbonate membrane filter.[48]

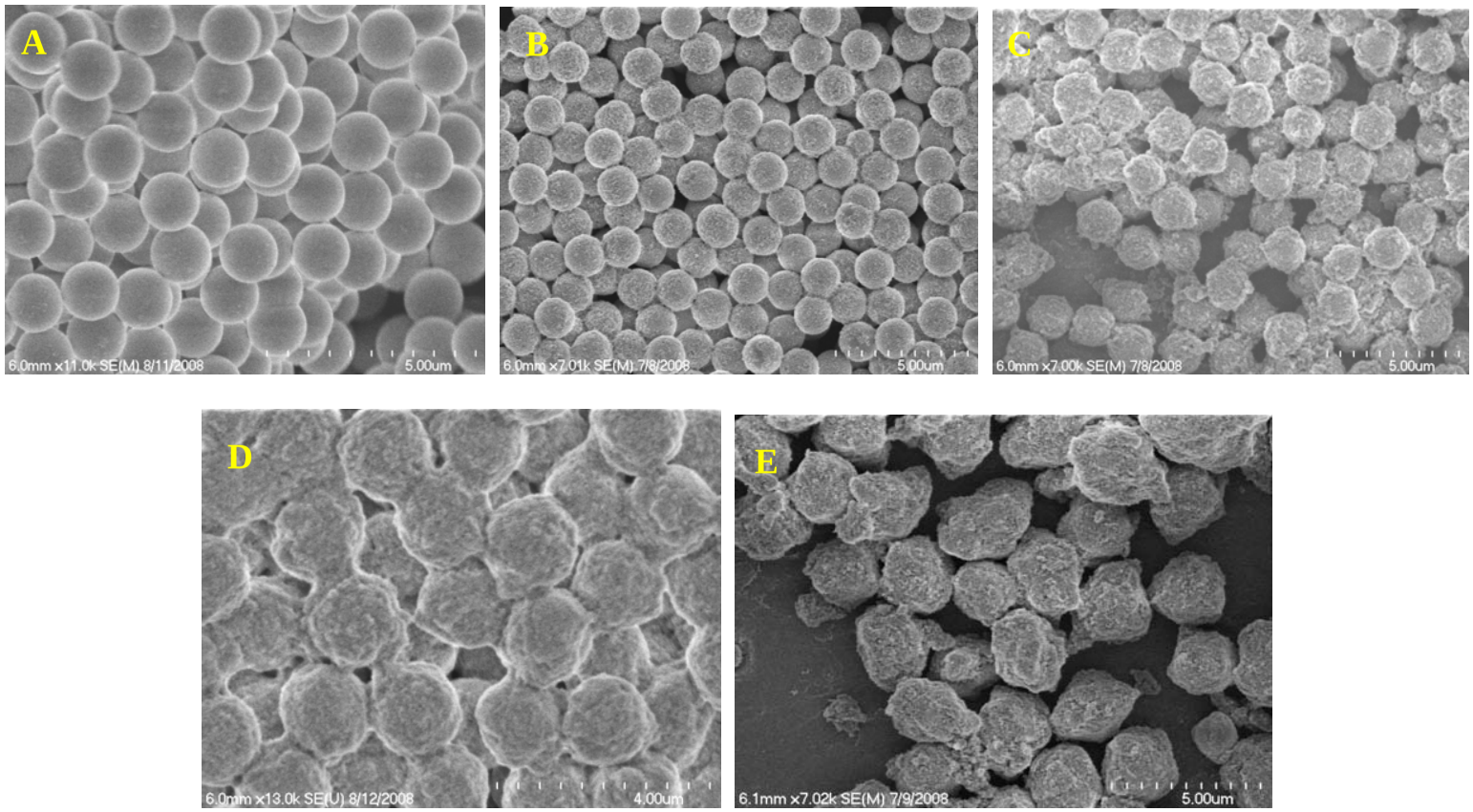

Figure 2-3: Images of the coating process. A) NPS, B) 1 full coating step, C) 3 full coating steps, D) 5 full coating steps, E) 10 full coating steps. 1.4 μm NPS core (Eprogen), 0.5%(w/w%) HMW PDDA, 10% (w/w%) Nalco 1034A (20 nm) colloidal silica

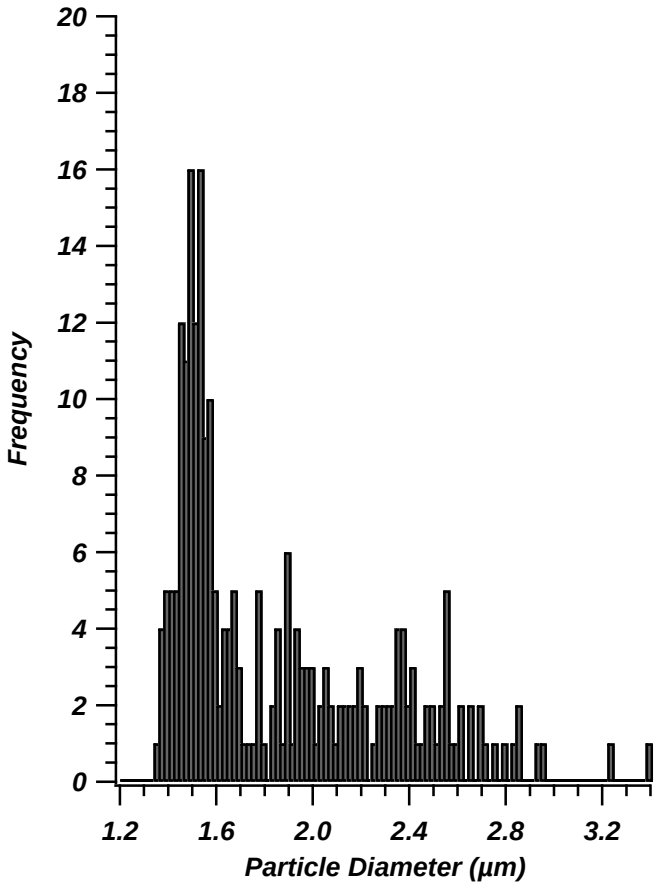

Figure 2-4: Particle size distribution of 1.4 μm core particles after 10 coating steps

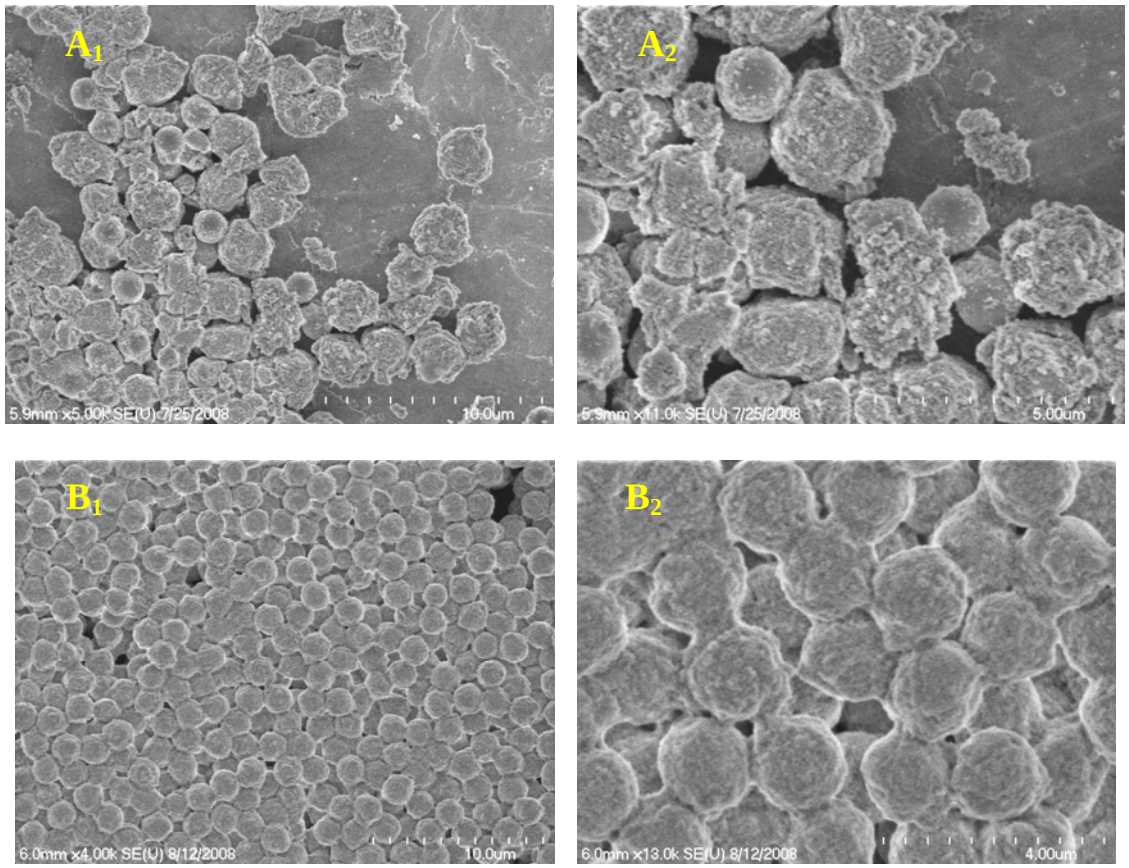

Figure 2-5: Comparison of Superficially Porous Particles after A_1) wide view of 10 coating step particles, A_2) close view of 10 coating step particles, B_1) wide view of 5 coating step particles, and B_2) close view of 5 coating step particles. 1.4 µm NPS core (Eprogen), 0.5% (w/w%) HMW PDDA, 10% (w/w%) Nalco 1034A (20 nm) colloidal silica

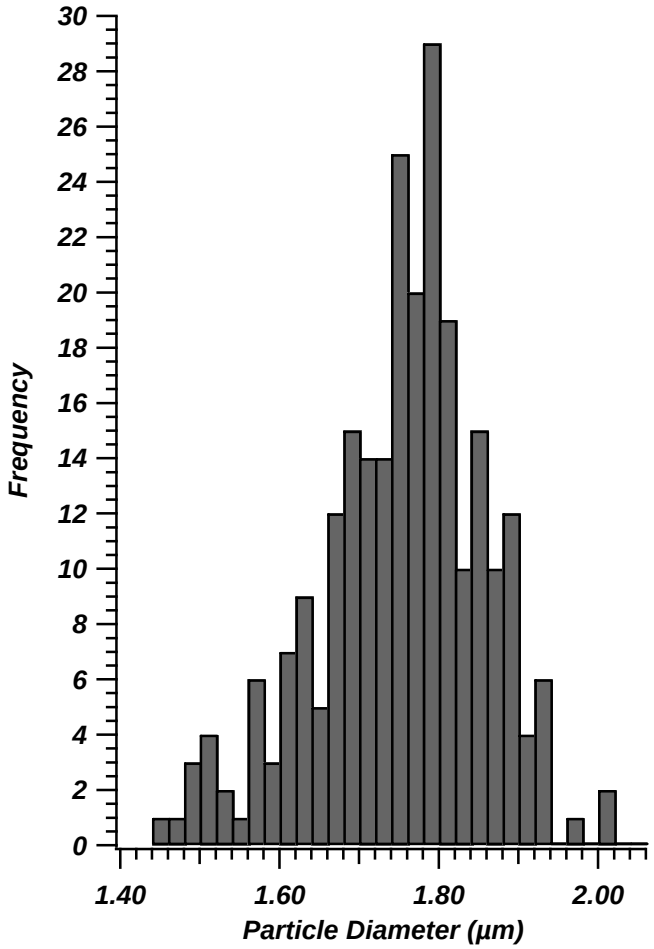

Figure 2-6: Particle size distribution of 1.4 μm core particles after 5 coating steps.

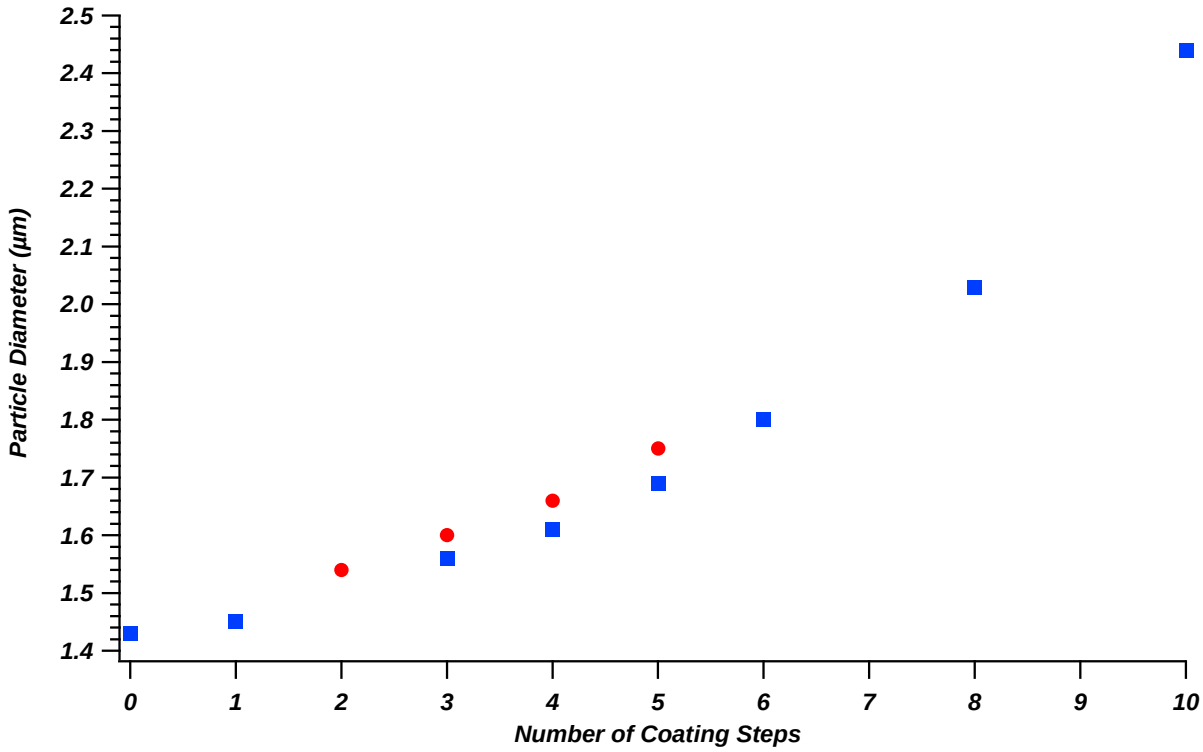

Figure 2-7: Growth Rate Comparison Based on Number of Coating Steps. (●) 5 Coating Step Preparation (■) 10 Coating Step Preparation

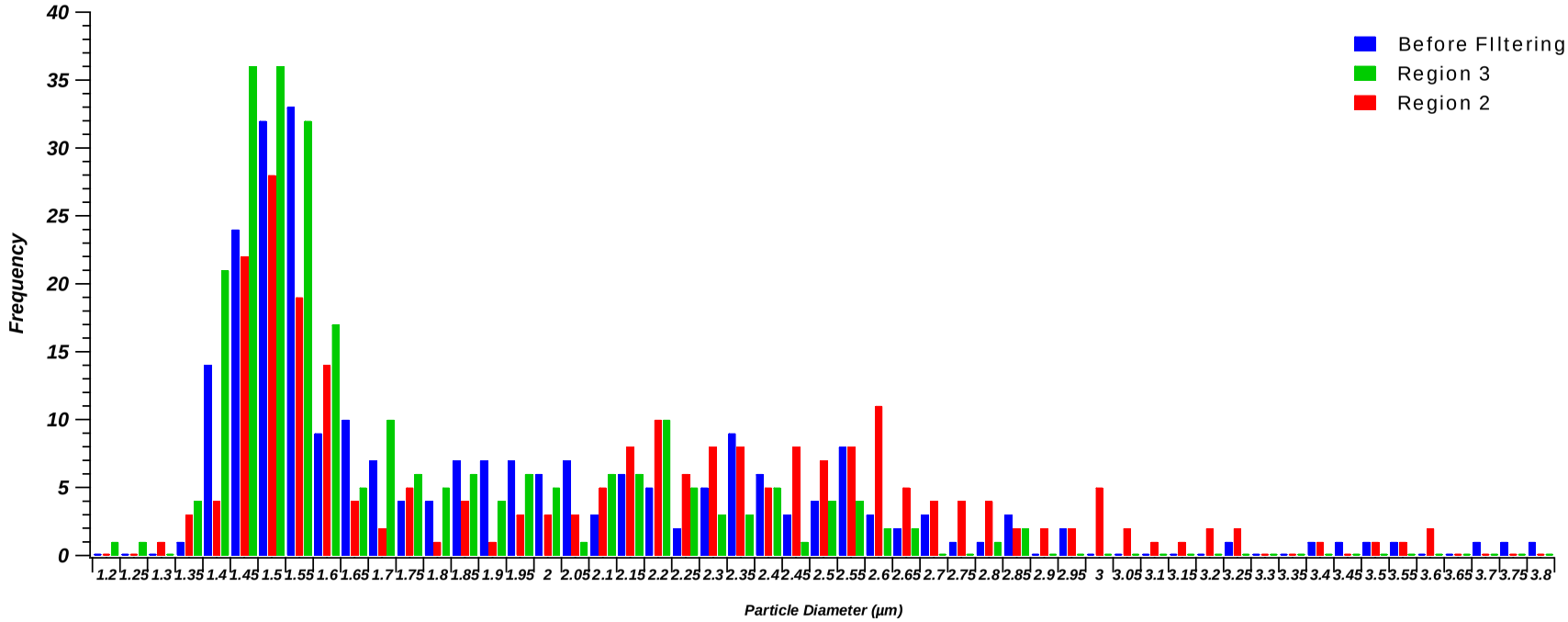

Figure 2-8: Particle size distribution of the 10 coating layer particles after sizing using the reversible flow sieving device.

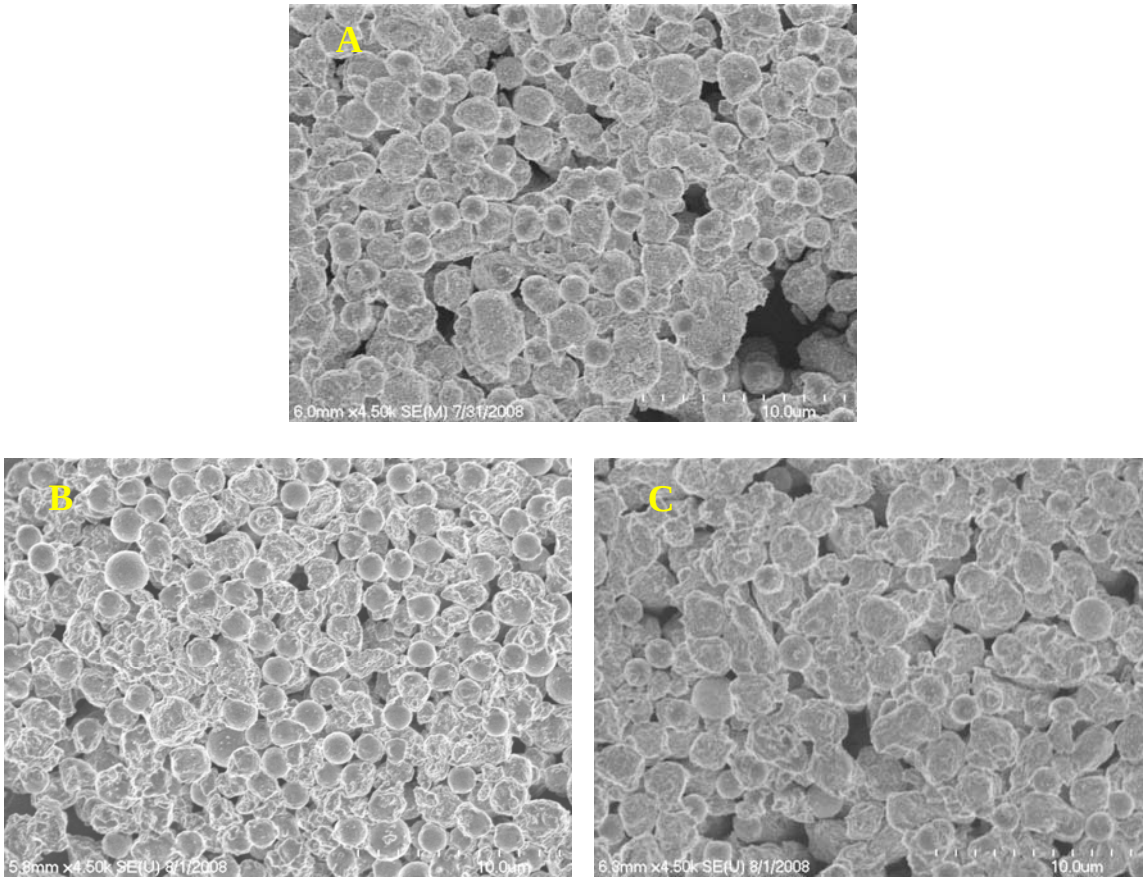

Figure 2-9: Comparison of particles sized with particle filtration apparatus. A) before filtering, B) within region 3 (2-3 μm), C) within region 2 (> 3 μm). 1.4 μm NPS core (Eprogen), 10 alternating layers of 0.5% (w/w%) HMW PDDA and 10% (w/w%) Nalco 1034A (20 nm) colloidal silica

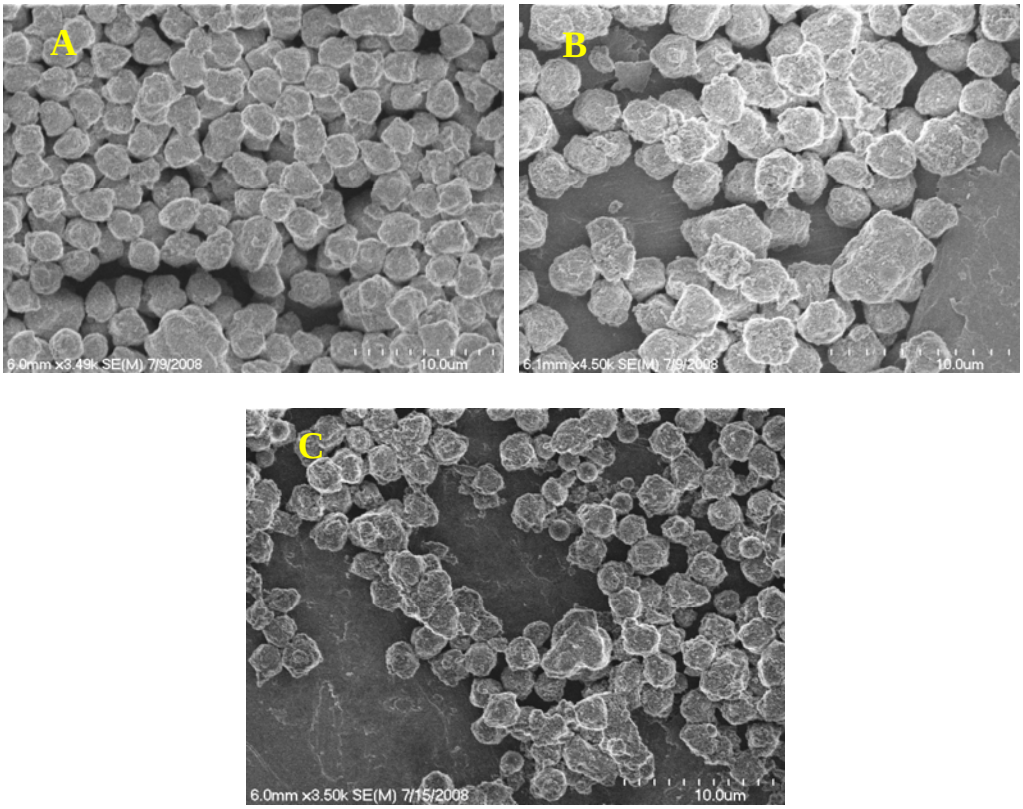

Figure 2-10: Comparison of particles sized with top loaded filtration apparatus . A) before filtering, B) removal of particles with 2.0 µm Nylon filter, C) removal of particles larger than 5 µm with nylon filter. 1.4 µm NPS core (Eprogen), 10 alternating layers of 0.5% (w/w%) HMW PDDA and 10% (w/w%) Nalco 1034A (20 nm) colloidal silica

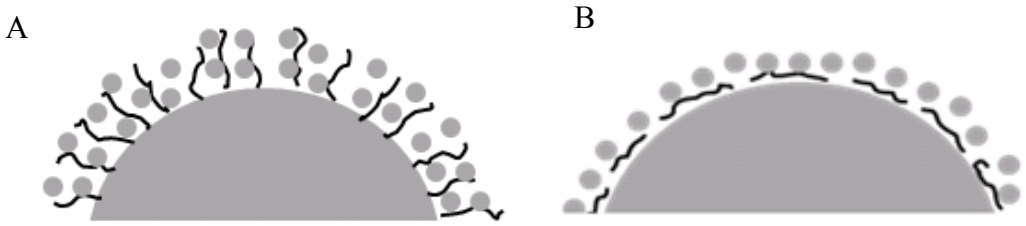

Figure 2-11: Diagram of theoretical polyelectrolyte orientation on NPS. A) Polyelectrolyte perpendicular to the NPS surface, B) polyelectrolyte parallel to the NPS surface

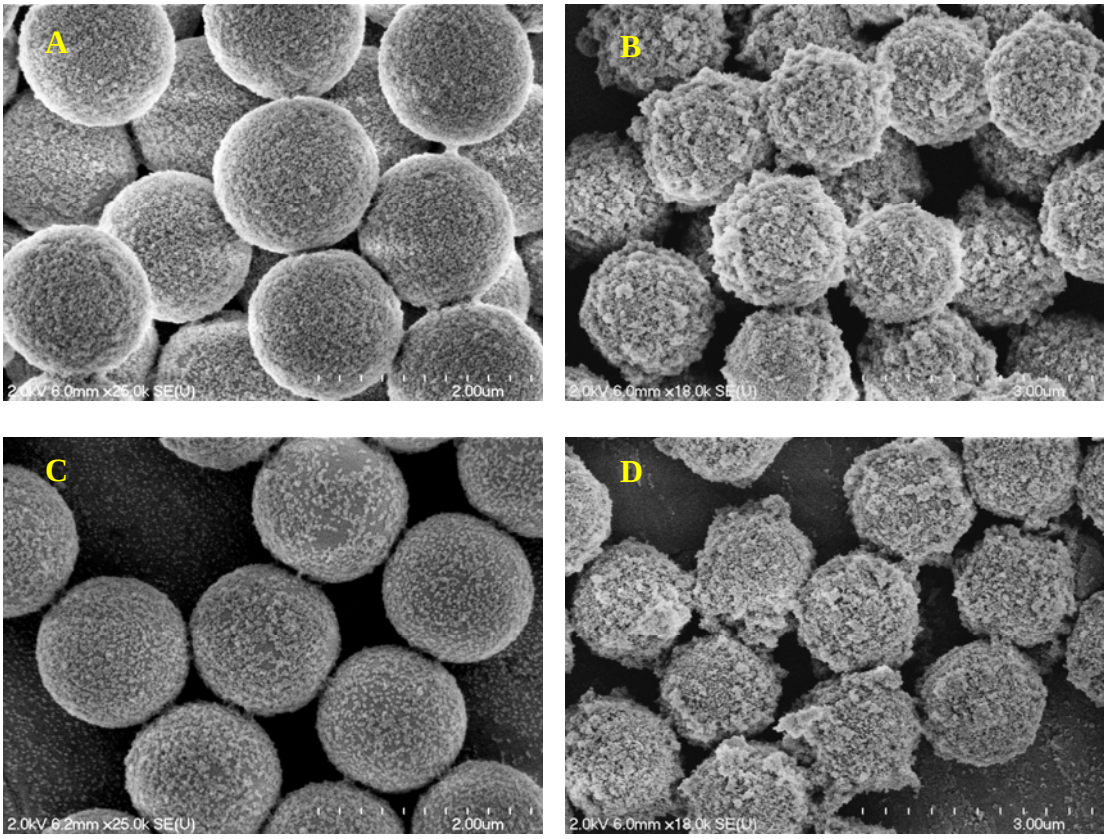

Figure 2-12: Comparison of polyelectrolyte molecular weight. A) one coat 0.5% (w/w%) LMW PDDA and 10% (w/w%) Nalco 1034A (20 nm), B) three alternating coats of 0.5% (w/w%) LMW PDDA and 10% (w/w%) Nalco 1034A (20 nm), C) one coat 0.5% (w/w%) HMW PDDA and 10% (w/w%) Nalco 1034A (20 nm), D) three alternating coats of 0.5% (w/w%) HMW PDDA and 10% (w/w%) Nalco 1034A (20 nm) colloidal silica

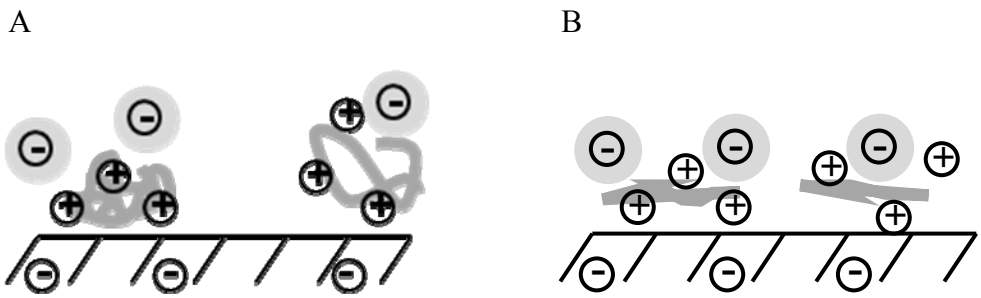

Figure 2-13: Diagram of effect of polyelectrolyte molecular weight on surface thickness variations and roughness. (A) HMW, side view (B) LMW, side view

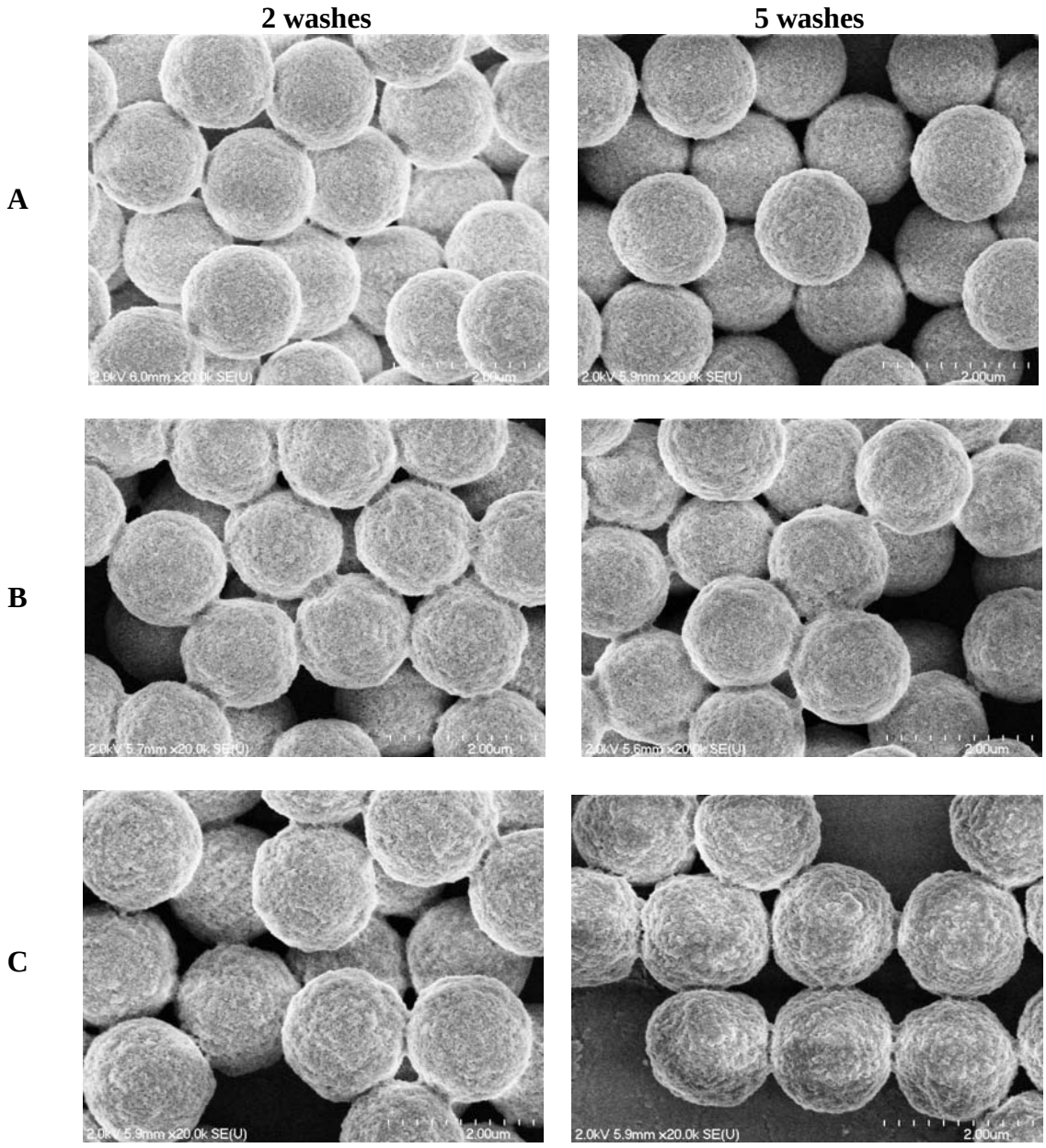

Figure 2-14: Effect of the number of polyelectrolyte washes on the surface uniformity and webbing between particles. A) One full layer B) two full layers C) three full layers 1.4 μm NPS (Eprogen), 0.5% (w/w%) LMW PDDA, 10% (w/w%) AS-30 (12 nm) colloidal silica

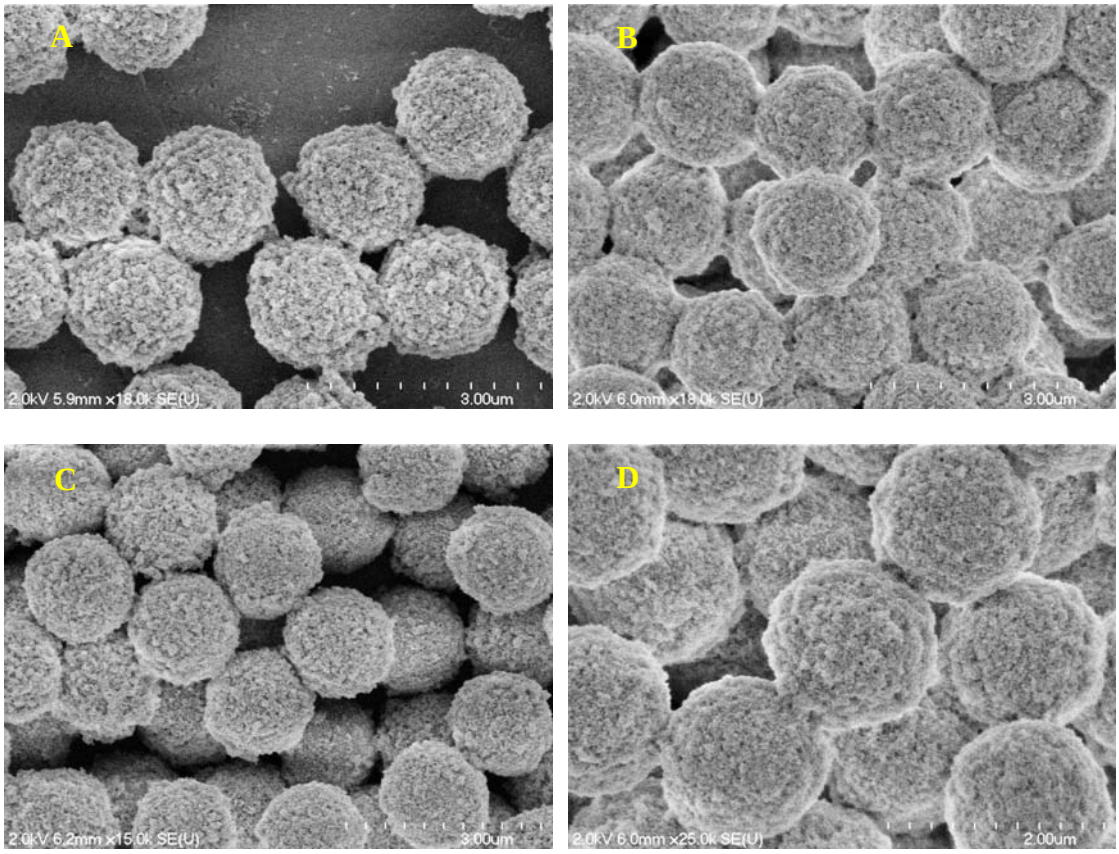

Figure 2-15: Effect of polyelectrolyte concentration (w/w%). A) 0.5%, B) 0.25%, C) 0.1%, D) 0.05%. 1.4 μm NPS (Eprogen), coated with three alternating layers of LMW PDDA and Nalco 1034A (20 nm) colloidal silica

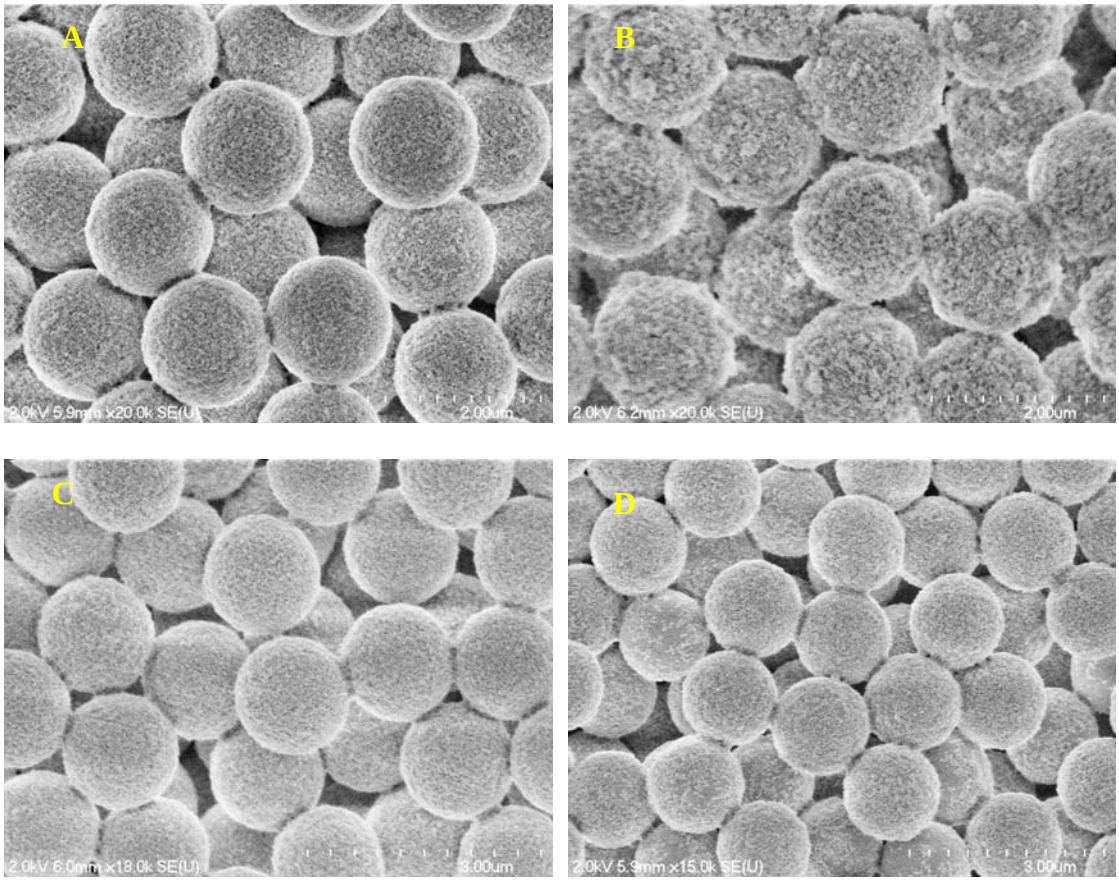

Figure 2-16: Effect of polyelectrolyte concentration (w/w%). A) 0.5%, B) 0.25%, C) 0.1%, D) 0.05%. 1.4 μm NPS (Eprogen), coated with one alternating layer of LMW PDDA and Ludox AS-30 (12 nm) colloidal silica

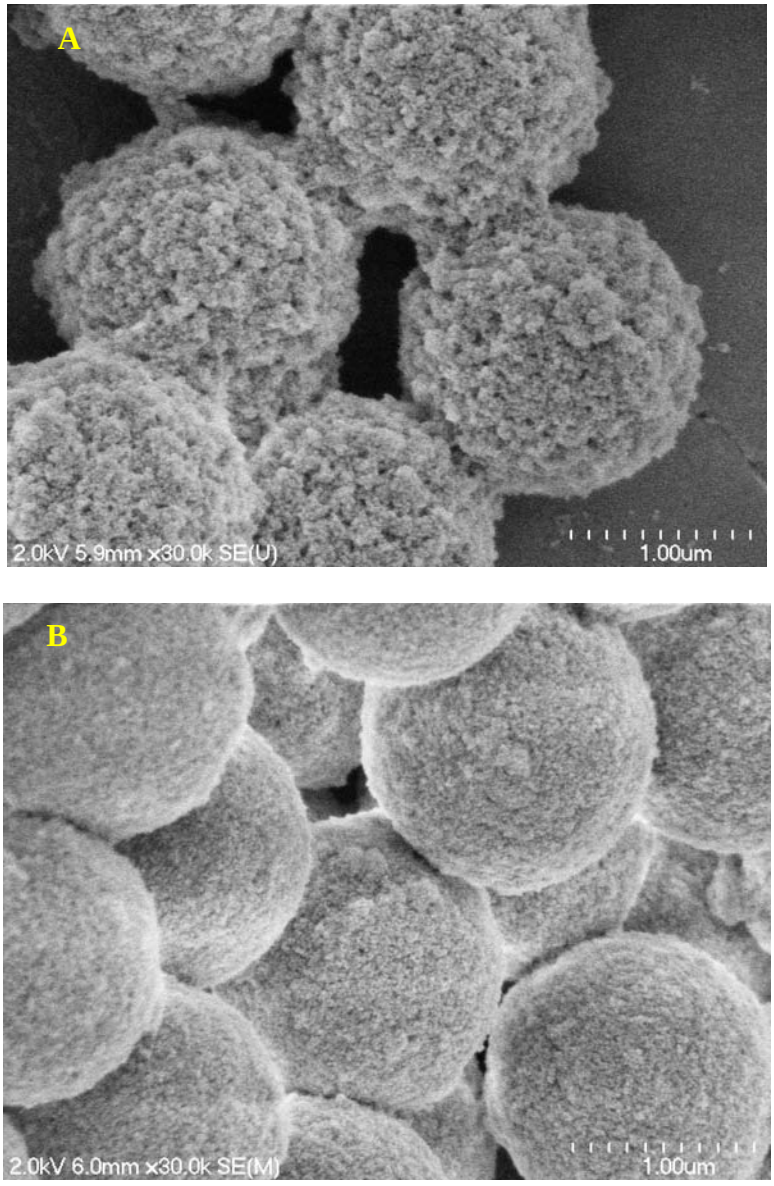

Figure 2-17: Comparison of colloidal silica stabilization pH. A) 10% (w/w%) Nalco 1034A (20 nm), pH = 2.8, B) 10% (w/w%) Nalco 1030 (13 nm), pH = 10.2. 1.4 μm NPS (Eprogen), coated with three alternating layers of 0.5% (w/w%) LMW PDDA and colloidal silica

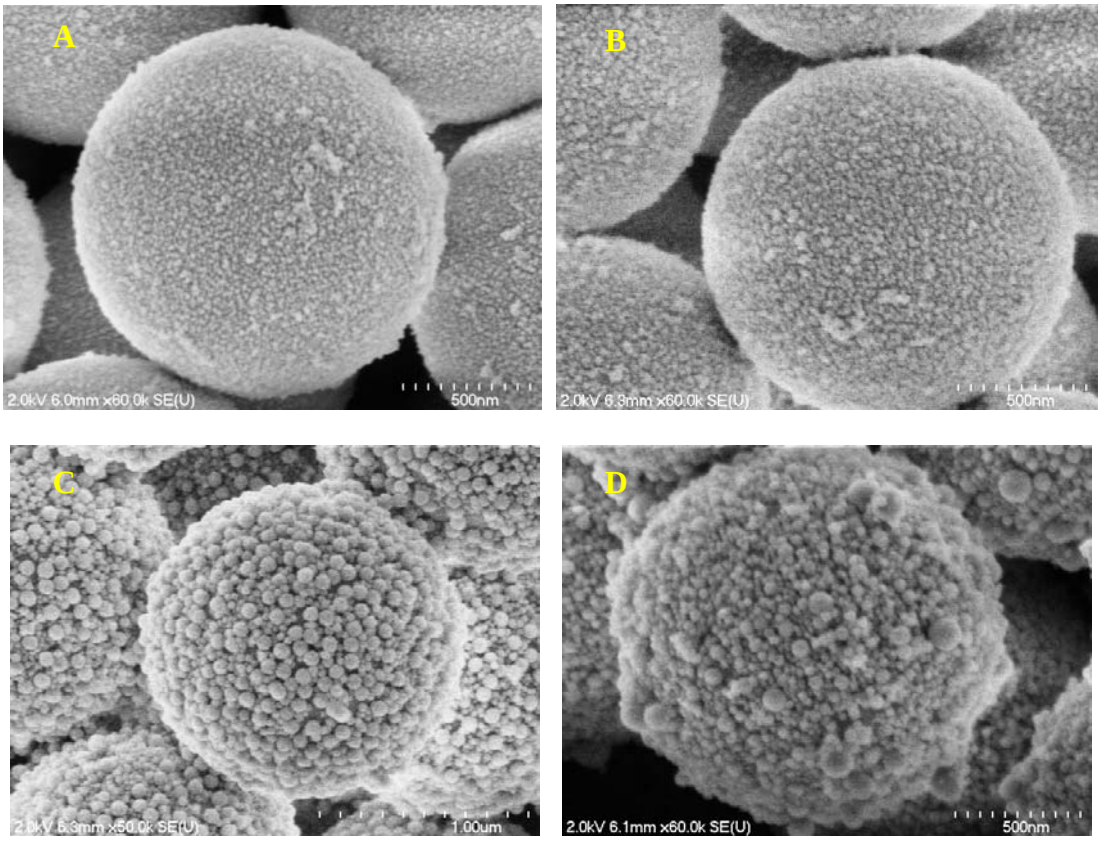

Figure 2-18: Comparison of colloidal silica size. A) NexSil 8 (8 nm), B) Nalco 1030 (13 nm), C) NexSil 85 (85 nm), D) NexSil 125 (125 nm). 1.4 µm NPS (Eprogen), coated with one alternating layer of 0.5% (w/w%) LMW PDDA and 10% (w/w%) colloidal silica

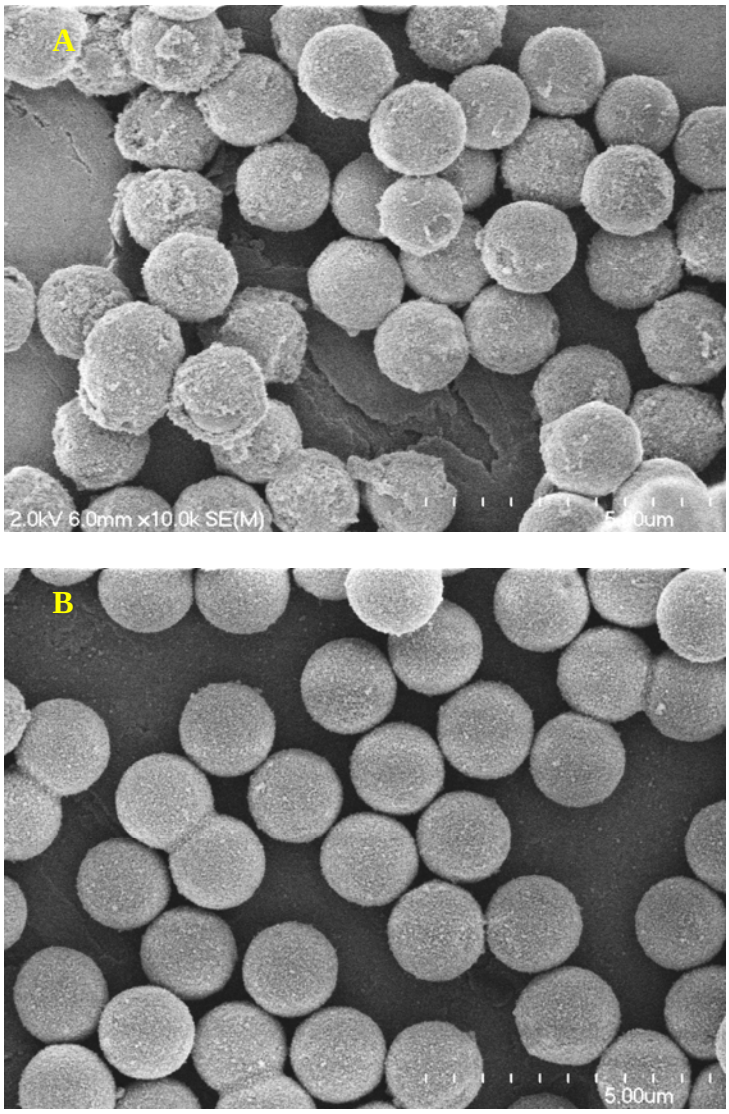

Figure 2-19: Comparison of solution mixing method. A) Centrifuge tube mixing, B) Beaker with stir bar mixing. 1.4 μm NPS (Eprogen), coated with three alternating layers of 0.5% (w/w%) LMW PDDA and 10% (w/w%) Nalco 1030 (13 nm) colloidal silica

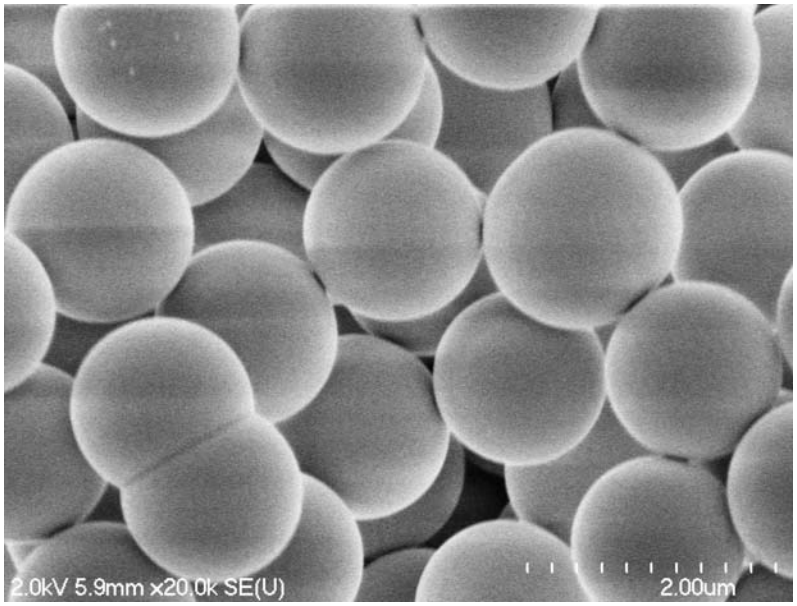

Figure 2-20: SEM image of NPS starting material indicating the presence of fused multiplets

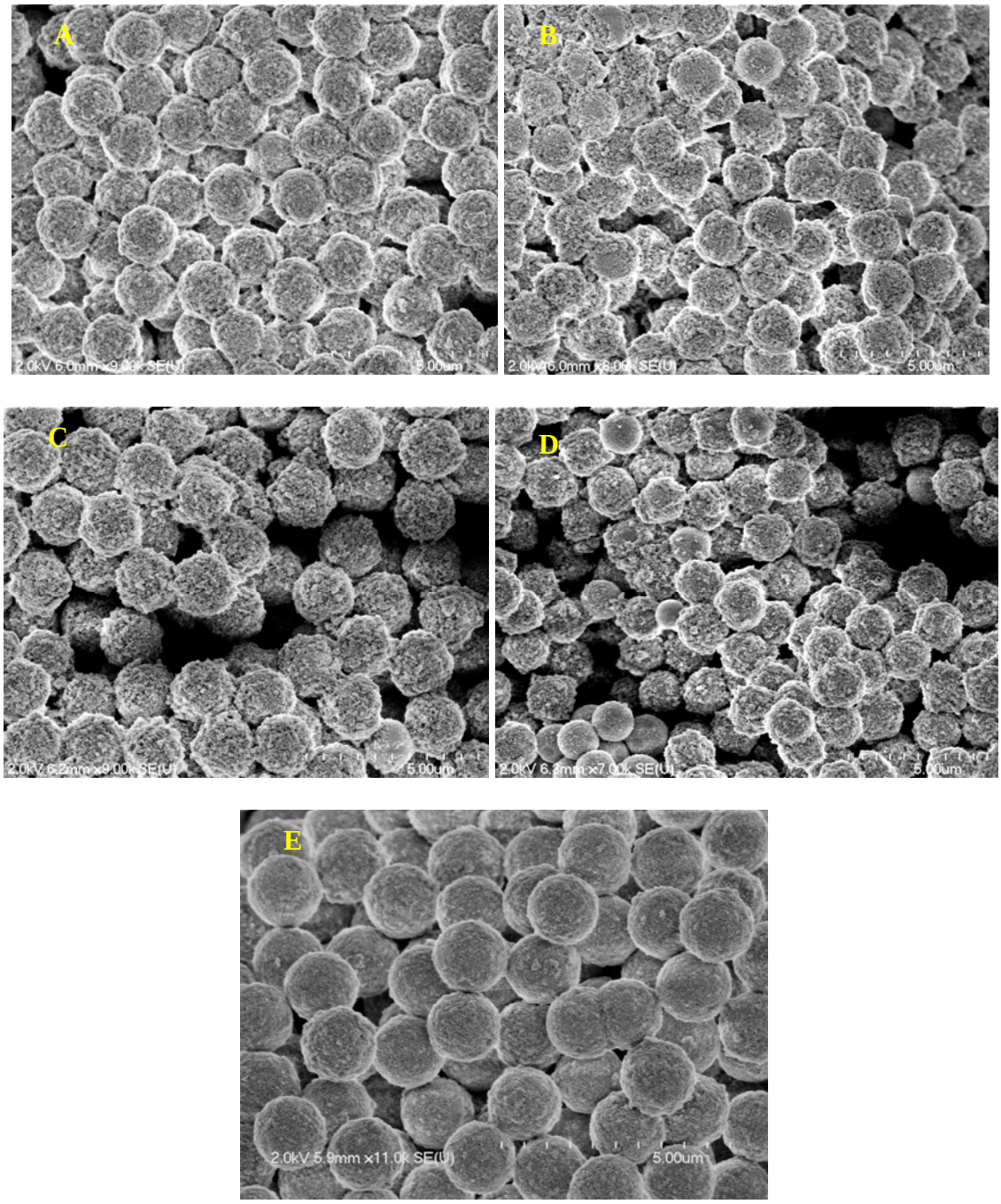

Figure 2-21: Comparison of drying temperature. A) 25˚C, B) 50˚C, C) 80˚C, D) 105˚C, E) lyophilization. 1.4 µm NPS (Eprogen), coated with three alternating layers of 0.5% (w/w%) LMW PDDA and 10% (w/w%) Nalco 1030 (13 nm) colloidal silica

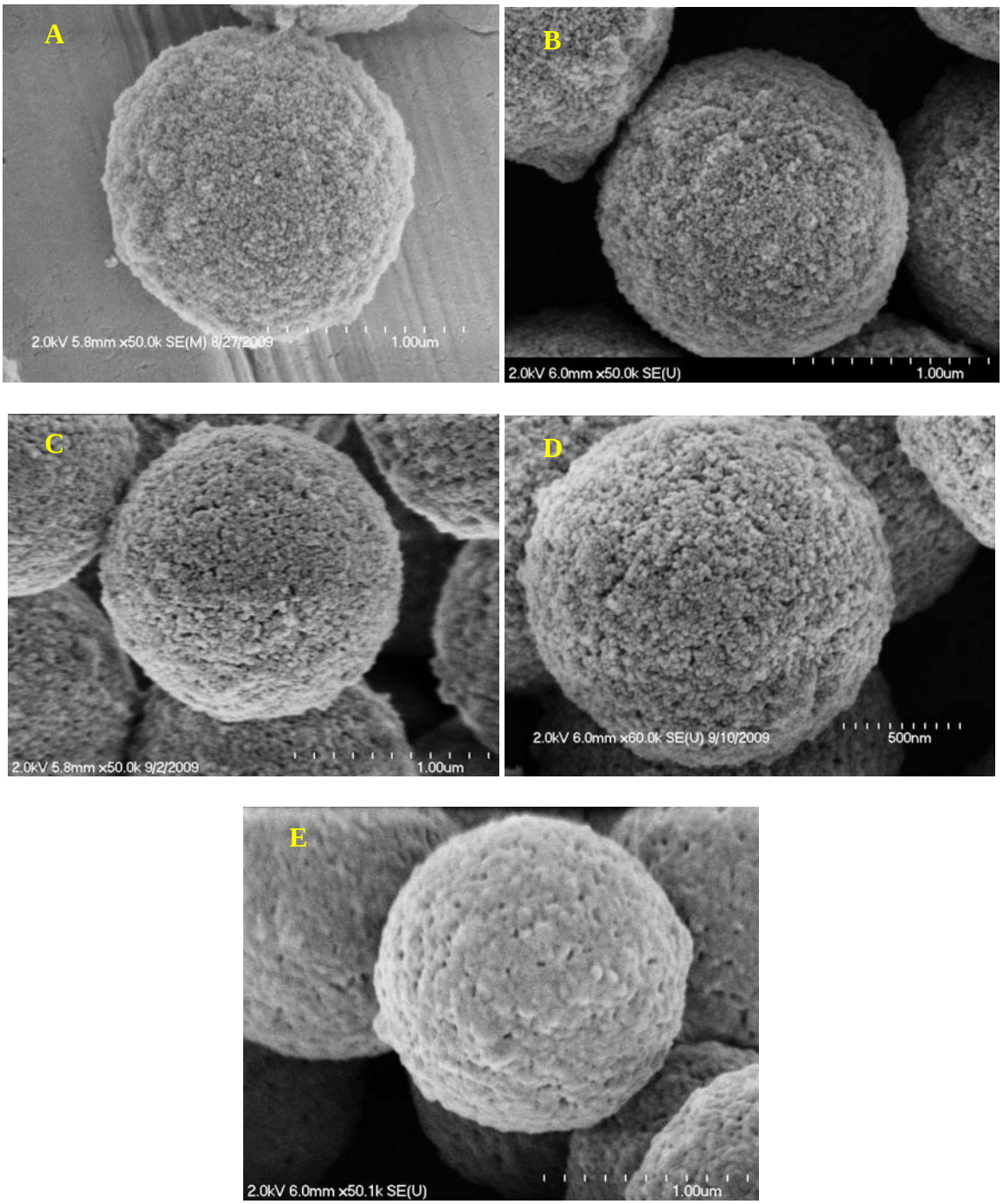

Figure 2-22: Comparison of sintering temperature. A) 855˚C, B) 900˚C, C) 950˚C, D) 980˚C, E) 990˚C. 1.4 µm NPS (Eprogen), coated with three alternating layers of 0.5% (w/w%) LMW PDDA and 10% (w/w%) Nalco 1030 (13 nm) colloidal silica

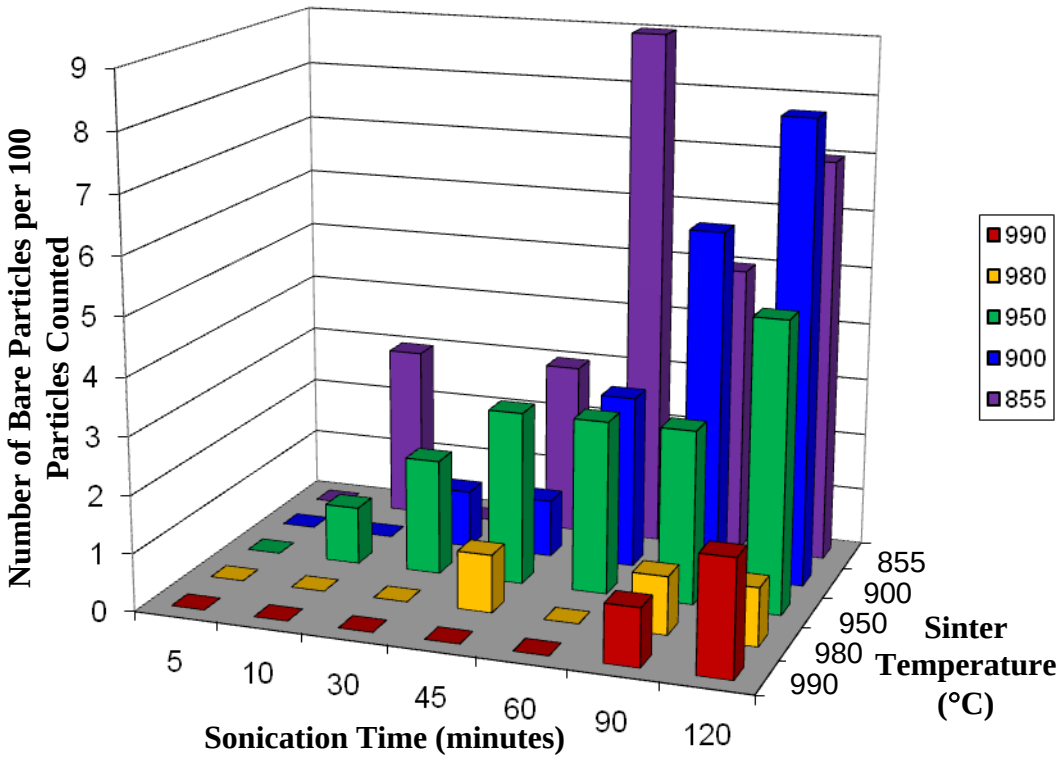

Figure 2-23: Comparison of sintering temperature effect on particle mechanical strength. Sonication of 3 mg/mL aqueous slurry solutions

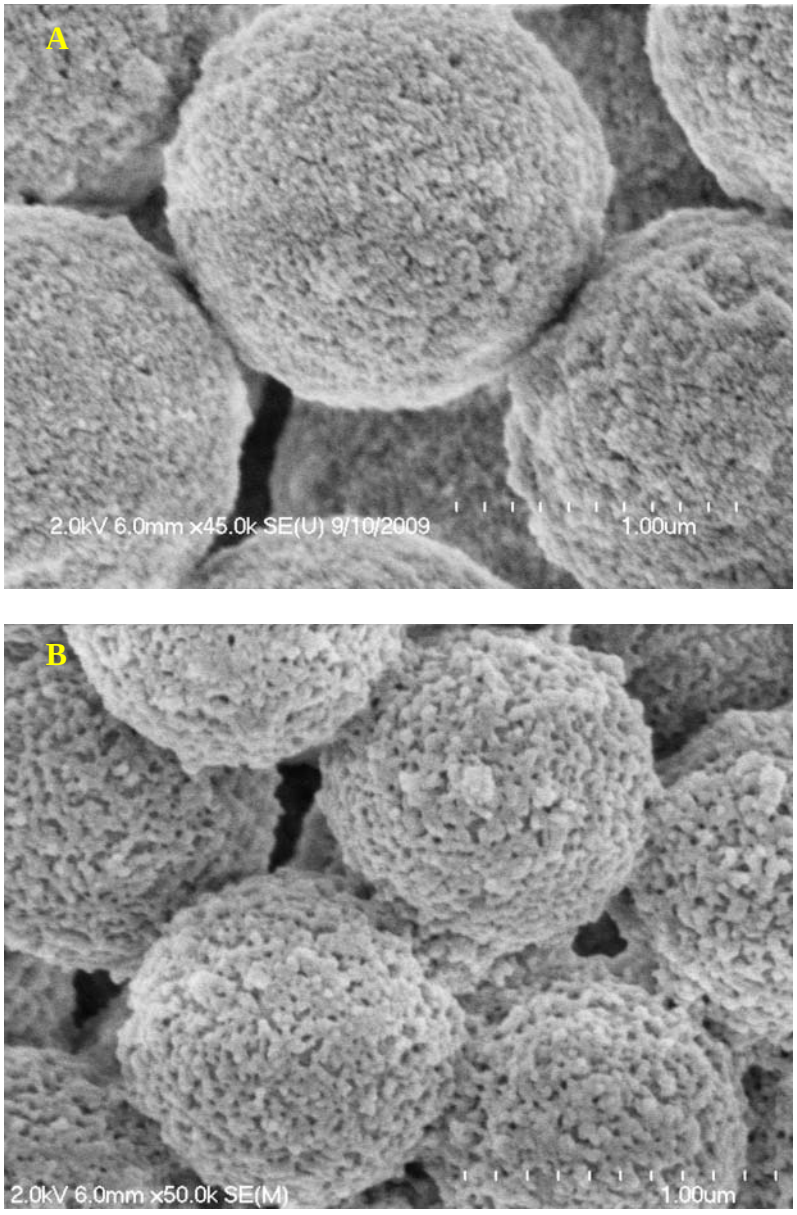

Figure 2-24: Comparison of surface melting when sintered at 980˚C. A) Batch 1 B) Batch 2. Both batches used the same NPS core particles, 0.5% (w/w%) LMW PDDA solution, and 10% (w/w%) Nalco 1030 (13 nm) solution

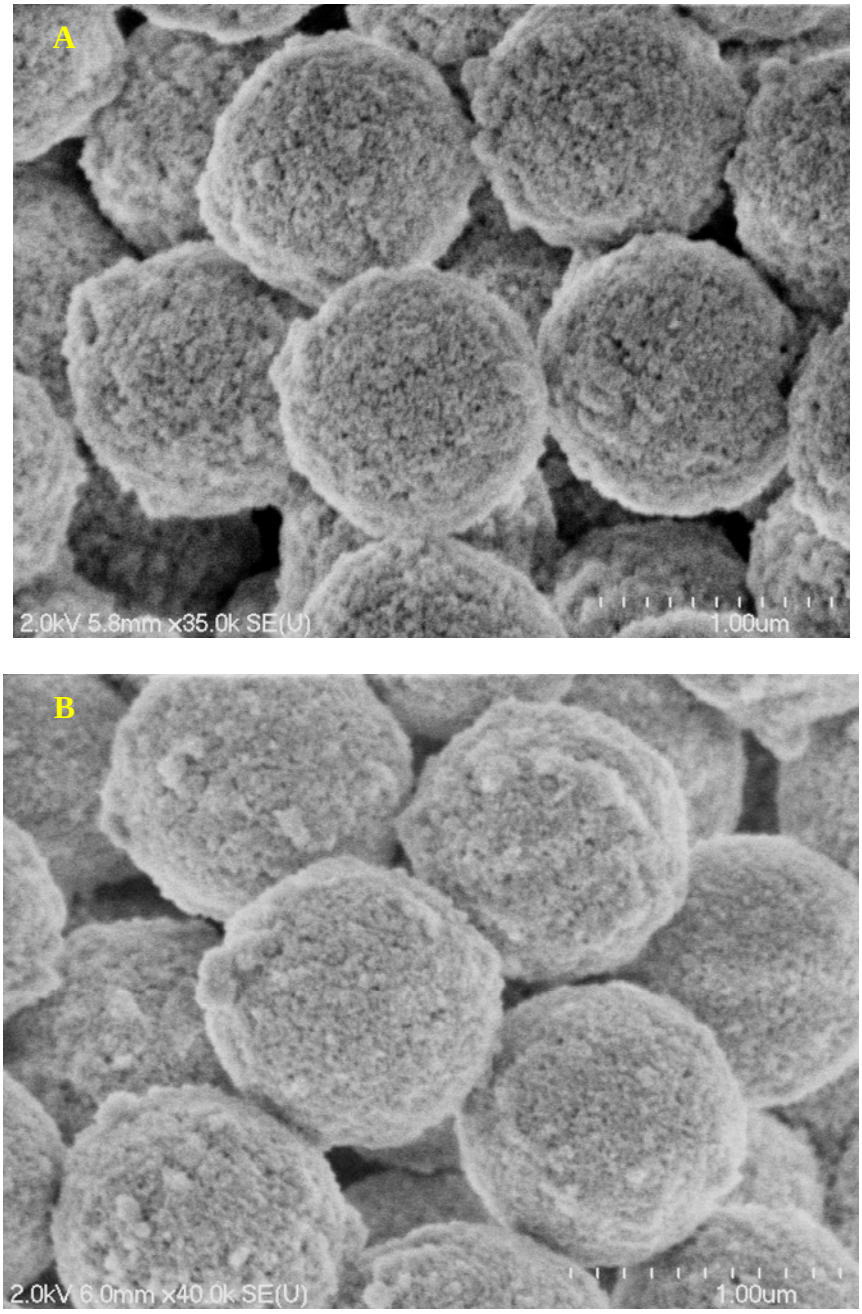

Figure 2-25: Comparison of surface melting when sintered at 980˚C. A) Batch 1 B) Batch 2. Both batches used the same NPS core particles, 0.5% (w/w%) LMW PDDA solution, and 10% (w/w%) Ludox AS-30 (12 nm) solution

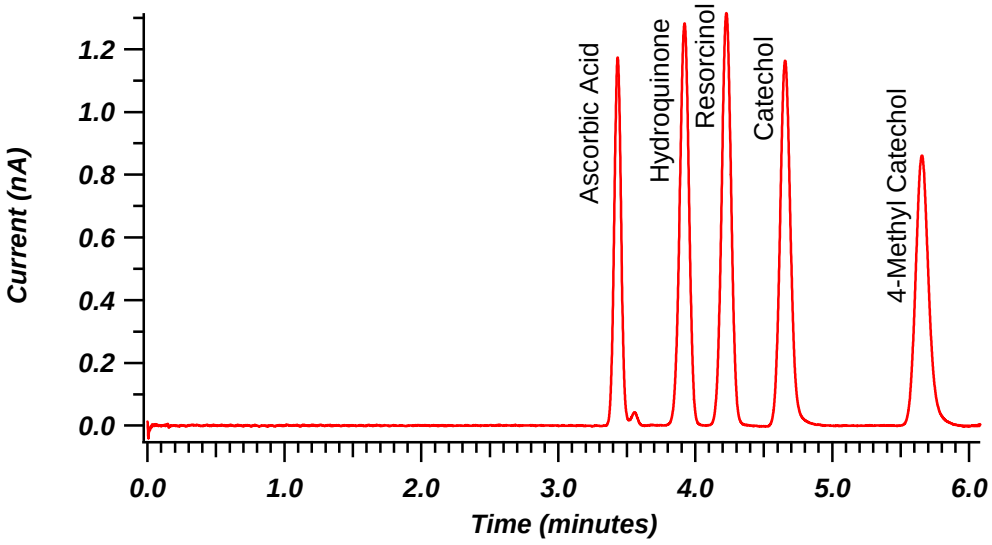

Figure 2-26: Chromatogram for Column LB1-68 at the optimum linear velocity. Particles with 10 coating layers, bonded with C18, and singly endcapped. 30 μm i.d. x 12.5 cm, run in 70/30 water/ACN 0.1% TFA, h_{min} (HQ) = 3.0, u_{opt} = 0.06 cm/sec (5600 psi), k' (4MC) = 0.61.

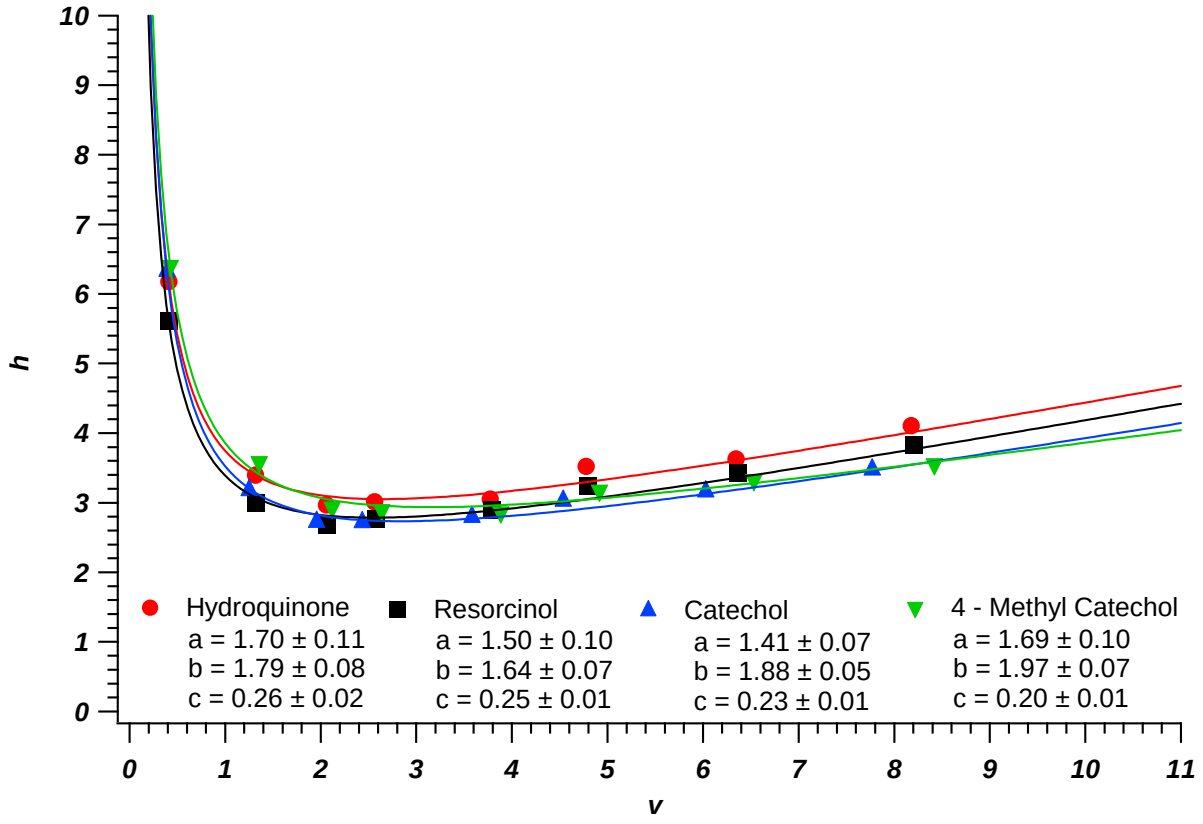

Figure 2-27: Reduced parameters plot for Column LB1-68. Particles with 10 coating layers, bonded with C18, and singly endcapped. 30 µm i.d. x 12.5 cm, run in 70/30 water/ACN 0.1% TFA, h_{min} (HQ) = 3.0, u_{opt} = 0.06 cm/sec (5600 psi), k' (4MC) = 0.61

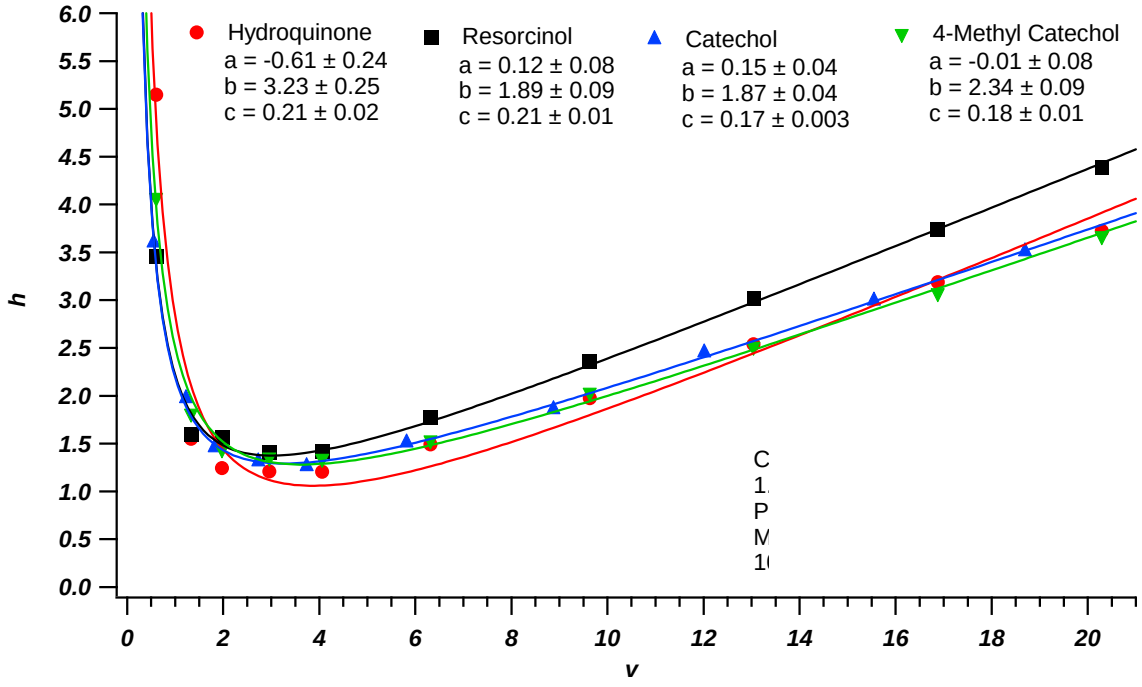

Figure 2-28: Reduced parameters plot for Column LB6-1. 1.9 µm Acquity C18 particles, 30 µm i.d. x 19.8 cm, run in 50/50 water/ACN 0.1% TFA, h_{min} (HQ) = 1.2, u_{opt} = 0.19 cm/sec (6600 psi), k' (4MC) = 0.53

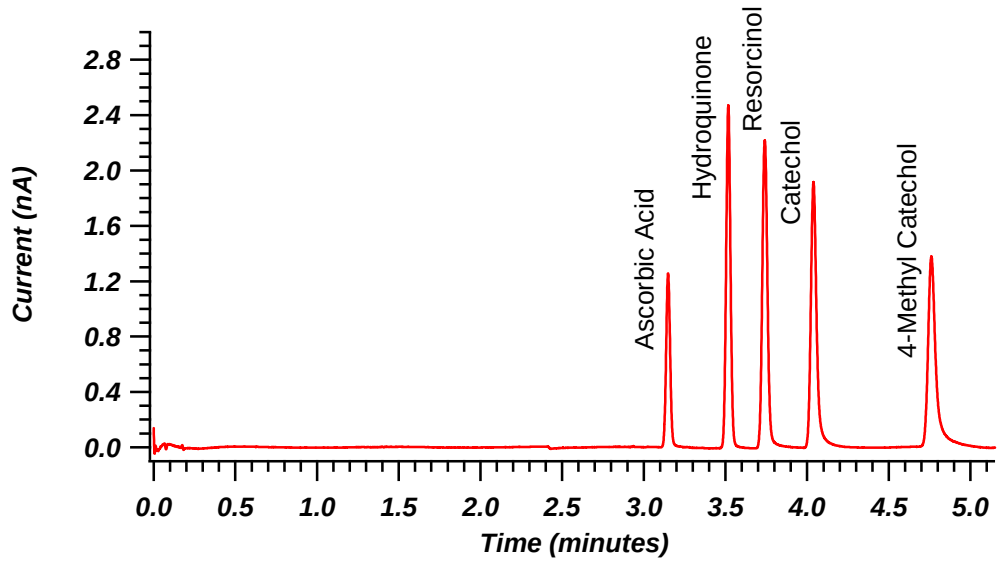

Figure 2-29: Chromatogram for Column LB1-95 at the optimum linear velocity. Particles with 5 coating layers, bonded with C18, and singly endcapped. 30 µm i.d. x 24.3 cm, run in 70/30 water/ACN 0.1% TFA, h_{min} (HQ) = 1.7, u_{opt} = 0.13 cm/sec (8900 psi), k' (4MC) = 0.45

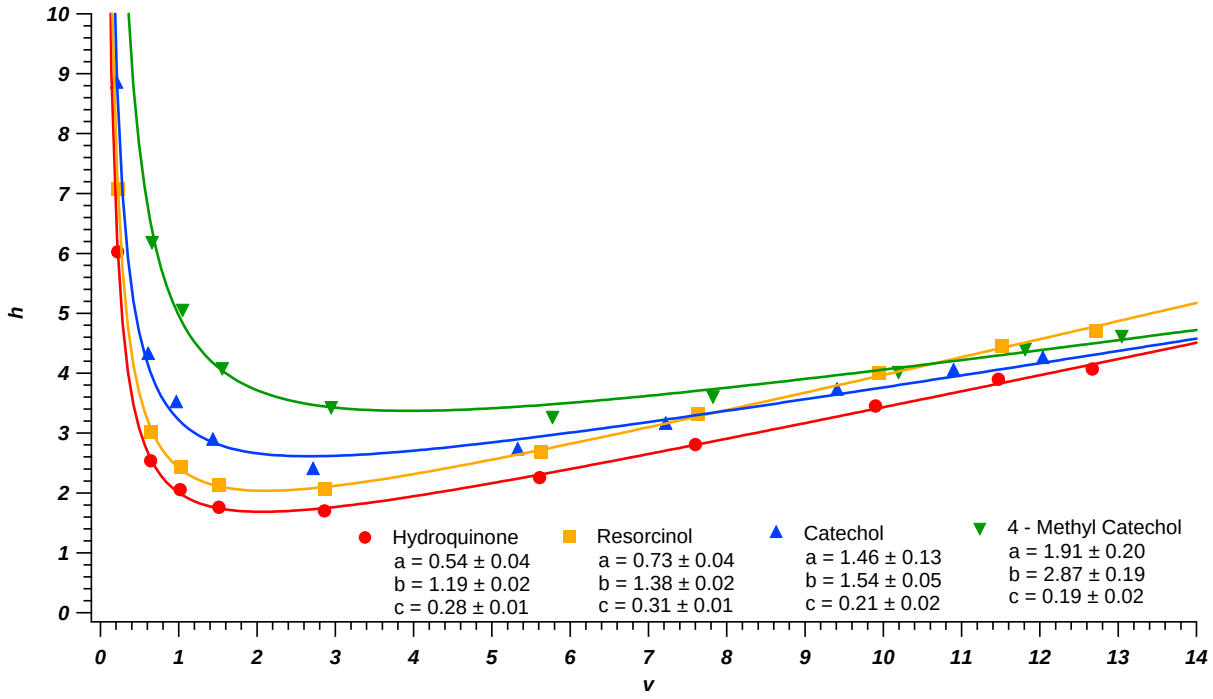

Figure 2-30: Reduced parameters plot for Column LB1-95. Particles with 5 coating layers, bonded with C18, and singly endcapped. 30 µm i.d. x 24.3 cm, run in 70/30 water/ACN 0.1% TFA, h_{min} (HQ) = 1.7, u_{opt} = 0.13 cm/sec (8900 psi), k' (4MC) = 0.45

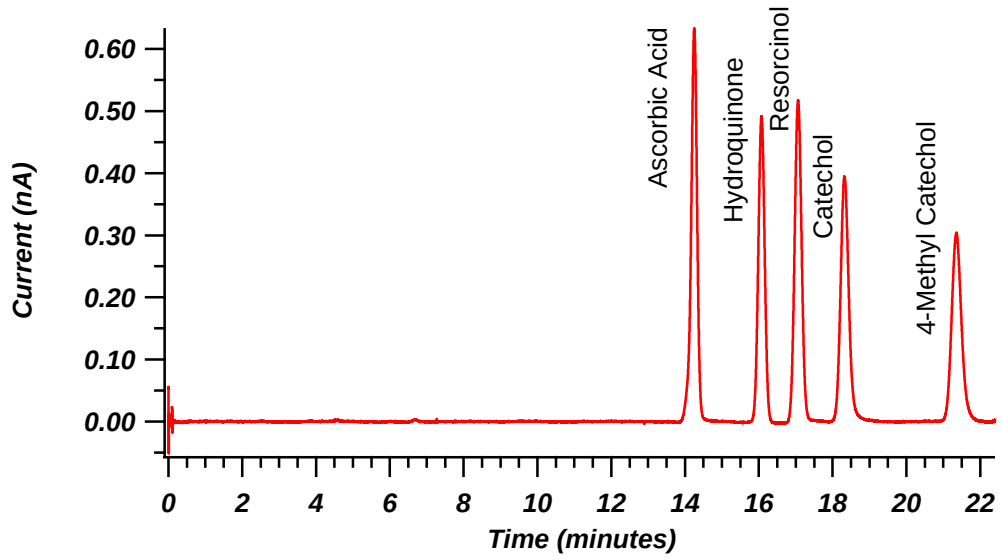

Figure 2-31: Chromatogram for Column LB1-103B at the optimum linear velocity. Particles with 5 coating layers, bonded with C18, and doubly endcapped. 30 µm i.d. x 28.3 cm, run in 70/30 water/ACN 0.1% TFA, h_{min} (HQ) = 3.9, u_{opt} = 0.03 cm/sec (2400 psi), k' (4MC) = 0.48

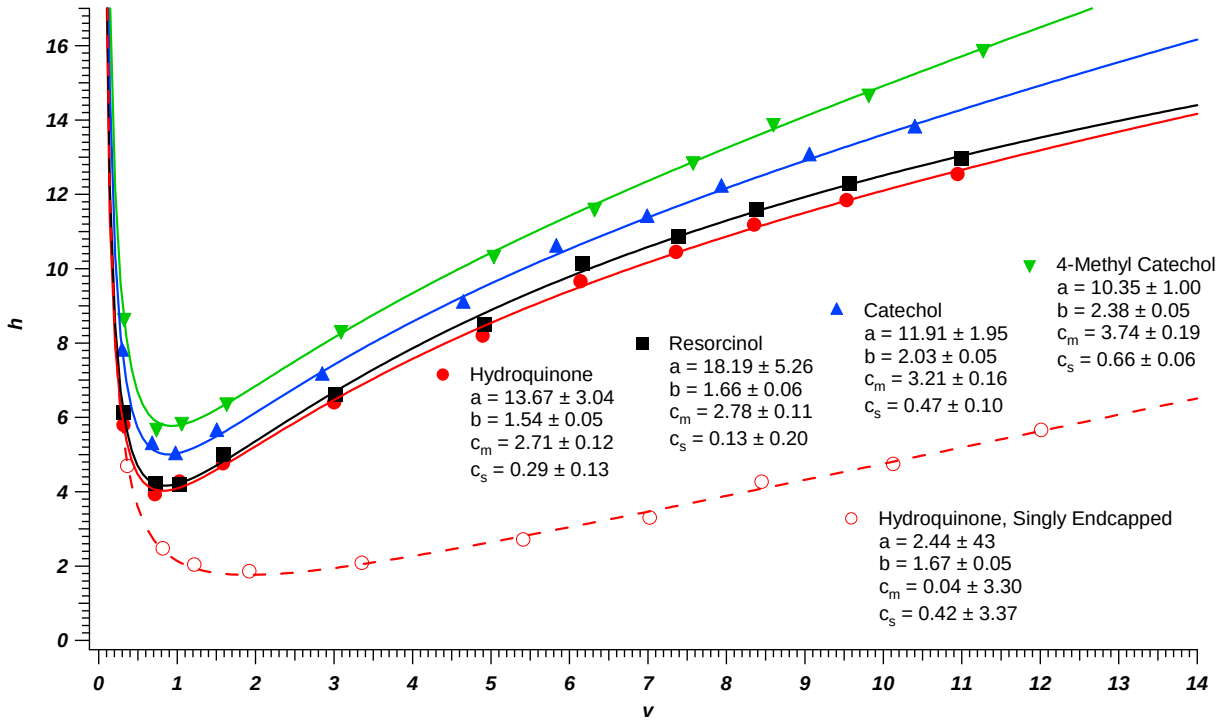

Figure 2-32: Reduced parameters plot for Column LB1-103B. Particles with 5 coating layers, bonded with C18, and doubly endcapped. 30 µm i.d. x 28.3 cm, run in 70/30 water/ACN 0.1% TFA, h_{min} (HQ) = 3.9, u_{opt} = 0.03 cm/sec (2400 psi), k' (4MC) = 0.48

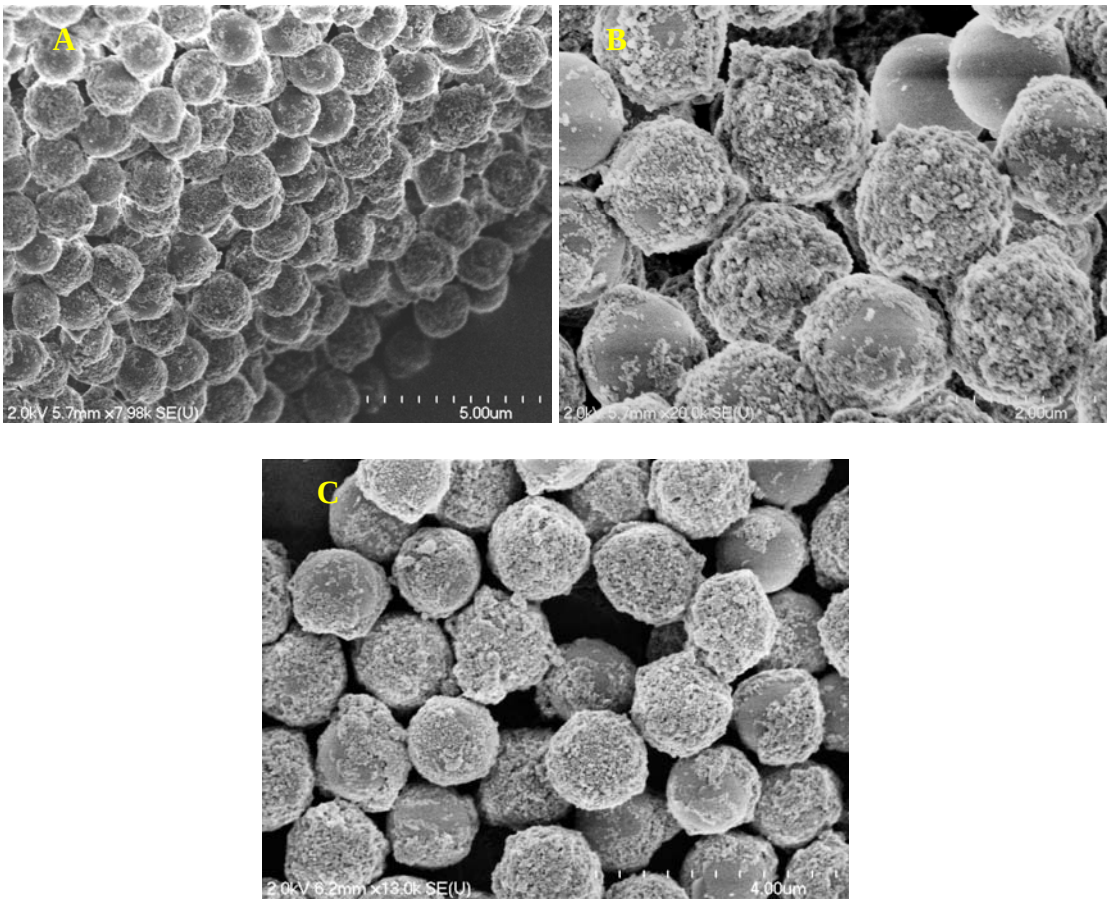

Figure 2-33: SEM images indicating particle structural degradation. A) intact column bed, B) free particles from extruded bed, C) particles after boding and endcapping. 1.4 μm NPS (Eprogen), coated with three alternating layers of 0.5% (w/w%) LMW PDDA and 10% w/w%) Nalco 1034A (20 nm) colloidal silica

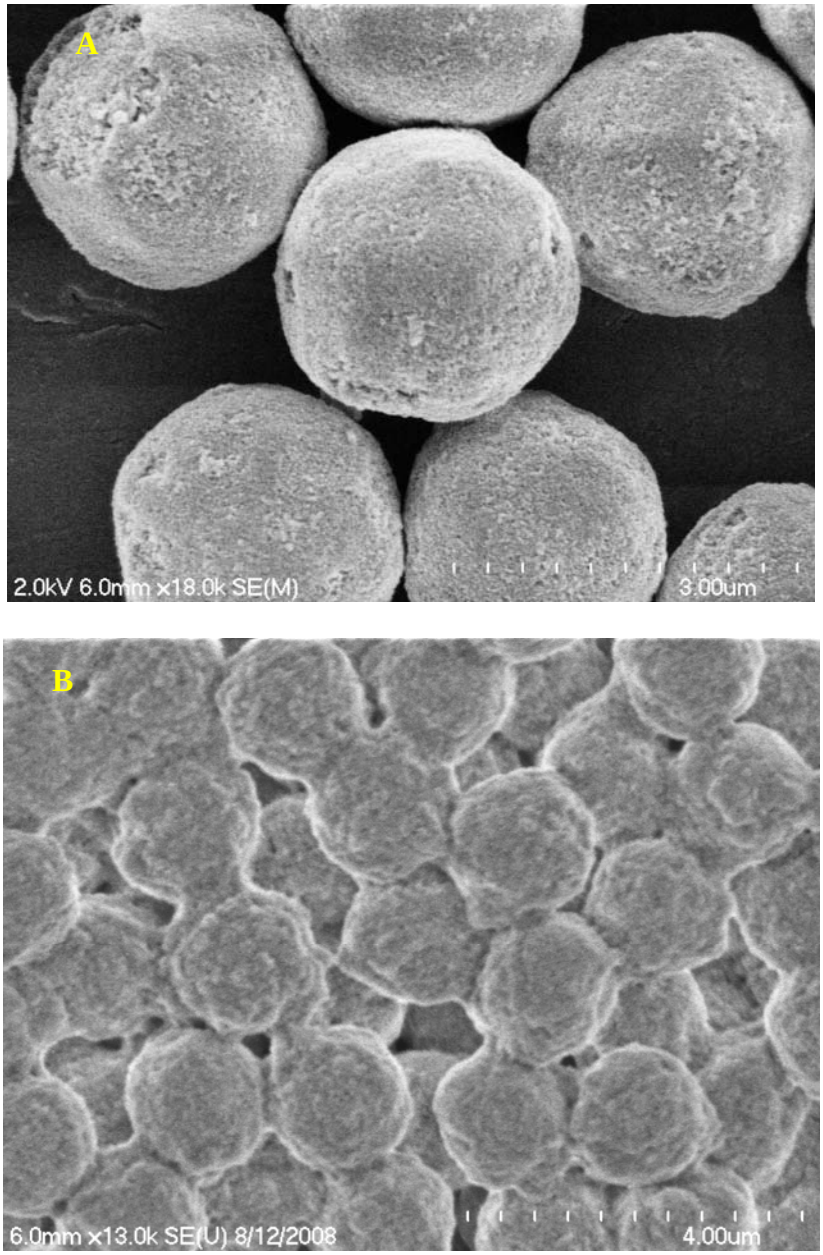

Figure 2-34: Comparison of the particle surface roughness. A) 2.6 μm Kinetex B) 5 layer particles

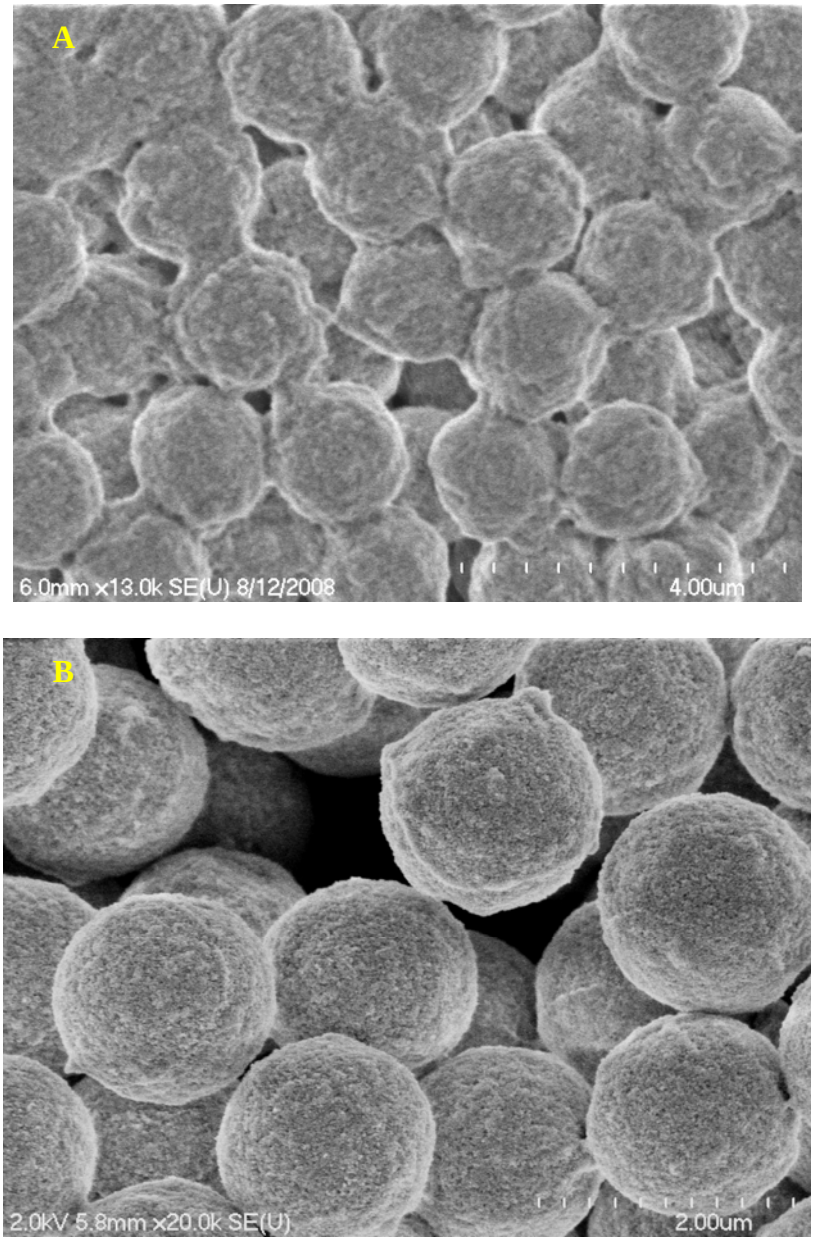

Figure 2-35: Comparison of original 1.7 μm particles (A) and particles with revised conditions based on experimentation contained within this chapter (B)

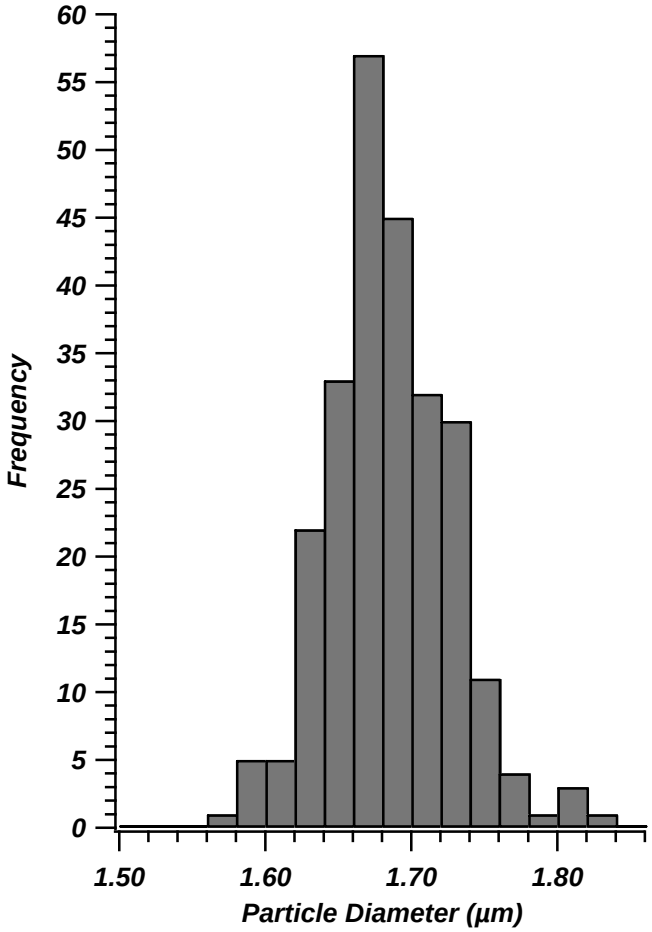

Figure 2-36: Particle size distribution of 1.4 µm core particles after 3 coating steps with revised synthesis parameters determined within this chapter.

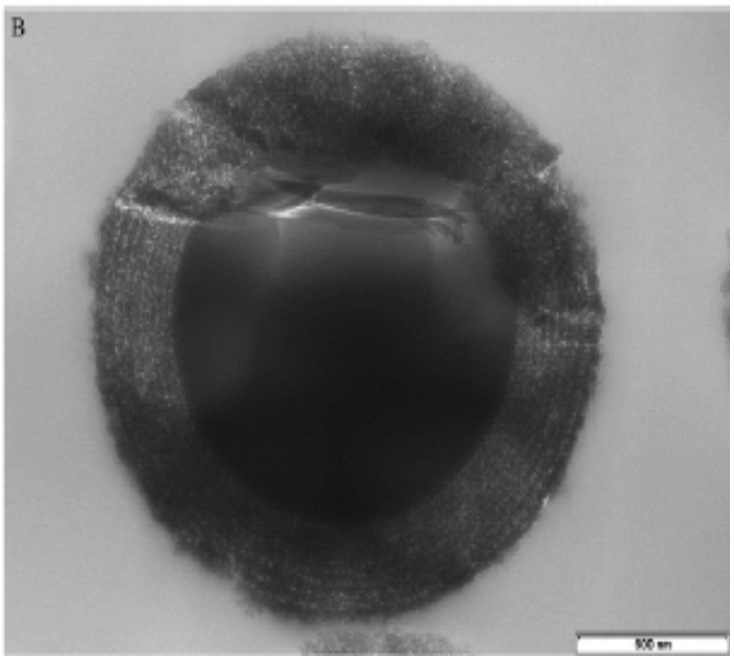

Figure 2-37: Illustration of the ring structure of the porous layer of 1.7 μm Kinetex particles.[27]

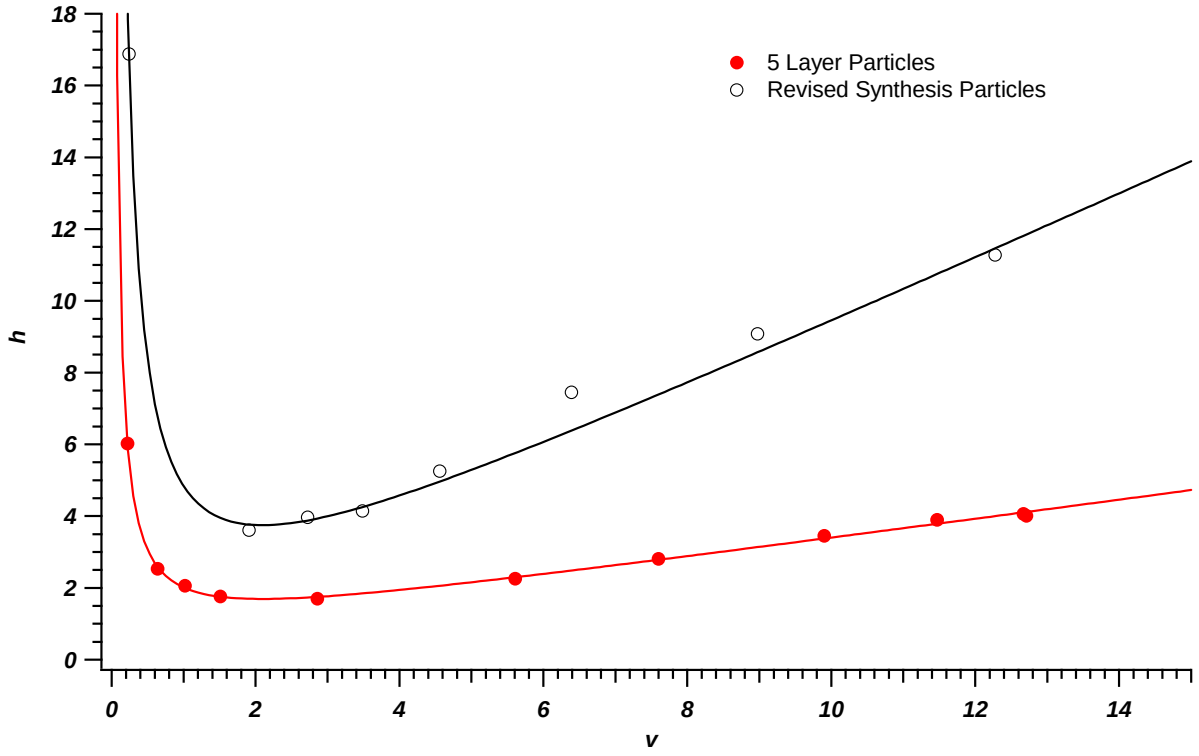

Figure 2-38: Hydroquinone chromatographic performance comparison of 5 layer particles and particles synthesized by the revised conditions. 30 µm i.d. columns run in 70/30 water/ACN with 0.1% TFA

CHAPTER 3: SYNTHESIS AND CHROMATOGRAPHIC EVALUATION OF 1.1 μm SUPERFICIALLY POROUS PARTICLES

3.1 INTRODUCTION

3.1.1 Initial Developments and Areas for Improvement

Pellicular particles were introduced by Horvath *et al.* to carry out efficient separations with lower pressure requirements for fast analyses.[1,2] These materials showed performance advantages over totally porous particles of similar size, but have been overshadowed until recently.[3, 4] Current development of superficially porous particles by J.J. Kirkland has led to the commercialization of the product termed Halo. Following the initial development of these particles, most other manufacturers have released similar products due to the improved chromatographic efficiency of superficially porous particles over totally porous particles.[5, 6]

While there have been significant advances in the development of superficially porous particles in recent years, there are still areas where improvement is possible. To date, the smallest superficially porous particles available have a particle diameter of 1.7 μm (Kinetex by Phenomenex). Further improvements to chromatographic performance, however, can be expected by moving to even smaller diameter particles. Based on the dependence of the *A*-term and *C*-term on the particle diameter, reduction in the particle diameter should lead to greater efficiency.[7]

$$A \propto d_p \tag{3-1}$$

$$C \propto d_p^2 \quad (3\text{-}2)$$

While decreasing the particle diameter leads to an increase in the required system pressure, the advent of ultrahigh pressure liquid chromatography has made this improvement in efficiency possible.[8] Another area with potential for improving efficiency is the porous layer thickness of the particle. It has been proposed by Horvath *et. al.* that a porous layer volume less than 35% of the total particle volume will be most beneficial based on the balance of maintaining analyte resolution and increasing efficiency.[9] Furthermore, based on the diffusion rate of macromolecules, it is predicted that the thinner the porous layer the more efficient the mass transfer, and therefore the better the chromatographic performance of the column.[9] While efficiency is improved with a very thin porous layer, the drawback of this is the decrease in sample loading capacity. A balance between these two variables must be achieved to give the most desirable performance characteristics.

3.1.2 Desirable Silica Characteristics

To enable uniform surface coverage of polyelectrolyte and colloidal silica, particle surface charge and aggregation must be regulated. The hydroxylated surface of a silica particle has been found to have a point of zero charge at a pH of approximately 2.[10] At and below this pH the positively charged polyelectrolyte would not be attracted to the neutral silica surface and vice versa in the case of colloidal silica. Increasing the pH to 6, the negative surface charge concentration increases, but remains low. Past this point, up to a pH of 10.7 the negative surface charge is found to dramatically increase, but at pH values above 8 the silica begins to dissolve so caution must be exercised.[10] To allow for complete surface coverage by the polyelectrolyte and colloidal silica, the charge density must be finely tuned through pH to allow enough charge for electrostatic attraction, but not too much

surface charge which would promote repulsion between the silica particles not allowing colloidal silica adhesion.

A further synthesis concern is colloidal silica particle aggregation. While particle aggregation through the formation of siloxane bridges is not typically found for silica particles larger than 100 nm, the colloidal silica used in the synthesis procedure is susceptible to this behavior. As the sol concentration is increased there is a marked rise in viscosity and long-term instability leading to gelling. Furthermore, at any concentration the formation of a gel occurs rapidly around a pH of 5-6, but above a pH of 7 no gel is formed because the particles are highly charged. There is temporary stability at pH values between 1.5-3, but gel formation occurs at a variable rate depending on the size of the colloidal silica particles.[10] This particle aggregation dependence on pH must be monitored to produce uniformly coated superficially porous particles without the presence of colloidal silica aggregates.

3.1.3 Particle Functionalization

The stationary phase ligand surface coverage and the degree of homogeneity on the particle surface have been found to vary depending on the ligand used and the reaction conditions. This functionalization variation leads to inconsistency in retention and band broadening contributions to the theoretical plate height. The best bonding reaction conditions produce a surface coverage, χ, of 4 μmol/m^2, which represent coverage of only 50% of the free silanols on the surface.[11]

$$\chi = \frac{\%C}{100 \cdot nC \cdot 12 \cdot SSA \cdot \left(1 - \frac{\%C}{100} \cdot \frac{MW - 1}{nC \cdot 12}\right)} \tag{3-3}$$

The percent carbon from elemental analysis, *%C*, number of carbons in the attached ligand, *nC*, specific surface area, *SSA*, and molecular weight of the attached ligand, *MW* are used to calculate the bonding surface coverage of the particles. The presence of the ligand side groups prevents higher surface coverage due to steric hindrance. Variation in the surface coverage and homogeneity occurs when the water content of the solvents is not controlled, there is water remaining on the particle surface, or multidentate ligands are used.[12-13] Multidentate ligands such as di-functional silanes produce attachment with only one siloxane bond one-half of the time while the other half are bonded by two siloxane bonds.[11] This results in no greater surface coverage, but produces slightly more stable bonding chemistry. Furthermore, due to the presence of an additional leaving group on the di-functional ligand with only one siloxane bond, an additional silanol group is produced. Therefore the number of free silanols is the same as for bondings using a mono-functional silane. When a tri-functional silane is used, the amount of free silanols is found to be greater than that for mono- and di-functional slianes since tridentate siloxane bond formation is impossible.[11] Further variation of the bonded phase occurs when di- and tri-functional silanes are used due to the ability of polymerization, particularly when water is present in the system. For these reasons, a mono-functional silane is typically used to ensure production of a reproducible, dense, and homogeneous monomeric layer.[12]

These variations in surface bonding have been found to affect the chromatographic performance of these materials through analyte adsorption to silanols, mass transfer resistance, and variation in column packing density.[11, 14] The presence of acidic silanols leads to adsorption of basic compounds leading to increased tailing and a higher density of surface silanols has been found to lead to a more densely packed column.[11, 12, 14] One

mechanism for reducing the number of silanols after functionalization is endcapping with trimethylchlorosilane, which has been found to systematically reduce the number of silanols and reduce surface heterogeneity.[15] An additional consequence of the bonding chemistry variations is the effect on the mass transfer resistance. When multi-functional silianes are used there is a higher likelihood of hindered mass transfer leading to a decrease in chromatographic efficiency.[11, 14]

In addition to the number of bonding sites of the ligand, variations in performance can occur due to the particle pre-treatment, reaction solvent, and the selected base activator. Particles which have been previously heat treated require pre-treatment with a strong acid to allow efficient stationary phase ligand surface coverage.[16] The heating of silica causes the condensation of silanols to form siloxane bridges, which will reversibly form silanols over time. To produce a reproducible, high surface coverage bonding, the silica particles must be fully re-hydroxylated to prevent formation of silanols over time. Additionally, it has been found that the reaction solvent has a significant influence on the kinetics of the silanization reaction. It was found that N,N-dimethylformamide and dichloromethane showed faster reaction kinetics and the greatest surface coverage.[17] To a lesser extent, but still important to the reaction is the base activator used. Imidazole has been favored due to the formation of reactive imidizole intermediates.[17]

Taking all of these reaction variations and resulting bonding densities into consideration, the chromatographic performance can greatly vary with minor changes in the reaction conditions. Of particular interest for studies within this chapter are the differences between the mono- and tri-functional silane and the reactivity of the base activator in relation to chromatographic performance.

3.1.4 Column Efficiency Relationship to Aspect Ratio

The aspect ratio of the column (d_c/d_p) has been found to greatly affect the chromatographic performance of a column.[18-30] While one study has shown that the aspect ratio does not affect the chromatographic efficiency or flow resistance, the remainder show significant improvements in efficiency as the aspect ratio is decreased.[27] The decrease in the aspect ratio has been associated with a disproportionate decrease in the reduced plate height predicted to be due to variations in the transcolumn porosity profiles.[18-20, 24 ,26] Two distinct packing regions within the column bed are found to be present. A more ordered, open packing structure near the column wall, and a random, densely packed region near the center of the column.[18, 19, 24, 26] From studies by Knox and Parcher it was found that the ordered wall region subsides after 6 particle diameters from the wall.[25] Other studies have shown persistence of this wall region over a greater number of particle diameters, but improved performance is still observed when decreasing aspect ratio independent of the specific location of the transition point.[19, 24] The removal of the random, densely packed core region at low aspect ratios allows for a more homogeneous radial velocity profile leading to a decrease in the *A*-term. Furthermore, the distance an analyte has to diffuse to sample all representative flow paths is inherently smaller when decreasing the column inner diameter, thereby contributing to the decrease in the *A*-term contribution to the theoretical plate height. Further variation in the packing structure at large aspect ratios has been found to be due to the presence of particle size segregation.[26] At higher aspect ratios, smaller particles are found to selectively pack against the column wall leading to even greater variation in the flow profile which leads to a decrease in performance.

According to the majority of aspect ratio studies it was found that as the aspect ratio is decreased, the packing density also decreases due to the reduction of the densely packed core region. The effect of the packing density on column performance, particularly the *C*-term, has been found to vary. Studies by Hsieh and Jorgenson found that the *C*-term increased with decreasing packing density.[18] This was attributed to the increased distance an analyte must travel between particles due to the lower packing density, which slows down the rate of mass transfer. Contrary to this, studies by Karlsson and Novotny and Kennedy and Jorgenson found that as the porosity was decreased there was a significant decrease in the *C*-term due to the coupled nature of the A-term and *C*-term.[24, 28] Based on these findings, column packing variations should be diminished as the aspect ratio approaches one. This allows for true assessment of the efficiency of the packing material independent of the packing process.

3.1.5 Band Broadening Relationship to Capacity Factor

The capacity factor, *k'*, has been found to vary as a function of pressure and to affect the chromatographic efficiency through the *B*- and *C*- terms of the van Deemter equation.[31-34] The *A*-term does not have any dependence on the *k'* and thus will not vary with *k'* changes.

The expanded B-term shows the dependence on the *k'*:

$$B = 2\gamma_M D_M + 2k'\gamma_S D_S \tag{3-4}$$

Where γ_M and γ_S are the obstruction factors that account for the diffusion restricted by the particles in the mobile phase and stationary phase, respectively; and D_M and D_S are the diffusion coefficients in the mobile phase and stationary phase, respectively. Therefore, as the *k'* is increased the *B*-term is found to increase.[33, 35, 36]

In addition to the *B*-term, the *C*-term also increases with *k'*.[31, 34] The contributions to the resistance to mass transfer term are from the mobile phase, stationary phase, and stagnant mobile phase. Each of these contributions to the *C*-term reveals a dependence on the *k'*.

$$C_M = \frac{(1 + 6k' + 11k'^2)d_p^2}{(1 + k')^2 D_M \mathrm{X}} \tag{3-5}$$

$$C_S = \frac{2k' d_f^2}{3D_S (k' + 1)^2} \tag{3-6}$$

$$C_{MSt} = \frac{(1 - \phi + k')^2 d_p^2}{30(1 - \phi)(1 + k')^2 \gamma' D_m} \tag{3-7}$$

Where d_p is the particle diameter, d_f is the stationary phase film thickness, X is the packing structure parameter, ϕ is the fraction of mobile phase stagnant within the pores of the particles, and γ' is the intraparticle obstruction factor. As *k'* increases, both the C_M and C_{MSt} terms continue to increase. The C_M term will increase at a faster rate due to the larger *k'* expression in the numerator. The C_S term increases rapidly at low *k'* values, but as *k'* continues to increase a maximum will be reached and then begin to decrease. As seen in Figure 3-1, the total *C*-term contribution rapidly increases at low *k'*, but then levels off at higher *k'* values. For the column packing densities and analytes used in this study the *k'* values are less than 1.5, which is in the rapidly changing region indicating that small changes in the observed *k'* values should also show large variation in the *C*-term contribution. While increased packing density theoretically indicates decreased performance, experimentally the

observed relationship between the packing density and column performance does not consistently indicate a direct relationship.[18, 31]

3.2 MATERIALS AND METHODS

Modifications to the Kirkland protocol were made to provide a more suitable synthesis of smaller diameter superficially porous particles that meet the criteria of monodisperse particle size and robust particle structure.[6] The particles were synthesized by alternating a layer of positively charged polyelectrolyte and negatively charged colloidal silica on a non-porous silica (NPS) core in a similar manner as discussed in Chapter 2.

3.2.1 NPS Solution pH

NPS particles, 1.0 μm, purchased from Fiber Optic Center Inc. (New Bedford, MA) were heated at 1000°C for 24 hours in a Thermo Scientific Lindberg Blue M Furnace (Waltham, MA) to produce 0.9 μm particles with a particle diameter RSD of 1.7%. The calcined NPS core particles were then re-hydroxylated in 10% (v/v%) aqueous nitric acid under reflux conditions for sixteen hours. The particles were washed with deionized water until the pH of the aqueous solution was equal to approximately 5 and then dried under heated vacuum at 80°C for sixteen hours. To evaluate the particle surface coverage dependence on pH, a portion of the 10% (w/w%) aqueous NPS core solution was adjusted to pH 2.3 with 10% (v/v%) aqueous nitric acid while the remaining NPS core solution was used with no pH adjustment. After one coating step, particles were evaluated for surface coverage and uniformity using scanning electron microscopy (SEM).

3.2.2 Polyelectrolyte Layer

To determine the effect of varying the type and molecular weight of polyelectrolyte, a 0.5% (w/w%) aqueous solution of polyelectrolyte was prepared. The polyelectrolytes

investigated (Figure 3-2) were low molecular weight poly(diallydimethylammonium chloride), 100-200 kDa, (LMW PDDA); high molecular weight poly(diallyldimethylammonium chloride), 400-500 kDa, (HMW PDDA); polyethylenimine, 2 kDa, (PEI); low molecular weight poly(allylamine hydrochloride), 17 kDa, (LMW PAH); and high molecular weight poly(allylamine hydrochloride), 65 kDa, (HMW PAH). All polyelectrolytes used were purchased from Sigma-Aldrich (St. Louis, MO). The polyelectrolyte solution was added to NPS core solution without pH adjustment of the NPS core solution at the ratio of 5:1 (w:w) and stirred for ten minutes. The solution was washed in triplicate by adding 30 mL deionized water for every 100 mg of particles to a centrifuge tube, shaken thoroughly, and particles pelleted by centrifugation. The growth rate, surface coverage, and particle size distribution were determined for each case based on SEM images.

The effect of polyelectrolyte solution concentration was investigated using LMW PDDA solution concentrations of 1.0%, 0.5%, 0.1%, and 0.05% (w/w%). The growth rate, surface coverage, and particle size distribution was determined at each concentration based on SEM images.

The effect of ionic strength of the polyelectrolyte solution was investigated by preparing 0.5% (w/w%) LMW PDDA solutions at 0.2 M, 0.4 M, and 0.6 M NaCl. The growth rate, surface coverage, layer thickness, and particle size distribution for each sample was determined at each salt concentration based on SEM images.

3.2.3 Colloidal Silica Layer

The colloidal silica solutions used were Nyacol NexSil8 (8 nm), Nyacol NexSil85 (85 nm), Nyacol NexSil125 (125 nm) (Nyacol Nano Technologies Inc.; Ashland, MA), Ludox AS-30 (12 nm) (Sigma-Aldrich; St. Louis, MO), Nalco 1030 (13 nm), and Nalco 1060 (60

nm) (Nalco; Chicago, IL). A 10% (w/w%) solution of colloidal silica was combined with the LMW PDDA coated NPS cores at a ratio of 1:1 (w:w) and stirred for 15 minutes. The solution was then washed in triplicate by adding 30 mL deionized water for every 100 mg of particles to a centrifuge tube, shaken thoroughly, and particles pelleted by centrifugation. One coating layer for each colloidal silica size was prepared. Visual examination of surface uniformity and colloidal silica polydispersity were assessed by SEM. In addition to type of colloidal silica solution, the relationship between pH of the colloidal silica solution and the surface coverage was investigated by completing one coating step each with Ludox AS-30 colloidal silica solution at pH 3.5 and pH 9.5. The pH was adjusted with 10% nitric acid (v/v%) for the pH 3.5 solution. The surface covered was assessed visually at each pH by SEM.

3.2.4 Drying Method

Particles were dried at 25°C, 80°C, 105°C, and by vacuum lyophilization. A portion of each was placed on an aluminum SEM stub and images collected. Particles dried under each condition were visually inspected for surface uniformity and agglomeration.

3.2.5 Sintering Temperature

Following drying, the polyelectrolyte was removed by heating at 540°C for sixteen hours and then sintered. A batch of particles was sintered at various temperatures to determine the effect on particle strength, specific surface area, and pore size. The particles were heated in the furnace at 825°C, 900°C, 925°C, 945°C, and 1000°C for eighteen hours.

3.2.6 Particle Mechanical Stability Study

A portion of the sample sintered at each temperature was used to make a 3 mg/mL slurry solution in distilled water. Each solution was sonicated for 5, 10, 30, 60, 90, and 120

minutes using a Cole Parmer 8891 Sonic Bath (Vernon Hills, IL) to evaluate particle stability. At each time point, a portion of the sample was removed and placed on an aluminum SEM stub for imaging. At each temperature and timepoint 100 particles were counted. If a particle had any sign of a bare region, the particle was classified as a "bare" particle.

3.2.7 Particle Structure Characterization

Particle size distribution, growth rate, and surface coverage were evaluated by placing a sample aliquot on an aluminum SEM stub for imaging using a through-the-lens (TTL) detector on a Hitachi S-4700 cold cathode field emission SEM (Tokyo, Japan). Using these images, Image J software produced by the National Institute of Health (Bethesda, MD) was used to measure the diameter of 250 particles.

The porous layer thickness percent, T_p, was calculated as follows:

$$T_p = \frac{d_p - d_{core}}{d_p} \times 100 \tag{3-8}$$

where d_p is the number average total particle diameter and d_{core} is the NPS core number average diameter. The layer thickness growth rate, r, was calculated based on the number of coating steps, N, by:

$$r = \frac{d_p - d_{core}}{2} \times \frac{1}{N_C} \tag{3-9}$$

Elemental analysis was performed using a Perkin Elmer CHN/S O elemental analyzer Series 2400 instrument (Waltham, MA).

3.2.8 Zeta Potential

The zeta potentials of 10% (w/w%) aqueous solutions of AS-30 colloidal silica were tested at the pH values of 2, 3, 4, 6, 8 and 9 using a Malvern Zetasizer Nano ZS

(Worcestershire, UK). The pH was adjusted with 10% nitric acid (v/v%) for pH values below nine.

To determine the rate of uptake of polyelectrolyte by NPS, a 10% (w/w%) aqueous core solution was combined with a 0.5% (w/w%) aqueous solution of either HMW PDDA or LMW PDDA at a ratio of 1:5 (w:w). An aliquot of each sample was removed at 1, 5, 10, 15, 30, 45, 60, and 300 minutes and immediately washed with deionized water. Each sample was washed in triplicate by adding 30 mL deionized water for every 100 mg particles to a centrifuge tube, shaken thoroughly, and particles pelleted by centrifugation. The zeta potential of each sample was tested using a Malvern Zetasizer Nano ZS (Worcestershire, UK).

3.2.9 Surface Area and Pore Volume Measurements

The surface area, pore volume, and pore diameter measurements were carried out by Waters Corporation (Milford, MA) using a Micromeritics ASAP2420 (Norcross, GA) for Brunauer, Emmet, Teller (BET) analysis. Pore size and volume measurements by mercury intrusion were carried out by Waters Corporation (Milford, MA) using a Micrometrics AutoPore IV 9500 series pore size analyzer (Norcross, GA).

3.2.10 Particle Bonding and Endcapping

The first batch was used for initial chromatographic performance assessment. The second batch was bonded using a monofunctional silane rather than a trifunctional siliane for the determination of the relationship between the bonding method and chromatographic performance. The first batch was bonded according to U.S. patent 20020070168 with n-octadecyltrichlorosilane (Gelest; Morrisville, PA) in toluene with pyridine as the base activator.[37] Both toluene and pyridine were purchased from Sigma-Aldrich (St. Louis,

MO). The particles were then refluxed in a 4.5/1 (v/v) solution of acetone/0.12 M aqueous ammonium acetate to remove any excess polymerized bonding agent. Acetone and ammonium acetate were purchased from Thermo Fisher Scientific Inc. (Waltham, MA). The particles were then endcapped with trimethylchlorosilane (Gelest; Morrisville, PA) in toluene with pyridine as the base activator. Excess endcapping agent was removed by refluxing the particles in a 4.5/1 (v/v) solution of acetone/0.12 M aqueous ammonium acetate. This bonding and endcapping procedure was used for all studies except in the bonding method comparison study.

The second batch of particles was bonded following US Patent 201000761.[38] The particles were bonded with n-octyldecyldimethylchlorosiliane (Gelest; Morrisville, PA) in toluene with imidazole as the base activator. Both toluene and imidazole were purchased from Sigma Aldrich (St. Louis, MO). The particles were then endcapped with trimethylchlorosilane in toluene with imidazole as the base activator.

3.2.11 Column Packing

Fused silica capillary tubing (Polymicro Technologies, Inc., Phoenix, AZ) with an inner diameter (i.d.) of 30 μm and an outer diameter of 360 μm was used to pack all columns except two columns which used a 20 μm inner diameter (i.d.) to evaluate the effect of column i.d. on chromatographic performance. The columns were prepared with outlet frits as outlined in Chapter 2. The procedure for packing capillary columns has be previously described.[11, 39-41] Briefly, the particles were suspended in a slurry solvent at a concentration of 3 mg/mL. The slurry solvents investigated were acetone, methanol, hexane, 67:33 hexane:acetone, 10 mM triethylammonium phosphate (TEAP) in acetone, and solvent X. Solvent X is a mixture of solvents readily available, but is a proprietary solvent suggested

by Waters Corporation. Therefore, the exact preparation cannot be divulged. All solvents were purchased from Fisher Scientific (Waltham, MA) and were filtered with a 0.2 μm PTFE filter before use. The slurry was sonicated for 10 minutes using a Cole Parmer Ultrasonic Cleaner 8891 (Vernon Hills, IL). A packing reservoir was then filled with the slurry solution and acetone was used as the pushing solvent. The capillary column was placed in a UHPLC fitting and secured to the column packing apparatus. Column packing was initiated at 3000 psi and as the bed began to form the pressure was gradually increased until reaching 30,000 psi at a rate of 3000 psi per centimeter of bed growth. The packing process was stopped by slowly releasing the pressure when the desired column length was reached.

After the desired column length was reached, the column was pressurized to ~45,000 psi and flushed with several column volumes of 50/50 water/ACN with 0.1% trifluoroacetic acid (TFA) mobile phase (Fisher Scientific; Waltham, MA). The pressure was slowly released and re-pressurized to ~10,000 psi. A temporary inlet frit was then put in place using a heated wire stripper (Teledyne Interconnect Devices, San Diego, CA). The column was then clipped to the desired final length. The permanent inlet frit was then prepared using a procedure described by Maiolica et. al..[42] The column inlet was gently pressed on a glass microfiber filter (Reeve Angel; Clifton, NJ) that was previously wetted with 1:1 (v:v) ratio of potassium silicate (Kasil) and formamide. The Kasil was used as received from PQ Corporation (Valley Forge, IA) and formamide was from Sigma Aldrich (St. Louis, MO). After a few minutes, the glass microfiber filter had hardened, but to ensure it could withstand the running pressures, the frit was set in place using an electric arc device.

To determine the effect of packing pressure on column performance and packing density, a column was packed at lower pressure in methanol. The column was packed as

previously stated but the final packing pressure was only 15,000 psi, and the flushing pressure was 30,000 psi. After chromatographic analysis, this column was then cut in half and the outlet was re-fritted with a Kasil frit. This short column was then analyzed.

3.2.12 Column Evaluation

The detailed experimental set-up used to perform isocratic UHPLC has been previously described and was carried out as described in Chapter 2.[32, 40, 41, 43]

The mobile phase used for chromatographic evaluation was 80/20 water/ACN with 0.1% TFA. The isocratic test mixture contained L-ascorbic acid, which served as the dead time marker, hydroquinone (HQ), resorcinol (R), catechol (C), and 4-methyl catechol (4MC). The concentration of each sample in the test mixture was ~200 μM.

The columns that were used for this experiment were evaluated on the basis of chromatographic performance and retentivity. Column performance analysis was carried out as described in Chapter 2.

3.3 RESULTS AND DISCUSSION

3.3.1 Synthesis

Using the parameters suggested by Kirkland as starting conditions and the knowledge base from working with 1.7 μm particles to develop the 1.1 μm superficially porous particles, problems related to non-uniform coating and particle agglomeration were encountered, Figure 3-3.[6] To overcome these difficulties, the synthesis parameters were investigated and altered accordingly.

3.3.1.1 Effect of NPS Solution pH

Based on the 2007 Kirkland patent, it was suggested to adjust the pH of the NPS core solution to a pH of 2.3.[6] The hydroxylated surface of silica has a point of zero charge at a

pH of 2.0, which would indicate that very little attraction between the silica and the polyelectrolyte would occur at the recommended pH.[11] As the pH of the silica solution is increased, the negative surface charge is also increased. Initial studies were carried out using the recommended pH of 2.3; however, frequently partially or completely bare particles were observed. When the pH of the core solution was left unadjusted (pH ~ 5), particles were consistently characterized by a greater surface coverage, Figure 3-4. As predicted, a higher pH solution forms a higher density of negative surface charge on the silica particles which more strongly attract the positively charged polyelectrolyte leading to greater colloidal silica surface coverage.

3.3.1.2 Effect of Polyelectrolyte Molecular Weight

The molecular weight, type, concentration, and ionic strength of the polyelectrolyte solution was evaluated. Although it was initially thought that using a higher molecular weight polyelectrolyte would lead to a thicker porous layer per coating step and thus a quicker synthesis process, the polyelectrolyte molecular weight may likely result in particle agglomeration for smaller diameter particles. Kirkland found that using 100–200 kDa PDDA led to five layers of nanoparticles, while 400–500 kDa PDDA led to fifteen layers of nanoparticles per coating cycle.[6] While this has been seen experimentally, studies of polyelectrolytes indicate that the higher the net charge of the polymer, the less polyelectrolyte that will be adsorbed on the substrate due to electrostatic repulsion between the polymer chains.[44] In contrast to the results obtained by Kirkland, our results indicate no difference in growth rate or particle size when coating particles with low versus high molecular weight PDDA, Table 3-1A. This may be explained by the self limiting nature of polyelectrolyte adsorption. Polyelectrolyte is only adsorbed until the NPS surface charge is

neutralized.[44] Therefore, independent of the polyelectrolyte molecular weight, roughly the same thickness of polyelectrolyte is coated on the NPS surface, Figure 3-5. This is further confirmed by the similar zeta potential polyelectrolyte uptake curves for each polyelectrolyte molecular weight, Figure 3-6. The particles coated with HMW PDDA were also found to yield a wider particle size distribution following coating with colloidal silica and were found to have areas of non-uniform colloidal silica adhesion and agglomeration as shown in Figure 3-7. These results correlate well with previous observations that as the molecular weight of the polyelectrolyte is increased, aggregates begin to form and in variable amounts, Figure 3-8.[45] From previous studies it has also been indicated that the type and pH of colloidal silica can lead to varying amounts of aggregates on the surface as will be discussed in section 3.3.1.7.

In comparison to the molecular weight studies with PDDA, two molecular weight variations of PAH, 17 kDa and 65 kDa, were investigated, both of which are much lower molecular weight than LMW PDDA. The growth rate and particle size was greater for both PAH variants when compared to PDDA and greater variation was found between the two molecular weights of PAH compared to PDDA, Table 3-1A.

3.3.1.3 Effect of Type of Polyelectrolyte

Comparing the different polyelectrolytes based on their structural characteristics rather than molecular weight also indicate sources of potential differences in coating thickness. The growth rate and particle size obtained when using PEI were in line with the values for PAH, but were greater than that for PDDA, Table 3-1A. The thicker coat obtained with PAH and PEI can be accounted for by their higher charge densities. As the charge density of a polyelectrolyte is increased, a more extended conformation is formed due to

electrostatic repulsion, which would allow for greater access to colloidal silica.[46, 47] Both PEI and PAH coated particles also showed a wider particle size distribution and were visibly less uniform than particles coated with PDDA, Figure 3-9 When an additional coating step was added to the 1.14 μm LMW PDDA coated particles, the diameter grew to 1.22 μm with a particle size distribution RSD of 2.2%. This indicates that the narrower particle size distribution of PDDA coated particles is not due to the smaller particle diameter after three coating steps. The charge on both PAH and PEI are dependent on the solution pH, ionic strength, and presence of other charged species, whereas the charge on quaternary polycations, such as PDDA, is independent of these variables.[48] Based on the concentration of ionic species in the solution, the charge and therefore the conformation of PAH or PEI can vary, which could lead to variations in surface coverage. While the growth rate was greater for PEI and PAH coated particles, the narrower particle size distribution and particle surface uniformity produced when using PDDA was considered to be more important in our synthesis method. Having a naturally narrow particle size distribution has the benefit of requiring no complicated sizing method after the synthesis is complete.

3.3.1.4 Effect of Polyelectrolyte Concentration

As previously mentioned, synthesizing smaller diameter particles may require the concentration of the polyelectrolyte solution to be decreased to reduce particle agglomeration. The concentration of 0.5% (w/w%) was suggested in the literature and was found to work well for 1.7 μm superficially porous particles.[6] Therefore, this was the initial starting concentration for our synthesis of 1.1 μm superficially porous particles. When the concentration of LMW PDDA was decreased to 0.1% and 0.05% (w/w%), particles with bare regions resulted, Figure 3-10. In contrast, increasing the concentration to 1.0% (w/w%)

showed particles with a greater growth rate, but also a slightly wider particle size distribution as shown in Table 3-1B. There were minimal signs of particle agglomeration at the higher concentration, but again the advantage of having a narrower particle size distribution was held in higher regard than the growth rate. Therefore, a concentration of 0.5% (w/w%) was used for all further studies.

3.3.1.5 Effect of Polyelectrolyte Solution Ionic Strength

The last study that was carried out with respect to the polyelectrolyte solution was the effect of the solution ionic strength on surface coverage and growth rate. The ionic strength is believed to affect the thickness of the coating layer as a result of shielding the charge along the polyelectrolyte chain by ions in the solution. This shielding effect causes the polyelectrolyte to become thicker in a globule conformation rather than a coil adsorbed parallel to the substrate when no salt is present, Figure 3-11.[44, 49] The extent of shielding determines the area of the chain exposed to the colloidal silica and therefore the thickness of the porous layer.[6] While it may be advantageous to increase the coating thickness and reproducibility, it has also been found that increasing the ionic strength of the solution leads to an increase in surface roughness.[44] Based on previous studies by others where the ionic strength of the solution was adjusted to increase layer thickness, the NaCl concentration range of 0.02 – 2.00 M was evaluated.[6, 49, 50] When the range of 0.0-0.6 M NaCl was investigated, no advantages in growth rate were noted with the use of LMW PDDA, Figure 3-12. After one coating step, the particle diameter for the solution without salt addition and for the 0.6 M salt solution was found to be 1.01 μm and 1.02 μm, respectively. An additional coating step did not lead to any significant difference in the particle diameter or particle size distribution at 1.08 μm (3.2% RSD) without salt addition and 1.10 μm (3.6% RSD) for the

0.6 M salt solution Visually, it was seen that as the salt concentration was increased, the presence of webbing between particles was more evident. While literature had suggested that the surface roughness would increase as the ionic strength was increased, there was no indication of this trend. Since there was no significant increase in porous layer thickness with increased ionic strength, in order to reduce the possibility for particle contamination from sodium in the salt solution in subsequent studies, no salt was added to the polyelectrolyte solution.

3.3.1.6 Effect of Type of Colloidal Silica

Next, the effect of the size and manufacturer of the colloidal silica on the surface coverage and uniformity was assessed. The attributes of colloidal silica that are desirable are a monodisperse solution that produces a uniform, repeatable surface coverage. As seen in Figure 3-13, all colloidal silica solutions below 15 nm were found to have a narrow particle size distribution and produced a uniform surface coverage. Independent of the manufacturer, as the colloidal silica size was increased, the degree of polydispersity of the colloidal silica and the resulting superficially porous particles was found to increase, Table 3-2. As the polydispersity of the colloidal silica increases it is more difficult to form a smooth surface coverage due to the variation in size of the colloids. Initial studies were performed with the 12 nm colloidal silica based on the monodisperse nature of the colloids and the uniform surface coverage.

3.3.1.7 Effect of Colloidal Silica Solution pH

The next point of evaluation was the effect of colloidal silica solution pH on NPS core surface coverage. It was observed that the colloidal silica solution quickly formed a gel as the pH was lowered from the storage pH of ~9 to the recommended pH of 3.5. This

indicated that the colloidal silica was forming aggregates at the lower pH values. The zeta potential was found to become more positive, closer to 0 mV, as the pH became more acidic, Table 3-3. Lower zeta potential values indicate a lower charge density on the particle leading to a decrease in charge repulsion between particles.[51] Since colloidal silica aggregation was not an attribute that we felt would help lead to uniform particles, it was believed that a more uniform coating would be obtained if the solution pH was left unadjusted at a pH of ~9. However, as seen in Figure 3-14, the high pH solution was found to not coat the polyelectrolyte covered NPS cores. These findings indicate that highly charged colloids at unadjusted pH may neutralize more charge on the polyelectrolyte per adhered colloidal silica particle or have such a high electrostatic repulsion that the individual colloidal silica particles cannot come in close proximity of each other leading to low colloidal silica surface coverage. To produce a high density surface coating without signs of aggregates on the particle surface, a pH of 3.5 was used, adjusted immediately before use.

3.3.1.8 Effect of Drying Method

After the desired porous layer thickness is achieved, the particles are dried before removing the polyelectrolyte. Particles were dried at 25°C, 80°C, and 105°C. As seen in Figure 3-15, bare particles, particle agglomeration, and a decrease in surface uniformity were found to be present at each temperature. There have been studies indicating that heat drying causes surface deformities and leads to a loss in surface area and pore volume for silica materials.[52] It is believed that in heat drying, the water inside the pores is quickly evaporated and pulls off part of the porous shell in the process of vapor formation and evacuation. In addition, bare regions may result from drying the particles in close contact with each other, allowing neighboring particles to pull off the porous layer of its nearest

neighbor as a result of remaining polyelectrolyte. In order to overcome these problems, lyophilization was investigated as a more gentle technique which dries the particles with a solvent layer protecting them from their neighbors. The process of lyophilization has been found to preserve the structure of materials without any shrinkage in contrast to the deformity found due to the rapid removal of water by evaporation.[53, 54] When a portion of the particles was dried by lyophilization, the particles were found to exhibit no sign of agglomeration or bare regions, Figure 3-15-D.

3.3.1.9 Effect of Sintering Temperature

Lastly, based on the initial difficulties with porous layer degradation, it was considered that the recommended sintering temperature of 825°C may not be high enough to produce particles mechanically robust enough to withstand bonding and packing procedures as evidenced by bare particles present when extruding the bed of a capillary column packed with particles sintered at 825°C, Figure 3-16. The goal in increasing the sintering temperature is to increase particle strength without particle melting or reduction in surface area or pore volume. Physical characteristics and particle stability were assessed for particle sinter temperatures of 825°C, 900°C, 925°C, 945°C, and 1000°C. At 1000°C, the surface of the particles was visually melted, and therefore no further physical measurements were made for these particles. While the melting temperature of pure silica is in the range of 1500°C, the presence of impurities such as sodium from the synthesis process can affect their surface properties and in turn lower the melting point.[54, 55] Slightly lower temperatures than 1000°C were investigated, but were found to show visual signs of melting until the temperature was decreased to 950°C. While we did not see visual external signs of melting below 950°C, there may be melting occurring below the surface. Based on the BET

measurements, seen in Table 3-4, it was found that the surface area of the particle decreased as the temperature was increased. This is an indication that there is some interior melting occurring when using the higher sintering temperatures. The particle stability was assessed by carrying out a sonication study to determine if there is a significant increase in stability when a higher sintering temperature is used. For all temperatures, there was limited particle degradation seen due to sonication, with 5% being the highest percentage of bare particles found at 900°C, Table 3-4. Since there was limited loss of surface area and increased particle strength at 945°C, this temperature was determined to be the most suitable.

In comparison to the 1.7 μm particles synthesized and characterized in Chapter 2, the 1.1 μm particles were prepared without pH adjustment of the NPS core solution, with base stabilized, sodium free colloidal silica, and were sintered at 945°C. These variations allowed for production of monodisperse, uniformly coated particles having a smaller total particle diameter.

3.3.2 Particle Structure Characterization

Upon synthesis of 1.1 μm superficially porous particles, physical characteristics such as the particle size distribution and porous layer thickness needed to be determined. From the revised particle synthesis methodology described above, the particle size distribution RSD was 2.2%, Figure 3-17. When the particle size distribution of the Halo 2.7 μm, Kinetex 2.6 μm particles, and Kinetex 1.7 μm particles were measured in our lab the RSD values were found to be 4.0%, 11.7%, and 6.1%, respectively. All these values are much tighter than the particle size distribution for totally porous particles, which is typically in the range of 15-20%.[56] The uniformity of the revised layering process is further indicated when comparing the final particle size distribution to that of the NPS core material, 1.7%.

While the particles synthesized in-house have significantly less surface area than the commercially available products, as seen in Table 3-5, it has been indicated in the literature that the porous layer thickness of commercial products may be too thick for highly efficient separations of macromolecules. According to Horvath and coworkers, it is recommended that the porous layer thickness percent of superficially porous particles be less than 13% of the total particle diameter for large molecules.[9] The porous layer thickness percent of Halo 2.7 μm, Kinetex 2.6 μm, and Kinetex 1.7 μm are 41%, 24%, and 28% of the total particle diameter, respectively, all of which are higher than the recommended porous layer thickness for increased efficiency.[9] The porous layer thickness of the particles synthesized in-house is 18%.

3.3.3 Column Performance

The 1.1 μm particles with 12 nm colloidal silica, synthesized by the revised conditions were then bonded and endcapped to allow column packing and performance assessment. The test analytes were found to be well resolved, Figure 3-18, but peak tailing was found to be present. This tailing was found to also be present for the dead time marker, ascorbic acid, which should have no interaction with the stationary phase and therefore not show any tailing due to the bonding chemistry or the particles. Thus, the peak asymmetry is due to a system band broadening source. When the column was viewed after running, no gap in the bed was found to be visible and the column was found to be correctly seated in the injector. No visible sources of system broadening were found to be present, but small column gaps may be present that were too small to see by eye.

The overall performance of these particles, shown in Figure 3-19 does not meet the theoretical values. The minimum plate height, h_{min} = 4.3, was found to be approximately

double the theoretical value and the *c*-term, 1.06, was approximately five times higher than predicted. There was no observed curvature in the higher linear velocity region indicating that the packing structure was still intact. This was confirmed by images of the extruded column bed, Figure 3-20-B, indicating that there were no particles found to be falling apart. Although, as observed in Figure 3-20-A, there were several regions where voids in the bed were found to be present as indicated by the red circles. These non-uniformities in the bed structure would lead to greater flow path variability, which would increase the *a*-term contribution to the theoretical plate height. While the extent to which these gaps would increase the *a*-term in not exactly known, they do contribute to the higher than expected *a*-term values. When comparing the *a*-term values between the analytes, it is found that the a-term decreases as analyte retention increases rather than remaining constant for all analytes as would be predicted. This trend occurs due to the relaxation of the *a*-term by the *c*-term.[11] As the *c*-term increases, the contribution to the theoretical plate height from the *a*-term is found to decrease due to the coupling of these terms. The presence of coupling between these terms indicates the presence of a poor column packing structure.

The *c*-term increase is associated with regions of the particle bed structure with slower mass transfer. As seen in Figure 3-20-B, there are a large number of particles with colloidal silica aggregates present and while not visible in this image some regions appeared to be melted. The presence of colloidal silica aggregates would lead to regions of greater resistance to mass transfer due to a thicker porous layer and would be exacerbated for the more retained analytes. Further indications of a large mass transfer resistance has been shown for particles with a rugose surface as is the case here.[42] An additional contribution to the resistance to mass transfer would be non-uniform bonding and endcapping. Unreacted

silanols would lead to increased tailing, reducing the column performance, and the presence of polymerized bonding agent would lead to a greater stationary phase film thickness increasing the mass transfer resistance. Both of these characteristics have been found to be present in variable amounts depending on the procedure used to bond and endcap the particles.[58] For silica particles, the greatest surface coverage has been found to cover 50% of the free silanol groups, but is variable depending on the reaction conditions.[11] The increased stationary phase film thickness is most likely found to be present when using a tri-functional silane for the bonding procedure.[59] When using this type of bonding agent, any water present in the reaction will lead to the formation of bonding agent oligimers by intramolecular condensation and allow for attachment to the silica particle.[59] To address these problems, the bonding and endcapping procedure can be varied.

3.3.3.1 Effect of Bonding and Endcapping Method

The initial bonding and endcapping procedure used was based on US patent 20020070168.[37] This procedure uses a tri-functional silane, pyridine as the base activator, and has a washing step. As previously mentioned, the use of a tri-functional silane is more likely to lead to silane polymerization which would increase the stationary phase film thickness and the resistance to mass transfer contribution to the theoretical plate height. Within this method, the washing step which uses an ammonium acetate/acetone mixture to remove any excess silane may also lead to removal of the bonded phase if the washing time is not fine tuned.[37] This would lead to a greater number of free silanols available for analyte interaction, leading to increased peak tailing.

A revised bonding and endcapping procedure was carried out based on US patent 20100076103 to improve the separation efficiency of the particles.[38] This procedure uses a

mono-functional silane, imidazole as the base activator, and does not include a washing step. The use of a mono-funtional silane does not allow polymerized bonding agent to be attached to the silica particle which should produce a more uniform surface coverage. While dimerization of the bonding agent can occur, there are no remaining reaction sites available for attachment to the silica particle. For this reaction, the use of a washing step is not required because surface polymerization is not possible. Furthermore, the more reactive imidazole is used in place of pyridine. A comparison of the separation with particles bonded with each method is shown in Figure 3-21. Both bonding procedures allowed for resolution of the test analytes and little tailing was found to be present. When comparing the peak width between the two methods, it is evident that the new bonding procedure is superior to the original method. The peak width of hydroquinone for the initial bonding procedure and the new procedure was found to be 0.13 minutes and 0.10 minutes, respectively. This translates to 225,000 plates/meter for the old bonding procedure and 375,000 plates/meter for the new bonding procedure. This performance improvement is seen in the reduced parameters plot, Figure 3-22, which shows an improvement of the *a*-term and *c*-term for the new bonding procedure particles. The h_{min} for the particles bonded with mono-functional silane, 2.2, is close to what is predicted, but the *c*-term is still slightly higher than expected. This would indicate that the bonding procedure may require further improvement to decrease the resistance to mass transfer. A further area for improvement is the removal of the colloidal silica aggregates on the surface leading to regions of non-uniform porous layer thickness.

Also, interesting is the observed decrease in the *a*-term for the new bonding procedure particles, but no change in the capacity factor. This would indicate that both columns have the same amount of stationary phase per column volume, which was confirmed

from percent carbon measurements. The initial bonding method and revised method particles were found to have 3.11% and 3.25% carbon, respectively. This performance improvement without an associated change in carbon load may be explained by the number of bonding sites on the bonding agent allowing polymerization, Figure 3-23. The use of a tri-functional silane would produce particles with no additional bonding agent due to polymerization blocking access to unreacted silanols, but would make particles with a greater number of free silanols. It would have been expected that with the change in packing structure uniformity as indicated by the *a*-term, an associated change in packing density would have occurred, but this was not found.[11] Therefore, the likely cause for the improvement in performance was the reduction in free silanols leading to decreased peak broadening.

3.3.3.2 Effect of Column Inner Diameter

The column performance is believed to be highly dependent on the packing structure of the column bed. The inability to properly pack the particles in the column lead to decreased performance, not directly representing the performance of the particles. To determine if the poor performance was related to column packing or directly to the particles, columns with a smaller inner diameter were packed. By decreasing the aspect ratio of the column, the packing is found to have improved radial homogeneity, therefore reducing the contribution of the packing process and allowing for direct determination of the performance of the particles.[18, 19, 60] While an aspect ratio of approximately six is suggested to completely eliminate the radial inhomogeneity, any decrease in aspect ratio should show efficiency improvements if column packing is at fault.[18, 20-23, 61] For two separate batches of particles, the performance was found to improve when decreasing the column inner diameter, Figures 3-24 and 3-25. In both cases there was a drastic improvement in the

a-term indicating that the packing structure uniformity was improved and that the packing process was partly at fault for the higher than predicted reduced plate heights. Between the two sets of particles, there was variation in the effect of the column inner diameter on the *c*-term. It has been found previously that the *c*-term decreases with increasing column inner diameter because the packing density is greater for columns with a larger inner diameter allowing for faster mass transfer.[18] This was not seen for either of the superficially porous particle batches described here, Figure 3-24 and 3-25. For the first batch of particles the *c*-term was found to improve when decreasing the column inner diameter and for the second batch the *c*-term was found to be independent of column inner diameter. This decrease in the c-term with inner diameter has been seen previously in our lab and is explained by an improvement in the homogeneity of the packing density across the column diameter.[18, 31] Columns with a large aspect ratio are found to have a loosely packed wall region and a densely packed core approximately five particle diameters from the wall. By decreasing the aspect ratio the densely packed core region diminishes leaving only the uniform wall region packing structure.

These results indicate that the poor performance is mainly due to the packing structure of the column bed. There is still some deviation from the predicted values, particularly with regard to the *c*-term, but further improvements may be possible with variation of the packing procedure.

3.3.3.3 Effect of Packing Solvent

One of the ways that column performance is improved is by varying the slurry solvent allowing for a more uniform column bed structure.[62] Variation of the slurry solvent has been carried out in our lab previously for totally porous particles and has been found to

produce columns with large variations in performance.[31] The contributions to the theoretical plate height most affected by changes in the slurry solvent are the *a*-term and *c*-term. The variation of the slurry solvent is thought to vary the amount of particle aggregation that occurs in the slurry. If the particles prefer to interact with another particle rather than the slurry solvent the amount of aggregation within the slurry will be high. Therefore, it is predicted that the best slurry solvent will be one that disperses the particles and allows for individual particles to pack into the column rather than aggregates. More detailed studies of the effect of the slurry solvent will be discussed in Chapter 5, but an initial investigation into this effect will be discussed here.

Six different slurry solvents were investigated in terms of column performance and column bed packing structure, Figure 3-26. All of the solvents were found to have h_{min} values between four and five except for solvent X, Table 3-6A This was interesting because slurry solvents similar to solvent X have routinely been found to be the best slurry solvent for totally porous particles.[31] This indicates that there are intrinsic differences between totally porous particles and superficially porous particles. Superficially porous particles have a greater density than that of totally porous particles, but the skeleton material and bonding chemistry should be similar. Another difference is the particle size distribution of the superficially porous particles, being lower than that found for totally porous particles. This narrower particle size distribution may allow for the particles to pack differently than totally porous particle which then does not require the properties supplied by solvent X. Further variation is the more rugose surface of superficially porous particles as compared to totally porous particles. The rougher particle surface has a higher resistance to slippage leading to a

less dense packing structure.[63] This surface roughness has been found to affect the ease of producing a stable packing and has a large impact on the wall region microstructure.[21]

Of the solvents investigated, methanol was found to give the lowest *c*-term. The presence of a protic solvent, such as methanol, may elevate the hydrogen bonding occurring between free silanols on the particles and allow for hydrogen bonding with the solvent. This might lead to a more disperse particle solution and a more uniform packing structure. The addition of a salt to acetone was investigate to determine if charge attraction or repulsion was playing a role in column packing. If electrostatic attraction between particles was causing particle aggregation the addition of a salt (TEAP) would reduce the interaction between the particles by shielding the charge. By increasing the ionic strength, the performance was found to not improve indicating that charging effects are not affecting the column packing performance.

Comparing the packing density of these columns, columns packed in hexane/acetone, methanol, and 10 mM TEAP in acetone were found to be more densely packed based on their *k'* values, Table 3-6 A. This would indicate that these solvents did not cause particle agglomeration, but allowed for individual particles to build the column bed. Contrary to this, when viewing the build-up of the column bed for these solvents it was found that particles would come into the column as a group of particles while with the other solvents that produced lower density packings, this was not observed. The observation of particle groups may be an artifact of the packing rate of the column. Particles may quickly enter the column and build up closer to the inlet and traverse the column as a group. Therefore, not packing in aggregates, but packing too quickly to see individual particles build-up the column bed. Since the packing density for the columns produced from these solvents were similar, but the

a-term varied, packing of individual particles does not seem to be the main attribute affecting the non-uniformity of the bed causing the high *a*-term, Table 3-6A, although it was found that methanol, an aggregating solvent, produced a column with the lowest c-term. A less aggregating solvent would cause particles to form a tighter column bed structure when packing. This does not correlate to a lower packing density which has been found to lead to a lower *c*-term.[31]

3.3.3.4 Effect of Packing Pressure

Since the slurry solvent was found to affect the packing density of the resulting packed bed, the effect of packing density on performance was investigated. To vary the packing density, two columns were prepared at different packing pressures. It was believed that packing at a lower pressure would lead to a less densely packed bed when using the same slurry solvent.[64] Contrary to this prediction, it was found that the columns packed at higher pressure had a lower *k'*, indicating a less densely packed bed, Figure 3-27. This effect is most likely due to the packing rate of the column. At a higher packing pressure, the rate at which the particles enter the column is higher, which does not allow time for the particles to rearrange to form a tight packing structure. On the other hand, at lower pressure the particles are coming into the column slow enough to allow for arrangement of the particles to form a random, close-packed structure leading to a higher packing density than that of the high pressure column. This was further confirmed by assessing the packing density of the front half of the low pressure column. The front half of the column, which would have packed faster, was found to have a lower *k'* than the entire column. This is in agreement with the results seen for the column packed at high pressure.

In addition to the packing density, the column performance was assessed in terms of the relationship to the packing pressure. The column packed at high pressure was found to have the best column performance in terms of the h_{min}, *a*-term, and *c*-term, Table 3-6B. The performance correlation to high pressure and therefore the packing rate was further confirmed by the improved performance of the front half of the low pressure packed column over the entire column, Figure 3-28. Therefore, a faster packing rate leads to a better performing column independent of slurry solvent. Another way to improve the packing rate of the column bed is to increase the concentration of the particles in the slurry, which will be discussed in 5.3.3.

3.3.3.5 Comparison to Commercial Products

To further investigate if the performance of the in-house particles was due to the packing structure or the particles, the performance of commercial products was tested. The commercial products were tested by packing the particles in-house in the same manner as carried out for particles synthesized in-house. The reduced parameters plot was used to compare their performance, Figure 3-29. The majority of the commercial products were found to have similar performance as the 1.1 μm and 1.7 μm particles made in-house. The 1.7 μm Kinetex particles greatly deviated from the performance of the other particles tested. Based on the imaging of these particles, Figure 3-30, it was found that a large number of the particles were found to be stuck together. These long chains of particles would make it difficult to pack and lead to a large variation of flow paths within the column.

Accounting for the particle diameter of the particles, the performance resulting for the particles synthesized in-house have been found to be superior to the commercial products. The number of theoretical plates normalized by the length of the column for the 2.7 μm Halo

and 1.1 μm UNC were 200,000 and 375,000 plates/meter for hydroquinone at the optimum linear velocity.

The agreement of the other commercial products with the particles made in-house indicate that the in-house particles are of equivalent performance, but it is the packing of the superficially porous particles that is causing the deviation from theory and from the results seen for mm bore HPLC columns. Therefore, the column packing procedure must further be investigated to produce superior columns to those currently available.

3.4 CONCLUSIONS

The synthetic route for 1.1 μm superficially porous particles has been revised to produce monodisperse particles with uniform surface coverage and layer thickness. These particles were found to perform as well as commercially available products, but degraded performance has been found for 30 μm bore UHPLC columns. The slurry solvent was found to affect the chromatographic performance due to different particle-solvent interactions. Fine tuning of the slurry solvent is required for the production of highly efficient columns. The packing structure was further indicated as causing poor performance by finding that decreasing the aspect ratio led to improved performance. This poor packing process is predicted to be closely tired to the packing rate of the column.

3.5 REFERENCES

[1] Horvath, C.; Lipsky, S.R. *J. Chrom. Science* 7 (1969) 109-116.

[2] Horvath, C.G.; Preiss, B.A.; Lipsky, S.R. *Anal. Chem.* 39 (1967) 1422-1428.

[3] Kirkland, J.J. *U.S. Patent 3505785* 1970.

[4] Kirkland, J.J. *Anal. Chem.* 64 (1992) 1239-1245.

[5] Snyder, L.; Kirkland, J. J.; Glajch, J.L. *Practical HPLC Method Development*, 2nd ed., Wiley, New York, 1997.

[6] Kirkland, J.J.; Langlois, T.J. *U.S. Patent 0189944 A1* 2007.

[7] Gritti, F.; Cavazzini, A.; Marchetti, N.; Guiochon, G. *J. Chrom. A* 1157 (2007) 289-303.

[8] Macnair, J.E.; Lewis, K.C.; Jorgenson, J.W. *Anal. Chem.* 69 (1997) 983-989.

[9] Horvath, K.; Gritti, F.; Fairchild, J.P.; Guichon, G. *J Chrom. A* 1217 (2010) 6373-6381.

[10] Iler, R.K. *The Colloid Chemistry of Silica and Silicates*; Cornell University Press, New York, 1955.

[11] Neue, U.D. *HPLC Columns: Theory, Technology, and Practice*, Wiley-VCH, New York, 1997.

[12] Buszewski, B.; Nondek, L.; Jurasek, A.; Berek, D. *Chromatoraphia* 23 (1987) 442-446.

[13] Lork, K.D.; Unger, K.K.; Kinkel, J.N. *J. Chromatogr.* 352 (1986) 199-211.

[14] Gritti, F.; Guichon, G. *J. Chrom. A* 1128 (2006) 45-60.

[15] Gritti, F.; Guiochon, G. *J. Chrom. A* 1098 (2005) 82-94.

[16] Großmann, F.; Ehwald, V.; du Fresne von Hohenesche, C.; Unger, K.K. *J. Chrom. A* 910 (2001) 223-236.

[17] Kinkel, J.N.; Unger, K.K. *J. Chromatogr.* 316 (1984) 193-200.

[18] Hsieh, S.; Jorgenson, J.W. *Anal. Chem.* 68 (1996) 1212-1217.

[19] Wu, N.; Lippert, J.A.; Lee, M.L. *J. Chrom. A* 911 (2001) 1-12.

[20] Ehlert, S.; Rosler, T. Tallarek, U. *J. Sep. Sci.* 31 (2008) 1719-1728.

[21] Roblee, L.H.S.; Baird, R.M.; Tierney, J.W.; *AIChE J.* 4 (1958) 460-464.

[22] Benenati, R.F.; Brosilow, C.B. *AIChE J.* 8 (1962) 359-361.

[23] Ridgeway, K.; Tarbuck, K.J. *Chem. Eng. Sci.* 23 (1968) 1147-1155.

[24] Kennedy, R.T.; Jorgenson, J.W. *Anal. Chem.* 61 (1989) 1128-1135.

[25] Knox, J.H.; Parcher, J.F. *Anal. Chem.* 41 (1969) 1599-1606.

[26] Bruns, S.; Grinias, J.P.; Blue, L.E.; Jorgenson, J.W.; Tallarek, U. *Anal. Chem*. 84 (2012) 4496-4503.

[27] Eeltink, S.; Rozing, G.P.; Schoenmakers, P.J.; Kok, W.T. *J. Chrom. A* 1044 (2004) 311-316.

[28] Karlsson, K.E.; Novotny, M. Anal. Chem. 60 (1988) 1662-1665.

[29] McGuffin, V.L.; Novotny, M. *J. Chromtogr.* 255 (1983) 381-393.

[30] Wilson, W.H.; McNair, H.M.; Maa, Y.F.; Hyver, K.J. *J. High Resolut. Chrom.* 13 (1990) 18-21.

[31] Lieberman, R. *UNC Doctoral Dissertation* 2009.

[32] MacNair, J.E. Lewis, K.C.; Jorgenson, J.W. *Anal. Chem.* 69 (1997) 983-989.

[33] Knox, J.H.; Scott, H.P. *J. Chromatogr.* 282 (1983) 297-313.

[34] Jerkovich, A.D. *UNC Dissertation*, 2003.

[35] Desmet, G.; Broeckhoven, K.; De Smet, J.; Deridder, S.; Baron, G.V.; Gzil, P. *J. Chrom. A* 1188 (2008) 171-188.

[36] Crombeen, J.P.; Poppe, H.; Kraak, J.C. *Chromatographia* 22 (1986) 319-328.

[37] Zhiping, J.; Fisk, R.P.;O'Gara, J.; Walter, T.H.; Wyndham, K.D. *US Patent 20020070168* 2002.

[38] Wyndham, K.D.; O'Gara, J.E. *US Patent 20100076103* 2007.

[39] Martin, M.; Blu, G.; Guiochon, G. *J. Chrom. Science* 11 (1973) 641-654.

[40] Mellors, J.S. *UNC Doctoral Dissertation* 2005.

[41] MacNair, J.E.; Patel, K.D.; Jorgenson, J.W. *Anal. Chem.* 71 (1999) 700-708.

[42] Maiolica, A.; Borsotti, D.; Rappsilber, J. *Proteomics* 5 (2005) 3847-3850.

[43] Bergna, H.E.; Kirkland, J.J. *US Patent 4,447,492* 1984.

[44] Jayant, K.; Singh, N.H.; MacDiamond, A.G.; Sukant, T. *Handbook of Polyelectrolytes and Their Applications: Polyelectrolyte-Based Multilayers, Self-Assemblies, and Nanostructures*, Volume 1; American Scientific Publishers, California, 2002.

[45] Yu, J.; Wang, Z.; Chu, B. *Macromolecules* 25 (1992) 1618-1620.

[46] Jachimska, B.; Jasinski, T.; Warszynski, P.; Adamczyk, Z. *Colloids and Surfaces* 355 (2010) 7-15.

[47] Kirwin, L.J.; Papastavrou, G.; Borkove, M.; Behren, S.H. *Nano. Letters* 4 (2004) 149-152.

[48] Hoover, F. *J. Macromol. Sci.-Chem.* 6 (1970) 1327-1417.

[49] Steitz, R.; Leiner, V.; Seibrecht, R.; Klitzing, R. *Colloids and Surfaces* 163 (2000) 63-70.

[50] Decher, G.; Schmitt, *J. Prog. Colloid Poly. Sci.* 89 (1992) 160-164.

[51] Russel, W.R.; Saville, D.A.; Schowalter, W.R. *Colloidal Dispersions*; Cambridge University Press, New York, 1989.

[52] Jafarzadeh, M.; Rahman, I.A.; Sipaut, C.S. *J. Sol-Gel Sci. Technol.* 50 (2009) 328-336.

[53] Brinker, C.J.; Scherer, G.W. *Sol-Gel Science: The Physics and Chemistry of Sol-Gel Processing*, 1st ed.; Academic Press, New York, 1990.

[54] Wang, B.; Zhang, W.; Zhang, W.; Mujumdar, A.S.; Huang, L. *Drying Technology* 23 (2005) 7-32.

[55] Unger, K.K. *Porous Silica, its properties and uses as support in column liquid chromatography*; Elsevier Scientific Publishing, New York, 1979.

[56] DeStefano, J.J.; Langlois, T.J.; Kirkland, J.J. *J. Chrom. Sci.* 46 (2008) 254-260.

[57] Gritti, F.; Leonardis, I.; Abia, J.; Guiochon, G. *J. Chrom. A* 1217 (2010) 3819-3843.

[58] Gritti, F.; Guiochon, G. *J. Chrom. A* 1098 (2005) 82-94.

[59] Schmidt-Traub, H. *Preparative Chromatography of Fine Chemicals and Pharmaceutical Agents*; Wiley-VCH, New York, 1997.

[60] Patel, K.D.; Jerkovich, A.D.; Link, J.C.; Jorgenson, J.W. Anal. Chem. 76 (2004) 5777-5786.

[61] de Klerk, A. *AIChE J.* 49 (2003) 2022-2029.

[62] Kirkland, J.J.; DeStefano, J.J. *J. Chrom. A* 1126 (2006) 50-57.

[63] Gritti, F.; Guiochon, G. *J. Chrom. A* 1166 (2007) 30-46.

[64] Guan, Y.; Zhou, L.; Shang, Z. *J. High Res. Chrom.* 15 (2005) 434-436.

3.6 TABLES

A.

Polyelectrolyte	Layer Thickness Growth Rate (nm/coating step)	Average $d_{p,n}$ (μm)	RSD (%)
LMW PDDA	40	1.14	2.2
HMW PDDA	40	1.15	3.1
PEI	52	1.28	3.8
LMW PAH	56	1.30	6.5
HMW PAH	47	1.25	4.9

B.

LMW PDDA Concentration (w/w%)	Layer Thickness Growth Rate (nm/coating step)	Average $d_{p,n}$ (μm)	RSD (%)
1.0%	50	1.21	3.2
0.5%	40	1.14	2.2
0.1%	13	0.99	4.4
0.05%	4	0.93	3.6

Table 3-1: (A) Effect of molecular weight and type of polyelectrolyte on growth rate and particle size distribution. Layer thickness growth rate determined from three coating steps. 0.9 μm NPS (Fiber Optic Center), 0.5% polyelectrolyte, 10% AS-30 colloidal silica (pH = 3.5). (B) Effect of polyelectrolyte concentration on growth rate and particle size distribution. Layer thickness growth rate determined from three coating steps. 0.9 μm NPS (Fiber Optic Center), 10% AS-30 colloidal silica (pH = 3.5)

Type of Colloidal Silica	Number Average Particle Size (μm)	RSD (%)
NexSil8 (8 nm)	0.97	2.4
Ludox AS-30 (12 nm)	0.99	2.3
Nalco 1030 (13 nm)	0.96	4.0
Nalco 1060 (60 nm)	1.0	3.5
NexSil85 (85 nm)	1.0	3.2
NexSil125 (125 nm)	1.0	9.2

Table 3-2: Effect of the type of colloidal silica. NPS coated with one layer of LMW PDDA and colloidal silica.

pH	Average Zeta Potential (mV)	Standard Deviation
9.1	-50.6	1.4
8.0	-40.0	4.1
6.0	-19.1	1.1
4.0	-6.0	0.7
3.0	-3.6	0.7
2.0	-0.6	0.7

Table 3-3: Zeta potential as a function of pH for 10% (w/w%) AS-30 (12 nm) colloidal silica solution.

Sinter Temperature	Surface Area (m^2/g)	Total Pore Volume (cm^3/g)	Average Pore Diameter (Å)	Bare Particles (%)
825°C	63	0.11	67	4
900°C	61	0.11	69	5
925°C	57	0.11	69	2
945°C	52	0.10	71	0

Table 3-4: Effect of sintering temperature on specific surface area, pore volume, pore diameter, and rigidity. 0.9 μm NPS (Fiber Optic Center), 0.5% (w/w%) LMW PDDA, 10% (w/w%) AS-30 (12 nm) colloidal silica (pH = 3.5). Measurements made after three coating steps, drying by lyophilization, and removal of LMW PDDA by heating at 540°C.

	Core dp (μm)	Total dp (μm)	Porous Layer Thickness (μm)	SSA (m^2/g)	SPV (cm^3/g)	Pore Diameter (Å)
2.7 μm Halo*	1.7	2.9	0.6	124	0.29	77
2.6 μm Kinetex*	1.9	2.5	0.3	100	0.24	83
1.7 μm Kinetex*	1.3	1.8	0.3	98	0.24	84
1.1 μm UNC	0.9	1.1	0.1	52	0.10	71

Table 3-5: Physical characteristics of commercially available superficially porous particles (*) [57] and superficially porous particles synthesized in-house.

A.

Solvent	h_{min}	a	b	c	k’
Acetone	3.8	1.64	1.15	1.00	0.9
Hexane	3.1	-0.63	1.75	2.01	0.9
Hexane/Acetone	3.7	0.93	1.17	1.80	1.3
Methanol	3.7	2.41	1.00	0.58	1.3
Solvent X	6.3	4.65	0.47	2.69	0.6
10 mM TEAP in acetone	4.2	1.60	1.27	1.40	1.4

B.

Packing Pressure	h_{min}	a	b	C	k’
30,000 psi	3.0	0.95	1.84	0.54	1.2
15,000 psi	5.0	1.13	1.27	3.50	1.3

Table 3-6: Performance parameter for columns packed in A) different slurry solvents and B) at different packing pressure

3.7 FIGURES

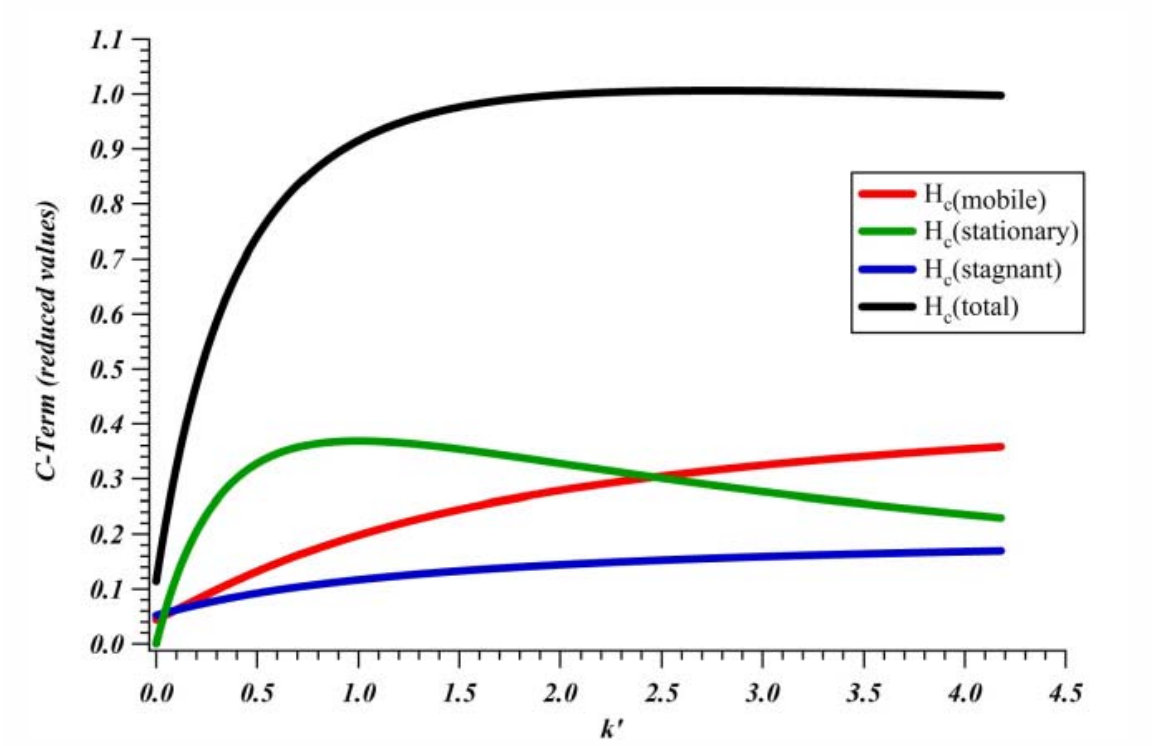

Figure 3-1: Theoretical curves for the contributions to the *c* term versus *k*' for an analyte. The blue trace is for the stagnant mobile phase term. The red trace is for the mobile phase term. The green trace is for the resistance to mass transfer in the stationary phase. The black trace is the total contribution to the *c* term as it varies with *k'*.[31]

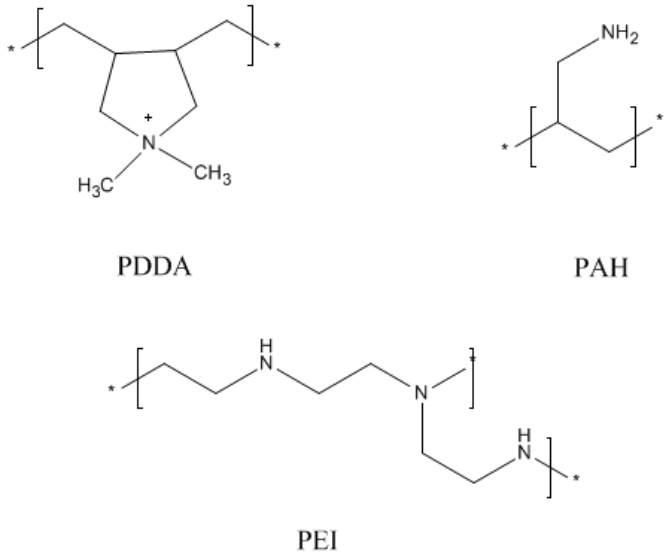

Figure 3-2: Polyelectrolyte structures

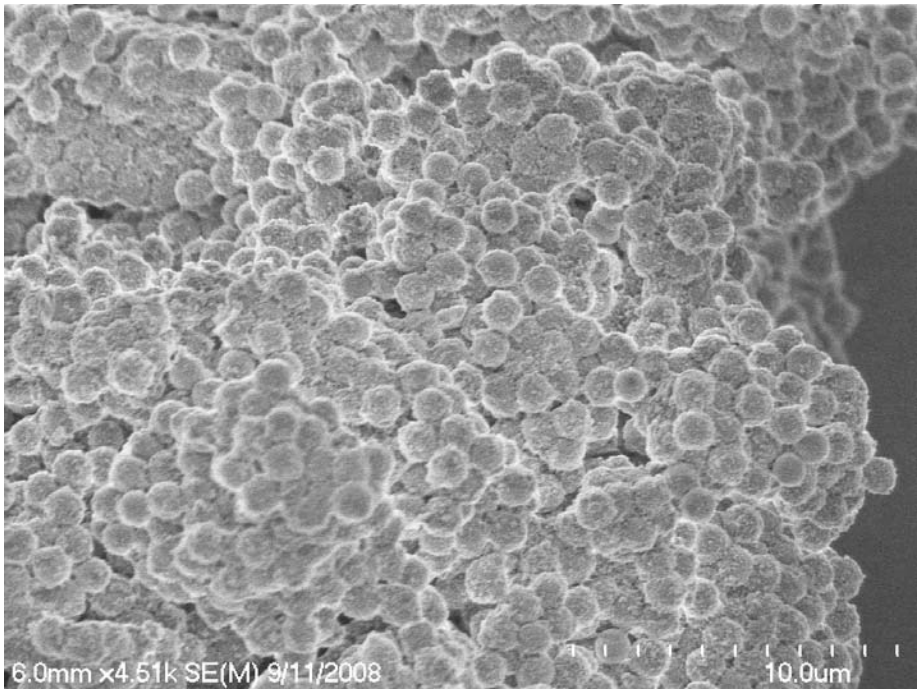

Figure 3-3: SEM image of the particle agglomeration seen in the initial synthesis of 1.1 μm superficially porous particles

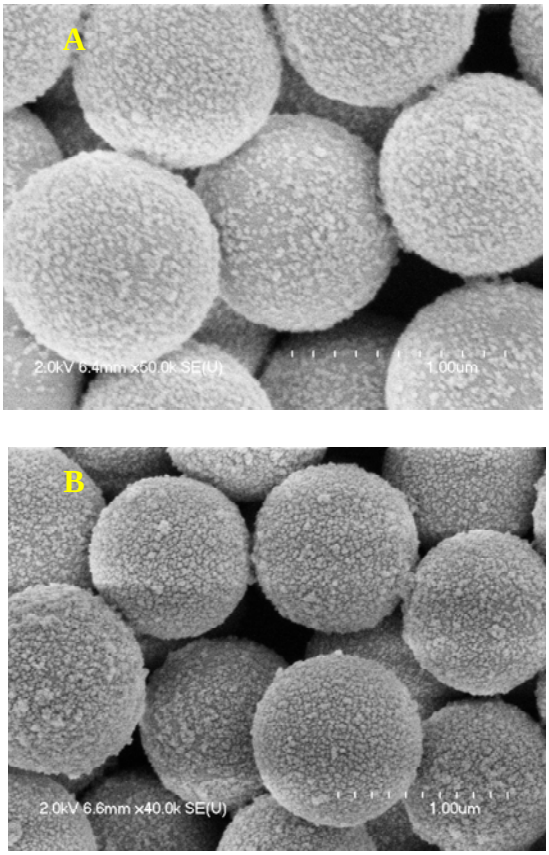

Figure 3-4: Effect of NPS core solution pH on surface coverage. One coating step, 0.9 µm NPS (Eprogen (Darien, IL)), 0.5% (w/w%) LMW PDDA, 10% (w/w%) AS-30 (20 nm) colloidal silica (pH = 3.5). (A) pH = 2.3; (B) pH = 5.5

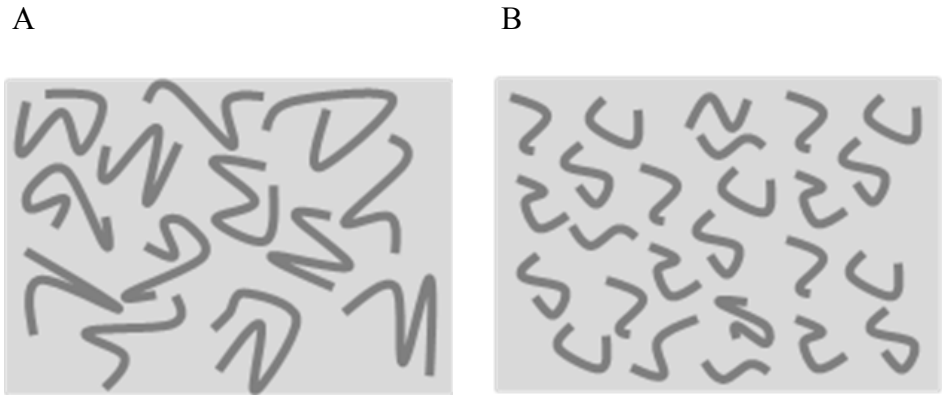

Figure 3-5: Diagram of effect of polyelectrolyte molecular weight (chain length) on surface coverage. (A) HMW, top view (B) LMW, top view

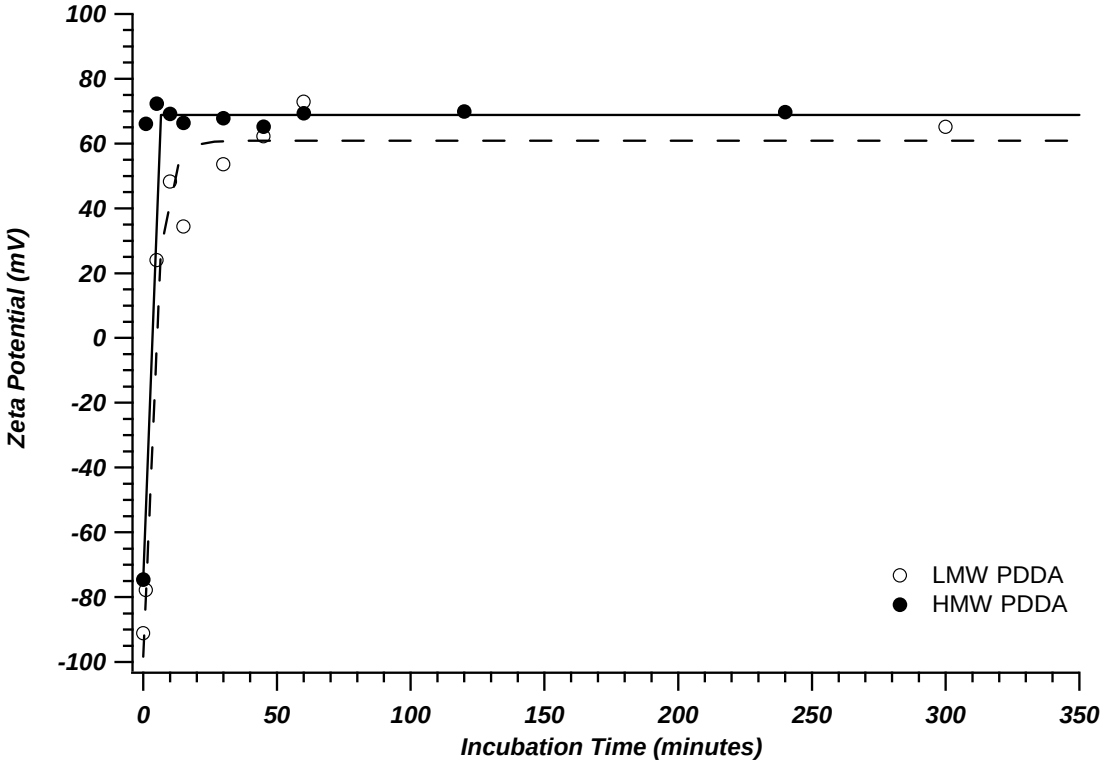

Figure 3-6: Comparison between LMW PDDA and HMW PDDA uptake

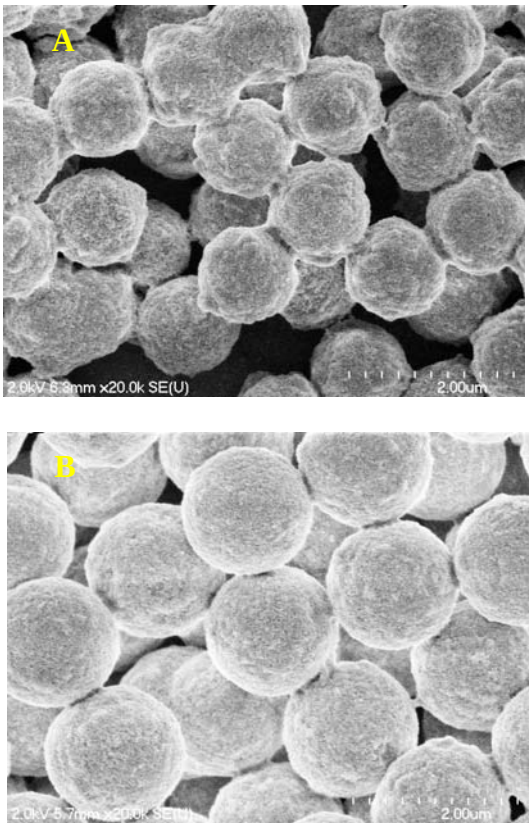

Figure 3-7: Effect of molecular weight of polyelectrolyte. Three coating steps, 0.9 μm NPS (Fiber Optic Center), 0.5% (w/w%) polyelectrolyte, 10% (w/w%) AS-30 (pH = 3.5). (A) HMW PDDA; (B) LMW PDDA

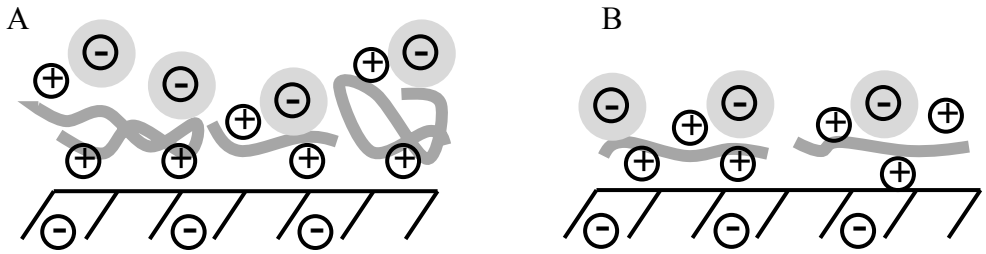

Figure 3-8: Diagram of effect of polyelectrolyte molecular weight on surface thickness variations and roughness. (A) HMW, side view (B) LMW, side view

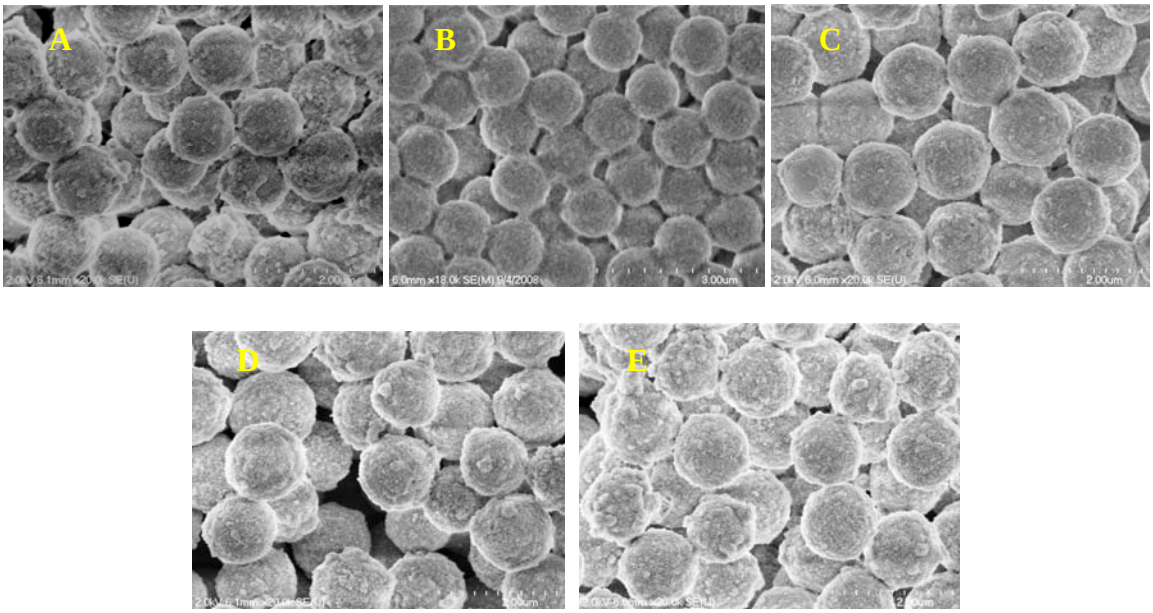

Figure 3-9: Effect of polyelectrolyte type on surface coverage and uniformity. A) LMW PDDA B) HMW PDDA C) PEI D) LMW PAH E) HMW PAH

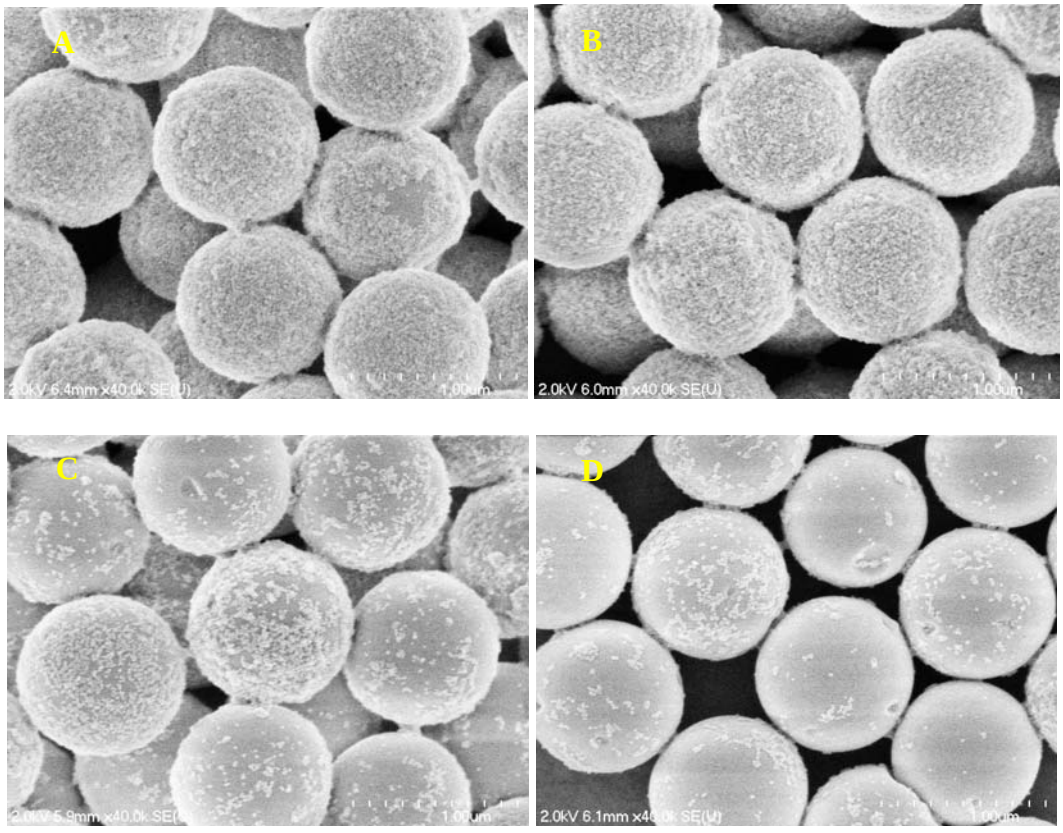

Figure 3-10: Effect of polyelectrolyte concentration (w/w%) on surface coverage. One coating step, 0.9 μm NPS (Fiber Optic Center), LMW PDDA, 10% (w/w%) AS-30 (pH = 3.5). (A) 1.0%; (B) 0.5%; (C) 0.1%; (D) 0.05

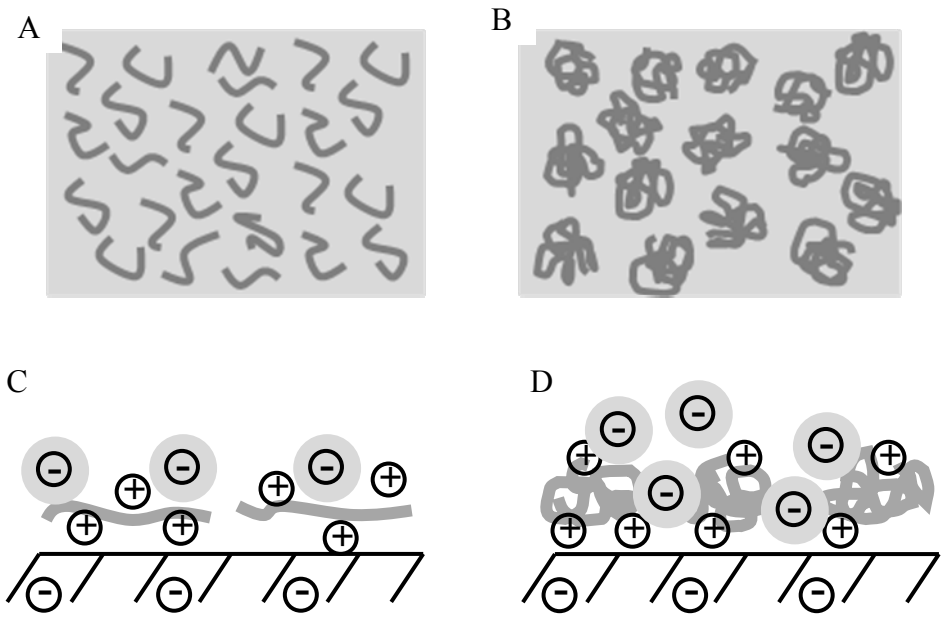

Figure 3-11: Diagram of effect of ionic strength on polyelectrolyte conformation and colloidal silica layer thickness. (A) low ionic strength, top view; (B) high ionic strength, top view; (C) low ionic strength, side view; (D) high ionic strength, side view

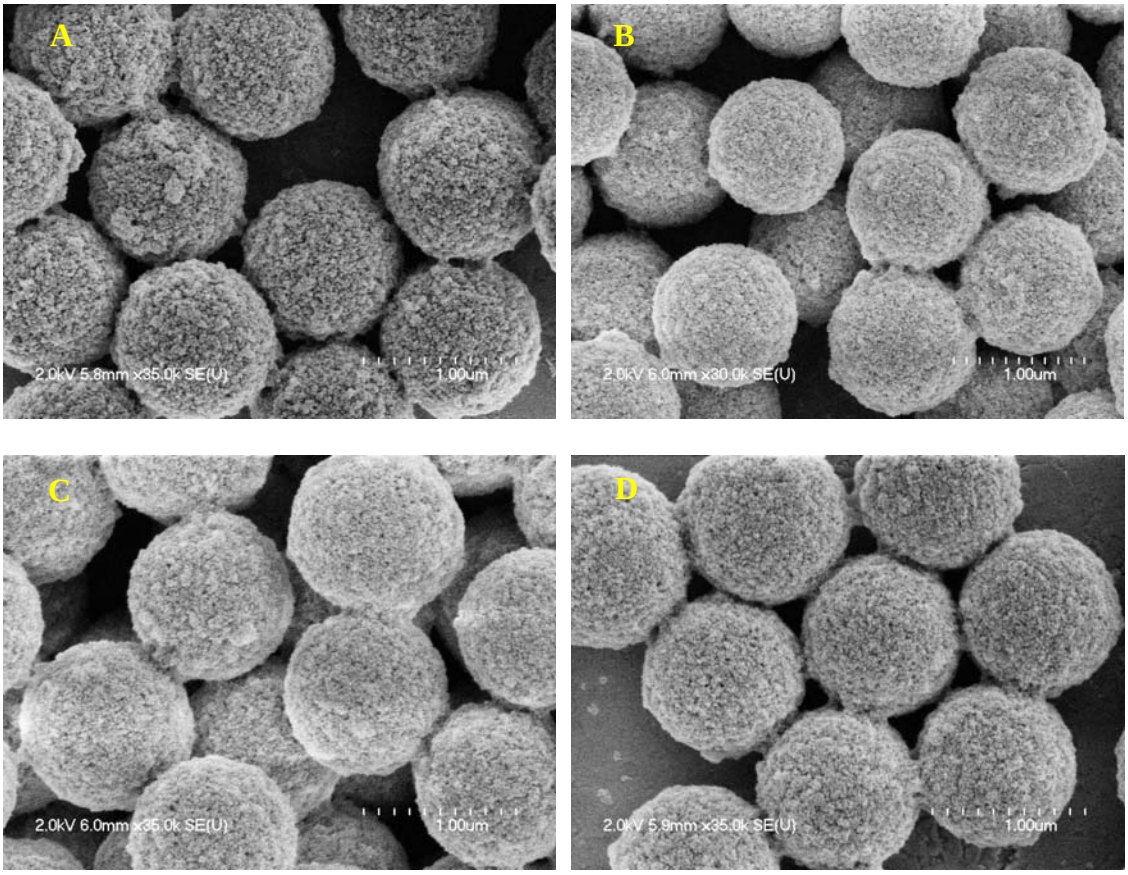

Figure 3-12: Effect of salt concentration on surface coverage, uniformity, and roughness. Two coating steps, 0.9 μm NPS (Eprogen (Darien, IL)), 0.5% (w/w%) LMW PDDA, 10% (w/w%) AS-30 (pH = 3.5). (A) 0.0 M NaCl; (B) 0.2 M NaCl; (C) 0.4 M NaCl; (D) 0.6 M NaCl

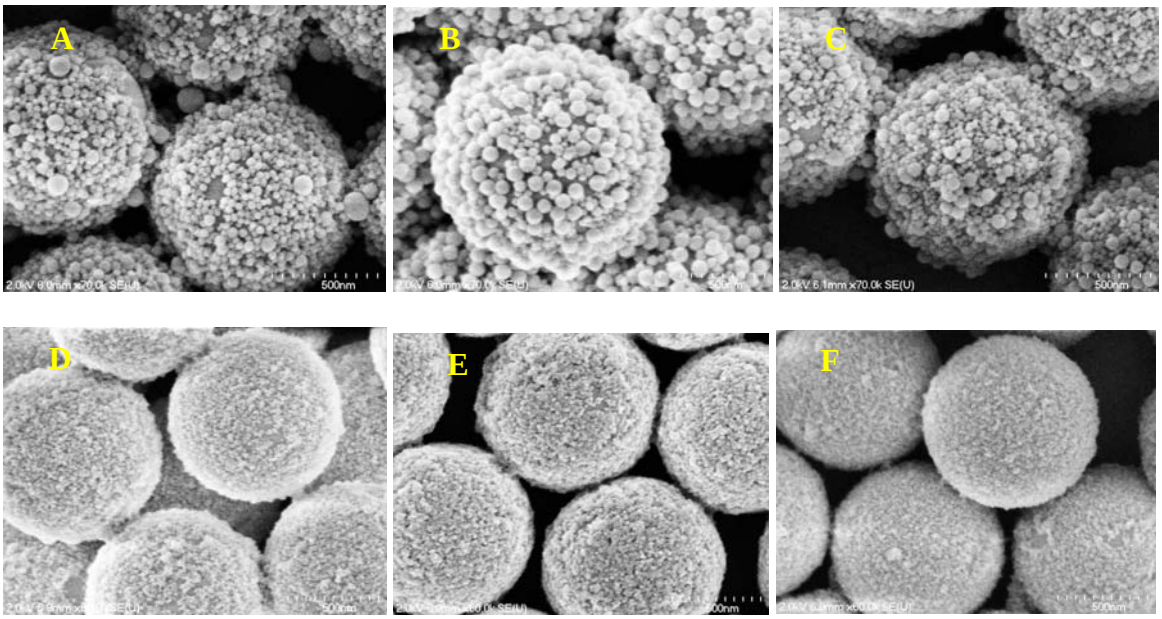

Figure 3-13: Comparison of colloidal silica size. One coating step, 0.9 μm NPS (Fiber Optic Center), 0.5% (w/w%) LMW PDDA, 10% (w/w%) colloidal silica (pH = 3.5). (A) Nyacol Nexsil125 (125 nm); (B) Nyacol NexSil85 (85 nm); (C) Nalco 1060 (60 nm); (D) Nalco 1030 (13 nm); (E) Aldrich, AS-30 (12 nm); (F) Nyacol, NexSil8 (8 nm)

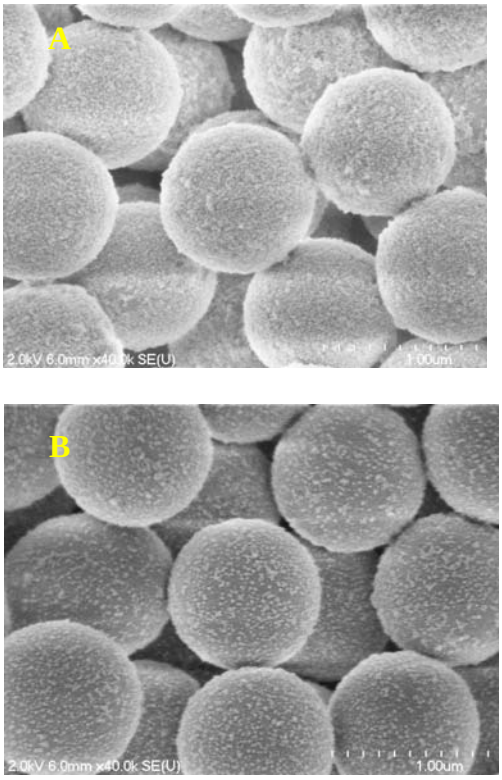

Figure 3-14: Effect of colloidal silica solution pH on NPS core surface coverage. One coating step, 0.9 μm NPS (Eprogen), 0.5% (w/w%) LMW PDDA, 10% (w/w%) AS-30 (20 nm) colloidal silcia. (A) pH = 3.5; (B) pH = 9.4

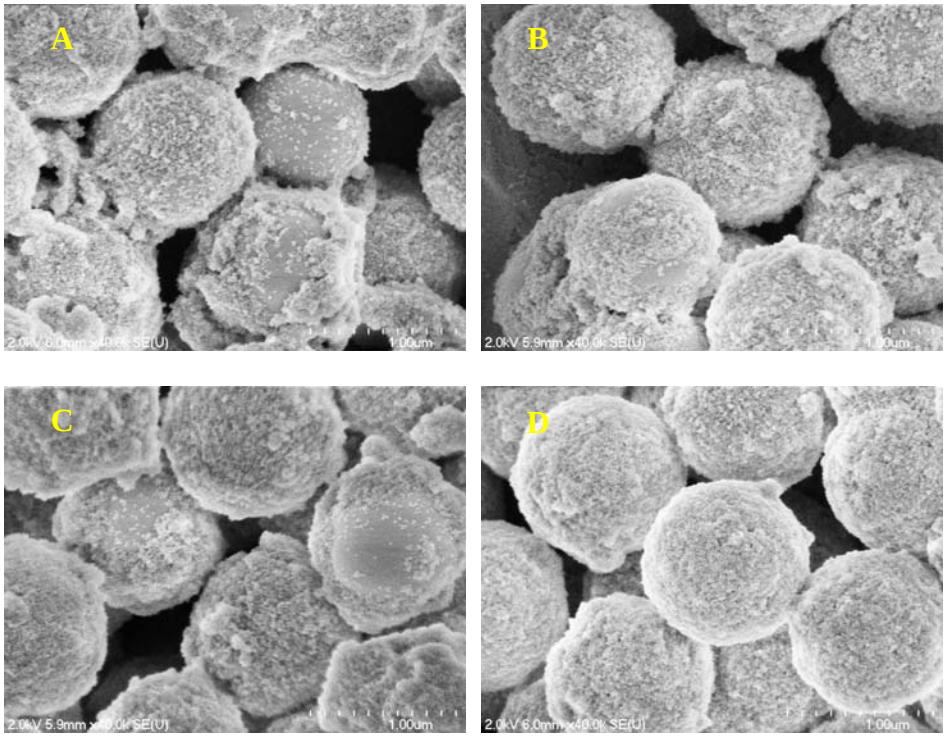

Figure 3-15: Effect of drying method on particle coverage and uniformity. Three coating steps, 0.9 μm NPS (Fiber Optic Center), 0.5% (w/w%) LMW PDDA, 10% (w/w%) AS-30 (20 nm) colloidal silica (pH = 3.5). (A) Dried at 25°C; (B) Dried at 80°C; (C) Dried at 105°C; (D) Lyophilized

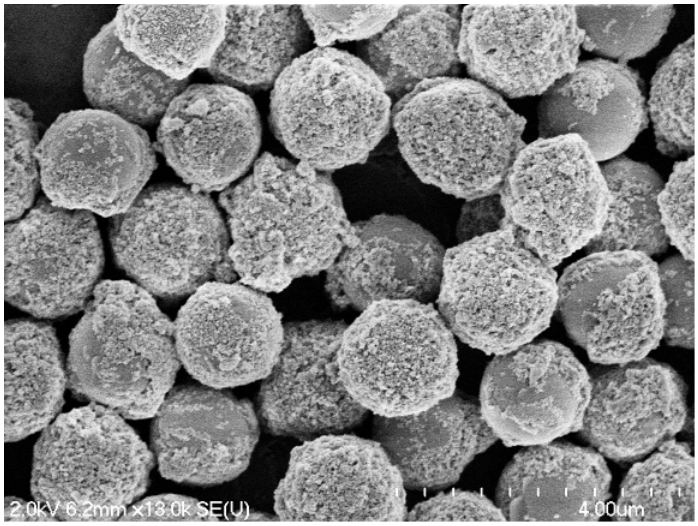

Figure 3-16: Particle degradation seen from extruded column bed. Three coating steps, 0.9 μm NPS (Eprogen (Darien, IL)), 0.5% (w/w%) LMW PDDA, 10% (w/w%) Nalco 1030 (13 nm) colloidal silica (pH = 3.5), sintered at 825°C, bonded and endcapped.

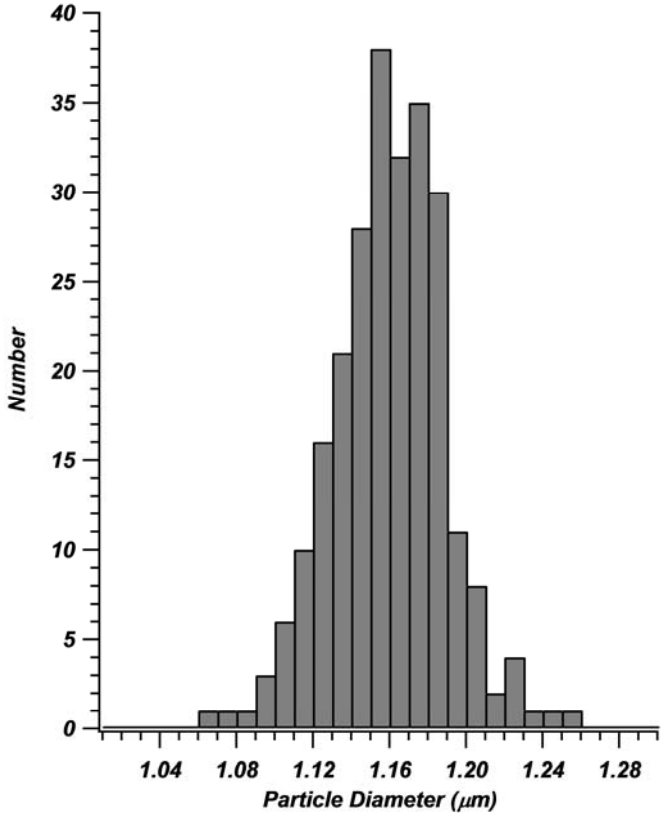

Figure 3-17: Particle size distribution of 1.1 μm ($d_{p,n}$) superficially porous particles. RSD = 2.2%

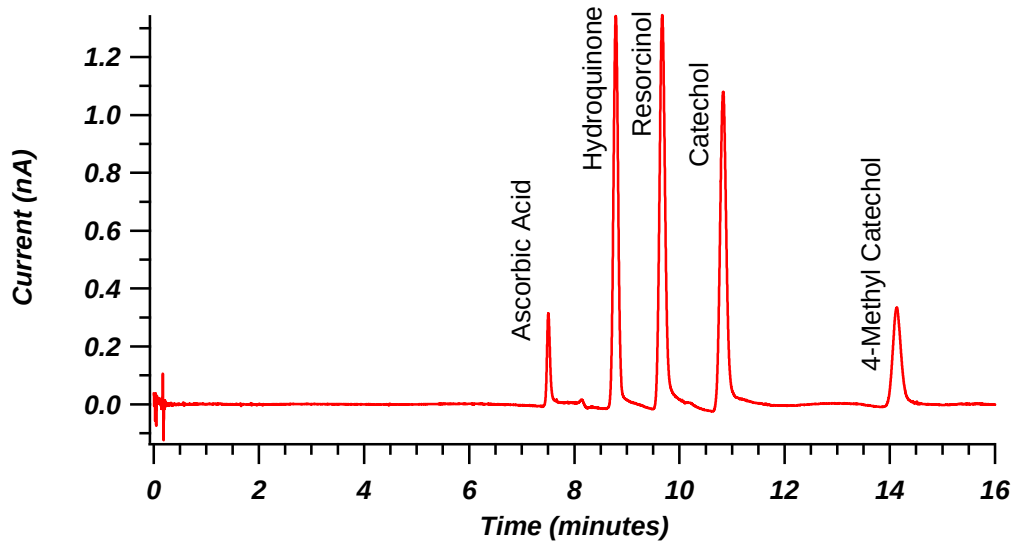

Figure 3-18: Example chromatogram for column LB3-104, particles LB3-102-1 bonded by U.S. patent 20020070168. Packed in acetone at 3 mg/mL. Mobile phase: 80/20 water/ACN 0.1% TFA, u_{opt} = 0.05 cm/sec (8300 psi) h_{min} (HQ) = 4.3, k' (4MC) = 0.9

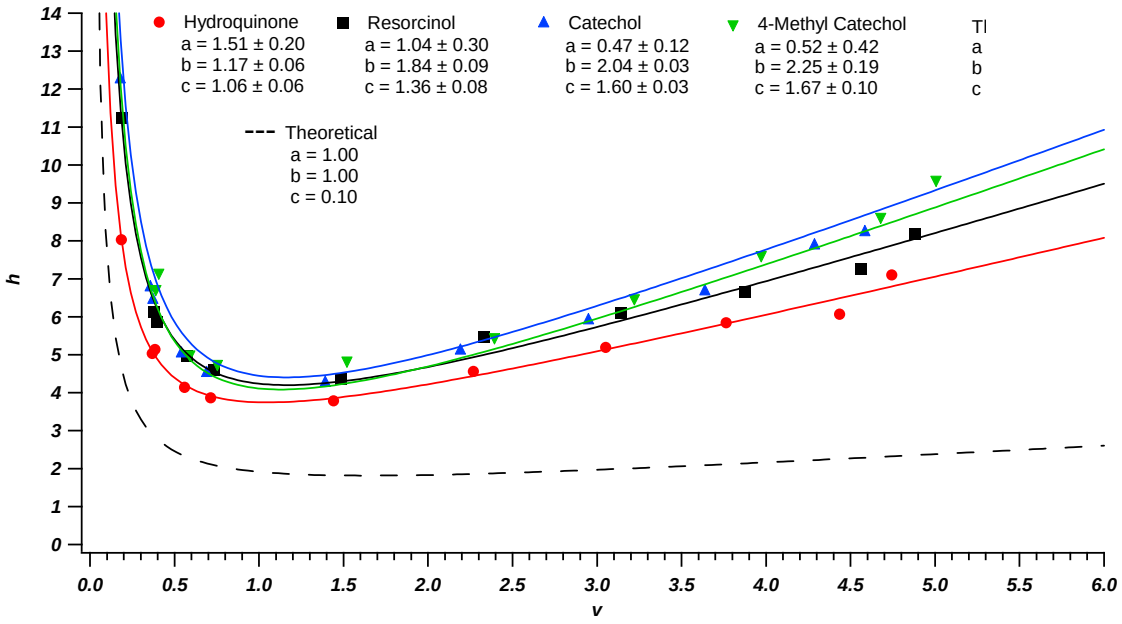

Figure 3-19: Reduced parameters plot for column LB3-104, particles LB3-102-1 bonded by U.S. patent 20020070168. Packed in acetone at 3 mg/mL. Mobile phase: 80/20 water/ACN 0.1% TFA, u_{opt} = 0.05 cm/sec (8300 psi). h_{min} (HQ)= 4.3, k' (4MC) = 1.2

A

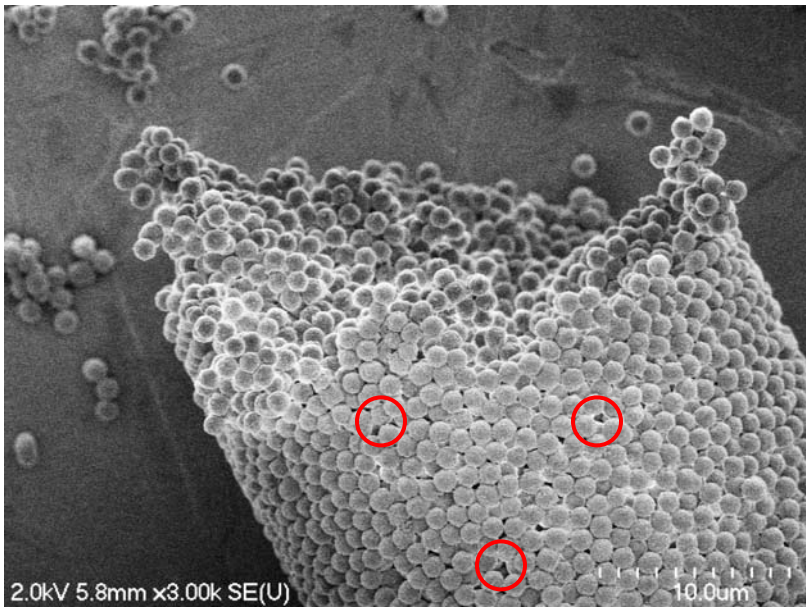

B

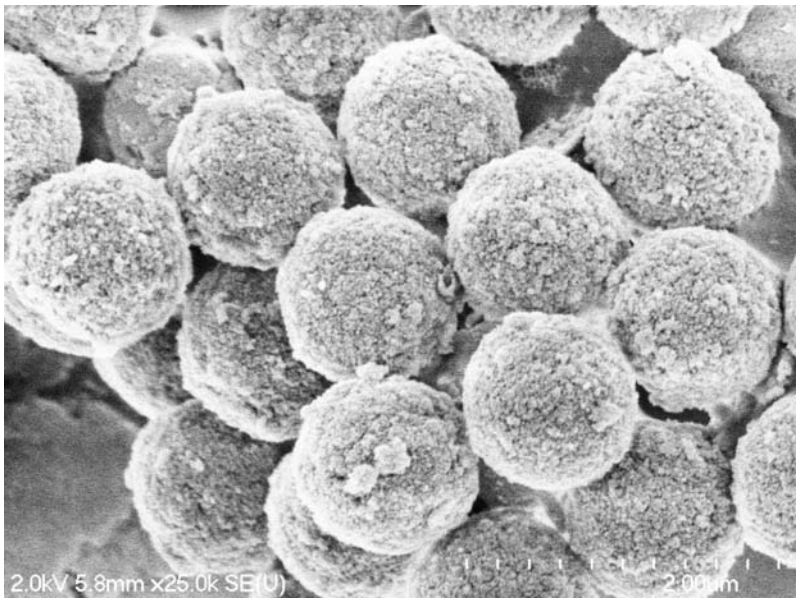

Figure 3-20: Images of Column LB3-104 extruded bed. A) image of column cross-section near column outlet where red circles highlight column voids B) expanded section of column cross-section

A

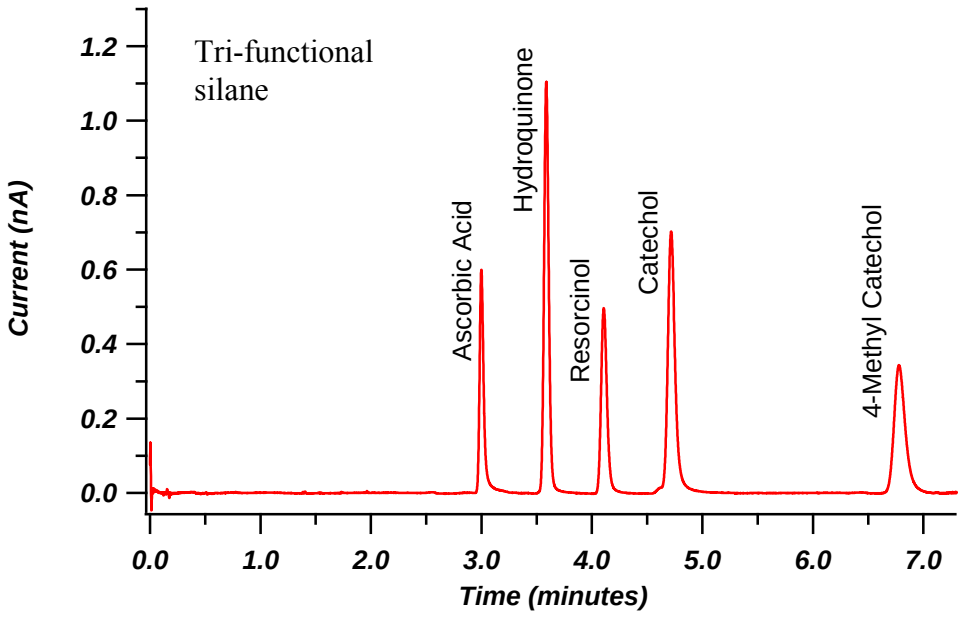

B

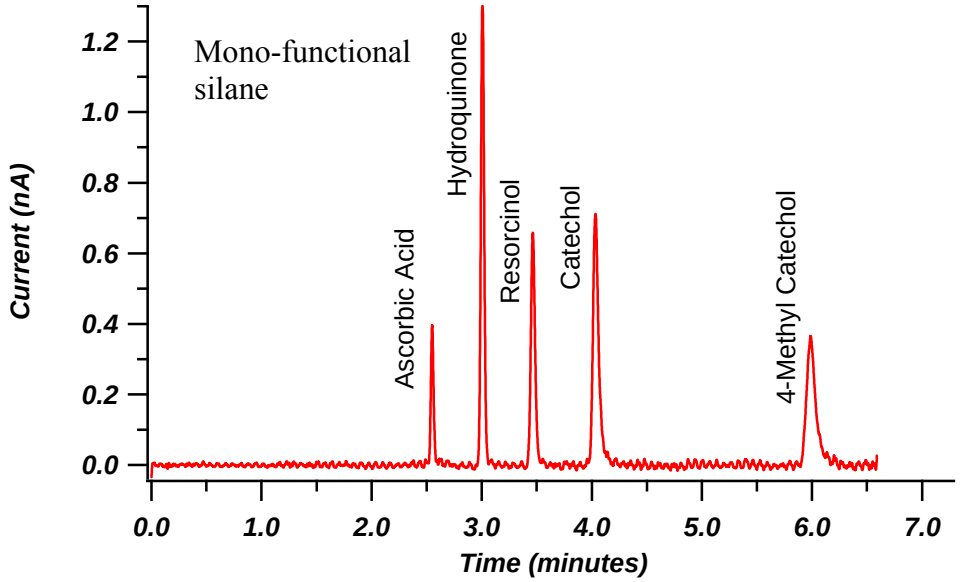

Figure 3-21: Example chromatogram comparison of different bonding and endcapping procedures. Mobile phase: 80/20 water/ACN 0.1% TFA. A) U.S. patent 20020070168, tri-functional silane, u_{opt} = 0.08 cm/sec (6900 psi), h_{min} (HQ) = 3.7, k' (4MC) = 1.3. B) U.S. patent 20100076103, mono-functional silane, u_{opt} = 0.12 cm/sec (6600 psi), h_{min} (HQ) = 2.2, k' (4MC) = 1.3

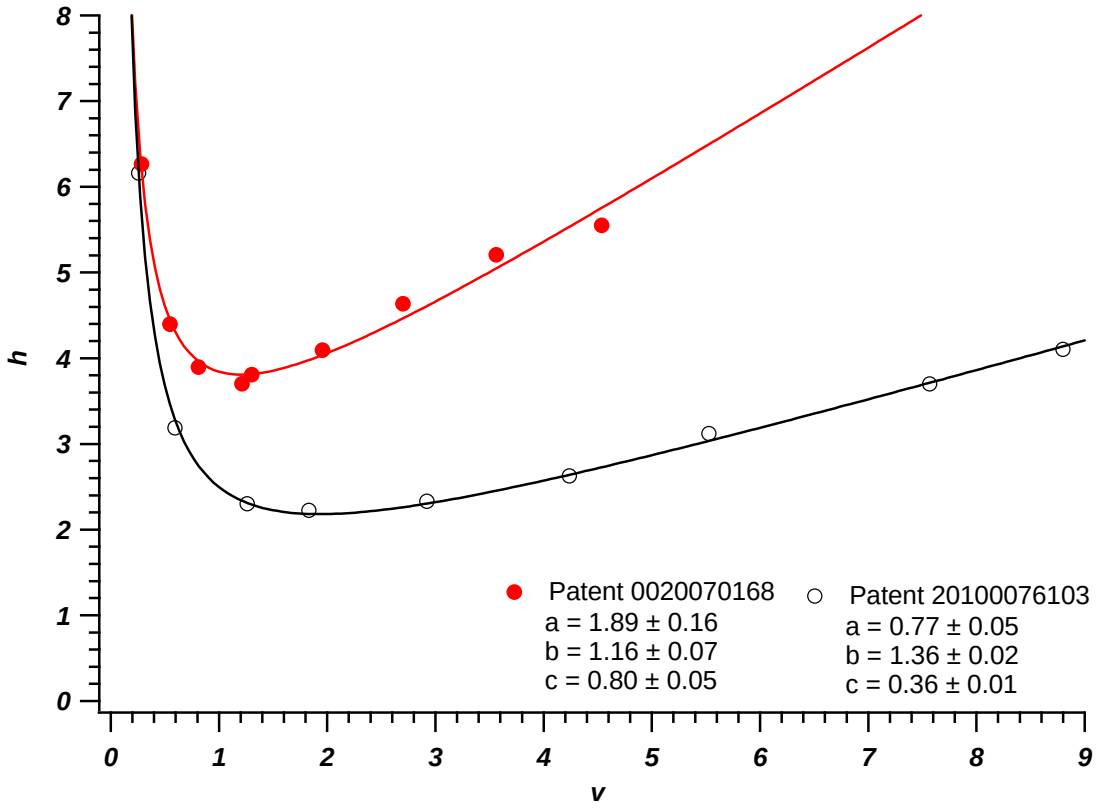

Figure 3-22: Reduced parameters plot for hydroquinone comparing different bonding and endcapping procedures. U.S. patent 20020070168, tri-functional silane: u_{opt} = 0.08 cm/sec (6900 psi), h_{min} (HQ)= 3.7, k' (4MC) = 1.3. U.S. patent 20100076103, mono-funtional silane: u_{opt} = 0.12 cm/sec (6600 psi), h_{min} (HQ) = 2.2, k' (4MC) = 1.3.

A

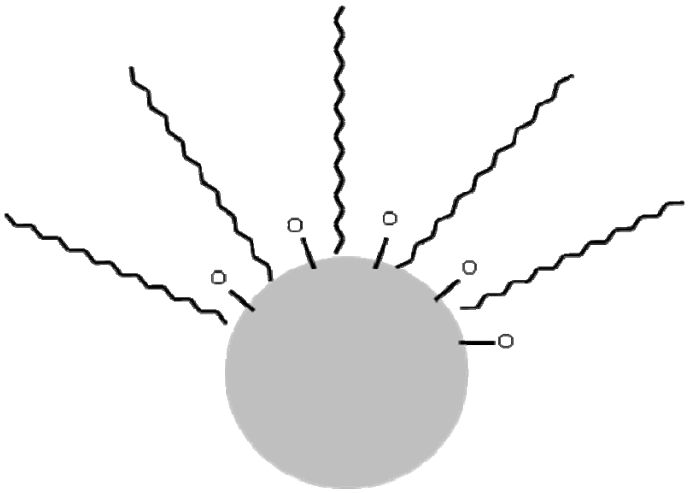

B

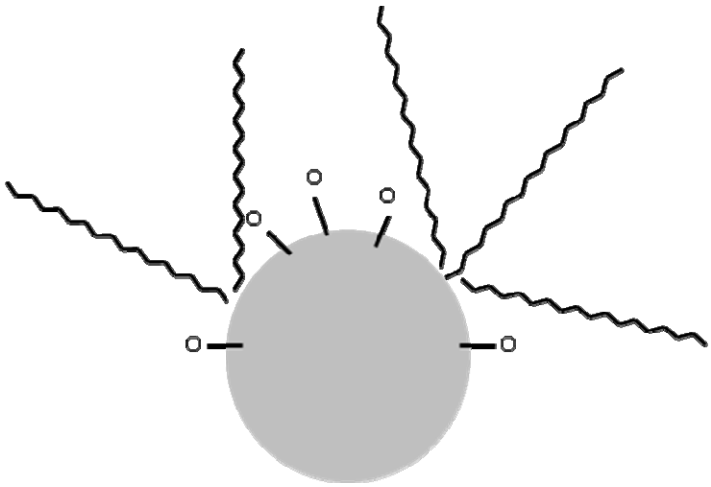

Figure 3-23: Diagrams of proposed bonding agent attachment. A) mono-functional silane, no polymerization, B) tri-functional siliane, polymerization

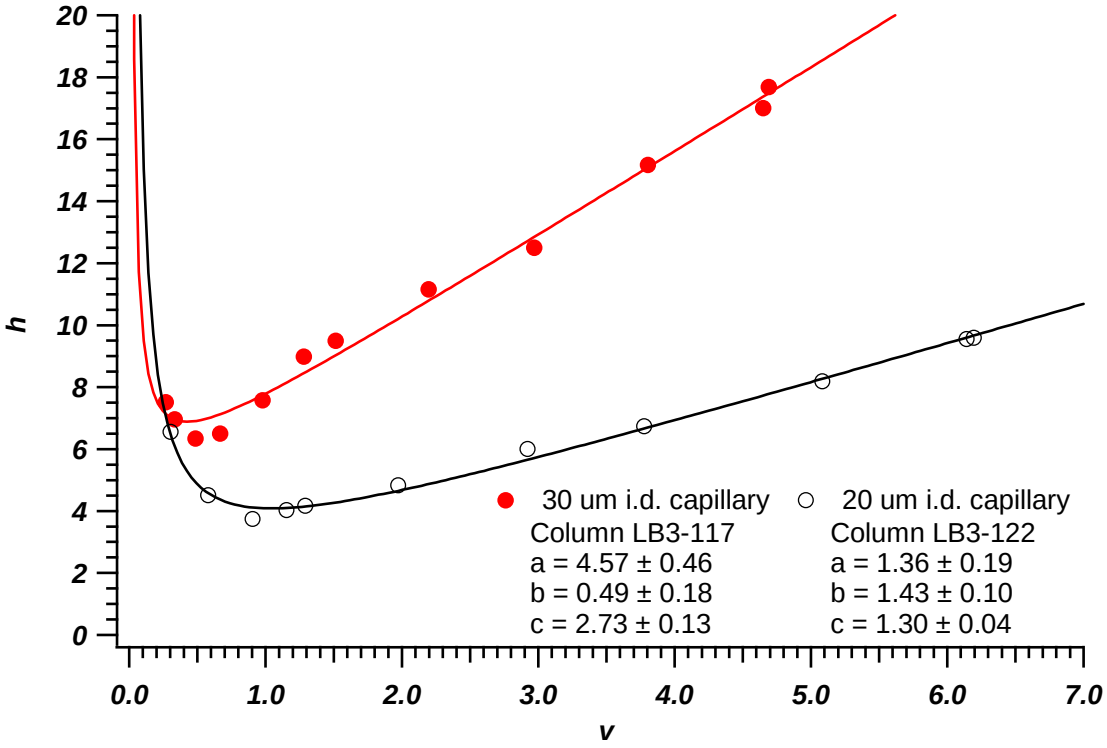

Figure 3-24: Reduced parameters plot for hydroquinone comparing the effect of the column inner diameter on column performance. Columns LB3-117 (30 µm i.d.) and LB3-122 (20 µm i.d.), LB3-104-3 particles bonded and endcapped using U.S. patent 20020070168, tri-functional silane, packed in solvent X. Mobile phase: 80/20 water/ACN 0.1% TFA. LB3-117: u_{opt} = 0.03 cm/sec (3600 psi), h_{min} (HQ) = 6.3, k' (4MC) = 0.58. LB3-122: u_{opt} = 0.06 cm/sec (5100 psi), h_{min} (HQ) = 3.7, k' (4MC) = 1.4

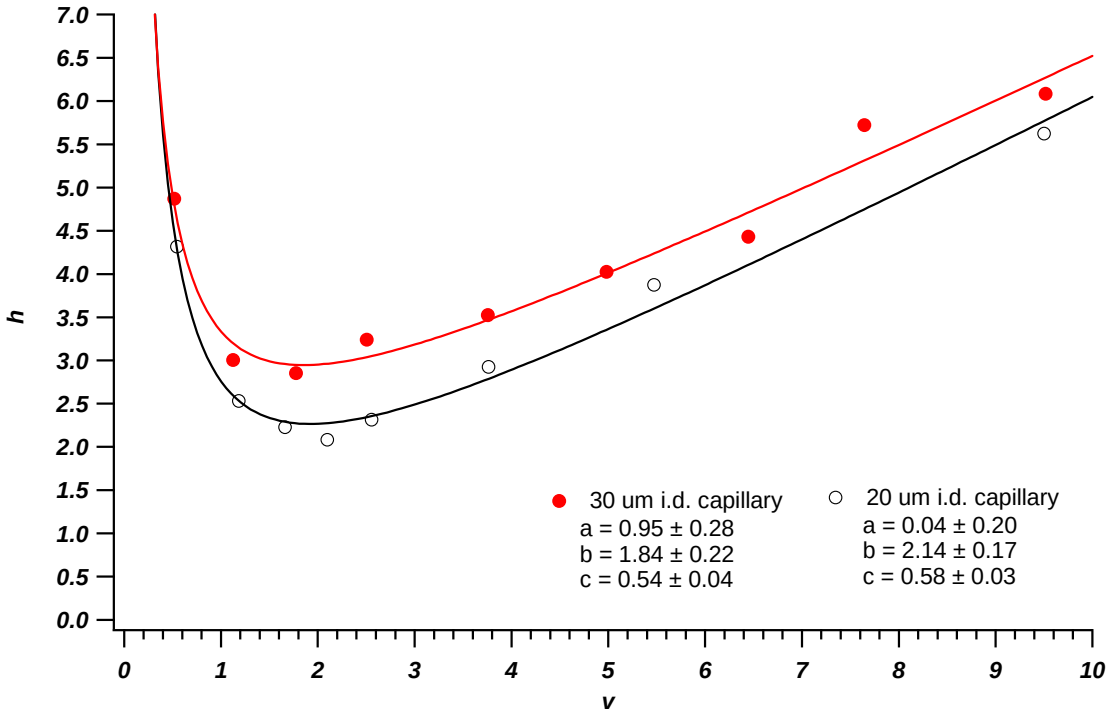

Figure 3-25: Reduced parameters plot for hydroquinone comparing the effect of the column inner diameter on column performance. Columns LB3-153 (30 µm i.d.) and LB4-12-C (20 µm i.d.), LB3-133-2 particles bonded and endcapped using U.S. patent 20020070168, tri-functional silane, packed in methanol. Mobile phase: 80/20 water/ACN 0.1% TFA. LB3-153: u_{opt} = 0.13 cm/sec (7000 psi), h_{min} (HQ) = 2.9, k' (4MC) = 1.1. LB4-12-C: u_{opt} = 0.13 cm/sec (18000 psi), h_{min} (HQ) = 2.1, k' (4MC) = 1.2.

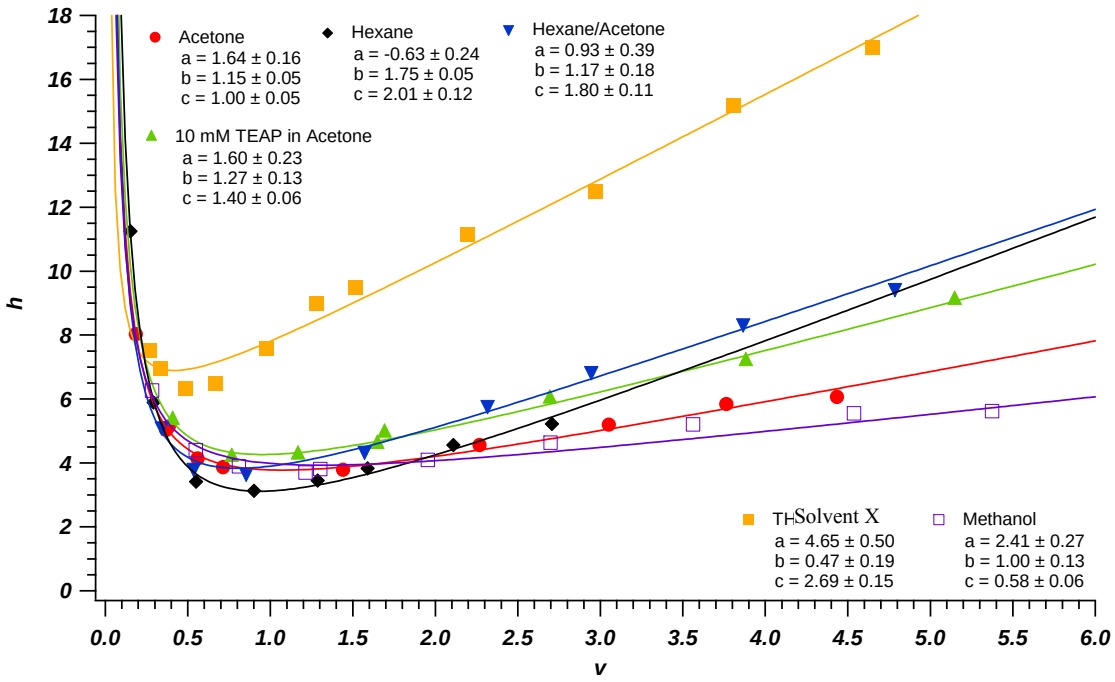

Figure 3-26: Reduced parameters plot comparing columns packed in different slurry solvents. LB3-104-3 particles, bonded and endcapped using U.S. patent 20020070168, tri-functional silane. Mobile phase: 80/20 water/ACN 0.1% TFA.

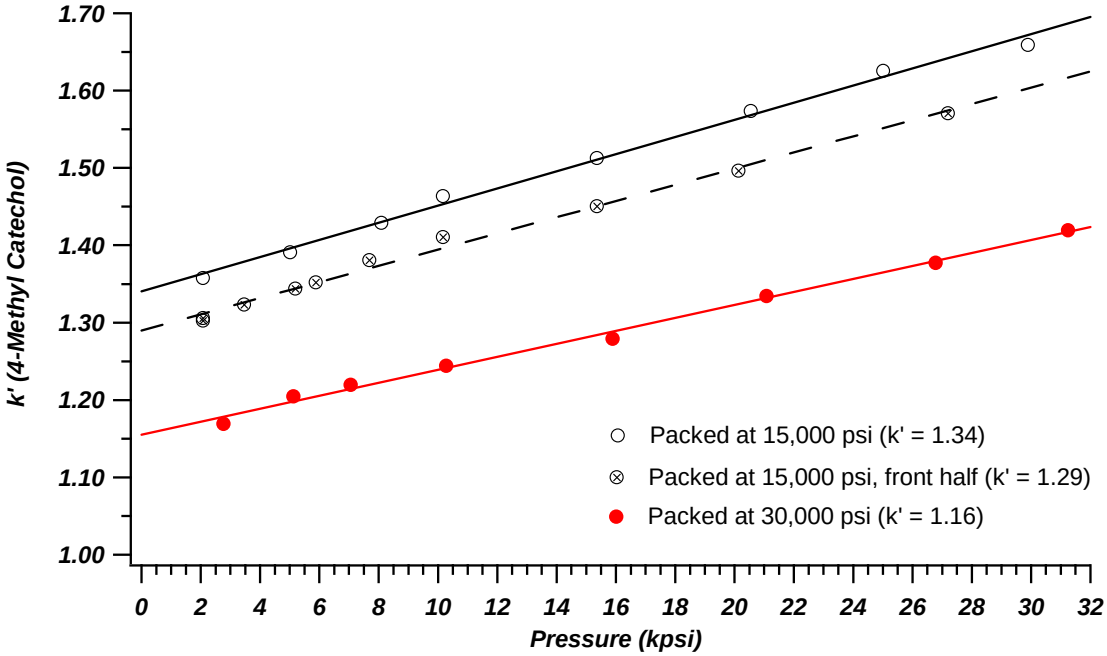

Figure 3-27: Effect of packing pressure on k'.

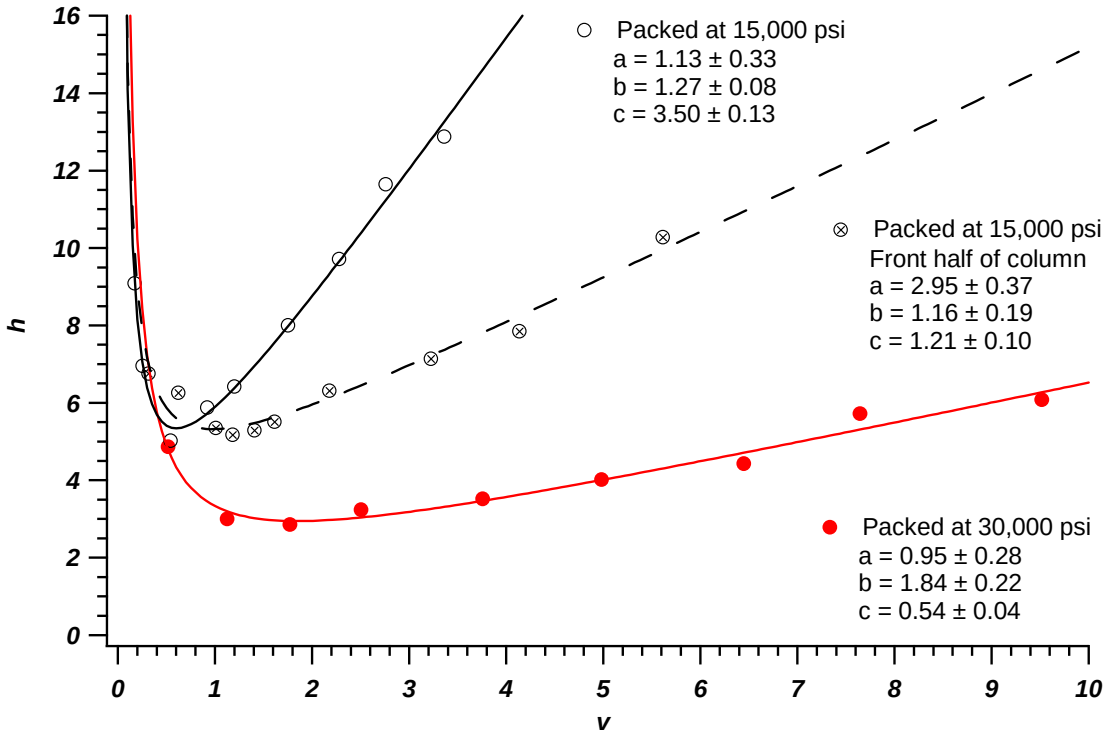

Figure 3-28: Effect of packing pressure on chromatographic performance. Particles LB3-133-2, bonded and endcapped with U.S. patent 20020070168, tri-functional silane, packed in methanol. Mobile phase: 80/20 water/ACN 0.1% TFA.

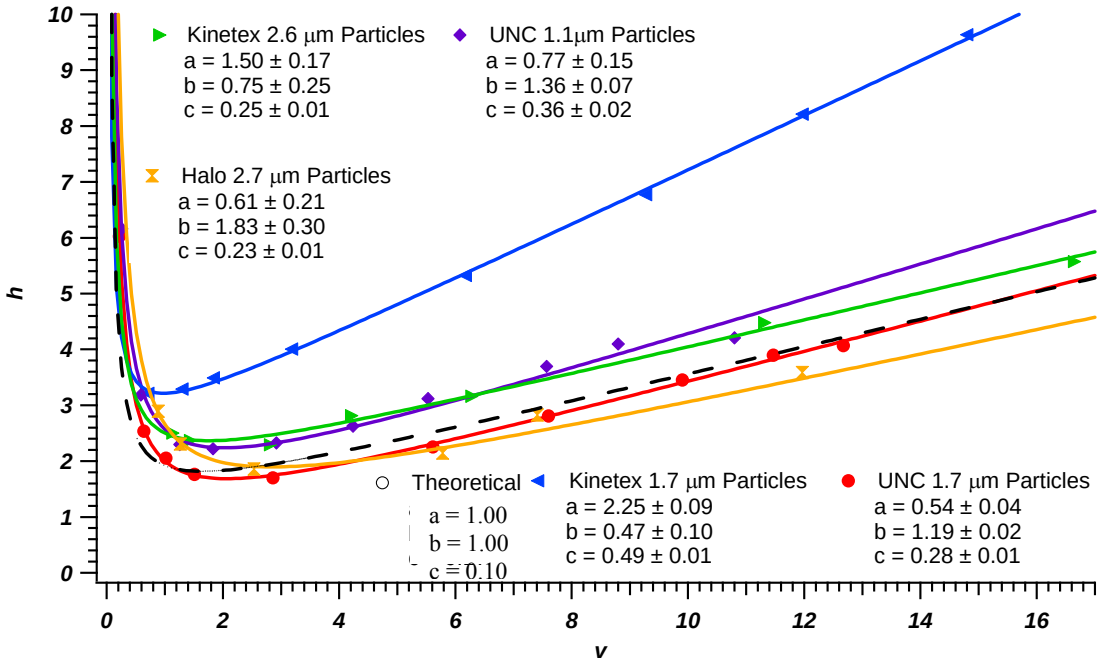

Figure 3-29: Reduced parameters plot comparing columns packed with particles synthesized in-house to those of commercial particles.

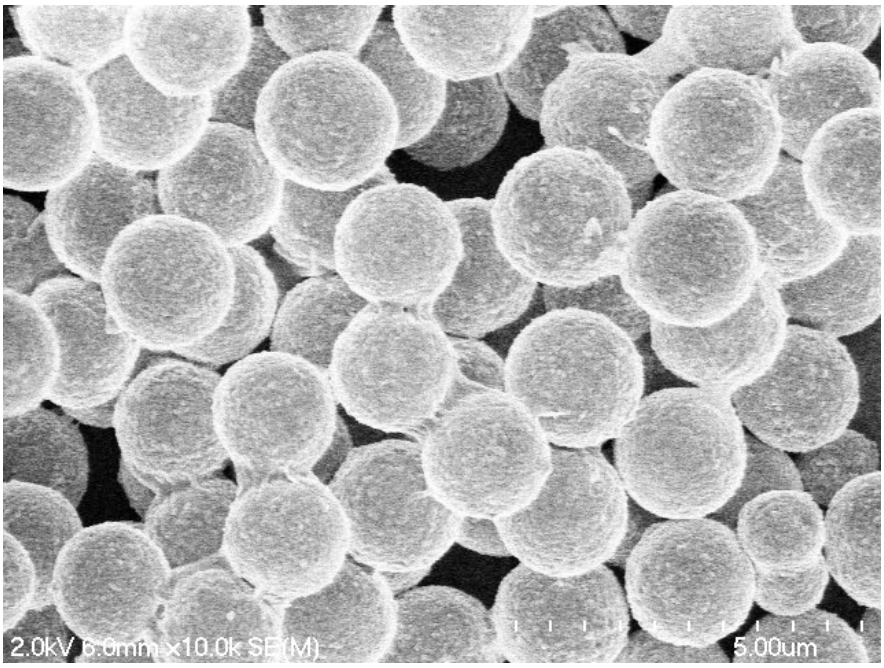

Figure 3-30: SEM images of 1.7 μm Kinetex particles showing the presence of particle multiplets.

CHAPTER 4: EFFECT OF COLLOIDAL SILICA DIAMETER ON PARTICLE PORE SIZE AND CHROMATOGRAPHIC PERFORMANCE

4.1 INTRODUCTION

Scientists have begun to focus on macromolecule separations in order to probe biological pathways, search for new therapeutic agents, and determine relationships between various organisms. The analysis of large peptides and intact proteins provides an additional layer of complexity over small molecules due to their physical size, which is the cause for the slow rate of diffusion. Slow diffusion as well as the protein conformation variation leads to more difficult separations and require the packing material pore size, stationary phase ligand length, and diffusion distance to be altered to produce efficient separations.

The physical characteristics of superficially porous particles lend themselves to improving the separation of macromolecules over totally porous particles. Since the *C*-term decreases as the distance over which mass transfer occurs decreases, and the *B*-term decreases as the mobile phase volume available for diffusion decreases, the solid core in superficially porous particles leads to improved efficiency. A theoretical comparison of van Deemter properties for totally porous particles versus superficially porous particles is illustrated in Figure 4-1 for small molecules. This gain in efficiency is predicted to be more dramatic for analytes that have low diffusion coefficients, such as large peptides (>30 amino acids) and proteins.

Another characteristic of superficially porous particles relates to the use of gradients for the separation of macromolecules. Studies have found that during gradient elution of peptides and proteins, the inner porous region of totally porous particles does not add any substantial sample loading capacity over superficially porous particles.[1, 2] This result is thought to be due to the sensitivity of proteins to changes in the mobile phase composition and their slower diffusion rates as compared to small molecules. When the organic concentration of the mobile phase is low, the majority of the analytes will be completely retained on the stationary phase on the exterior of the particle. As the organic mobile phase concentration is slightly increased, an analyte goes from being fully retained to completely unretained. Therefore, the analyte has almost no interaction with the stationary phase in the interior of a totally porous particle. Due to this behavior, using superficially porous particles should not greatly affect the sample loading capacity, but should allow for an increase in the column efficiency.

This phenomenon is not the case for small molecules that can easily traverse the entirety of the porous layer. While typical superficially porous particles have roughly 40% of the porous volume of totally porous particles, there is still a loss of loading capacity for small molecules. Thus, to prepare an improved packing material, a compromise of loading capacity versus improved chromatographic efficiency must be considered for analytes of varying size.

4.1.1 Effect of Pore Size on Separation Efficiency

The particle pore size has been found to greatly affect the separation efficiency and the biological activity of large peptides and proteins.[3-5] While the overall pore size of the packing material does play a role, it has been found that the absence of pores less than 200 Å is of greater importance for macromolecule separations. The presence of pores of equal or

smaller size than the analyte can lead to pore blockage or exclusion, which would lead to lower than expected retention and decreased resolution. Pores only slightly larger than the analyte or a pore network of varying size can lead to trapping of the analyte, producing broad peaks. Additionally, the use of small pores affects the unfolding of the protein and can lead to the loss of biological activity.[3]

To allow for the separation of a wide variety of analytes, it is preferred to have particle that allow for easy manipulation of the pore size. For many of the totally porous particle materials currently available the pore size is not easily tuned.[6] With the use of the layer-by-layer process to synthesize superficially porous particles, the ability to tune the pore size should be readily achieved by altering the size of the colloidal silica building the porous layers. By increasing the colloidal silica diameter used to construct the porous layers, the pore diameter should increase in a predictable fashion.[7, 8]

4.1.2 Effect of Bonded Chain Length on Retention

Within this chapter two bonded alkyl chain lengths are compared, C8 and C18. Based on previous findings, the length of the alkyl chain has been found to alter the retention and the nature of the analyte interaction, particularly for proteins.[3, 9-13] Generally, the retention of an analyte increases as the length of the bonded chain increases. While for small molecules a longer bonded chain is desired, as the analyte size grows the interaction with the stationary phase increases significantly leading to reduced resolving power for longer bonded alkyl chain lengths.[11,13]

Further deleterious effects to proteins have been found as the chain length increases such as loss of biological activity, reduced recovery, and formation of multiple conformations leading to peak multiplets.[10] The stationary phase ligand can significantly

affect the structure of the protein which can lead to loss of biological activity. The C18 ligand has been found to cause a greater extent of unfolding and at a greater rate than shorter ligands such as C8 and C4.[3,10, 14] The lower hydrophobicity and more rigid structure of the shorter ligands disrupt the protein to a lesser extent, therefore preserving the biologically active structure. Additionally, the use of longer ligands leads to reduced recovery of peptides and proteins. This loss of material on the column is believed to be due to the analyte size relative to the chain length and the pore size. As the stationary phase ligand length is increased, a greater number of adsorption sites are available and the amount of the analtye in contact with ligand increases. Both of these factors can hinder desorption since proteins are characterized by a narrow elution window and a multi-site binding pattern.[12] Lastly, the increased stationary phase ligand length can produce multiple peaks for the same analyte due to elution of the protein in various conformations. The greater the time a protein spends on the column the more conformational interconversion possible. Therefore, the increased retention with long chain ligands leads to a greater number of analyte conformations observed.[10] For these reasons it would be predicted that particles bonded with shorter alkyl chains would show greater efficiency for macromolecules.

4.1.3 Desirable Porous Layer Thickness Based on Analyte Size

The physical characteristics of superficially porous particles lend themselves to increased chromatographic efficiency through the presence of a solid core, therefore decreasing the diffusion distance within the particle. The presence of the core decreases the diffusion volume available for analyte broadening due to longitudinal diffusion and reduces the presence of the stagnant mobile phase mass transfer resistance contribution to the theoretical plate height. Independent of analyte size, the thinner the porous layer of the

particle the greater the efficiency, but also lower loading capacity. Furthermore, the decrease of the porous layer thickness requires reducing the eluent strength to maintain chromatographic retention and resolution.

A thinner porous layer is more advantageous for larger, slow diffusing analytes. Previous studies have found that for small molecules there was only a slight improvement in chromatographic performance for superficially porous particles over totally porous particles. On the other hand, for proteins dramatic improvements are seen as the porous layer thickness is decreased.[15] For these reasons, particles synthesized in-house have a porous layer less than 10% of the total particle diameter.

4.2 MATERIALS AND METHODS

4.2.1 Synthesis of 1.1 μm Superficially Porous Particles

Two batches of 1.1 μm particles were synthesized as described in Chapter 3. One batch was prepared with 12 nm colloidal silica and the other with 28 nm colloidal silica. Ludox AS-30 (12 nm) and Ludox AS-40 (28 nm) were purchased from Sigma Aldrich (St. Louis, MO). The particles were prepared using 0.5% (w/w%) LMW PDDA (Sigma Aldrich; St. Louis, MO) and 10% (w/w%) colloidal silica solutions. Three alternating layers were coated on 0.9 μm NPS cores (Fiber Optic Center; New Bedford, MA) for each colloidal silica size. The particles were dried by lyophilization at 30 mg particles/1.7 mL centrifuge tube. The particles were then heated at 540°C for 16 hours to remove the polyelectrolyte, followed by sintering at 940°C for 18 hours.

4.2.2 Synthesis of 1.6 μm Superficially Porous Particles

A batch of 1.6 μm particles were synthesized in a similar manner as described for the synthesis of 1.1 μm particles. A larger diameter particle was found to be necessary for the

initial synthesis with 67 nm colloidal silica due to difficulties with particle agglomeration with 1.1 μm particles. 1.4 μm NPS cores (EIChrom; Dillon, IL.) were coated with a single layer of 0.5% (w/w%) HMW PDDA (Sigma Aldrich; St. Louis, MO) and 5% (w/w%) 67 nm NexSil85 (Nyacol Nano Technologies, Inc.; Ashland, MA). The colloidal silica solution was adjusted to a pH of 2.0 with 5% (v/v%) aqueous nitric acid. After each coating step, the particles were washed in triplicate by allowing the particles to settle overnight. DI water was added to the particles in a 50 mL centrifuge tube, 30 mL water for every 100 mg particles, gently shaken, and allowed to settle on the bench top overnight or until all particles had settled to the bottom of the tube. The supernatant was then decanted and another portion of DI water was added. After one complete layer was attached, the particles were dried by lyophilization at 10 mg particles/1.7 mL centrifuge tube. The particles were then heated at 540°C for 16 hours to remove the polyelectrolyte, followed by sintering at 940°C for 18 hours.

4.2.3 Particle Characterization

Particle size distribution, growth rate, and colloidal silica surface coverage were evaluated by placing a sample aliquot on an aluminum SEM stub for imaging using a through-the-lens (TTL) detector on a Hitachi S-4700 cold cathode field emission SEM (Tokyo, Japan). Using these images, Image J software produced by the National Institute of Health (Bethesda, MD) was used to measure the diameters of 250 particles.

The porous layer thickness, T_p, was calculated as follows:

$$T_p = \frac{d_{p,n} - d_{core}}{2} \tag{4-1}$$

where $d_{p,n}$ is the number average total particle diameter and d_{core} is the NPS core number average diameter.

The ratio of the pore diameter to the core particle diameter was used to determine the closeness of the colloidal silica layer structure to close packed particles.

$$R_{cs} = \frac{d_{pore}}{d_{cs}} \tag{4-2}$$

where d_{pore} is the average pore diameter of the particle as determined by BET analysis and d_{cs} is the number average diameter of the colloidal silica coated on the NPS core. If the colloidal silica particles are arrange in a close packed arrangement the R_{cs} value would be equal to 0.15.

Elemental analysis was performed using a Perkin Elmer CHN/S O elemental analyzer Series 2400 instrument (Waltham, MA). The surface area, pore volume, and pore diameter measurements were carried out on non-bonded particles by Waters Corporation (Milford, MA) using a Micrometrics ASAP2420 (Norcross, GA) for Brunauer, Emmet, Teller (BET) analysis. Pore size and volume measurements by mercury intrusion were carried out on non-bonded particles by Waters Corporation (Milford, MA) using a Micrometrics AutoPore IV 9500 series pore size analyzer (Norcross, GA). The particle size of non-bonded particles determined by disc centrifuge was carried out by Waters Corporation (Milford, MA) using a CPS disc centrifuge (CPS Instruments; Newtown, PA). The plotted range was set by the maximum particle diameter and minimum particle diameter measured. The ranges for the distribution table were set with five equally spaced ranges based on the log scale.

4.2.4 Particle Bonding and Endcapping

Particles functionalized with C18 were prepared according to U.S. patent 20100076103.[16] They were bonded with n-octadecyldimethylchlorosilane (Gelest; Morrisville, PA) in toluene with imidazole as the base activator. Both toluene and imidazole were purchased from Sigma-Aldrich (St. Louis, MO). The particles were then endcapped

with trimethylchlorosilane (Gelest; Morrisville, PA) in toluene with imidazole as the base activator.

Particles functionalized with C8 were prepared according to U.S. patent 20100076103.[16] They were bonded with n-octyldimethylchlorosilane (Gelest; Morrisville, PA) in toluene with imidazole as the base activator. The particles were then endcapped with trimethylchlorosilane (Gelest; Morrisville, PA) in toluene with imidazole as the base activator.

4.2.5 Column Packing

Fused silica capillary tubing (Polymicro Technologies, Inc., Phoenix, AZ) with an inner diameter (i.d.) of 30 μm and an outer diameter of 360 μm was used to pack all columns for small molecule characterization. Fused silica capillary tubing with an inner diameter of 75 μm and an outer diameter of 360 μm was used to pack all columns for peptide and protein characterization. The columns were prepared with outlet frits as outlined in Chapter 2. The procedure for packing capillary columns has be previously described.[17-20] Briefly, the particles were suspended in methanol (Fisher Scientific; Waltham, MA) at a concentration of 3 mg/mL. The slurry solvent was filtered with a 0.2 μm PTFE filter before use. The slurry was sonicated for 10 minutes using a Cole Parmer Ultrasonic Cleaner 8891 (Vernon Hills, IL). A packing reservoir was then filled with the slurry solution and acetone was used as the pushing solvent. The capillary column was placed in a UHPLC fitting and secured to the column packing apparatus. Column packing was initiated at 3000 psi, and as the bed began to form the pressure was gradually increased until reaching 30,000 psi at a rate of 3000 psi per centimeter of bed growth for the 30 μm i.d. columns. The 75 μm i.d. columns were packed

up to 20,000 psi. The packing process was stopped when the desired column length was reached by slowly releasing the pressure.

After the desired column length was reached, the column was pressurized to ~45,000 psi (30 μm i.d. columns) or 20,000 psi (75 μm i.d. columns) and flushed with several column volumes of 80/20 (v/v) water/acetonitrile (ACN) with 0.1% trifluoroacetic acid (TFA) mobile phase (Fisher Scientific; Waltham, MA). The pressure was slowly released and re-pressurized to ~10,000 psi. A temporary inlet frit was then put in place using a heated wire stripper (Teledyne Interconnect Devices, San Diego, CA). The column was then clipped to the desired final length. The permanent inlet frit was then prepared using a procedure described by Maiolica *et. al*..[21] The column inlet was gently pressed on a glass microfiber filter (Reeve Angel; Clifton, NJ) that was previously wetted with 1:1 (v:v) ratio of potassium silicate (Kasil) and formamide. The Kasil was used as received from PQ Corporation (Valley Forge, IA) and formamide was from Sigma Aldrich (St. Louis, MO). After a few minutes, the glass microfiber filter had hardened, but to ensure it could withstand the running pressures, the frit was set in place using an electric arc device.

4.2.6 Column Evaluation for Small Molecules

The detailed experimental set-up used to perform isocratic UHPLC has been previously described and was carried out as described in Chapter 2.[19, 20, 22, 23]

The mobile phase used for chromatographic evaluation of the 1.1 μm particles was 80/20 (v/v) water/ACN with 0.1% TFA. The mobile phase used for chromatographic evaluation of the 1.6 μm particles was 90/10 (v/v) water/ACN with 0.1% TFA. The isocratic test mixture contained L-ascorbic acid, which served as the dead time marker, hydroquinone

(HQ), resorcinol (R), catechol (C), and 4-methyl catechol (4MC). The concentration of each sample in the test mixture was ~200 μM.

The columns that were used for this experiment were evaluated on the basis of chromatographic performance and retentivity. Column performance and analysis was carried out as described in Chapter 2.

The peak symmetry was assessed by determining the tailing factor, T_f, for each test analyte.

$$T_f = \frac{w_{full,5\%}}{2w_{front,5\%}} \tag{4-3}$$

Where the peak width at 5% of the maximum height, $w_{full,5\%}$, and the front half width at 5% of the maximum height, $w_{front,5\%}$, are used to determine the extent of the asymmetry.[17]

The column retentivity was evaluated by plotting the k' of each analyte versus the applied pressure. A line of best fit was made through the data points giving the y-intercept, k' at atmospheric pressure. The k' at atmospheric pressure for 4MC was used to compare the retentivity and packing density of different columns. The retentivity of a column can be used to compare the relative density of packing, assuming the same bonding and endcapping coverage, because it is directly related to the phase ratio.

4.2.7 Column Evaluation for Peptides and Proteins

The gradient and sample injection was carried out by capillary ultra-high performance LC-MS^E (UPLC-MS^E) using a Waters nanoAcquity LC system and a Waters Q-TOF Premier mass spectrometer (Milford, MA). Mobile phase A consisted of HPLC grade water with 0.1% formic acid and mobile phase B consisted of HPLC grade acetonitrile with 0.1% formic acid (Fisher Scientific; Waltham, MA). A 1.0 uL injection of 100 fM enolase digest was made in partial loop, direct injection mode for all columns except the Acquity BEH column

which was run in trapping mode. Separations were performed on an analytical column with a 75 μm i.d. and packed with one of the three types of particles synthesized. The column temperature was regulated at 40°C. Connection with the mass spectrometer was achieved by connecting approximately 20 cm of 20 μm i.d. capillary from the outlet of the column directly to the nanoflow lockspray-ESI source fitted with a 20 μm i.d. capillary pulled to 10 μm at the tip. The standard solution for the reference channel of the nano-lockspray was 200 fmol/μL glu-fibrinopepetide, which was supplied by an auxiliary pump on the nanoAcquity system at 0.5 μL/min. The full gradient for the separation is specified in Table 4-1.

The Q-TOF Premier was operated in positive ionization mode with the lockspray enabled and the reflectron operated in V mode. The sample cone and extraction cone were held at +35V, and +4V, respectively. The scan time for the low energy, elevated energy, and reference scans was 0.6 seconds across the *m/z* range from 100 to 1900. The collision energy was held at 5V for the low energy scans, 6V for the reference scans, and ramped from 15 – 40V during the elevated energy scan. The reference channel was sampled every 30 seconds.

The same instrument and instrumental conditions stated for the peptide separation were used for protein separation. The sample was a mixture of thyroglobulin 700 kDa), β-lactoglobulin (18.4 kDa), RNase-A (13.7 kDa), cytochrome c (12.3 kDa), myoglobin (17.0 kDa), and bovine serum albumin (BSA) (66.5 kDa). The column temperature was maintained at 65°C.

For the peptide separations, the peak capacity of the column was calculated as follows:

$$P_c = 1 + \frac{\Delta t}{4\sigma_t R_s} \tag{4-4}$$

Where Δt is the length of the gradient, R_s is the resolution between consecutive peak pairs, and σ_t is the peak standard deviation in time units for the *m/z* 644 peak. For all analyses, the length of the gradient was equal to 30 minutes and the resolution was set to one.

The peak width for the *m/z* 644 peak was calculated at 5% of the peak maximum height. To determine the peak width of β-lactoglobulin, the raw protein deconvolution data was run through AutoME. Noise was removed through the Standard Definition Filter (StDef Filter) in LabView designed by James RJ Parks. The intensity threshold and the signal-to-noise multiplier were set to 200 and 2, respectively. Following noise removal, the harmonics were removed using the StDef Filter. The peak width for β-lactoglobulin was determined from the generation of a 3D plot of intensity, mass, and retention time generated from the StDef Filter.

4.3 RESULTS AND DISCUSSION

4.3.1 Physical Characteristics

All of the particles synthesized were found to be monodisperse and have uniform surface coverage. The particle size distribution for all of the particles was found to be narrower than for commercially available particles (RSD = 5%).[15] The relative standard deviation for the 12 nm, 28 nm, and 67 nm colloidal silica coated particles was 2.1%, 3.8%, and 3.8%, respectively, Figures 4-2 through 4-4. The RSD for the 12 nm coated particles is comparable to that for the NPS core particles, 1.7%, but the larger colloidal silica coated particles showed increased variability. This increased variability would be expected for the 67 nm colloidal silica due to the increased polydispersity of the colloidal silica particles. While the size of the colloidal silica coating the NPS particles can be partially controlled (selectively coating larger particles) by adjusting the pH, there is still a greater variability in

size than for the 12 nm and 28 nm colloidal silica. The colloidal silica diameter on the 67 nm coated particles ranged from 40 nm to 80 nm. The wider particle size distribution for the 28 nm coated particles was not expected. Comparison of the surface coating shows that the 28 nm coated particles are slightly less uniform than the 12 nm coated particles, Figure 4-5. This variation does not seem to be due to a wider colloidal silica particle size distribution, but due to the decreased uniformity of the coating.

In addition to measurement of the particle size and distribution using SEM images, the particle size was also assessed using disc centrifuge analysis, Figures 4-6 through 4-8. With this technique, the particles are dispersed in water and added to a sucrose gradient within the disc. The multiple distinct peaks seen in the disc centrifuge results indicate the presence of higher order multiplets. For all samples, multiplets up to four particles were observed. For each size of colloidal silica, the particle size measured by disc centrifuge was slightly greater than that measured from SEM images, but still in agreement. Additionally, the polydispersity index between all the particles was very similar, Table 4-2. This value is the ratio between the weight mean and the number mean, indicating a polydisperse sample when the value is greater than one.[17]

For all particle types, the fraction of particles in the expected size range was between 70% and 80%, with the 28 nm coated particles having the greatest number of particles in the predicted size range. For all the particles, the size range that had the next highest fraction of particles was in the region that would indicate the formation of particle doublets. While this may have had a contribution from the presence of doublets in the NPS starting material, it is believed that a number of doublets are also formed during the synthesis. The process of washing by centrifugation and the addition of the reagents have been found to lead to particle

agglomeration, as discussed in Chapters 2 and 3. The process of washing by settling has been found to reduce the number of particle agglomerates formed for particles with large diameter colloidal silica, but does not completely eliminated their formation. A batch of 28 nm coated particles was synthesized by settling, and the fraction of particles in the expected range was 70%, which is within the same range but slightly lower than that seen for the particles prepared by centrifugation, Table 4-3. While the settled particles were observed to have a smoother surface the amount of particle agglomeration was not reduced by settling. The increase in the number of particle doublets may have been due to the increased time of particle contact due to the slow rate of sedimentation by settling. For all the samples the disc centrifuge results show very few particles with higher order particle multiplets.

As the colloidal silica diameter was increased it was predicted that the pore size would increase accordingly. This was found to be the case for increasing the colloidal silica diameter from 12 nm to 28 nm, Table 4-4. The pore diameter increased and specific surface area decreased by 210% and 220%, respectively. This is in agreement with the increase in colloidal silica particle diameter of 230%. In contrast, while the pore size increased for the 67 nm coated particles, the same pore size growth trend was not found. The colloidal silica particle diameter was increased 560% over the 12 nm colloidal silica, but the pore diameter increased by only 290%. This discrepancy may be due to the multiple layers present on the 12 nm coated particles and the single layer present for the 67 nm coated particles. As multiple layers are added, the deviation from hexagonal close packing increases as observed by the increased irregularity in the surface uniformity. A single layer, as is the case with the 67 nm colloidal silica, will be almost perfectly close packed assuming monodisperse colloidal silica diameter. For monodisperse, close packed particles, the ratio of the pore

diameter to the colloidal silica particle diameter would be equal to 0.15. For the 12 nm and 28 nm colloidal silica coated particles R_{cs} is much higher than for close packed particles, but for the 67 nm coated particles the packing ratio is much lower (0.37) and is approaching that for close packed particles. This irregularity seen for the multiple layer, smaller diameter colloidal silica would produce larger pores than if only hexagonal close packing was present. In comparing the two particles with multiple layers, it can be inferred that the layering process is similar due to the correlation in pore size produced and colloidal silica diameter. The 12 nm coated particles were found to have a pore size similar to the majority of commercial superficially porous particles and suitable for small molecule analysis. The particles coated with the 28 nm colloidal silica have pores similar to the commercial peptide columns such as Halo-Peptide (Advanced Materials Technology), Poroshell 120 (Agilent Technologies), and Aeris (Phenomenex). The 67 nm colloidal silica coated particles are similar in pore size to the Poroshell 300 (Agilent Technologies) and Aeris WIDEPORE (Phenomenex) particles, but are much smaller in total particle diameter which should lead to improved efficiency. While increased pore diameter was seen, the pore size should be increased further to allow for application of large proteins and monoclonal antibodies which have been receiving increased attention recently.

The specific surface area of the particles was also measured and correlates well to predicted values. The specific surface area for the 28 nm colloidal silica coated particles decreased by 220% compared to the 12 nm particles. This correlates to the 230% increase in colloidal silica diameter. Taking the increased size and therefore weight of the core for the 67 nm colloidal silica coated particles and the presence of only one layer of colloidal silica, the specific surface area for these particles, 6 m^2/g, is as predicted from theoretical calculations

of hexagonal close packing of colloidal silica on a 1.4 μm NPS core, 6.4 m^2/g. Due to the thin porous layer, the surface area of the in-house particles was much lower than the commercially available products. While surface area is a concern, the potential efficiency gained by having a thinner porous layer should compensate for the loss in loading capacity. [2] Furthermore, due to the catch-and-release separation mechanism for macromolecules, this low surface area should have a loading capacity reduction less than expected.

4.3.2 Small Molecule Performance

The separation efficiency of the particles of varying pore size was assessed based on chromatographic performance of four catechols, each approximately 100 Da. From previous studies it has been found that the performance of small molecules is not affected by the pore size due to the relatively large pore space compared to the analyte size. The particles with 87Å and 187 Å pores allowed for complete resolution of the test analytes and produced symmetrical peaks for each analyte, Figure 4-9. The tailing factor for the 187 Å pore particles was slightly better, but not significantly different, Table 4-5. Both of these particles produced columns having greater than 300,000 plates/meter, which is much greater than that seen for 2.7 μm Halo, 2.6 μm Kinetex, and 1.7 μm Kinetex particles tested in our laboratory. The 2.7 μm Halo, 2.6 μm Kinetex, and 1.7 μm Kinetex particles were found to have 199,000 plates/meter, 162,000 plates/meter, and 183,000 plates/meter, respectively. The 248 Å pore particles did not perform as well as the smaller pore size particles. As seen in Figure 4-10, the peaks are much broader and show tailing for the more retained analytes. This column produced 189,000 plates/meter, which is in line with the commercially available product of similar particle diameter, 1.7 μm Kinetex.

Further assessment was carried out by comparing the reduced parameter plot of hydroquinone fit to the van Deemter equation for each type of particle, Figure 4-11. The performance of the 87 Å and 187 Å pore particles were found to have equivalent performance over the range of linear velocities tested. Due to the small size of the test analytes, all of the pore sizes investigated should not show any decrease in chromatographic performance due to hindered analyte diffusion. In contrast, the 248 Å pore particles did not perform as well as the other particles. The *c*-term value for these particles was equivalent to the smaller pore diameter particles, but deviation in performance was shown with an increase in the *a*-term. This would indicate that there was greater variation in the packed bed structure. These particles were found to have a rougher particle surface due to the use of larger size colloidal silica. The particle surface roughness has been found to affect the column packing previously, where the rough surface is predicted to produce a bed with a lower *a*-tem than that for a smooth particle.[24] In this previous study, the surface roughness was tested for particles with relatively small pore size material, while the particles under discussion have a much greater peak-to-valley distance due to the size of the colloidal silica used, Figure 4-5. This feature may lead to the inability of the particles to slip past each other while packing, which would lead to greater variations in the bed structure, in turn increasing the *a*-term contribution to the theoretical plate height.

The 248 Å pore particles were run in a lower eluent strength mobile phase due to the lower surface area, which does not allow for direct comparison of the capacity factors between the 248 Å pore particle column and the better performing, smaller pore particle columns. The relative comparison between the capacity factors for the 248 Å pore particles, 0.9, and that for the 87 Å and 187 Å pore particles, 1.3, indicate that the packing density of

the larger pore material is less dense than the smaller pore particle columns. Based on the amount of stationary phase per column volume, Table 4-6, it would be predicted that the retention of the 248 Å pore particles would be approximately 23% lower than the 87 Å and 187 Å pore particles with the same mobile phase, which would lead to a k' of approximately 1.0. Since a lower strength mobile phase was used for the 248 Å pore particles, it would be predicted that the capacity factor would be greater than this due entirely to the lower eluent strength, but this was not found to be the case. This indicates the presence of a lower amount of stationary phase per column volume and therefore a lower packing density for the 248 Å pore particles. Alternatively, when comparing the phase ratios between the columns, the results were not in agreement. The 87 Å and 187 Å pore particle columns were found to have the same k', but the phase ratio of the 187 Å pore particles was roughly half that found for the 87 Å pore particles. Since the same interparticle porosity was assumed for all columns, any packing density variations would not be taken into account making direct comparisons by phase ratio unreliable.

The performance of large molecules has been found to be affected by the length of the bonded ligand. Two batches of 248 Å pore particles were prepared, one bonded with C18 and the other with C8. Before analysis with peptides and proteins, the performance was assessed using our small molecule isocratic UHPLC set-up. Independent of bonded ligand length, all test analytes were well resolved and produced symmetrical peaks, Figure 4-12. Based on the reduced parameters plot of hydroquinone for these two columns, Figure 4-13, the *c*-term for the C8 column was found to be lower than for the C18 column. The increase in the efficiency as the capacity factor is decreased agrees with chromatographic theory.

4.3.3 Peptide Performance

As the pore size of the particle is increased, the particle should be better suited for the separation of molecules of increasing size. To asses each particle's performance for peptide separations, enolase digest was run and the chromatographic characteristics were assessed, Figure 4-14. As shown, all particles were found to separate several components of the enolase digest, but fewer peptides than typically seen with columns packed with totally porous particles was observed. Analyte adsorption was found to be the most dramatic for the 187 Å pore particles, but was evident for all particles bonded in-house as compared to commercial Acquity BEH particles, Figure 4-15C. This adsorption behavior is further indicated by the presence of peak tailing for the 87 Å pore particles, indicating the presence of a secondary adsorption mechanism. The presence of surface adsorption was not further tested, but may be caused by incomplete bonding and endcapping ligand surface coverage. Further refinement of the bonding method may lead to improvement in analyte recovery. The small pores of the 87 Å pore particles may have also contributed to the peak broadening due to hindered movement of the peptides within the pores.

Of the peaks present, the peaks at *m/z* of 644 was always present and were used to better asses the chromatographic performance, Table 4-5. The peak width of the *m/z* 644 peak was found to improve as the pore size was increased. While the pore size may have a slight effect, particularly for the 87 Å pore particles, the increased surface coverage of the bonded stationary phase ligand as the pore size was increased is more likely the reason for the improved peak shape. Accordingly, as the peak width was improved the peak capacity was also found to increase.

As a performance comparison, the particles synthesized in-house were compared to 1.5 μm NPS particles, C18 bonded in-house and commercial 1.9 μm Acquity BEH C18 particles Figure 4-15. As previously mentioned, a large amount of analyte adsorption was found to be present on columns bonded in-house, as indicated by the 1.5 μm NPS and 248 Å pore particles. In comparing the performance of the *m/z* 644 peak, all three columns were found to produce similar peak widths and peak capacities. While the goal was to produce columns of higher efficiency than currently available products, the performance should be able to be improved if the bonding method can reduced the amount of peptide surface adsorption.

As mentioned previously, another factor thought to contribute to the separation of larger analytes is the length of the bonded ligand on the particle. As the analyte size is increase, the stationary phase chain length is many times decreased to a C8 or C4 to improve the rate of mass transfer and reduce recovery loss. To asses the effect of the stationary phase chain length on peptide performance, a batch of 248 Å pore particles was synthesized and bonded with both C18 and C8. The particles bonded with the C8 ligand were found to have worse performance than the particles bonded with C18, Figure 4-16. As seen by the large peak in the beginning of the chromatogram for the C8 column, silanes were constantly eluting from the column. The silane peak would often times be seen at the beginning of the run, but was also found to be present at later elution times. The silane elution may be the bonding or endcapping reagent washing off the column. This would explain the increased peak broadness for this column due to increased silanol interaction. Therefore, C8 may not actually perform worse than the C18 if a proper and effective bonding technique is carried out.

4.3.4 Protein Performance

The separation of proteins should be best achieved by using particles in which all pores are larger than the test analytes. The effect of the pore size on the separation of a protein mixture was evaluated with the superficially porous particles synthesized in-house. All three pore sizes produced lower than expected resolution between the analytes, Figure 4-17. While in all cases the chromatographic efficiency was low, there was some improvement seen when the pore size was increased. For the 87 Å pore particles, only RNAse-A and myoglobin were found to be resolved, Figure 4-18, and the peak width for myoglobin was found to be 9.0 minutes. This performance was predicted to be similar to that of a non-porous particle because all of the pores present should have been too small for a protein to enter, therefore acting as if non-porous. When compared to the results obtained for 1.5 μm NPS particles, the performance of the NPS particles was found to be slightly better. The elution of cytochrome c was observed and the myoglobin peak width decreased to 6.0 minutes, Figure 4-19. The inferior performance of the 87 Å pore particles may be due to the protein molecules becoming trapped in the small pores coated with stationary phase, therefore producing wider peaks. As the pore size of the superficially porous particles was increased to 187 Å, the resolution of cytochrome c was observed, but the peak width of myoglobin was found to be the same as that for the 87 Å pore particles, Figure 4-20. When the pore size was further increased to 248 Å, the intensity of the cytochrome c peak slightly increased and the peak width of myglobin was greatly decreased to 3.5 minutes, Figure 4-21. Previously, protein peak broadening has been found to be greatly affected by the presence of a trace level of metals which greatly affect silanol acidity and can act as chelating agents.[25] The amount of metals within these particles has not been tested and may be playing a role in the lower

than expected efficiency. While high efficiency was not observed, as the pore size was increased the resolution of cytochrome c became possible and the myoglobin peak was much narrower.

A further factor that has been found to play a role in the separation efficiency of proteins is the bonded ligand chain length. All previously discussed particles were bonded with C18, which is typically believed to be too long for use with proteins. To determine if the ligand chain length was affecting our separation efficiency, a batch of 248 Å pore particles was bonded with C8. As seen in Figure 4-22, the resolution of the analytes based on the chromatogram was not greatly improved with the use of C8, but based on the deconvolution profiles, increased resolution was observed, Figure 4-23. Both cytochrome c and β-lactoglobulin were observed and at a much higher intensity than seen with the C18 particles. Therefore, the use of a short ligand chain length did improve the efficiency of the separation and efficiency may be able to be further improved by using C4.

4.4 CONCLUSIONS

The pore size of the superficially porous particles was found to be adjustable by varying the size of the colloidal silica used in the coating process. When the same layering procedure is used, the pore size can be reliably predicted from the diameter of the colloidal silica used to build the porous layer. The small molecule performance of the 87 Å and 187 Å pore particles were found to have equivalent performance, which was slightly worse than theoretical predictions. The 248 Å pore particles were worse performing than the smaller diameter pore particles in terms of *a*-term, indicating a less uniform packing which may be due to the large size of the colloidal silica. All the particles were found to have a large amount of peptide adsorption due to inadequate bonding ligand surface coverage, but the

peak widths were similar to that seen for NPS particles and Acquity BEH particles. The separation of proteins was found to slightly improve as the pore size was increased, but for all cases very broad peaks were observed. The separation efficiency of proteins was further improved by the use of C8 instead of C18.

4.5 REFERENCES

[1] Urban, J.; Jandera, P.; Kucerova, Z.; van Straten, M.; Claessens, H. (2007). *J. Chrom. A* 116 (2007) 63-75.

[2] Gritti, F.; Guiochon, G. *J. Chrom. A* 1176 (2007) 107-122.

[3] Dillon, T.M.; Bondarenko, P.V.; Rehder, D.S.; Pipes, G.D.; Kleemann, G.R.; Speed Ricci, M. *J. Chrom. A* 1120 (2006) 112-120.

[4] Tanaka, N.; Kimata, K.; Mikawa, Y.; Hosoya, K.; Araki, T.; Ohtsu, Y.; Shiojima, Y.; Tsuboi, R.; Tsuchiya, H. *J. Chromagr.* 535 (1990) 13-31.

[5] Guan-Sajonz, H.; Guiochon, G.; Davis, E.; Gulakowski, K.; Smith, D.W. *J. Chrom. A* 773 (1997) 33-51.

[6] Unger, K.K.; Skudas, R.; Schulte, M.M. *J. Chrom. A* (2008) 393-415.

[7] Kirkland, J.J.; Truszkowski, F.A.; Ricker, R.D. *J. Chrom. A* 965 (2002) 25-34.

[8] Blue, L.E.; Jorgenson, J.W. *J. Chrom. A* 1218 (2011) 7989-7995.

[9] Rafferty, J.L.; Siepmann, J.I.; Schure, M.R. *J. Chrom. A* 1216 (2009) 2320-2331.

[10] Purcell, A.W.; Aguilar, M-I.; Hearn, M.T. Anal. Chem. 71 (1999) 2440-2451.

[11] Pearson, J.D.; Mahoney, W.C.; Hermodson, M.A.; Regnier, F.E. *J. Chrom.* 207 (1981) 325-332.

[12] Pearson, J.D.; Lin, N.T.; Regnier, F.E. *Anal. Biochem.* 124 (1982) 217-230.

[13] Hemetsberger, H.; Behrensmeyer, P.; Henning, J.; Ricken, H. *Chromatographia* 12 (1979) 71-76.

[14] McNay, J.L.; Fernandez, E.K. *Biotech. Bioeng.* 76 (2001) 224-232.

[15] Gritti, F.; Leonardis, I.; Abia, J.; Guiochon, G. *J. Chrom. A* 1217 (2010) 3918-3843.

[16] Wyndham, K.D.; O'Gara, J.E. *US Patent 20100076103* 2007.

[17] Neue, U.D.; *HPLC Columns: Theory, Technology, and Practice*, Wiley-VCH, New York, 1997.

[18] Martin, M.; Blu, G.; Guiochon, G. *J. Chrom. Science* 11 (1973) 641-654.

[19] Mellors, J.S. *UNC Doctoral Dissertation* 2005.

[20] MacNair, J.E.; Patel, K.D.; Jorgenson, J.W. *Anal. Chem.* 71 (1999) 700-708.

[21] Maiolica, A.; Borsotti, D.; Rappsilber, J. *Proteomics* 5 (2005) 3847-3850.

[22] MacNair, J.E.; Lewis, K.C.; Jorgenson, J.W. *Anal. Chem.* 69 (1997) 983-989.

[23] Bernga, H.E.; Kirkland, J.J. *US Patent 4,447,492* 1984.

[24] Gritti, F.; Guiochon, G. *J. Chrom. A* 1166 (2007) 30-46.

[25] Snyder, L.; Kirkland, J.J.; Dolan, J.W.. *Practical HPLC Method Development*, John Wiley & Sons Inc., New York, 3nd ed., 2010.

4.6 TABLES

Time (minutes)	Flow Rate (μL/min)	% Water	% Acetonitrile
0	0.300	95	5
30	0.300	60	40
33	0.300	15	85
38	0.300	15	85
40	0.300	95	5
90	0.300	95	5

Table 4-1: Gradient method used for separation of enolase digest and protein mixture by LC/MS. gradient applied as a linear ramp.

12 nm Coated Particles		28 nm Coated Particles		67 nm Coated Particles	
Number Diameter (μm)	1.21	**Number Diameter (μm)**	1.18	**Number Diameter (μm)**	1.71
Polydispersity Index	1.26	**Polydispersity Index**	1.23	**Polydispersity Index**	1.15
Diameter Range	**% Fraction**	**Diameter Range**	**% Fraction**	**Diameter Range**	**% Fraction**
0.57 – 0.87	0.20	0.60 – 0.86	0.30	0.61 – 0.90	0.82
0.87 – 1.25	71.91	0.86 – 1.24	79.18	0.90 – 1.25	0.82
1.25 – 1.80	23.09	1.24 – 1.79	17.23	1.25 – 1.80	70.77
1.80 – 2.60	4.07	1.79 – 2.58	2.72	1.80 – 2.60	23.81
2.60 – 3.74	0.59	2.58 – 3.73	0.45	2.60 – 3.75	3.77

Table 4-2: Summary of the results obtained from disc centrifuge analysis for each diameter colloidal silica coated particle.

28 nm Coated Particles_Centrifuged		28 nm Coated Particles_Settled	
Number Diameter (μm)	1.18	**Number Diameter (μm)**	1.21
Polydispersity Index	1.23	**Polydispersity Index**	1.44
Diameter Range	**% Fraction**	**Diameter Range**	**% Fraction**
0.60 – 0.86	0.30	0.60 – 0.86	1.46
0.86 – 1.24	79.18	0.86 – 1.24	69.92
1.24 – 1.79	17.23	1.24 – 1.79	21.6
1.79 – 2.58	2.72	1.79 – 2.59	5.36
2.58 – 3.73	0.45	2.59 – 3.73	1.39

Table 4-3: Comparison of the results obtained from disc centrifuge analysis for 28nm colloidal silica coated particles with washing by centrifugation or settling.

Colloidal Silica Diameter (nm)	Core d_p (μm)	Total d_p (μm)	Porous Layer Thickness (μm)	Pore Diameter/Colloidal Silica Diameter	SSA (m^2/g)	SPV (cm^3/g)	Pore diameter (Å)	%C (w/w/%)
12	0.9	1.1	0.10	0.73	49	0.12	87	3.9
28	0.9	1.1	0.10	0.67	22	0.10	187	2.0
67	1.4	1.6	0.08	0.37	6	0.03	248	0.7

Table 4-4: Physical characteristics of superficially porous particles synthesized in-house with varying colloidal silica diameter.

Colloidal Silica Diameter (nm)	Number of Theoretical Plates/meter for Hydroquinone	Tailing Factor for Hydroquinone	$w_{5\%}$, *m/z* 644 (minutes)	Peptide Peak Capacity	w_b, myoglobin (minutes)
NPS	374,000	1.1	0.40	76	6.0
12	322,000	1.0	0.92	33	9.0
28	318,000	1.1	0.54	57	9.0
85	189,000	1.2	0.46	66	3.5
Acquity BEH	437,000	0.92	0.32	95	Not Tested

Table 4-5: Chromatographic performance summary of particles of varying pore size. The width of the *m/z* 644 peak was calculated at 5% of the peak height maximum. For the calculation of the peak capacity, Δt was chosen to be the length of the gradient, R_s is the resolution between consecutive peak pairs, and σ_t is the peak standard deviation in time units for the *m/z* 644 peak. For all analyses, the length of the gradient was equal to 30 minutes and the resolution was set to one. The width of the myoglobin peak was calculated at the peak base from the 3D plots.

Particle Pore Size	Surface Area/column (m^2)	Phase Ratio
87 Å	6.7×10^{-3}	0.11
187 Å	6.7×10^{-3}	0.06
248 Å	1.4×10^{-3}	0.03

Table 4-6: Comparison of surface area per column of particles with varying pore size. See Appendix 2 for example calculation.

4.7 FIGURES

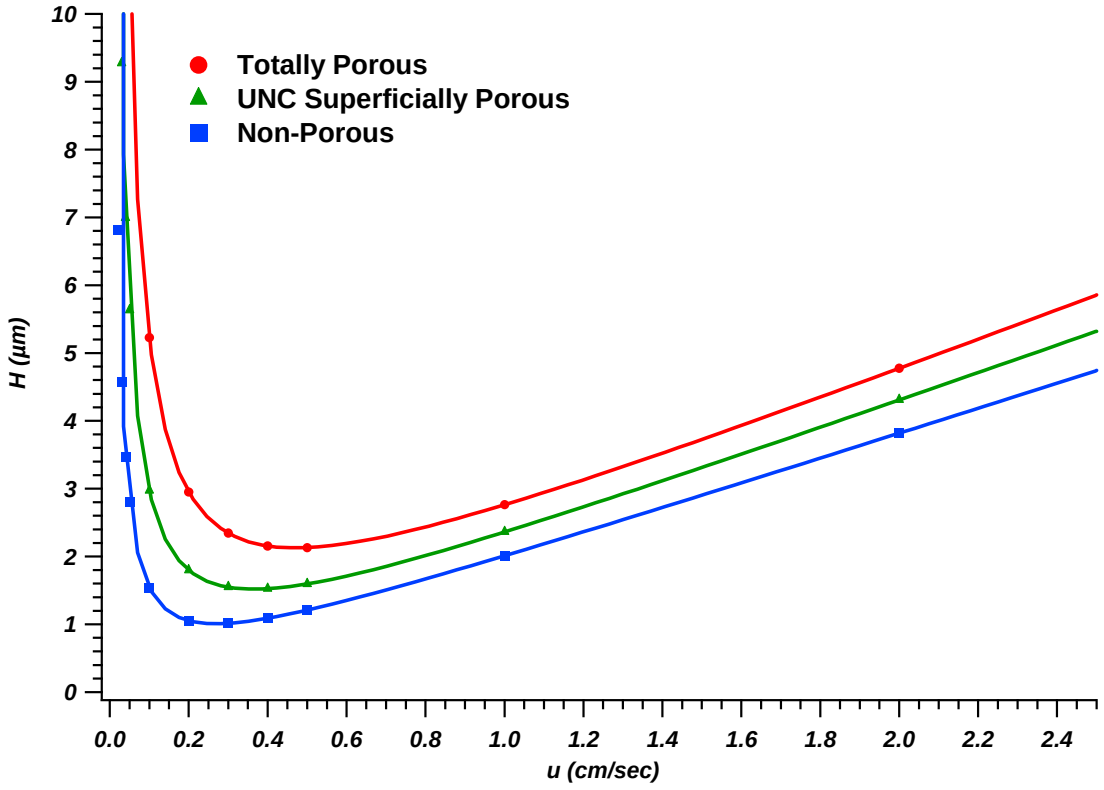

Figure 4-1: Comparison of predicted values for small molecules (D_m = 1 x 10^{-5} cm^2/sec) for totally porous particles, superficially porous particles, and non-porous particles

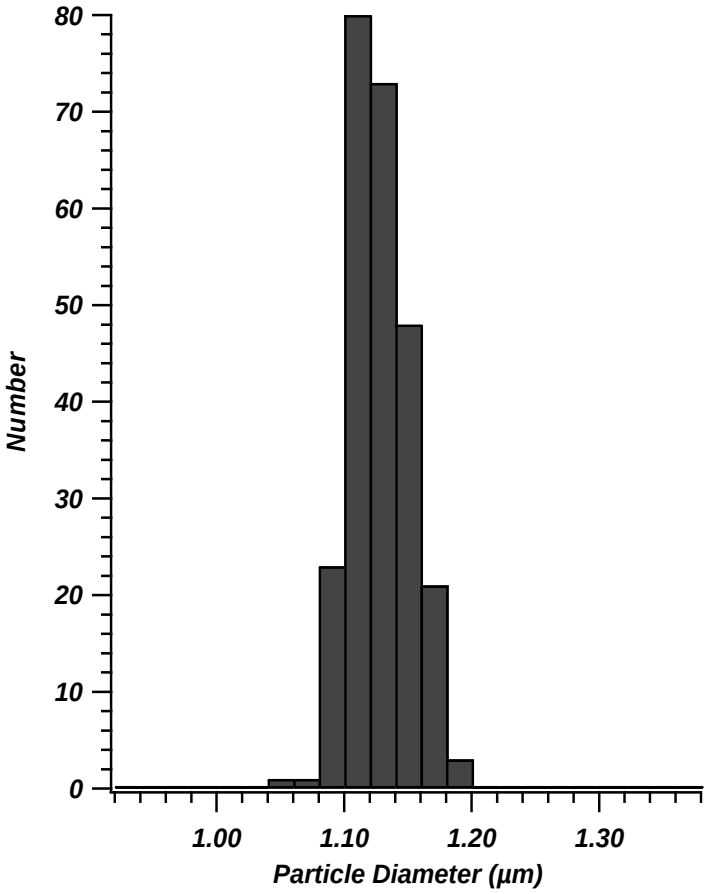

Figure 4-2: Particle size distribution of 1.1 μm ($d_{p,n}$) particles coated with 12 nm colloidal silica. RSD = 2.1%

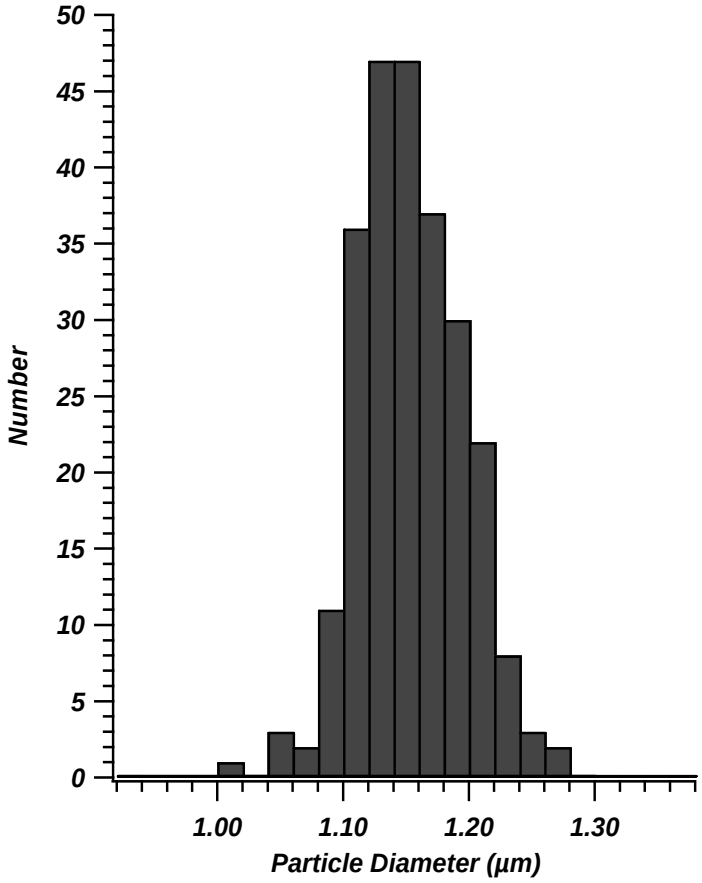

Figure 4-3: Particle size distribution of 1.1 µm ($d_{p,n}$) particles coated with 28 nm colloidal silica. RSD = 3.8%

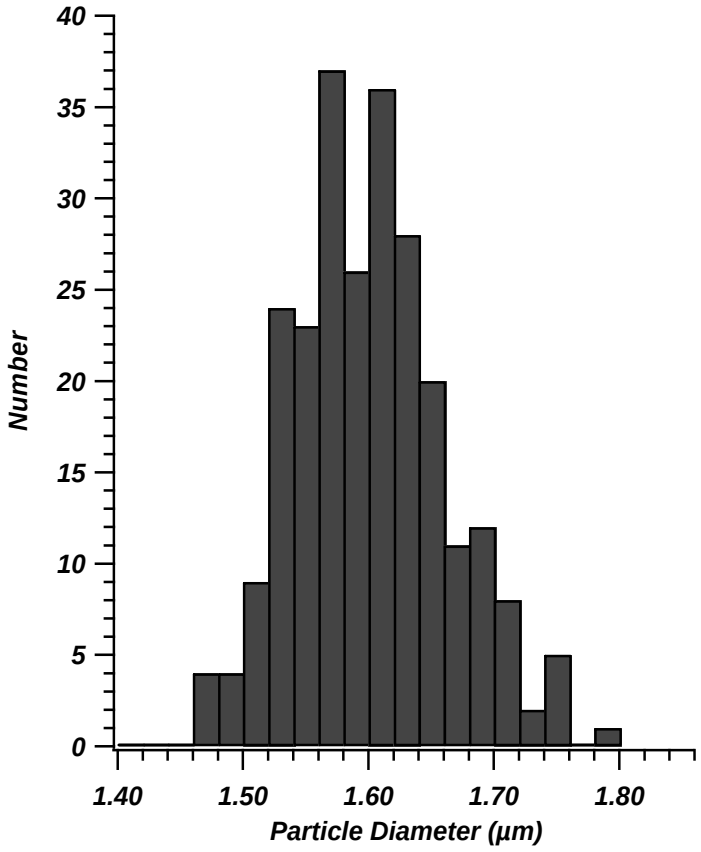

Figure 4-4: Particle size distribution of 1.6 μm ($d_{p,n}$) particles coated with 67 nm colloidal silica. RSD = 3.8%

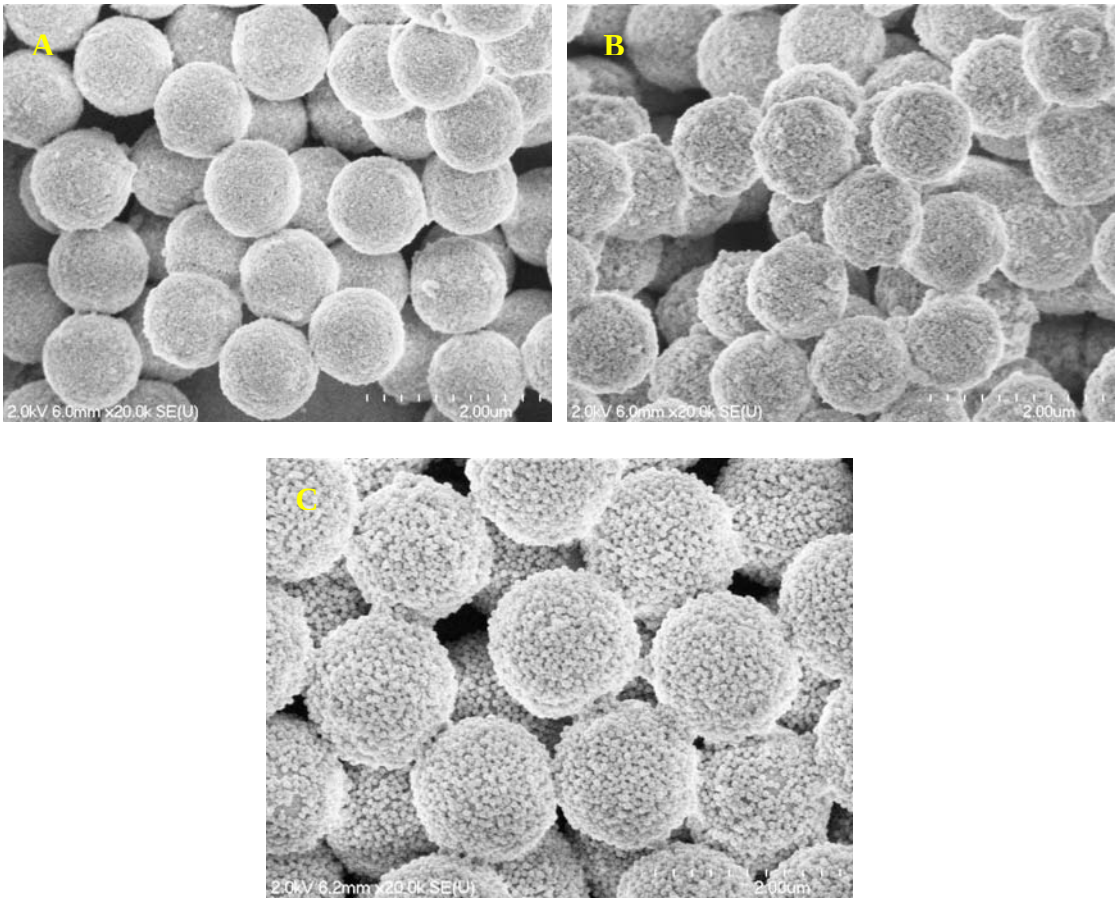

Figure 4-5: Images of particles coated with varying diameter of colloidal silica. A) 1.1 μm ($d_{p,n}$) with 12 nm colloidal silica B) 1.1 μm ($d_{p,n}$) with 28 nm colloidal silica C) 1.6 μm ($d_{p,n}$) with 67 nm colloidal silica

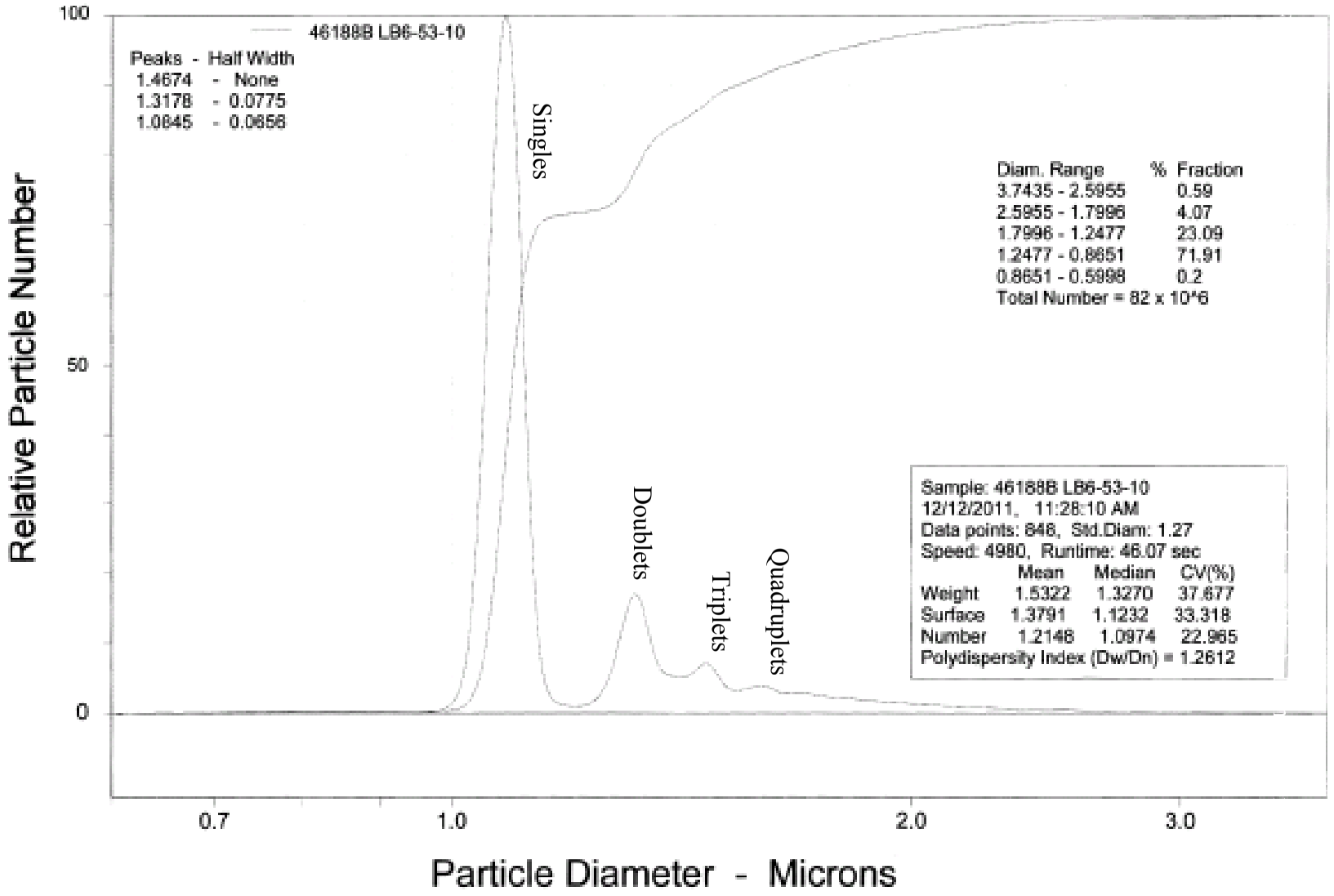

Figure 4-6: CPS Disc Centrifuge raw data for the 1.1 μm ($d_{p,n}$), 12 nm colloidal silcia.

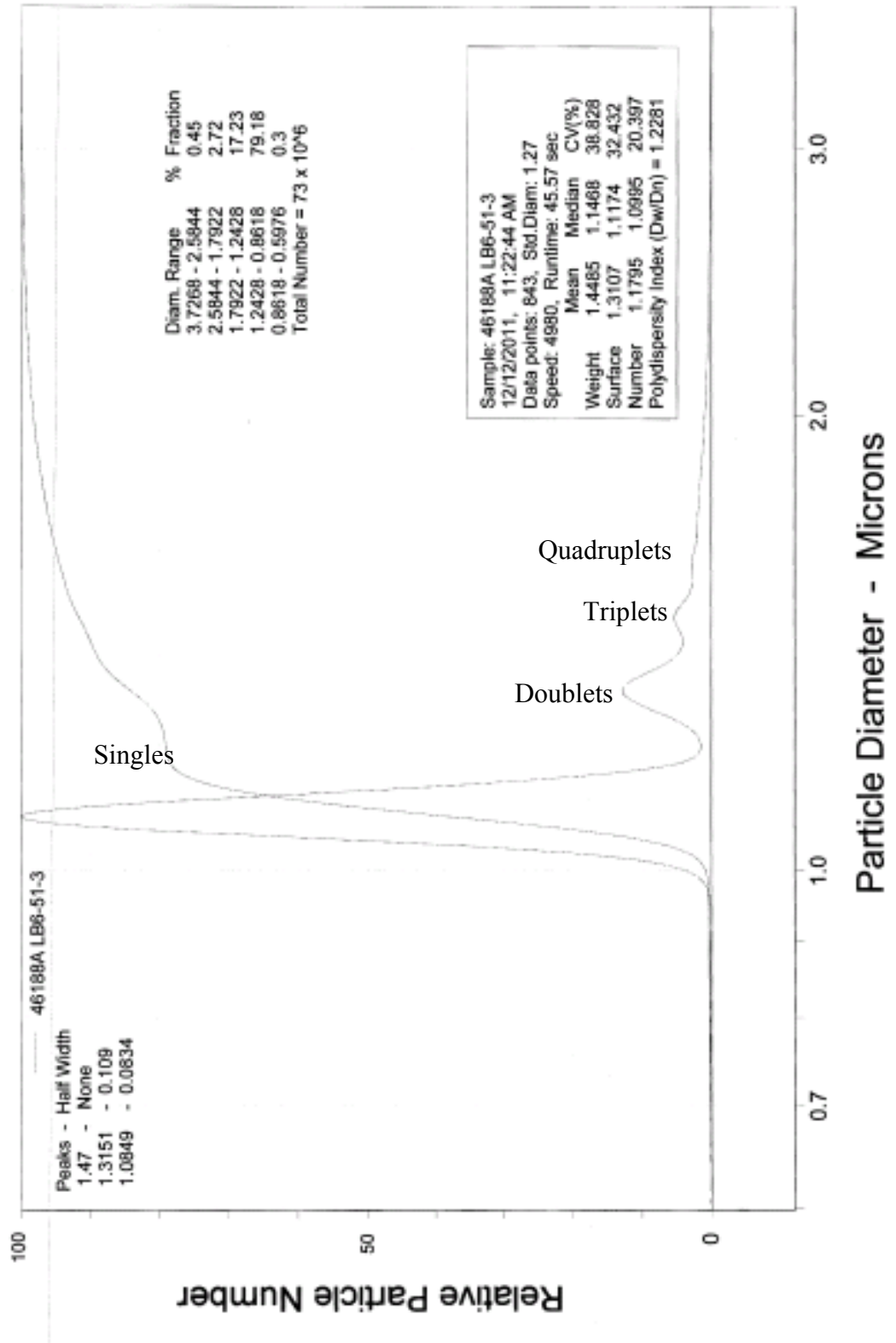

Figure 4-7: CPS Disc Centrifuge raw data for the 1.1 μm ($d_{p,n}$), 28 nm colloidal silica.

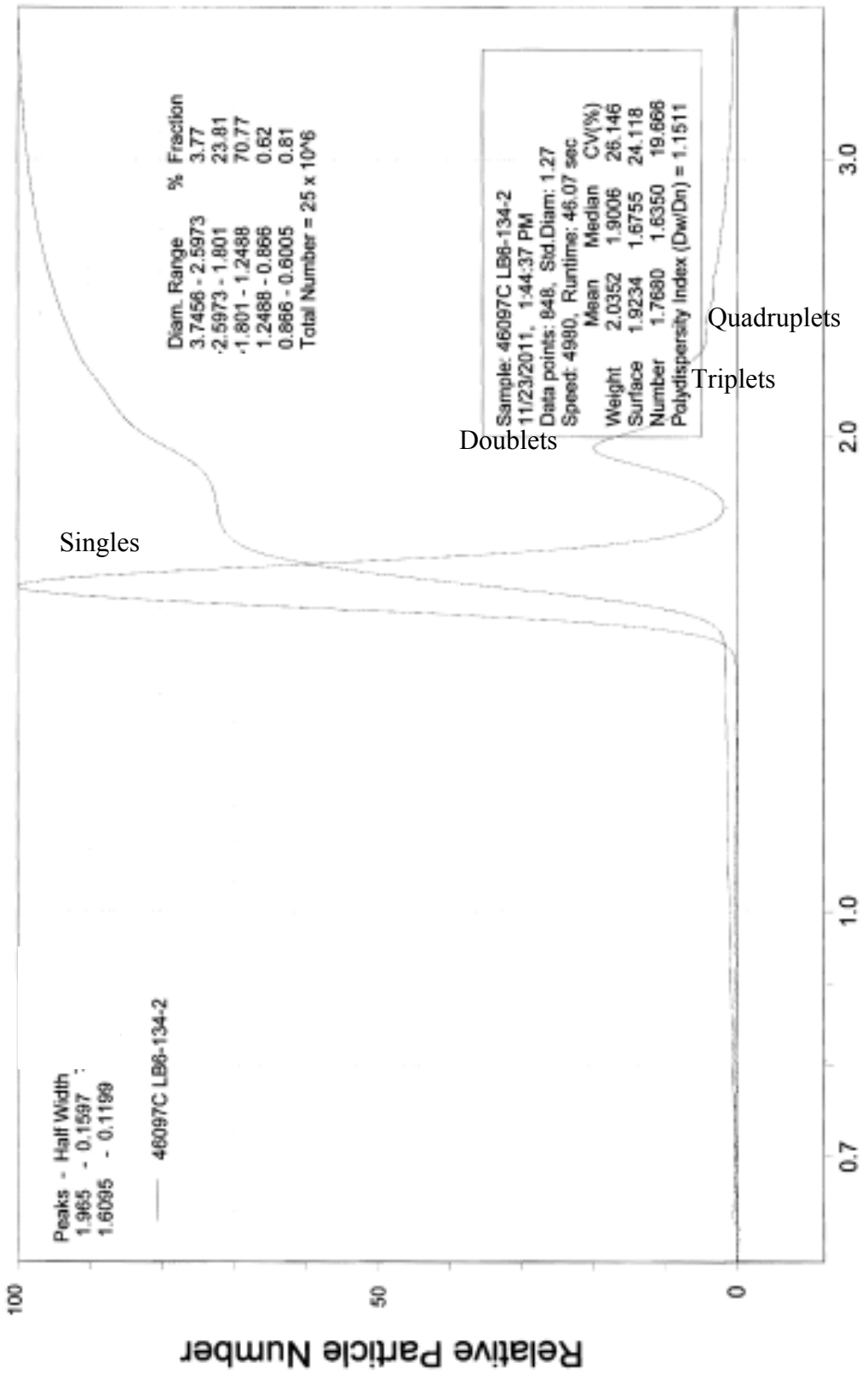

Figure 4-8: CPS Disc Centrifuge raw data for the 1.6 µm ($d_{p,n}$), 67 nm colloidal silcia.

A

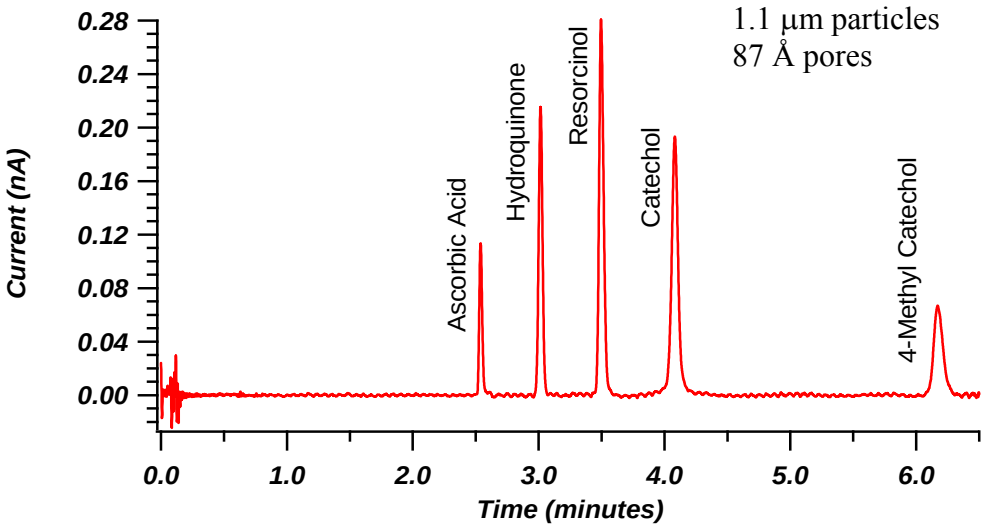

B

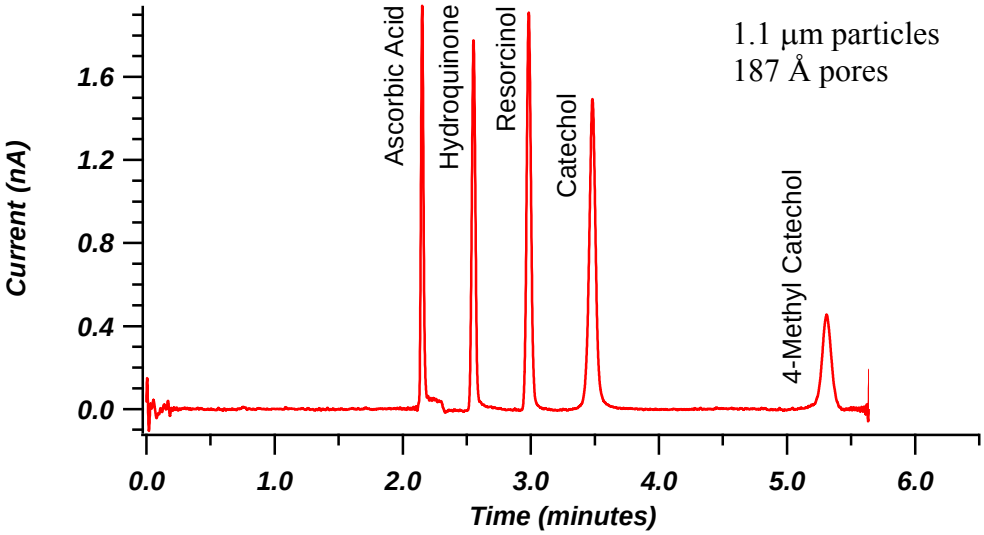

Figure 4-9: Example chromatograms for superficially porous particles of varying pore size for analysis of small molecules. A) Column LB7-32, LB6-75-1 particles (1.1 µm ($d_{p,n}$)), 12 nm colloidal silica C18 bonded, 30 µm x 16.9 cm, MP: 80/20 water/ACN 0.1% TFA, h_{min} (HQ) = 2.6, u_{opt} = 0.09 cm/sec (5000 psi), k'(4MC) = 1.3 B) Column LB7-33, LB7-23-3 particles (1.1 µm), 28 nm colloidal silica C18 bonded, 30 µm x 12.8 cm, MP: 80/20 water/ACN 0.1% TFA, h_{min} (HQ) = 2.6, u_{opt} = 0.16 cm/sec (8700 psi), k'(4MC) = 1.3

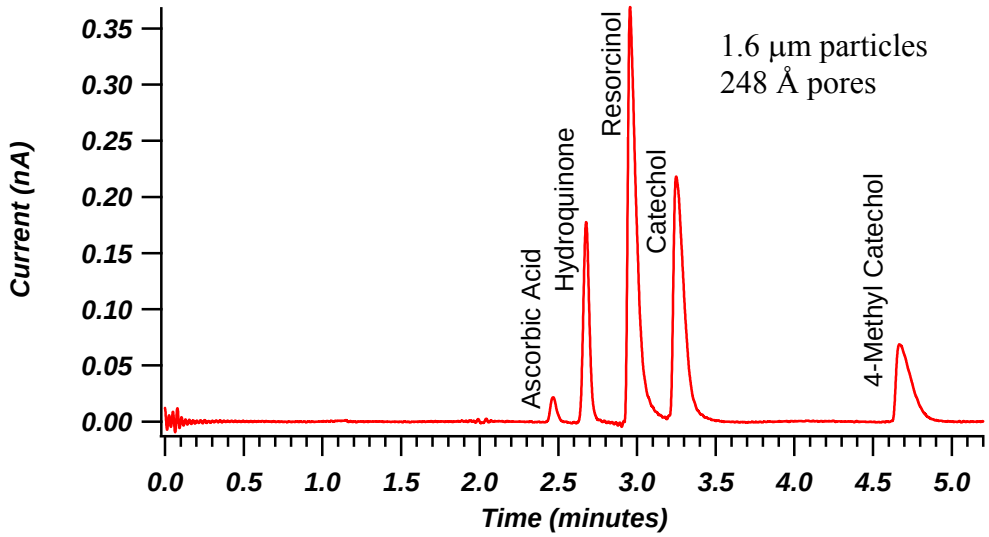

Figure 4-10: Example chromatogram for large pore superficially porous particles. Column LB7-23-C, LB6-111-3 particles (1.6 µm ($d_{p,n}$)), 67 nm colloidal silica, C18 bonded, 30 µm x 12.3 cm, MP: 90/10 water/ACN 0.1% TFA, h_{min} (HQ) = 3.3, u_{opt} = 0.08 cm/sec (2500 psi), k'(4MC) = 0.9

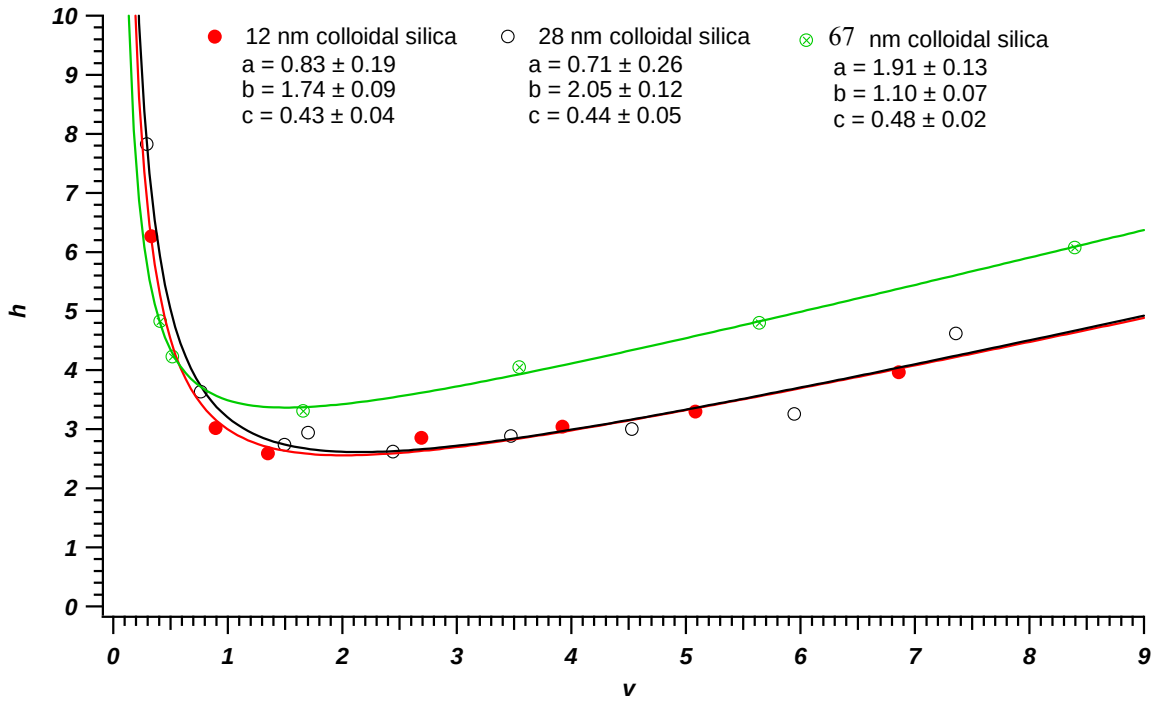

Figure 4-11: Reduced parameters plot comparison for superficially porous particles with varying pore size fit to the van Deemter equation.

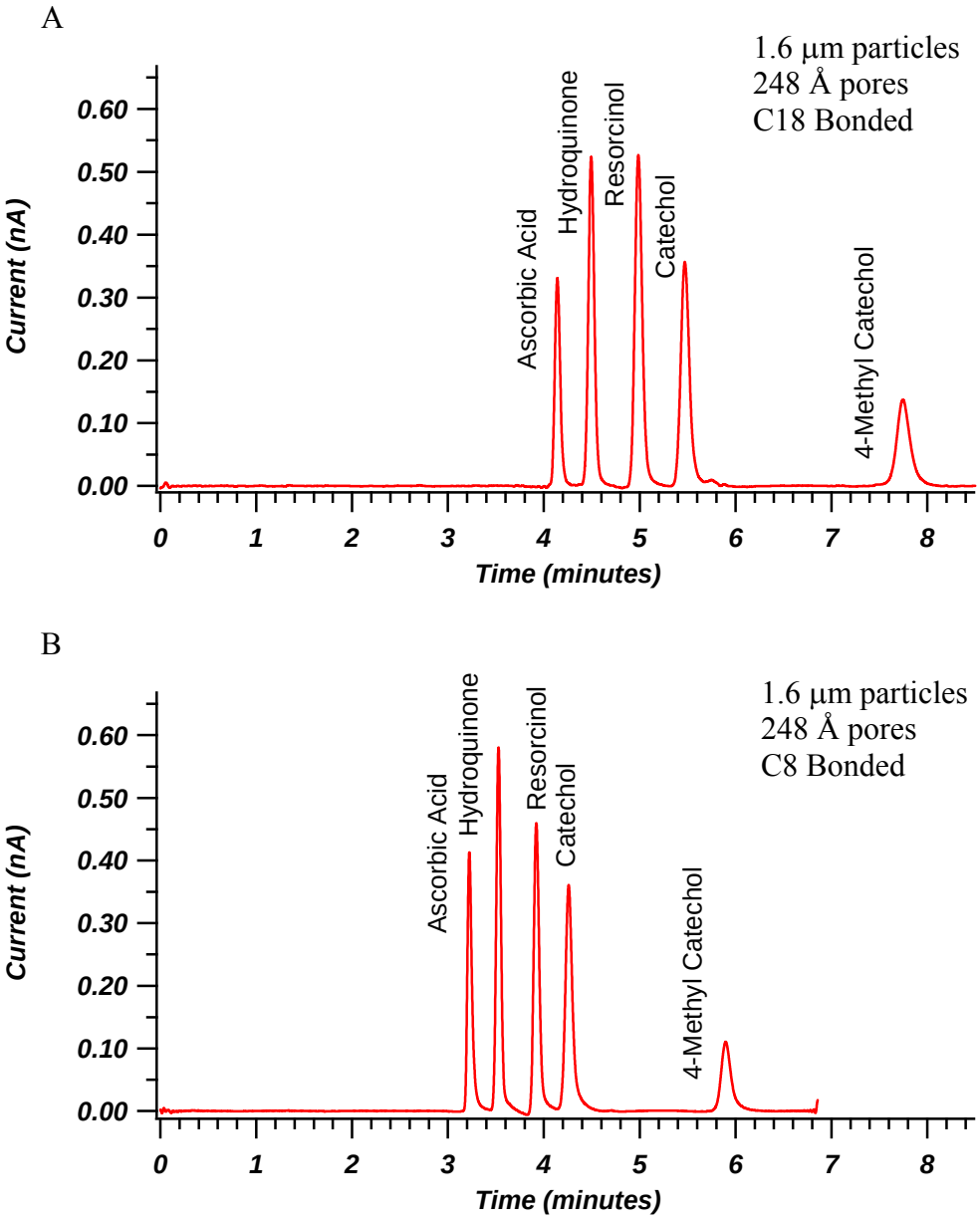

Figure 4-12: Example chromatograms for 1.6 µm ($d_{p,n}$), 67 nm coated superficially porous particles. A) Column LB6-112, LB6-102-6 particles, C18 bonded, 30 µm x 13.8 cm, MP: 90/10 water/ACN 0.1% TFA, h_{min} (HQ) = 3.7, u_{opt} = 0.06 cm/sec (2300 psi), k'(4MC) = 0.7 B) Column LB6-146-B, LB6-138-4 particles, C8 bonded, 30 µm x 13.4 cm, MP: 90/10 water/ACN 0.1% TFA, h_{min} (HQ) = 3.6, u_{opt} = 0.07 cm/sec (2300 psi), k'(4MC) = 0.8.

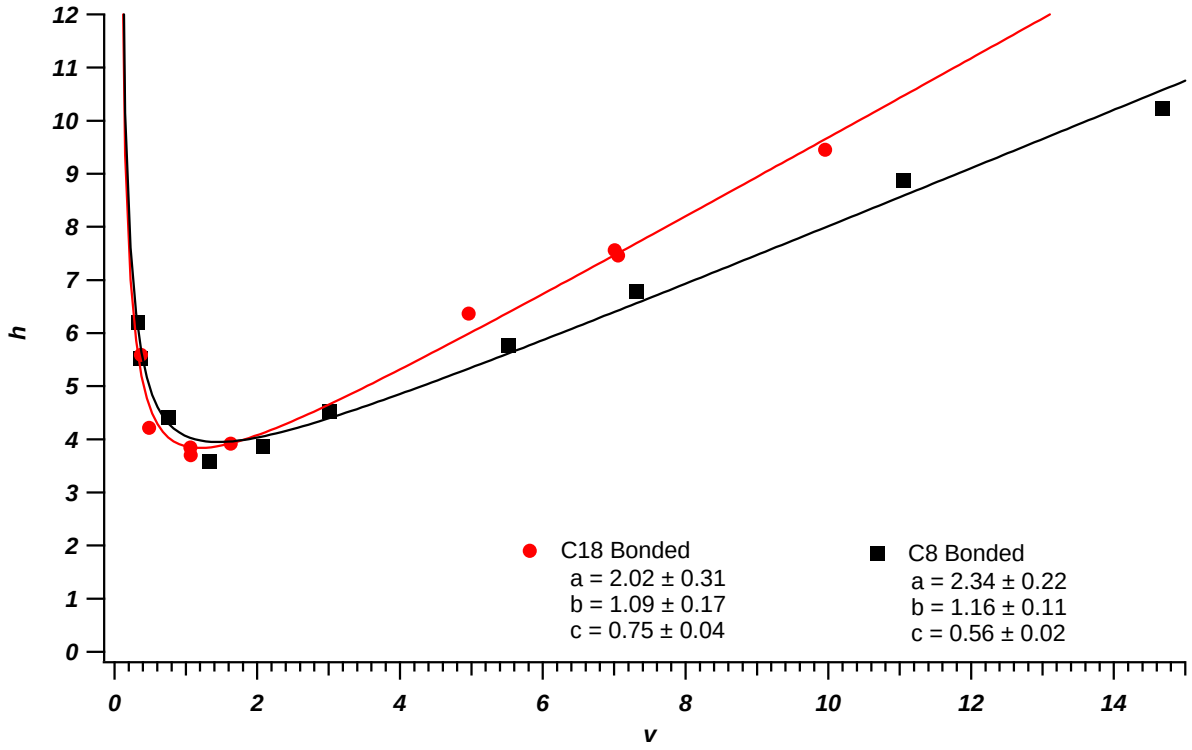

Figure 4-13: Example chromatograms for 1.6 µm ($d_{p,n}$), 67 nm coated superficially porous particles. C18 Bonded) Column LB6-112, LB6-102-6 particles, C18 bonded, 30 µm x 13.8 cm, MP: 90/10 water/ACN 0.1% TFA, h_{min} (HQ) = 3.7, u_{opt} = 0.06 cm/sec (2300 psi), k'(4MC) = 0.7 C8 Bonded) Column LB6-146-B, LB6-138-4 particles, C8 bonded, 30 µm x 13.4 cm, MP: 90/10 water/ACN 0.1% TFA, h_{min} (HQ) = 3.6, u_{opt} = 0.07 cm/sec (2300 psi), k'(4MC) = 0.8.

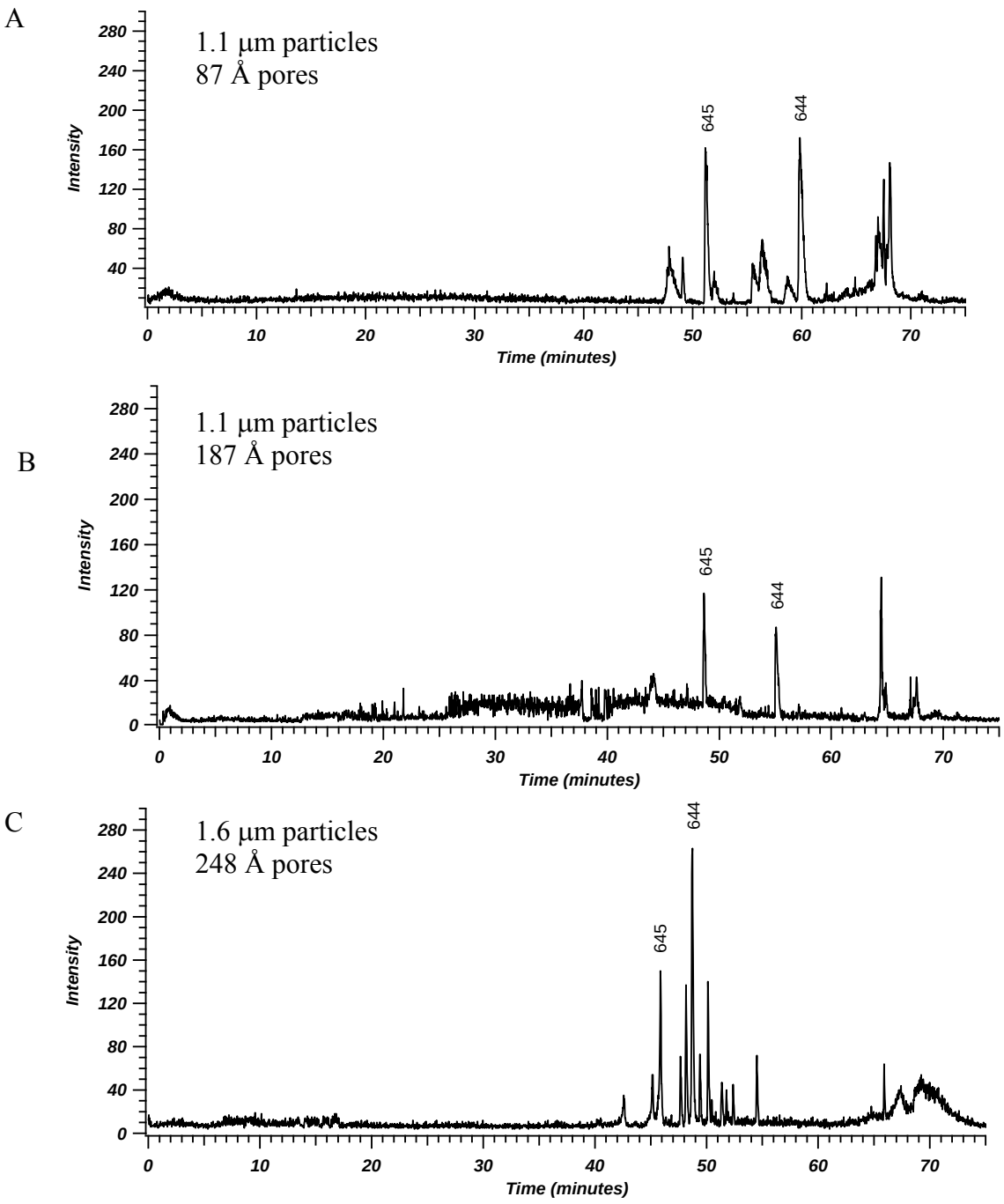

Figure 4-14: Example chromatograms for superficially porous particles of varying pore size for analysis of peptides of enolase digest. A) Column LB7-41, LB6-75-1 particles, C18 bonded, 75 µm x 16 cm B) Column LB7-41-B, LB7-23-3 particles, C18 bonded, 75 µm x 15 cm C) Column LB6-111, LB6-111-3 particles, C18 bonded, 75 µm x 27 cm

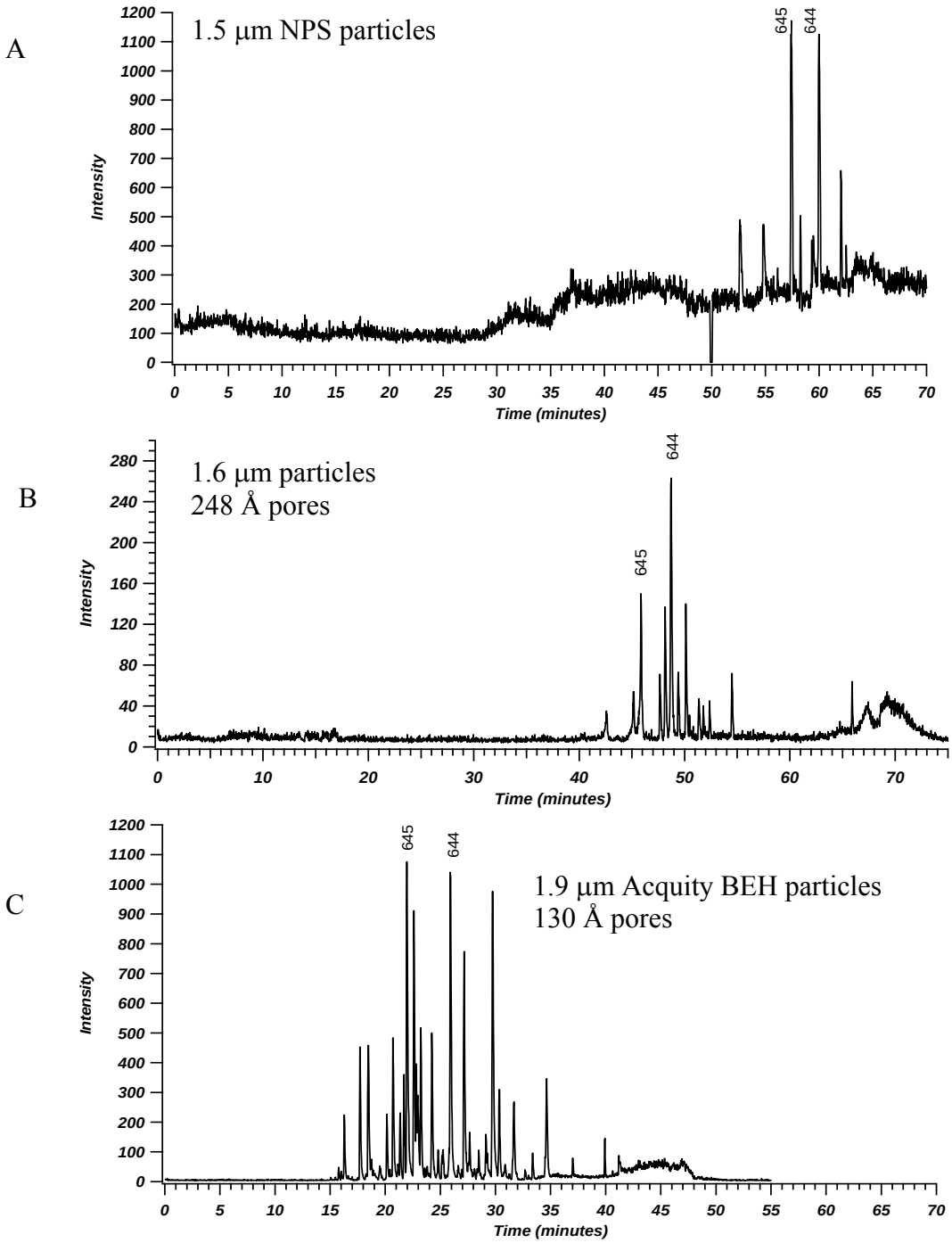

Figure 4-15: Example chromatogram of in-house superficially porous particles compared to non-porous particles and totally porous particles for analysis of peptides of enolase digest. A) Column LB6-150, 1.5 µm NPS, C18 bonded, 75 µm x 17 cm B) Column LB7-41, LB6-75-1 particles, C18 bonded, 75 µm x 16 cm C) Waters 1.9 µm Acquity BEH130, 75 µm x 25 cm

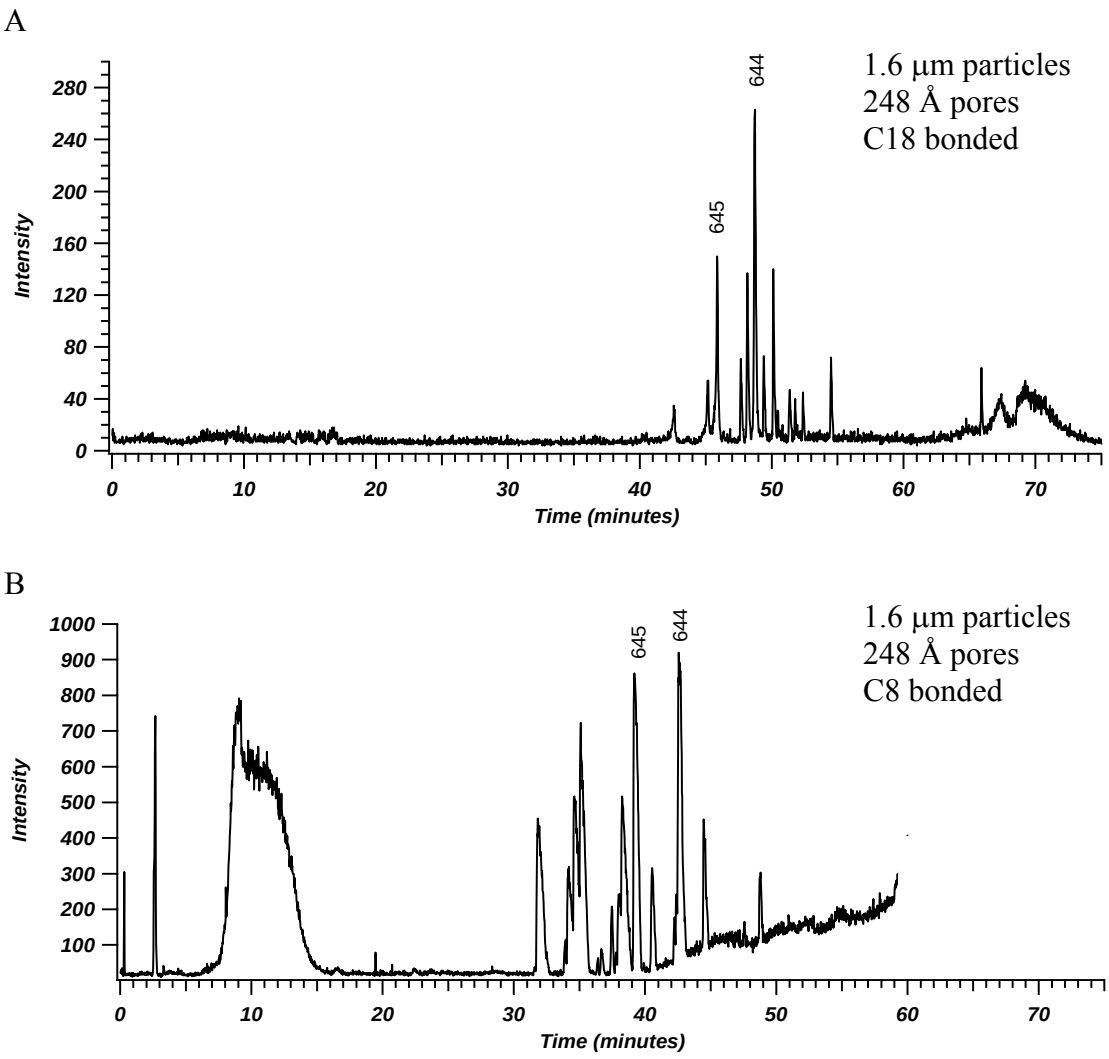

Figure 4-16: Example chromatograms for enolase digest separated using 1.6 µm particles coated with 85 nm colloidal silica variation in bonded ligand chain length. A) Column LB6-111, LB6-111-3 particles, C18 bonded, 75 µm x 27 cm B) Column LB6-146, LB6-138-4 particles, C8 bonded, 75 µm x 25 cm

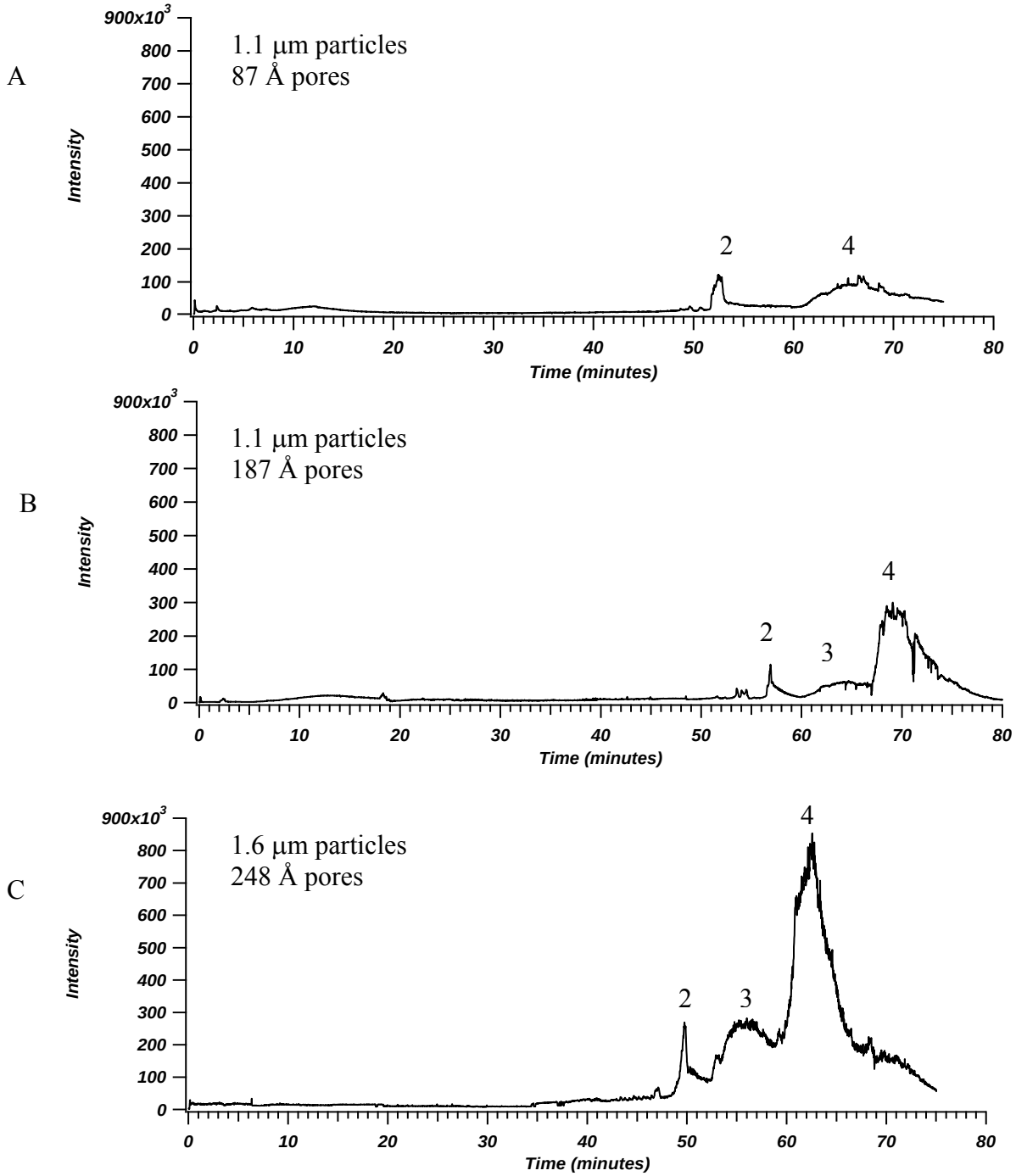

Figure 4-17: Example chromatogram for superficially porous particles of varying pore size for analysis of protein mixture. Mixture included thyroglobulin (1), β-lactogloulin (2), RNasa-A (3), cytochrome c (4), myoglobin (5), bovine serum albumin (6) A) Column LB7-41, LB6-75-1 particles, C18 bonded, 75 µm x 16 cm B) Column LB7-41-B, LB7-23-3 particles, C18 bonded, 75 µm x 15 cm C) Column LB6-111, LB6-111-3 particles, C18 bonded, 75 µm x 27 cm

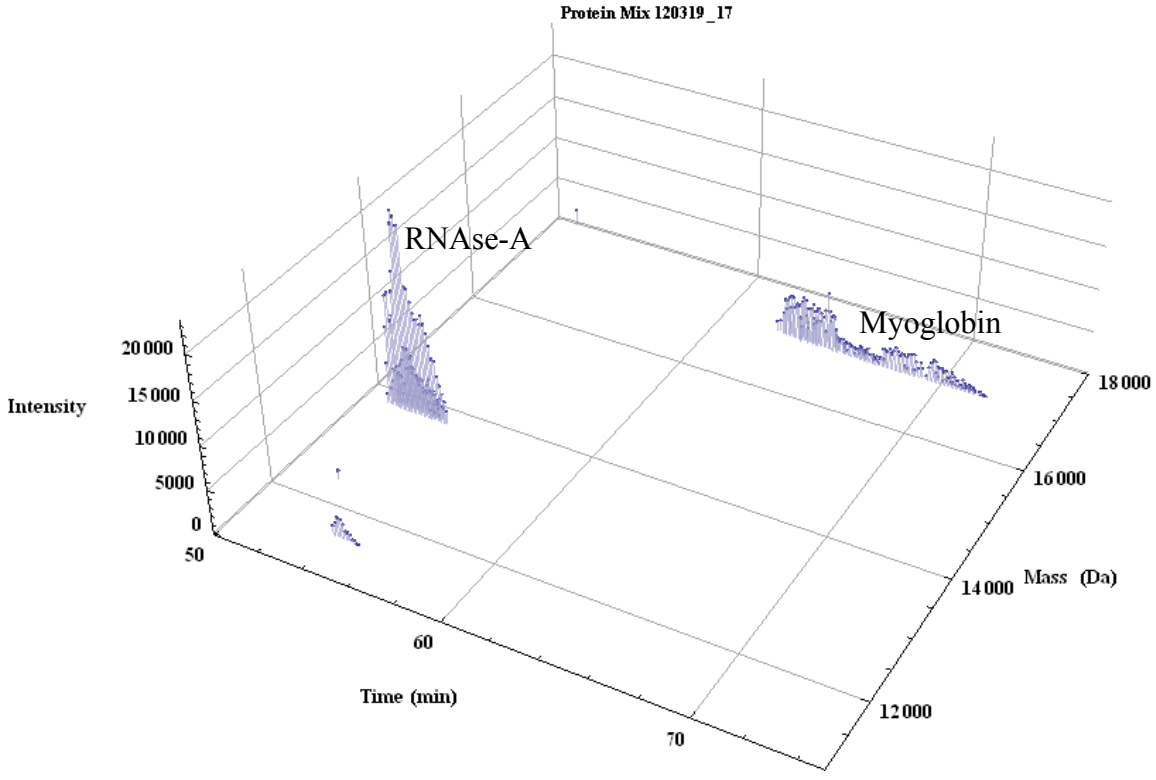

Figure 4-18: 3D plot for 87 Å pore particles

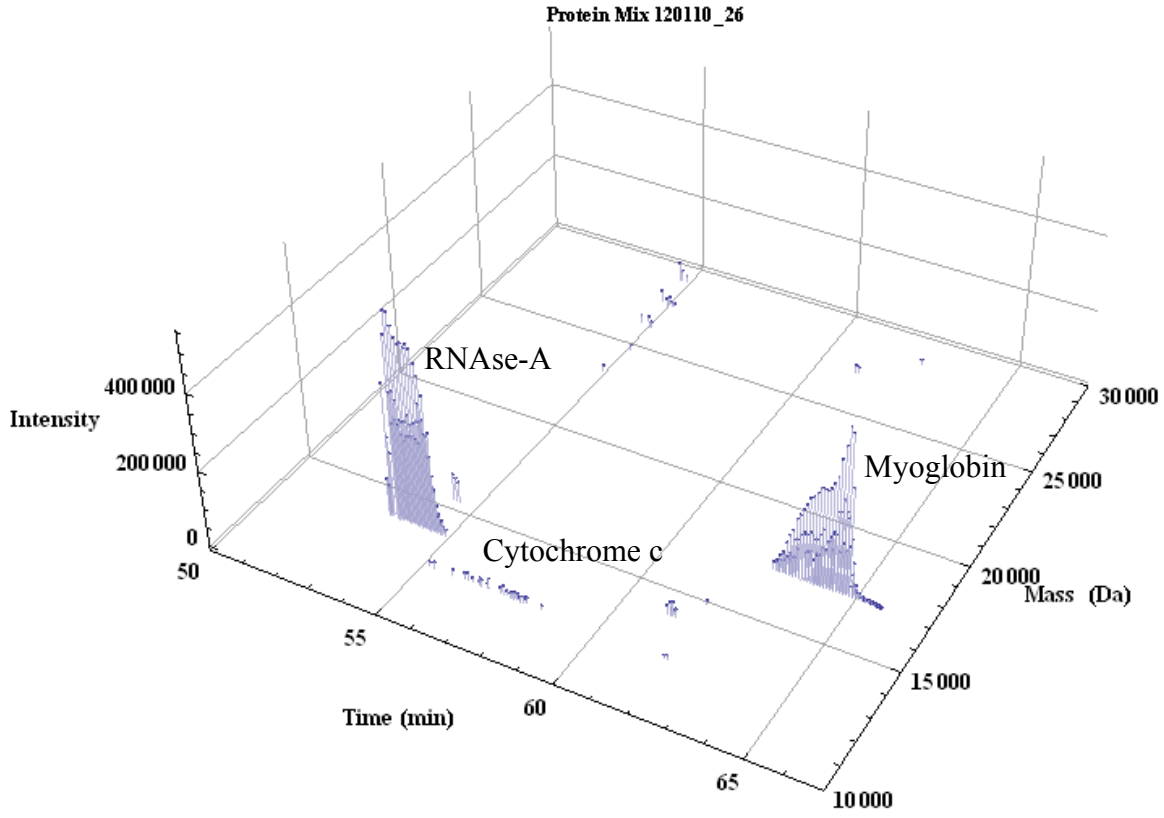

Figure 4-19: 3D plot for 1.5 μm NPS particles, C18 bonded.

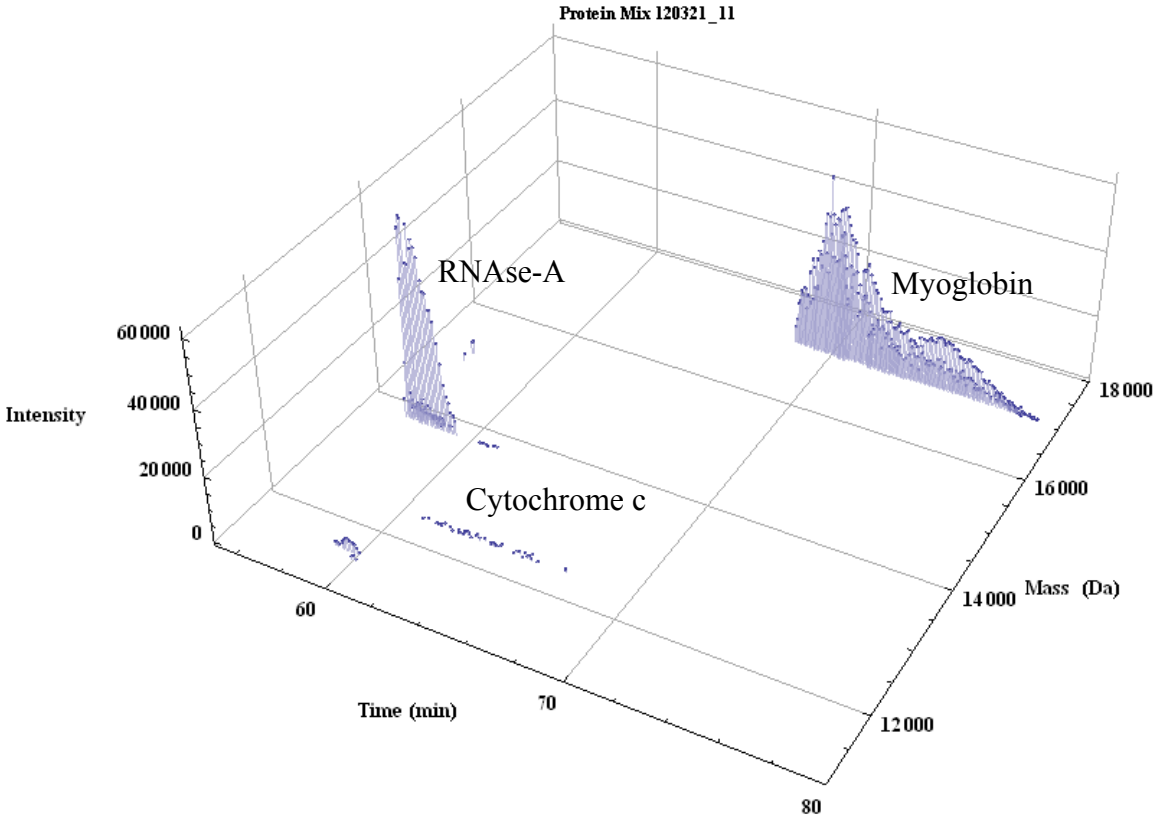

Figure 4-20: 3D plot for 187 Å pore particles

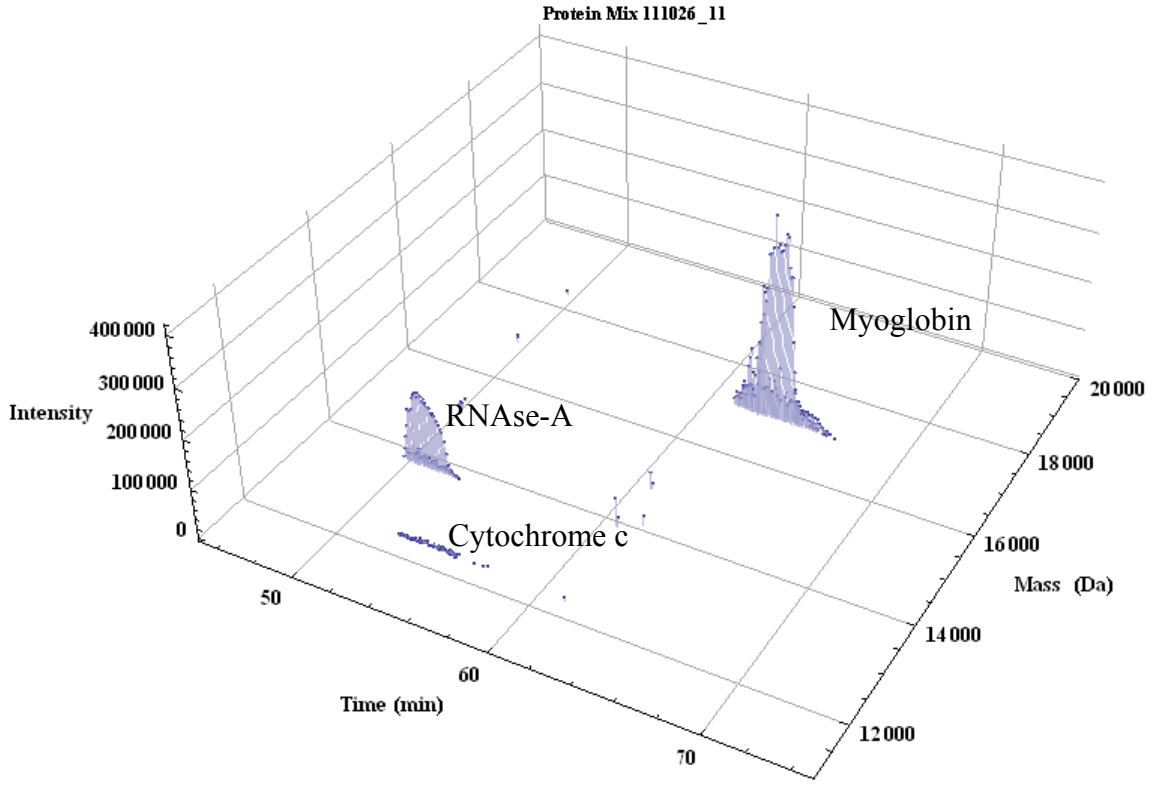

Figure 4-21: 3D plot for 248 Å pore particles bonded with C18

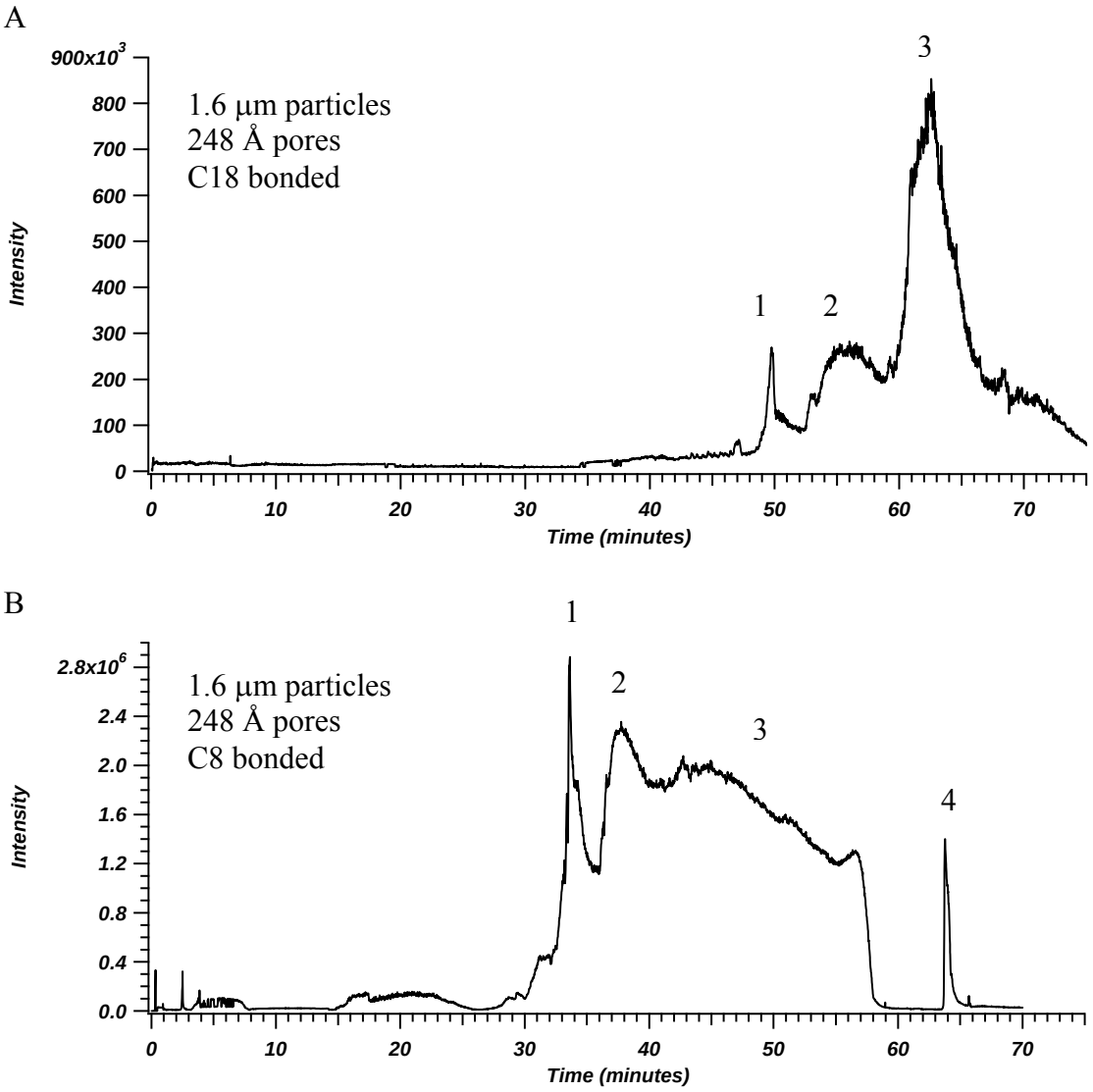

Figure 4-22: Example chromatograms for protein mixture separated using 1.6 µm particles coated with 85 nm colloidal silica variation in bonded ligand chain length. Mixture included thyroglobulin (1) RNasa-A (2) cytochrome c (3) myoglobin (4) β-lactogloulin (5) bovine serum albumin (6) A) Column LB6-111, LB6-111-3 particles, C18 bonded, 75 µm x 27 cm B) Column LB6-146, LB6-138-4 particles, C8 bonded, 75 µm x 25 cm.

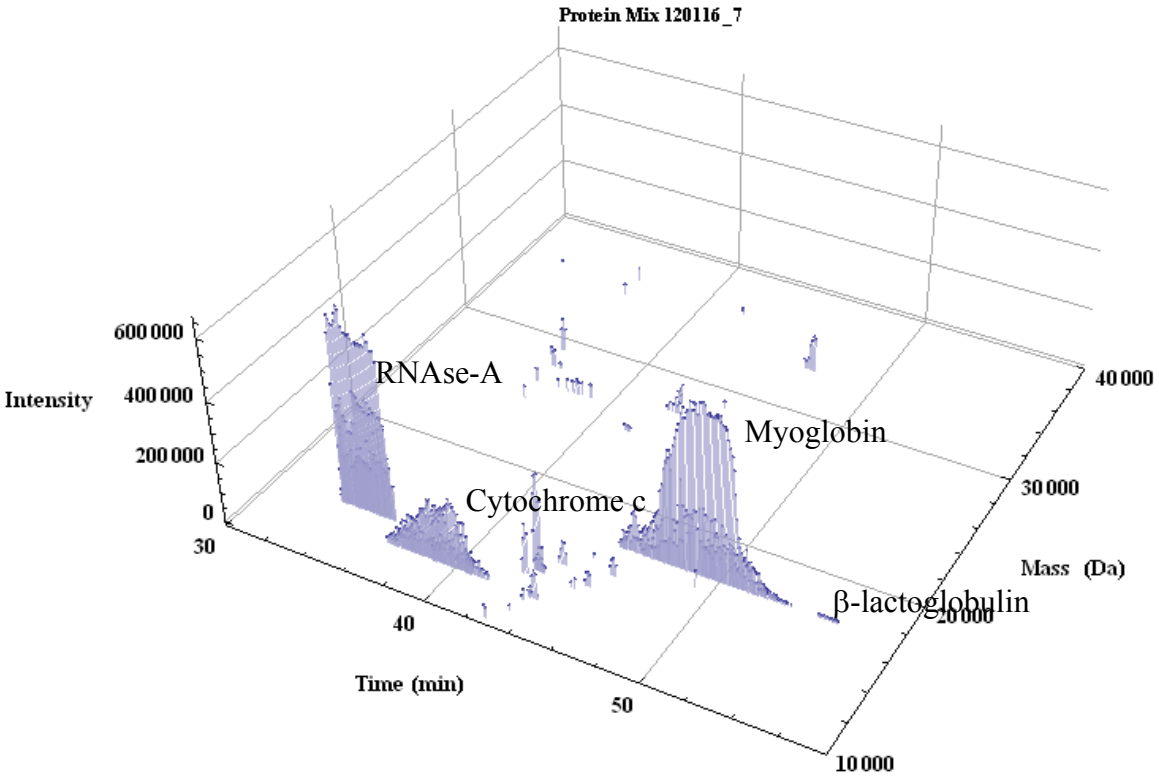

Figure 4-23: 3D plot for 248 Å pore particles bonded with C8.

CHAPTER 5: EFFECT OF COLUMN PACKING CONDITIONS ON CHROMATOGRAPHIC PERFORMANCE

5.1 INTRODUCTION

To produce highly efficient HPLC columns, the column packing procedure must produce stable, reproducible columns. Historically, it is believed that column packing is an art rather than science. Our lab has found this to be the case, and even greater difficulties in column packing have been found to be present for columns with particles of decreasing diameter.

5.1.1 Role of Column Packing on Performance

The column packing conditions have been found to greatly affect the packing efficiency and in turn the chromatographic performance. The process of column packing is not well understood and contradicting information pertaining to desired packed bed characteristics have been found. The structure of the packed bed is typically believed to most greatly affect the *A*-term contribution to the theoretical plate height, but contributions to the *B*- and *C*-terms have been found as well. With regards to the *A*-term, the concentration of the particle slurry has been found to affect the radial uniformity of the packed bed. At low slurry concentrations, when the packing rate is slow or at large aspect ratios, size segregation across the column diameter occurs.[1, 2] This radial inhomogeneity produces a greater number of flow paths available to an analyte, which increases the band broadening due to eddy dispersion.

The presence of a constant packing rate has been found to be crucial for producing a packed bed with longitudinal uniformity.[3] While a constant packing rate is targeted, it is common for the initial bed formed to pack more quickly due to the absence of a large length of packed bed producing elevated flow resistance. This variation in packing rate throughout the duration of bed formation typically produces a more loosely packed bed with a more rapid packing rate at the beginning of column packing.[3] The interparticle porosity of the packed bed has also been found to increase as the particle monodispersity improves.[4] Further bed density variation can be found to depend on the kinetic energy of the particles while packing. At high particle kinetic energy, such as with low viscosity solvents and at high pressures, particles can forcibly displace already packed particles leading to a more densely packed bed.[5] Each of these factors affect the packing density which can lead to large variations in the eddy dispersion between columns packed under different conditions.

In addition to the effect of bed structure and packing density on eddy dispersion, longitudinal diffusion and resistance to mass transfer are also affected. The longitudinal diffusion of the column is affected by the packing density due to the resulting variation in the interparticle mobile phase volume available for diffusion. The lower the packing density of the column, the greater the contribution from longitudinal diffusion to the theoretical plate height due to a larger interparticle volume than for a tightly packed column. Additionally, the packing density (as represented as k') has historically been thought to affect the mobile phase mass transfer resistance. As the packing density is increased, the C_m-term has been found to sharply increase.[6] Recent collaborative studies carried out in our lab in conjunction with the Tallarek group have found that this

decreased performance may be attributed to a velocity dependent coupled *A*-term rather than the C_m-term.[7] This performance variation was found to correlate to the column porosity and the performance of the column was increased as the radial homogeneity was improved. The increased mass transfer resistance for high density columns also relates to the number of particles per column volume. The greater the number of particles, the more stationary phase available for mass transfer, thus increasing the contribution to the theoretical plate height.[8] The resistance to mass transfer in the mobile phase has also been found to depend on the roughness of the particle surface. Due to the layer-by-layer approach used to produce some superficially porous particles, the particle surface roughness is greater than totally porous particles or superficially porous particles produced by a sol-gel process. This higher than expected mass transfer resistance of superficially porous particles produced by the layer-by-layer process has been attributed to the increased particle surface roughness.[9]

5.1.2 Historical Challenges with Column Packing

Due to the resulting bed structure and the column performance dependence on the column packing procedure, the ability to tightly control the packing parameters is desirable. The ability to control the resulting packing structure has been found to be very undependable and not well understood.[10] Many times each batch of particles requires modification of the packing conditions and small changes in the packing conditions can produce significant variation in packing density and thus column performance.[5,11 -13] Furthermore, difficulty in obtaining radial homogeneity of the bed is inherent due to the use of liquid as the particle dispersant. Due to the hydrodynamic flow profile, radial variation in the axial velocity in the column during the packing process results in

significant differences in the radial bed structure. Since the rate of particles building up the bed is greater in the center of the column than near the walls, a less dense packing structure would be expected in the center. Variation in the density across the bed is also due to the presence of the wall, which leads to a more ordered packing structure and has been found to cause a lower packing density in this more ordered region.[2]

These difficulties with column packing have been found to be exacerbated in moving to smaller diameter particles predicted to have greater efficiency.[4-6, 12] As the particle size is decreased the surface chemistry of the particle becomes more important due to the increase of the surface area to volume ratio.[4] Also, with the use of smaller diameter particles, the effective linear velocity of the particles at a specific pressure will be lower due to the higher flow resistance produced from the bed of smaller particles. Therefore, the pressure required to maintain an adequate packing rate is increased. These difficulties have impeded development of commercial columns packed with particles of decreasing diameter.

5.1.3 Predicted Efficient Packing Conditions

While the packing conditions are typically adjusted for each type and batch of particles, numerous studies have been performed to try to predict general parameters that produce efficient columns. The packing conditions that characterize a good packing slurry for millimeter bore HPLC columns, non-aggregating solvents, has been found to not work well for capillary columns as seen in Chapter 3. In contrast, slurry solvents that cause particles to aggregate have been found to produce more efficient capillary columns.[10, 13] For example, aggregating solvents such as acetonitrile and methanol have been found to be better than non-aggregating solvents, acetone, isopropanol and

tetrahydrofuran.[13] Contrary to this, Angus and coworkers found the opposite to be true indicating the difficulty in predicting appropriate packing conditions.[5]

Ultimately, the conditions that build a packed bed the fastest have been found to produce the most efficient columns with the least bed compaction over time leading to more stable separations. For this reason, slurry concentrations ranging from 7 to 40% (w/w%) have been found to produce efficient bed formation, but this range is still quite wide for easy determination of the appropriate packing concentration.[10, 12, 14] In addition to slurry packing concentration, the length of the column blank can affect the packing rate. The shorter the column blank, the greater the impact velocity of the particles, and therefore a faster packing rate.[5] This range of variables serve as a good starting conditions, but a large amount of optimization is still required.

5.1.4 Previous Methods for Predicting Suitable Slurry Solvent

The role of the particle-slurry solvent interaction is believed to be the greatest contributing factor to producing a well packed column. To account for this, the determination of the particle behavior in the slurry solution has been used to predict suitable packing conditions. These properties have typically been investigated by in-solution microscopy, determination of sedimentation velocity, and zeta potential measurements. Optical microscopy shows whether aggregation in solution is occurring at atmospheric pressure, but does not predict particle behavior at elevated pressure as is the case during packing.[10] This technique is still a good indicator of the differences between different slurry solvents.

The most common method used to determine the extent of particle aggregation in solution has been sedimentation velocity measurements. This method compares the

measured sedimentation velocity to the theoretical sedimentation velocity of individual particles based on the measured particle size from an ancillary method, such as SEM images. The theoretical sedimentation velocity (v_S) is calculated based on the measured volume average particle diameter, $d_{p,v}$, the density of the particle skeleton, ρ_{skel}, and the slurry solvent density, ρ_l, and viscosity, η

$$v_S = \frac{(1-\phi_p)^{-K_2} d_{p,v}^2 [\rho_{skel}(1-\varepsilon) + \rho_l(\varepsilon_f - 1)]g}{18\eta} \tag{5-1}$$

where ϕ_p is the volume fraction of the particles in the slurry solution, K_2 is the hindered settling constant which is a particle-solvent dependant constant typically taken as 5.4 for hard spheres, ε is the fraction of the particle occupied by pores (0.26 for the 12 nm coated particles and 0.21 for the 28 nm coated particles), ε_f is the fraction of pores filled with solvent (assumed pores completely filled with solvent), and g is the acceleration due to gravity.[15,16] Accordingly, an effective particle diameter, d_{eff}, based on the experimental sedimentation velocity can be calculated by rearranging equation 5-1.

$$d_{eff} = \sqrt{\frac{18 v_S \eta}{(1-\phi_p)^{-K_2}[\rho_{skel}(1-\varepsilon) + \rho_l(\varepsilon_f - 1)]g}} \tag{5-2}$$

This effective particle diameter can be used as an indication of the particle or particle aggregate size in solution.

A further measure of the degree of aggregation is the ratio, α, of the experimental sedimentation velocity and the theoretical velocity.

$$\alpha = \frac{v_{experimental}}{v_{theoretical}} \tag{5-3}$$

A stable solution, one without aggregation, has a α value of 1 and α greater than 1 for aggregating suspensions.

Another method to investigate the particle suspension properties is the measurement of the electrophoretic mobility and its correlation to the suspension zeta potential. A greater zeta potential value indicates the presence of electrostatic repulsion forces which promote non-aggregated particles in solution. Previous studies have shown values greater than +/- 30 mV to have enough repulsive forces to be non-aggregated.[17] While this technique offers valuable information, it is many times difficult to get accurate measurements because particle sedimentation interferes with the electrophoretic mobility measurement.

An additional technique used to determine the effective particle diameter in solution is dynamic light scattering (DLS). This technique measures the Brownian motion and relates this to the effective size of the particles. The slower the Brownian motion, the greater the size of the particle or particle aggregate. As with zeta potential measurements, DLS is susceptible to erroneous measurements due to particle sedimentation.[17]

In-solution microscopy, sedimentation, and DLS were investigated to determine which method, if any, most reliably predicts the production of a highly efficient column packing method. Development of a good solvent selection method would greatly reduce the time spent on the trial-and-error process of finding appropriate slurry packing conditions.

5.2 MATERIALS AND METHODS

5.2.1 In-Solution Microscopy

For each of the solvents listed in Table 5-1, a 3 mg/mL slurry of the 12 nm coated particles and the 28 nm coated particles described in Chapter 4 was prepared. To assess the effect of slurry concentration, a 7, 13, and 25 mg/mL solution in acetone and in methanol of the 28 nm coated particles was prepared. All solvents were purchased from

Fisher Scientific (Waltham, MA) and used as supplied. All slurry solutions were sonicated for 10 minutes using a Cole Parmer Ultrasonic Cleaner 8891 (Vernon Hills, IL). After sonication, 10 μL of the slurry solution was placed on a glass microscope slide and covered with a glass cover slip. The solution was then observed with a Wolfe oil immersion microscope equipped with an Edmund 1.25 oil lens (Edmund Optics; Barrington, NJ). Images were collected using DigiVu Microscope software. Solutions that were found to be aggregating solvents were perceived as being a potentially good packing solvent based on previous studies found in the literature for capillary columns.

5.2.2 Sedimentation Velocity

The sedimentation velocity and effective particle diameter were determined for 12 nm and 28 nm colloidal silica coated particles in the solvents listed in Table 5-1. The hexane, isopropanol (IPA), methanol (MeOH), tetrahydrofuran (THF), and acetone were purchased from Fisher Scientific (Waltham, MA) and used as supplied. For each slurry solvent, 3 mg of particles were placed in a 1.5 mL glass vial marked with a 1.0 cm window and 1.0 mL of slurry solvent was added, Figure 5-1. Additionally, the effect of slurry concentration on sedimentation rate was evaluated by preparing solutions at 5, 10, and 15 mg/mL in acetone for the 28 nm coated particles. Each solution was sonicated for 10 minutes using a Cole Parmer Ultrasonic Cleaner 8891 (Vernon Hills, IL), then immediately placed on the bench top to begin recording the sedimentation process. Video of the sedimentation was recorded using a Lenovo Thinkpad W510 laptop webcam (Morrisville, NC) and Debut video recording software (NCH Software).

The density and viscosity values for the pure solvents were taken from the CRC Handbook of Chemistry and Physics as stated for 25°C.[18] The density of the binary

solvent mixtures were determined by weighing 1000 μL of each solvent in triplicate on a Sartoruis GD603 analytical balance (Goettingen, Germany). The viscosity of the hexane :acetone mixtures were calculated based on the results of a plot of viscosity versus the mole fraction of hexane.[19] The viscosity of the acetone:methanol mixture was calculated based on a plot of viscosity versus mole fraction of acetone.[20] The viscosity of the hexane:isopropanol and acetone:isopropanol were calculated based on plots constructed from tabular values of viscosity and mole fraction.[21] The resulting density and viscosity values used for sedimentation rate calculations are listed in Table 5-2. The following constants were used based on literature values [15, 16] and specific values for these particles (see Appendix 3 for calculations): ρ_{skel} = 2.11 g/cm^3, ε (12 nm) = 0.26, ε_f (12 nm) = 0.26, ε (28 nm) = 0.21, ε_f (28 nm) = 0.21, ϕ = 0.0014, and K_2 = 5.4.

5.2.3 Dynamic Light Scattering

The effective particle diameter of each solution prepared for the sedimentation velocity study was measured by dynamic light scattering (DLS) using a Malvern Zetasizer Nano ZS (Worcestershire, UK). The zetasizer was equipped with a universal dip cell to allow use of measurements with organic solutions. The Z-average was used as the effective particle diameter, which is an intensity mean, not a number or volume average. This Z-average may be inaccurate if the distribution is very broad. The width of the distribution is measured by the DLS polydispersity index (DLS PDI). This polydispersity index is different from the polydispersity index defined in Chapter 4. The PDI for DLS is the ratio of the peak width of the particle size distribution to the intensity mean particle size. Typically a DLS PDI value of less than 0.1 is required to compare results to other methods. If the DLS PDI is between 0.1 and 0.5 the results can be

relatively compared to other zetasizer results. Values of greater than 0.5 result in an inaccurate Z-average value.

5.2.4 Stationary Phase Surface Coverage

To compare the stationary phase surface coverage for the 12 nm and the 28 nm colloidal silica coated particles the surface coverage, χ, was determined.

$$\chi = \frac{\%C}{100 * nC * 12 * SSA * (1 - \frac{\%C}{100} * \frac{MW - 1}{nC * 12})} \quad (5\text{-}4)$$

The %C values were obtained by elemental analysis using a Perkin Elmer CHN/S O elemental analyzer Series 2400 instrument (Waltham, MA). nC is the number of carbons in the stationary phase ligand (18), MW is the molecular weight of the stationary phase ligand, and SSA is the specific surface area of the particles which was carried out on non-bonded particles by Waters Corporation (Milford, MA) using a Micrometrics ASAP2420 (Norcross, GA) for Brunauer, Emmet, Teller (BET) analysis.

5.2.5 Column Packing

Fused silica capillary tubing (Polymicro Technologies, Inc., Phoenix, AZ) with an inner diameter of 30 μm and an outer diameter of 360 μm was used to pack all columns. The columns were prepared with outlet frits as outlined in Chapter 2. The procedure for packing capillary columns has be previously described.[22-25] Briefly, the 28 nm colloidal silica coated particles were suspended in a slurry solvent at a concentration of 3 mg/mL for all packing studies except the slurry concentration study which used a concentration of 25 mg/mL. The slurry solvents investigated were acetone, methanol, hexane and solvent X. All solvents were purchased from Fisher Scientific (Waltham, MA) and were filtered with a 0.2 μm PTFE filter before use. The slurry was sonicated for

10 minutes using a Cole Parmer Ultrasonic Cleaner 8891 (Vernon Hills, IL). A packing reservoir was then filled with the slurry solution and acetone was used as the pushing solvent. The capillary column was placed in a UHPLC fitting and secured to the column packing apparatus. Column packing was initiated at 3000 psi and as the bed began to form the pressure was gradually increased until reaching 30,000 psi at a rate of 3000 psi per centimeter of bed growth. The packing process was stopped when the desired column length was reached by slowly releasing the pressure.

After the desired column length was reached, the column was pressurized to ~45,000 psi and flushed with several column volumes of 80/20 water/ acetonitrile (ACN) with 0.1% trifluoroacetic acid (TFA) mobile phase (Fisher Scientific; Waltham, MA). The pressure was slowly released and re-pressurized to ~10,000 psi. A temporary inlet frit was then put in place using a heated wire stripper (Teledyne Interconnect Devices, San Diego, CA). The column was then clipped to the desired final length. The permanent inlet frit was then prepared using a procedure described by Maiolica *et. al*..[26] The column inlet was gently pressed on a glass microfiber filter (Reeve Angel; Clifton, NJ) that was previously wetted with 1:1 (v:v) ratio of potassium silicate (Kasil) and formamide. The Kasil was used as received from PQ Corporation (Valley Forge, IA) and formamide was from Sigma Aldrich (St. Louis, MO). After a few minutes, the glass microfiber filter had hardened, but to ensure it could withstand the running pressures, the frit was set in place using an electric arc device.

5.2.6 Column Evaluation

The detailed experimental set-up used to perform isocratic UHPLC has been previously described and was carried out as described in Chapter 2.[24, 25, 27, 28]

The mobile phase used for chromatographic evaluation was 80/20 water/ACN with 0.1% TFA. The isocratic test mixture contained L-ascorbic acid, which served as the dead time marker, hydroquinone (HQ), resorcinol (R), catechol (C), and 4-methyl catechol (4MC). The concentration of each sample in the test mixture was ~200 μM.

The columns that were used for this experiment were evaluated on the basis of chromatographic performance and retentivity. Column performance and analysis was carried out as described in Chapter 2.

5.3 RESULTS AND DISCUSSION

5.3.1 Particle Behavior at Atmospheric Pressure

5.3.1.1 In-Solution Microscopy

The behavior of the 12 nm and 28 nm colloidal silica coated particles in various slurry solvents was investigated by in-solution microscopy to determine if there were differences in the extent of particle aggregation in solution, Figures 5-2 and 5-3. The presence of aggregation has been found to work well for packing efficient capillary columns.[10, 13] Based on images collected for each sample, the degree of aggregation was used to determine the relative perceived performance of each slurry solvent. Based on the chemical aspects of the particle surface it would be expected that the particles would be most dispersed in a non-polar solvent, such as hexane, if the C18 chains are dominating the particle-solvent properties. A more polar solvent would be expected to cause little particle aggregation if the free silanols are dictating the particle-solvent behavior. Based on the polarity index, the solvents investigated vary in polarity as follows: methanol = acetone > tetrahydrofuran > isopropanol >> hexane.[29]

There are difficulties that arise when using in-solution microscopy to determine particle aggregation behavior due to the process of solvent evaporation during imaging. It was observed that as the solvent evaporated due to the heat of the microscope light, particles acting individually became aggregated in the evaporating solvent front. Therefore, care needed to be taken to obtain images before any substantial solvent evaporation occurred. To reduce any concentration effects the same concentration and same amount of sample was loaded onto each slide for observation with the exception of the slurry concentration study.

The 12 nm colloidal silica coated particle, results shown in Table 5-3, indicate that the binary solvent mixtures caused a greater amount of particle aggregation. Mixtures from solvents that did not cause aggregation individually were shown to cause aggregation when combined, such as acetone and methanol. The mixture of acetone and methanol or acetone and isopropanol have less dispersing power because the majority are hydrogen bonded together leading to less interaction with the particles.[30] This behavior would be observed for any mixture of a protic and aprotic solvent, but to varying degrees. From the perceived performance, it is seen that the polar solvents dispersed the particles more than the non-polar solvent, indicating that the particle-solvent properties are controlled more by the free silanols than the C18 functional groups. In the case of mixtures of a non-polar solvent with a polar solvent, the polar solvent is preferentially taken up by the silica.[31] This would lead to particle dispersion better than the solution with non-polar solvent alone, as was observed.

On the other hand, the dispersion properties of the 28 nm coated particles showed the opposite behavior, Table 5-4. The binary slurry solvents showed little aggregation,

while the individual solvents produced highly aggregated particles. This is further indication of the need for an assessment of the slurry solvent for each batch of particles. Individual solvents that showed particle aggregation did not produce aggregation as part of binary mixtures. This does correlate with the behavior seen with the 12 nm coated particles in that the individual slurry solvents act in a manner opposite the binary mixtures.

The external surface of the particles governs the type and extent of particle-solvent interactions present. The main difference between the external surface of the 12 nm and 28 nm coated particles is the stationary phase surface coverage. The 12 nm coated particles were found to have 4.0 μmol/m^2 C18 while the 28 nm coated particles have 4.4 μmol/m^2 C18. This indicates that there is a greater amount of the non-polar functional group and a decrease in the free silanols for the 28 nm coated particles. This difference may have lead to the differences in effective dispersion solvents.

In addition to slurry solvent, the slurry concentration has been found to play a role in column packing and performance. For the 28 nm coated particles, a slurry solution in methanol was made at varying concentrations, Figure 5-4. At all concentrations, aggregation was found to be present. As the concentration was increased, the size of the aggregates increased, but independent of concentration the proportion of single particles present did not change. Since aggregation has been found to produce capillary columns with higher efficiency, a high slurry concentration in methanol would be predicted to work well.

For comparison, the 28 nm coated particles were slurried in acetone at varying concentrations, Figure 5-5. As with methanol, no significant changes between

concentrations were observed. At all concentrations some aggregation was seen, but not nearly to the extent seen with methanol. Therefore, varying the concentration for these solvents did not affect the state (aggregated versus non-aggregated) of the particles.

5.3.1.2 Sedimentation Velocity and Effective Particle Size

The sedimentation velocity of particles in solution is related to the effective particle size in solution. The larger the particle, the greater the sedimentation velocity. One difficulty with this method is the bias to the smallest particles in solution. This is due to the start and end time determination by visually monitoring the particle front. Therefore, only solutions that are entirely aggregated will show a larger effective particle size than that measured from SEM images. In order to accurately determine the sedimentation velocity and effective particle diameter, the values must be scaled by the density and viscosity of the solvent. Not scaling for each solvent would cause the calculated effective particle diameter to be artificially low for solvents with a high viscosity and artificially high for solvents with low viscosity.

The majority of the 12 nm coated particles were found to show an effective particle diameter close to the value determined from SEM images as expected from the bias towards small particles, Table 5-5. Of those that showed aggregation, hexane was found to produce the largest effective particle size. This indicates that the particle properties in solution are dictated by the free silanols rather than the C18 functional groups. Furthermore, it was found that the aggregation behavior of the particles in hexane could be overcome by adding acetone to the solution. While addition of isopropanol to hexane had a less significant effect on relieving the aggregation caused by hexane. This is as would be expected based on their polarity values of 5.1 for acetone and 3.9 for

isopropanol.[29] In comparison to the results obtained from in-solution microscopy, the aggregation behavior of the binary solvents was indicated by both methods, but the aggregation seen with hexane from sedimentation was not seen with in-solution microscopy.

For the 28 nm colloidal silica coated particles, hexane again showed the greatest amount of particle aggregation and the addition of acetone and isopropanol relieved some of these aggregation affects as was seen with the 12 nm coated particles, Table 5-6. The majority of the effective particle diameters for the 28 nm coated particles correlated well to that seen for the 12 nm coated particles. The exception being the 1:1 acetone:methanol slurry solvent, which showed no aggregation with the 28 nm coated particles, but produced slight aggregation with the 12 nm coated particles. These results again indicate that the particle-solvent interactions are dictated by the free silanols present. The results obtained from in-solution microscopy did not correlate well with the sedimentation results. In particular, methanol and acetone were predicted to be good packing solvents by in-solution microscopy based on the observation of particle aggregates, but based on sedimentation these were found to produce the smallest effective particle diameters. Therefore, a consistent prediction with these particles cannot be made based on these two techniques.

Additional investigation of the 28 nm coated particles was carried out by varying the particle slurry concentration in acetone. From previous studies, it has been found that a higher solution concentration produces a more efficient column due to increased packing rate.[10, 12, 14] From these previous results and predictions that a more concentrated solution would lead to a higher amount of aggregation due to the greater

chance of particle-particle contact it would be expected that the higher concentration solutions would show a higher effective particle size. This was found to not be the case for solutions up to 15 mg/mL. All solutions were found to have a effective particle size equal to that measured by SEM images. From these results, no changes in packing and performance would be predicted from the physical interaction of the particle in solution at higher concentrations.

When comparing the two types of particles by sedimentation, the results were much more consistent than seen with in-solution microscopy. While this may in fact be the case, the slight changes in particle aggregation may have been masked by measurement of the sedimentation velocity due to the bias toward smaller particles. While aggregation may have been present, it would not have been detected unless the entirety of the solution was aggregated. To overcome this bias and gain more valuable information from this technique it would require the measurement of the absorbance as a function of time at a single vertical position in the solution. This will still show some problems due to the scattering of light in the solution, but should be more valuable than visual measurement.

5.3.1.3 Particle Size by Dynamic Light Scattering

The effective particle diameter for the 12 nm and 28 nm colloidal silica coated particles was assessed by dynamic light scattering. By this technique, the effective particle diameter was determined in the selected slurry solvents. The 12 nm coated particles were found to show 1:1 hexane:isopropanol, tetrahydrofuran, and hexane as the most aggregating solvents, Table 5-7. Both tetrahydrofuran and hexane produced effective particle diameters greater than the upper size limit, 6 μm, of the instrument. As

with the previous methods, this indicates that the dispersing properties are governed more by the free silanols than the bonded hydrophobic ligand. The results from DLS do not agree with the results found by in-solution microscopy. For example, particles in 2:1 hexane:acetone and 2:1 acetone:hexane were measured as individual particles by DLS, but were mainly aggregated as viewed by in-solution microscopy.

Similarly, the 28 nm coated particles were found to highly aggregate in hexane and tetrahydrofuran, Table 5-8. On the other hand, in isopropanol the particle size was found to be much smaller than the size of an individual particle. This skewed measurement was found to be common when measuring isopropanol solutions due to the high viscosity of isopropanol leading to error in the measurement of Brownian motion. Also in agreement with the 12 nm coated particles, some of the results from DLS for the 28 nm coated particles were found to contradict those found for in-solution microscopy. For example, 1:1 hexane:IPA was measured as acting individually by DLS, but was one of the most aggregating by in-solution microscopy. Further discrepancy was found for the degree of aggregation measured. For both methanol and 1:1 acetone:hexane, minor aggregation was measured by DLS, but by in-solution microscopy very large aggregates were observed.

To investigate the reliability of the measurements obtained by DLS, multiple measurements of the same sample were made. For the acetone slurry, the z-average measurements were found to be 2.9 μm and 2.3 μm and for THF the initial value was over the size limit, but the second measure measurement was 5.3 μm. Neither of these values is drastically different from each other, but the variation is still at least 30%. Some of this lack of reproducibility may have been due to the inaccurate determination of the

Brownian motion due to particle sedimentation. Therefore, based on the variability seen from the DLS results, the results from in-solution microscopy were held in higher regard.

5.3.2 Prediction of Column Performance

For the 28 nm coated particles, slurry solvents predicted to produce the most efficient and least efficient columns based on the sedimentation and in-solution microscopy results were selected. The performance of each of these columns was assessed to determine if there is a technique that can accurately predict a suitable slurry solvent.

The solvent typically selected as the slurry solvent for totally porous particles in our group is acetone. In the case of superficially porous particles synthesized in-house, methanol is typically a better slurry solvent. Figure 5-6 shows chromatograms for columns packed in each of these solvents, further indicating the improved efficiency of a methanol slurry for superficially porous particles. The number of theoretical plates per meter for the column packed in acetone and methanol were 132,000 plates/meter and 239,000 plates/meter, respectively. Other solvents investigated, solvent X and hexane were used to determine their packing and chromatographic efficiency. The chromatography at the optimum linear velocity for columns packed with these solvents is shown in Figure 5-7. The hydroquinone peak width at half height for the acetone, methanol, hexane, and solvent X columns were found to be 0.11 minutes, 0.06 minutes, 0.07 minutes, and 0.10 minutes, respectively. Using the half height peak width to predict the minimum reduced plate height, the h_{min} value for hexane would be predicted to be closer to that for methanol than for acetone or solvent X, but this was found to not be the case. This indicates that the peak symmetry plays a large role in the performance since

the number of theoretical plates is calculated by iterative statistical moments rather than peak width or peak area and height.

Comparing the reduced parameter plots for the four columns to the values theoretically predicted, it was found that the performance of all columns was not meeting the expectations, Figure 5-8. The methanol packed column was found to be closest to the theoretical values, having a h_{min} of 3.5 and a *c*-term of 0.86, but was still quite far from the predicted h_{min} of 2.0 and *c*-term of 0.10. Comparing the other columns, all had roughly the same h_{min} values, but the *c*-term widely varied.

In comparison to the methods used to predict a suitable packing solvent, the in-solution microscopy indicates a better correlation to column performance than sedimentation velocity. Methanol was seen by in-solution microscopy to yield highly aggregated slurries and produced the most efficient column. Accordingly solvent X was found to allow the particles to act individually in solution and produced an inefficient column. This was further evidence that an aggregating solvent produced a more efficient column than a solvent that reduces particle-particle interactions. This particle aggregation may reduce the ability of particle size segregation during packing, leading to improved chromatographic efficiency. Both hexane and acetone were seen to form small aggregates in solution, but in roughly similar amounts, correlating well to their similar chromatographic performance. Based on in-solution microscopy, the particles in hexane were slightly less aggregated than in acetone, which would predict the hexane column to be slightly worse performing than the acetone column, but this was not seen. Therefore, in-solution microscopy may only be able to differentiate vast differences in particle aggregation for translation into column performance.

In comparison, the sedimentation method did not correlate well to the column performance. The most aggregating solvent, as determined by the effective particle diameter, was found to be hexane, but did not produce the highest efficiency column. Furthermore, methanol, acetone, and solvent X were found to have very similar effective particle diameters, but showed widely varying performance. Therefore, the use of sedimentation velocity to determine effective particle diameter was not found to be a good performance predictor in this case.

5.3.3 Effect of Slurry Concentration on Performance

Based on previous studies from other groups and current research in our lab, it has been found that for totally porous particles and non-porous particles, a high slurry concentration produces columns with higher efficiency. Concentrations found in the literature varied from 7 to 40% (w/v%) [10, 12, 14] and a concentration of 2.5% (w/v%) was found to work best for 1.0 μm totally porous particles packed in our lab. Historically our lab has used a 0.3% (w/v%) solution for column packing. Therefore, for the majority of the column packing studies this was the concentration used.

To determine the effect of the slurry concentration on column performance, a column packed with a 0.3% (w/v%) solution and one with a 2.5% (w/v%) solution were compared. Based on the chromatographic performance at the optimum linear velocity it is evident that the higher slurry concentration packed a more efficient column, Figure 5-9. The number of theoretical plates per meter for the hydroquinone peak for the 0.3% (w/v%) slurry and 2.5% (w/v%) slurry were found to be 173,000 plates/meter and 318,000 plates/meter, respectively. As seen in each chromatogram, an ascorbic acid impurity was found to be present, but this did not interfere with the determination of the

dead time for ascorbic acid. No performance assessment was carried out for ascorbic acid and therefore column assessment is not affected by the unresolved impurity. Further confirmation of the improved efficiency of the higher concentration slurry column can be seen in Figure 5-10. Both the *a*-term and the *c*-term were found to significantly improve and the packing density was increased for the higher concentration slurry column. The *c*-term reduction has been explained by a decreased distance between particles for a more densely packed bed, thus reducing the time for mass transfer in the mobile phase.[32] The decrease in the *a*-term may be attributed to the predicted effect of the increased packing rate for the higher slurry concentrations which lead to improved radial homogeneity.[7]

5.3.4 Effect of Surface Roughness on Performance

From previous studies it was found that the use of centrifugation for particle washing led to particle agglomeration that was carried through to the final particles. It was predicted from other synthesis studies that the particle agglomeration would be reduced by washing by settling. As seen from the disc centrifuge results discussed in Chapter 4, the use of settling for washing did not reduce the amount of particle agglomeration, but did improve the surface uniformity. As seen in Figure 5-11, the presence of colloidal silica aggregates on the superficially porous particle surface was reduced by washing by settling.

As seen in Figure 5-12, the efficiency of 1.1 μm, 28 nm coated particles was slightly improved by the removal of the colloidal silica aggregates of the settle washed particles. There was a slight increase in the number of theoretical plates obtained for the settle washed particles, 356,000 plates/meter, over the centrifuge washed particles, 318,000 plates/meter. There was also a modest improvement in the *c*-term contribution,

Figure 5-13. The lower slope in the higher linear velocity region indicates the presence of a velocity dependent *a*-term.[7] This can be explained by the reduction in colloidal silica aggregates on the settled particles that may allow for a more homogeneous packing structure. The similar performance between to two types of particles indicates that the washing method only slightly improves the performance for a large increase in production time.

5.4 CONCLUSIONS

Both the slurry solvent and slurry concentration play a critical role in the chromatographic performance of the resulting column. Historically the selection of a suitable slurry solvent and concentration has been by trial-and-error which can be very time consuming. In-solution microscopy, sedimentation velocity, and particle size by dynamic light scattering were carried out to determine if a performance prediction technique could be developed. The use of dynamic light scattering to determine the particle size was not useful because accurate measurements could not be obtained due to the sedimentation of the particles. The determination of the effective particle size by sedimentation has been most commonly used in our lab, but is biased to the smallest particles present. Taking this into consideration, sedimentation was not found to accurately predict a good slurry solvent. The most useful technique was found to be in-solution microscopy. Based on this technique, the most aggregating solvent was found to produce the most efficient column for those slurry solvents tested. From the performance analysis, a slurry solvent of methanol and a particle concentration of 2.5% (w/v%) was found to produce the most efficient column.

5.5 TABLES

Solvent
Acetone
Methanol (MeOH)
Isopropanol (IPA)
Tetrahydrofuran (THF)
Hexane
Solvent X
1:1 Hexane:Isopropanol
1:1 Acetone:Isopropanol
1:1 Acetone:Methanol
1:1 Acetone:Hexane
2:1 Hexane:Isopropanol
2:1 Isopropanol:Hexane
2:1 Acetone:Hexane
2:1 Hexane:Acetone

Table 5-1: Solvents used to investigate solution properties of 12 nm and 28 nm colloidal silica coated particles by in-solution microscopy, sedimentation, and dynamic light scattering.

Solvent	Density (g/cm^3)	Viscosity (cP)
Acetone	0.786	0.306
Methanol (MeOH)	0.791	0.548
Isopropanol (IPA)	0.785	1.96
Tetrahydrofuran (THF)	0.889	0.455
Hexane	0.655	0.294
Solvent X	0.804	0.790
1:1 Hexane:Isopropanol	0.702	0.900
1:1 Acetone:Isopropanol	0.797	0.600
1:1 Acetone:Methanol	0.857	0.400
1:1 Acetone:Hexane	0.779	0.300
2:1 Hexane:Isopropanol	0.726	0.670
2:1 Isopropanol:Hexane	0.700	1.35
2:1 Acetone:Hexane	0.817	0.300
2:1 Hexane:Acetone	0.744	0.300

Table 5-2: Summary of densities and viscosities used to calculate the sedimentation rate.

Slurry Solvent	Observations	Perceived Performance
2:1 IPA:Hexane	All multiplets	1
1:1 Acetone:Hexane	All multiplets	2
2:1 Acetone:Hexane	Singles and large aggregates	3
2:1 Hexane:Acetone	Singles and large aggregates	4
1:1 Acetone:Methanol	Singles and large aggregates	5
1:1 Acetone:IPA	Singles and large aggregates	6
Hexane	Mainly multiplets, some singles	7
1:1 Hexane:IPA	Half multiplets, half singles	8
Isopropanol	Mainly singles, some multiplets	9
Tetrahydrofuran	Mainly singles, some multiplets	10
Acetone	Mainly singles, some multiplets	11
Solvent X	Mainly singles, some multiplets	12
Methanol	Mainly singles, some multiplets	13
2:1 Hexane:IPA	Mainly singles	14

Table 5-3: Summary of perceived performance of 1.1 μm particles coated with 12 nm colloidal silica by in-solution microscopy.

Slurry Solvent	Observations	Perceived Performance
1:1 Acetone:MeOH	All large aggregates	1
Methanol	Singles and large aggregates	2
Acetone	Multiplets	3
1:1 Hexane:IPA	Multiplets	4
Isopropanol	Multiplets	5
2:1 Acetone:Hexane	Mulitplets	6
Hexane	Mulitplets	7
Tetrahydrofuran	Some singles and multiplets	8
1:1 Acetone:IPA	Some singles and multiplets	9
2:1 IPA:Hexane	Mainly singles, some multiplets	10
2:1 Hexane:IPA	Mainly singles, some multiplets	11
2:1 Hexane:Acetone	Singles and a couple multiplets	12
1:1 Hexane:Acetone	Singles and a couple multiplets	13
Solvent X	Singles and a couple multiplets	14

Table 5-4: Summary of perceived performance of 1.1 μm ($d_{p,n}$) particles coated with 28 nm colloidal silica by in-solution microscopy.

Slurry Solvent	Theoretical Sedimentation Velocity (cm/sec)	Experimental Sedimentation Velocity (cm/sec)	Effective Particle Diameter (μm)	α
Isopropanol	3.9×10^{-5}	3.6×10^{-5}	1.2	0.9
Acetone	2.5×10^{-4}	2.7×10^{-4}	1.2	1.1
1:1 Acetone:Hexane	2.5×10^{-4}	2.8×10^{-4}	1.3	1.1
2:1 Acetone:Hexane	2.5×10^{-4}	2.6×10^{-4}	1.2	1.0
2:1 Hexane:Acetone	2.6×10^{-4}	2.8×10^{-4}	1.2	1.1
Methanol	1.4×10^{-4}	1.5×10^{-4}	1.2	1.1
Tetrahydrofuran	1.5×10^{-4}	1.7×10^{-4}	1.2	1.1
Solvent X	9.5×10^{-5}	1.2×10^{-4}	1.3	1.3
2:1 Hexane:IPA	1.2×10^{-4}	1.7×10^{-4}	1.4	1.4
2:1 IPA:Hexane	6.0×10^{-5}	8.6×10^{-5}	1.4	1.4
1:1 Acetone:IPA	1.3×10^{-4}	1.8×10^{-4}	1.5	1.4
1:1 Hexane:IPA	9.0×10^{-5}	1.4×10^{-4}	1.5	1.6
1:1 Acetone:MeOH	1.8×10^{-4}	2.8×10^{-4}	1.5	1.6
Hexane	2.8×10^{-4}	1.4×10^{-3}	2.7	5.0

Table 5-5: Summary of sedimentation rate and effective particle diameter for 1.1 μm ($d_{p,n}$) particles coated with 12 nm colloidal silica.

Slurry Solvent	Theoretical Sedimentation Velocity (cm/sec)	Experimental Sedimentation Velocity (cm/sec)	Effective Particle Diameter (μm)	α
Methanol	1.5×10^{-4}	1.3×10^{-4}	1.1	0.9
Tetrahydrofuran	1.6×10^{-4}	1.4×10^{-4}	1.1	0.9
Acetone (3 mg/mL)	2.6×10^{-4}	2.5×10^{-4}	1.2	1.0
Acetone (5 mg/mL)	2.6×10^{-4}	2.7×10^{-4}	1.2	1.0
Acetone (10 mg/mL)	2.6×10^{-4}	2.7×10^{-4}	1.2	1.0
Acetone (15 mg/mL)	2.6×10^{-4}	2.7×10^{-4}	1.2	1.0
1:1 Acetone:Hexane	2.7×10^{-4}	2.9×10^{-4}	1.2	1.1
2:1 Acetone:Hexane	2.6×10^{-4}	2.6×10^{-4}	1.2	1.0
1:1 Acetone:MeOH	1.9×10^{-4}	1.9×10^{-4}	1.2	1.0
2:1 Hexane:Acetone	2.8×10^{-4}	2.6×10^{-4}	1.2	0.9
Isopropanol	4.1×10^{-5}	4.1×10^{-5}	1.2	1.0
Solvent X	1.0×10^{-4}	1.0×10^{-4}	1.2	1.0
Water (After SDS treatment)	6.9×10^{-5}	7.0×10^{-5}	1.2	1.0
1:1 Acetone:IPA	1.3×10^{-4}	1.6×10^{-4}	1.3	1.2
1:1 Hexane:IPA	9.6×10^{-5}	1.2×10^{-4}	1.3	1.3
2:1 Hexane:IPA	1.3×10^{-4}	1.7×10^{-4}	1.4	1.3
2:1 IPA:Hexane	6.4×10^{-5}	8.4×10^{-5}	1.4	1.3
Hexane	3.0×10^{-4}	9.8×10^{-4}	2.2	3.3

Table 5-6: Summary of sedimentation rate and effective particle diameter for 1.1 μm ($d_{p,n}$) particles coated with 28 nm colloidal silica.

Slurry Solvent	DLS Particle Size (μm)	DLS Polydispersity Index
2:1 Hexane:Acetone	1.0	0.42
2:1 Acetone:Hexane	1.2	0.38
1:1 Acetone:Hexane	1.6	0.49
1:1 Acetone:Methanol	1.6	0.18
2:1 IPA:Hexane	1.6	0.33
Methanol	1.6	0.15
Isopropanol	1.8	0.22
Solvent X	2.0	0.46
1:1 Acetone:IPA	2.1	0.56
Acetone	2.9	0.43
2:1 Hexane:IPA	3.0	0.72
1:1 Hexane:IPA	3.4	0.35
Tetrahydrofuran	> upper size limit	N/A
Hexane	> upper size limit	N/A

Table 5-7: Summary of effective particle size measurements by dynamic light scattering for 1.1 μm ($d_{p,n}$) particles coated with 12 nm colloidal silica in various slurry solvents

Slurry Solvent	DLS Particle Size (μm)	DLS Polydispersity Index
Isopropanol	0.3	0.18
1:1 Acetone:IPA	0.8	0.36
1:1 Hexane:IPA	0.9	0.19
2:1 IPA:Hexane	1.1	0.21
2:1 Hexane:IPA	1.3	0.54
Acetone	1.4	0.10
1:1 Acetone:Methanol	1.9	0.35
Methanol	1.9	0.25
2:1 Hexane:Acetone	2.3	0.49
1:1 Acetone:Hexane	2.4	0.50
2:1 Acetone:Hexane	2.8	0.50
Solvent X	3.6	0.87
Hexane	> size limit	N/A
Tetrahydrofuran	> size limit	N/A

Table 5-8: Summary of effective particle size measurements by dynamic light scattering for 1.1 μm ($d_{p,n}$) particles coated with 28 nm colloidal silica in various slurry solvents.

5.6 FIGURES

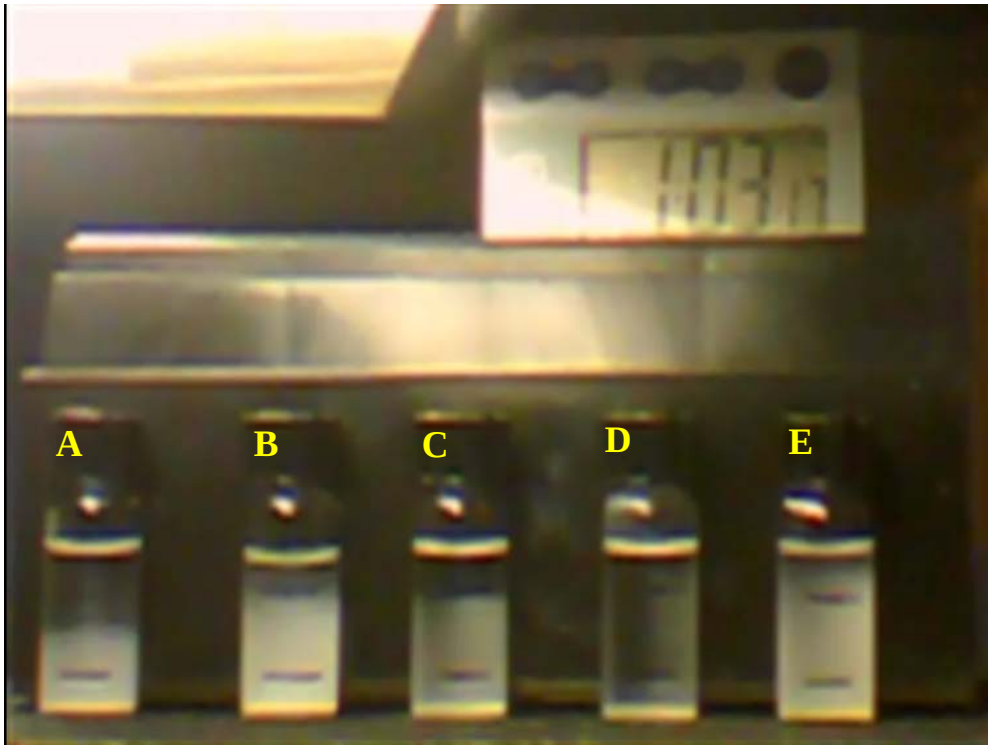

Figure 5-1: Example of sedimentation rate and effective particle size measurement set-up. A) acetone B) methanol C) tetrahydrofuran D) hexane E) isopropanol

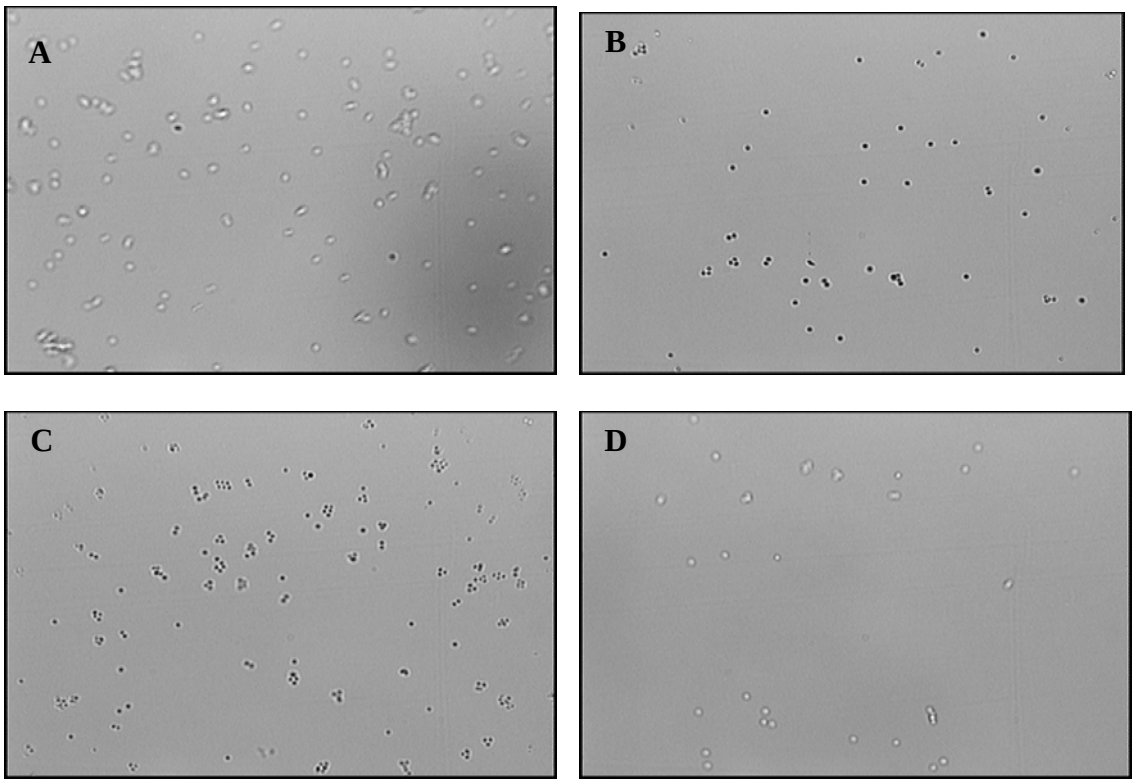

Figure 5-2: Images of 1.1 μm ($d_{p,n}$) particles coated with 12 nm colloidal silica by in-solution microscopy. A) acetone B) methanol C) hexane D) solvent X

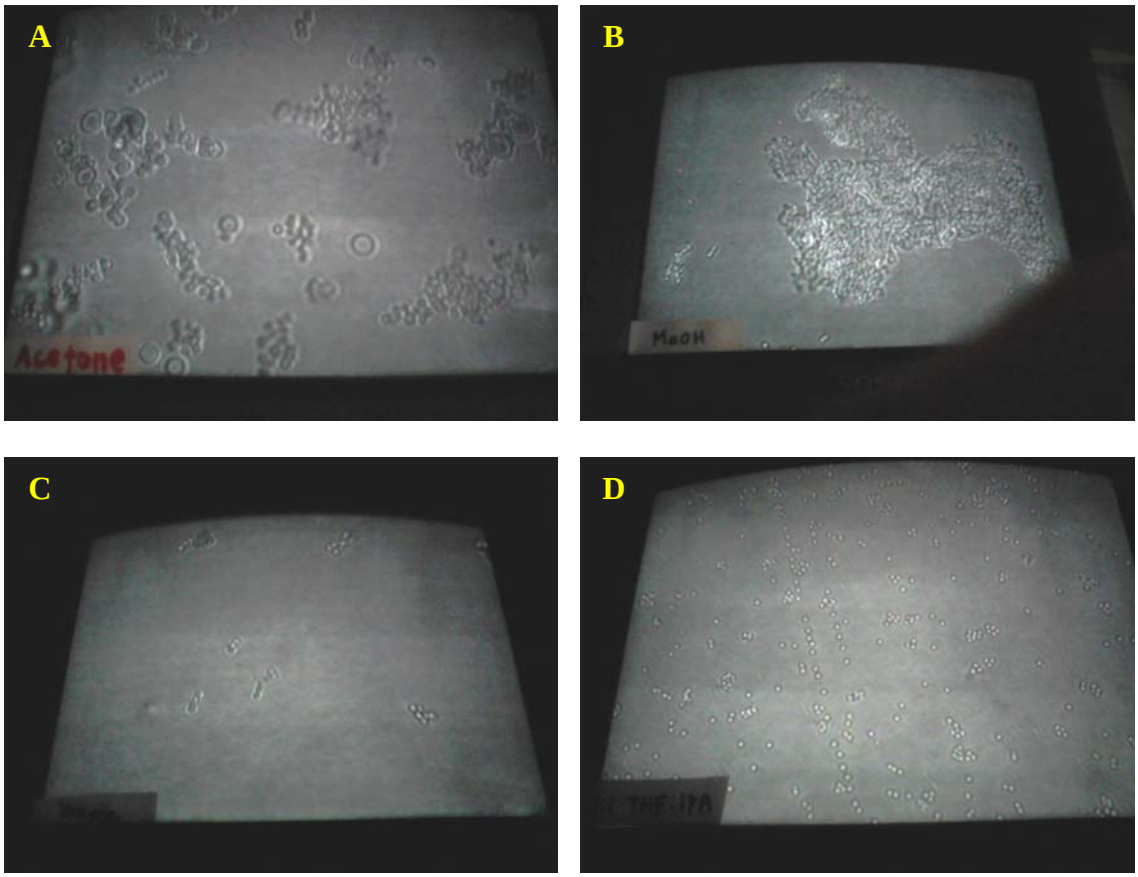

Figure 5-3: Images of 1.1 μm ($d_{p,n}$) particles coated with 28 nm colloidal silica by in-solution microscopy. A) acetone B) methanol C) hexane D) solvent X

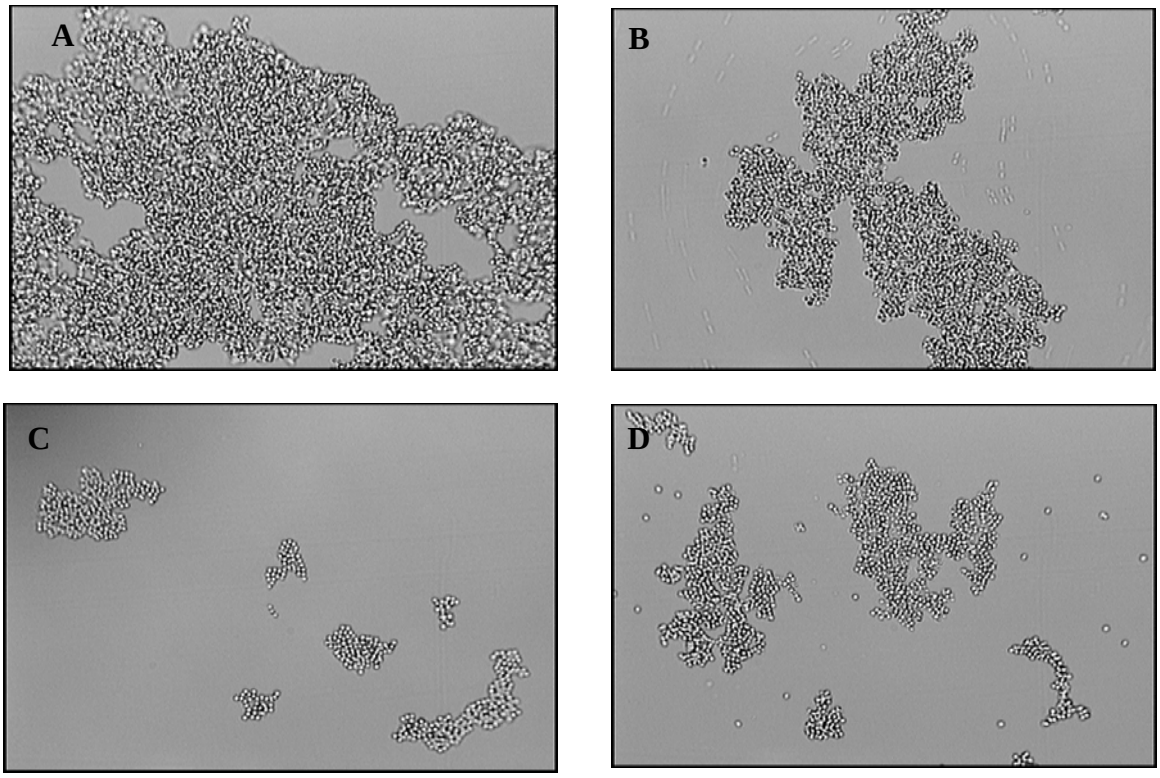

Figure 5-4: Images of 1.1 μm ($d_{p,n}$) particles coated with 28 nm colloidal silica by in-solution microscopy in methanol at varying concentrations. A) 25 mg/mL B) 13 mg/mL C) 7 mg/mL D) 3 mg/mL

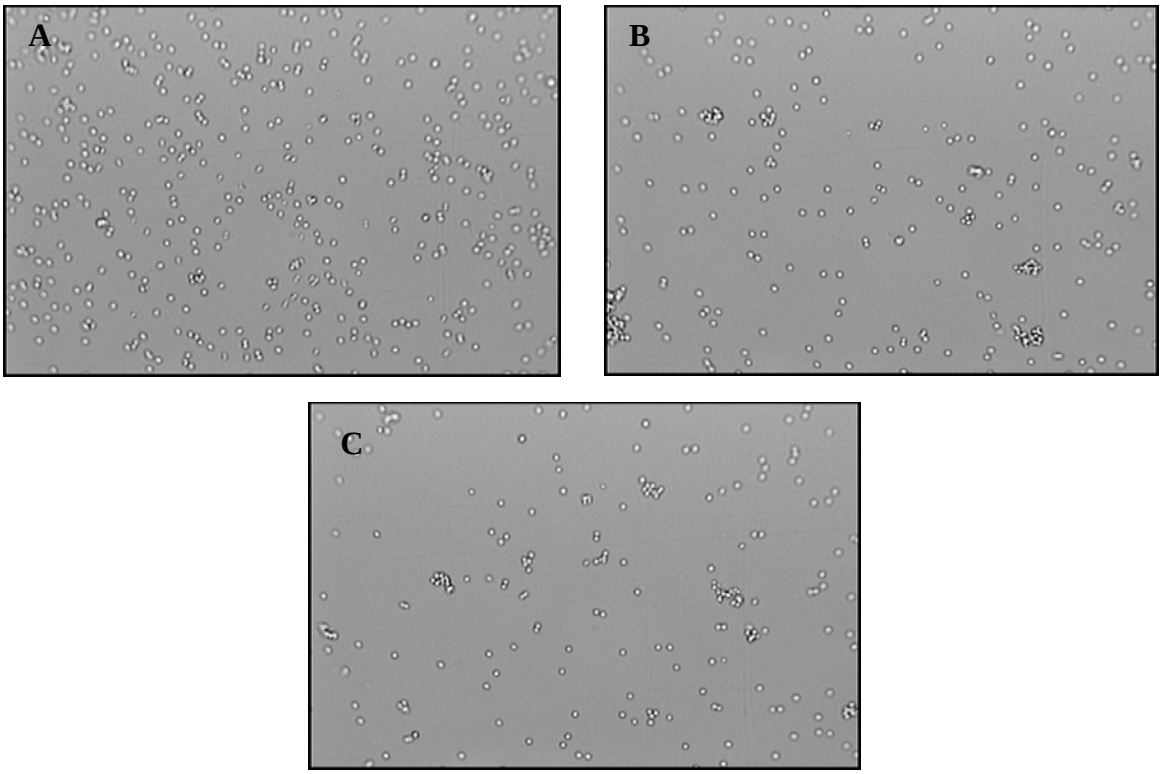

Figure 5-5: Images of 1.1 μm ($d_{p,n}$) particles coated with 28 nm colloidal silica by in-solution microscopy in acetone at varying concentrations. A) 25 mg/mL B) 13 mg/mL C) 7 mg/mL

A

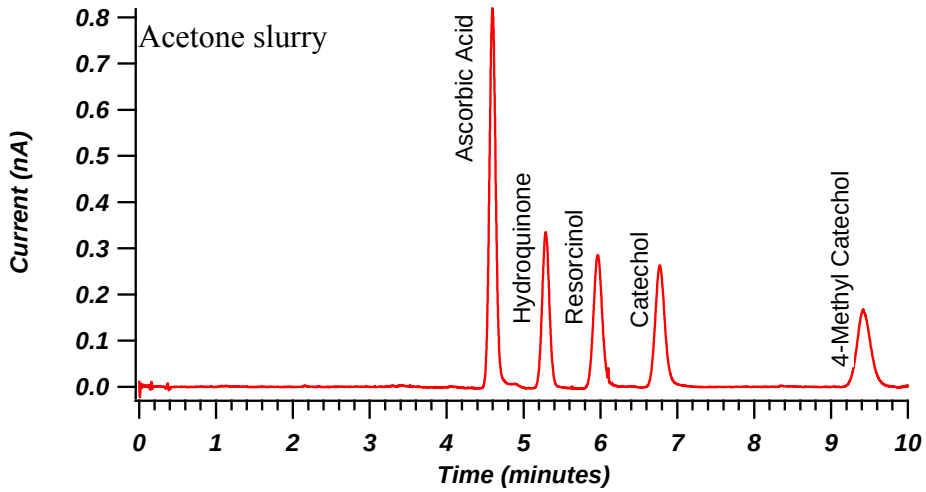

B

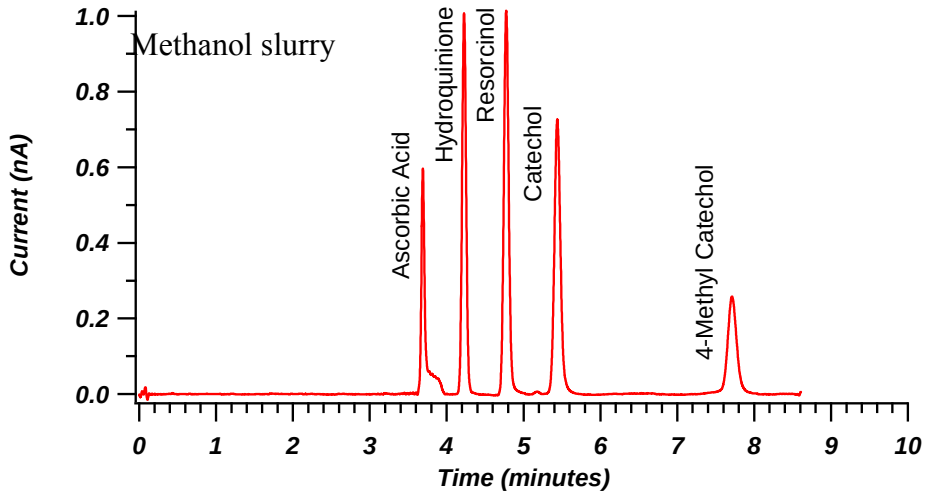

Figure 5-6: Example chromatograms for columns packed with 1.1 µm ($d_{p,n}$) particles coated with 28 nm colloidal silica in varying slurry solvent. A) acetone, Column LB6-81, LB6-57-4 particles, 30 µm x 11.6 cm, h_{min} (HQ) = 6.3, u_{opt} = 0.04 cm/sec (2400 psi), k'(4MC) = 1.04 B) methanol, Column LB6-153-C, LB6-57-4 particles, 30 µm x 12.5 cm, h_{min} (HQ) = 3.5, u_{opt} = 0.07 cm/sec (4400 psi), k'(4MC) = 1.04

A

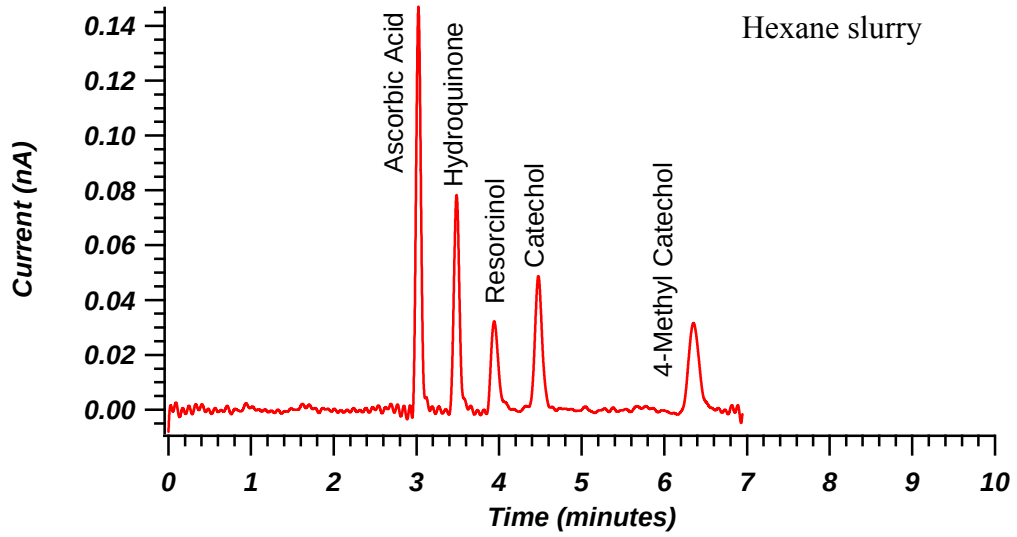

B

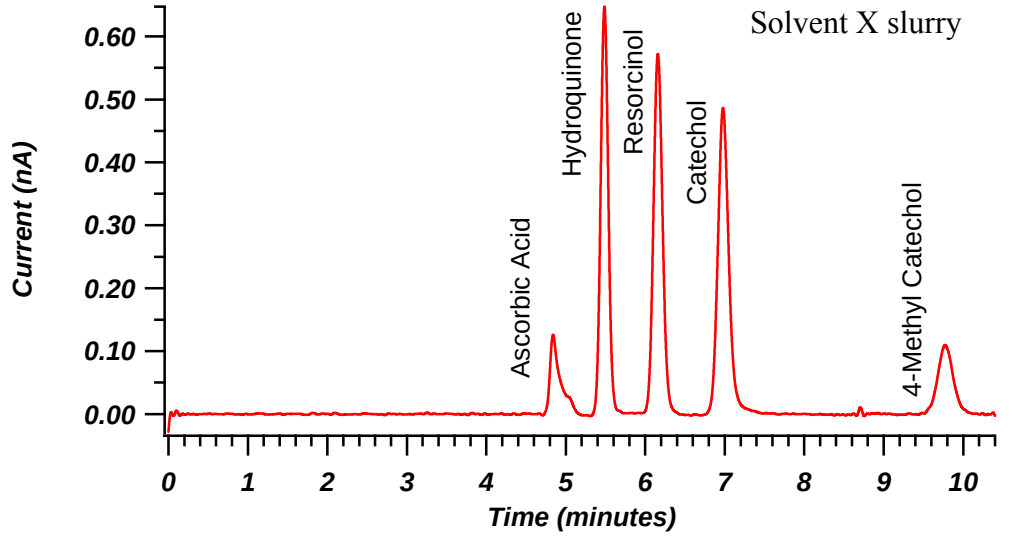

Figure 5-7: Example chromatograms for columns packed with 1.1 µm ($d_{p,n}$) particles coated with 28 nm colloidal silica in varying slurry solvent. A) hexane, Column LB7-20, LB6-57-4 particles, 30 µm x 10.2 cm, h_{min} (HQ) = 6.1, u_{opt} = 0.06 cm/sec (3000 psi), k'(4MC) = 1.06 B) solvent X, Column LB6-153-A, LB6-57-4 particles, 30 µm x 12.6 cm, h_{min} (HQ) = 6.8, u_{opt} = 0.03 cm/sec (1800 psi), k'(4MC) = 0.98

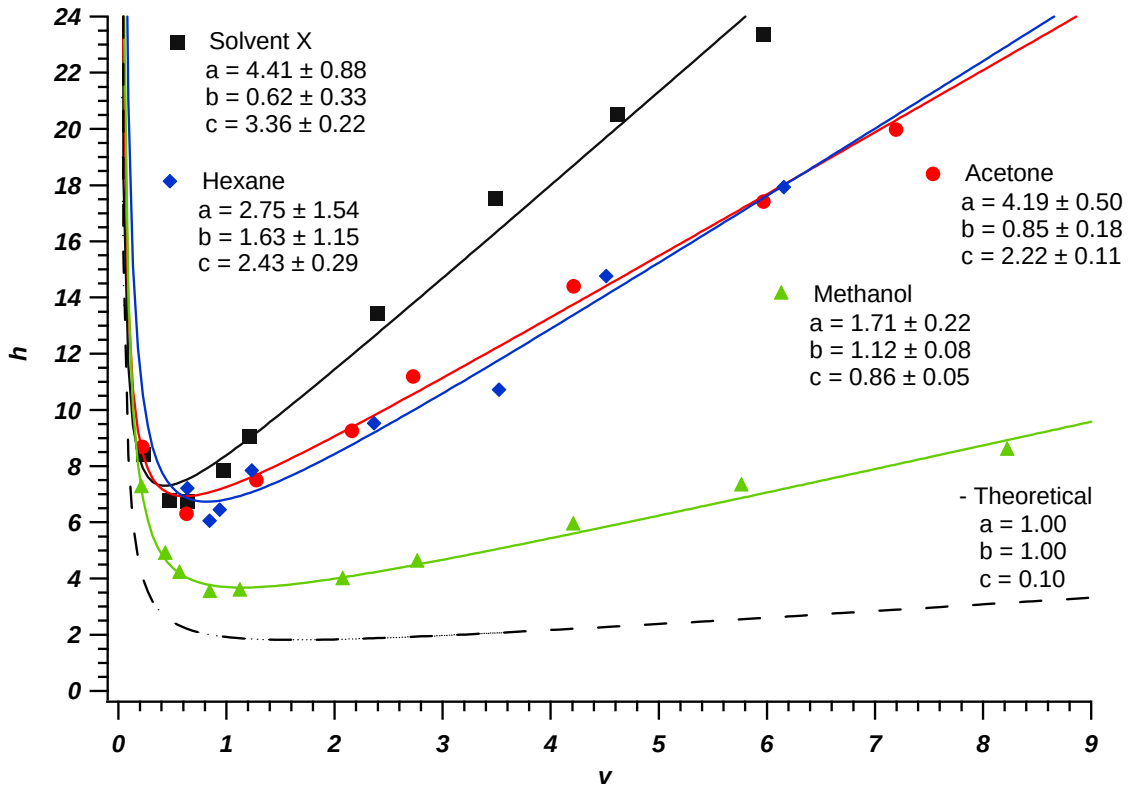

Figure 5-8: Reduced parameters plot comparison for columns packed with 1.1 µm ($d_{p,n}$) particles coated with 28 nm colloidal silica in varying slurry solvent. A) acetone B) methanol C) hexane D) solvent X

A

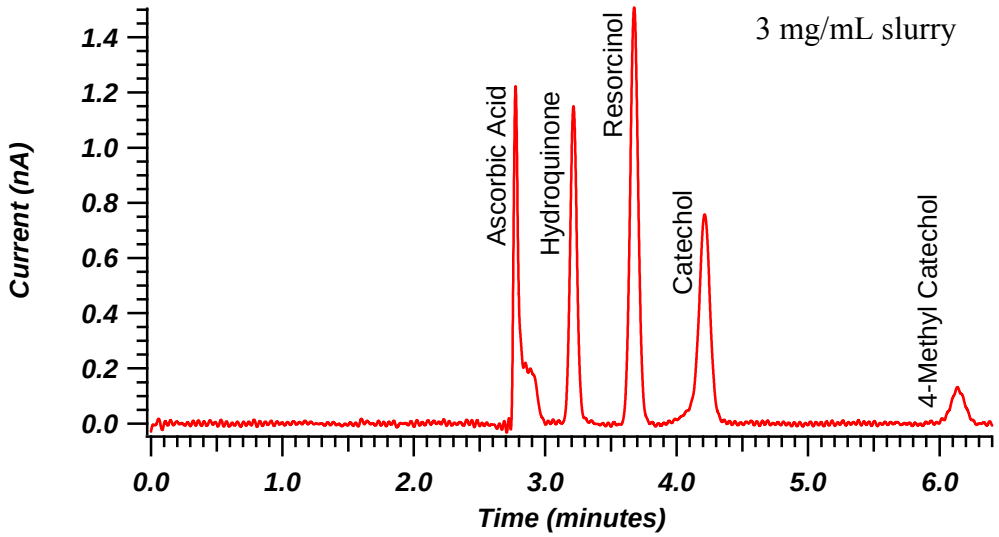

B

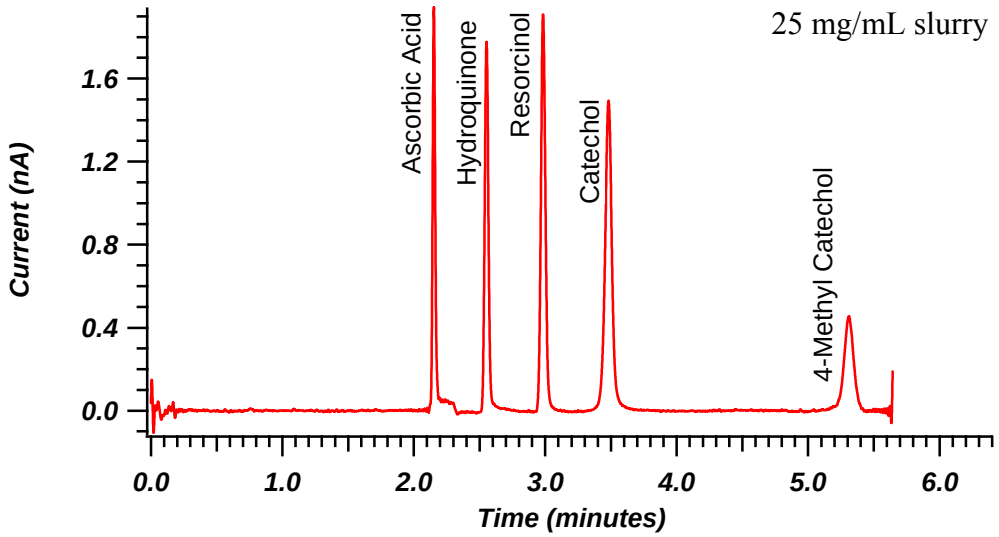

Figure 5-9: Example chromatograms for columns packed with 1.1 µm ($d_{p,n}$) particles coated with 28 nm colloidal silica at varying slurry concentration. A) Column LB7-38, LB7-23-3 particles, slurry concentration = 3 mg/mL, 30 µm x 10.2 cm, h_{min} (HQ) = 4.8, u_{opt} = 0.06 cm/sec (2600 psi), k'(4MC) = 1.2 B) Column LB7-33, particles LB7-23-3, slurry concentration = 25 mg/mL, 30 µm x 12.8 cm, h_{min} (HQ) = 2.6, u_{opt} = 0.16 cm/sec (8700 psi), k'(4MC) = 1.3

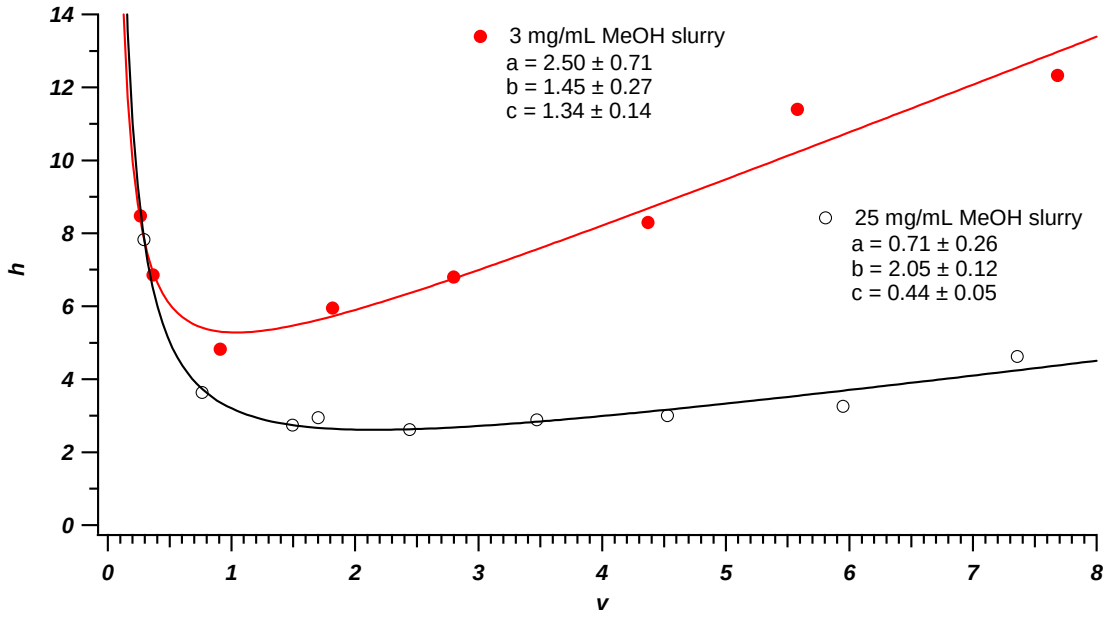

Figure 5-10: Reduced parameters plot comparison of hydroquinone for columns packed with 1.1 µm ($d_{p,n}$) particles coated with 28 nm colloidal silica at varying slurry concentration fit to the van Deemter equation.

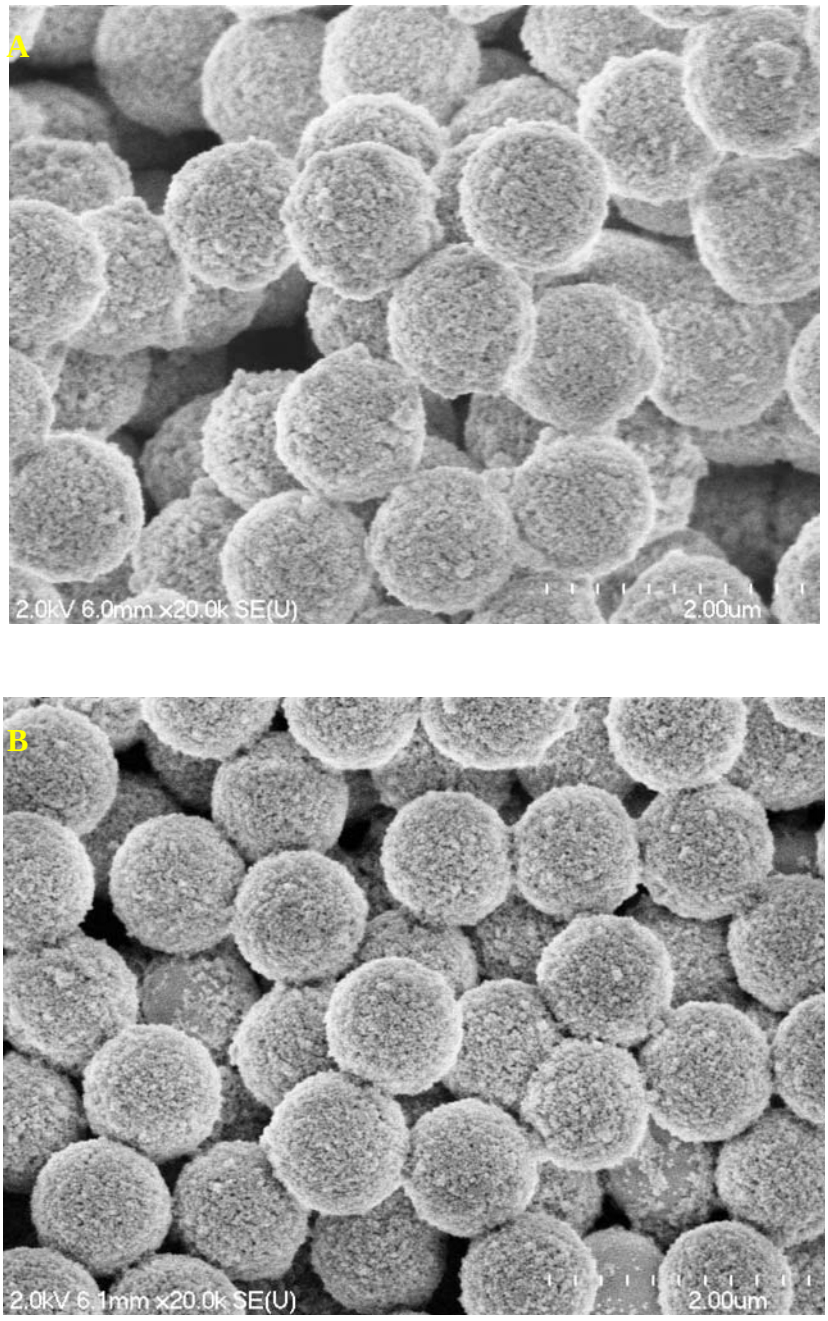

Figure 5-11: Images of 28 nm colloidal silica coated particles prepared by different washing methods. A) Centrifuged B) Settled

A

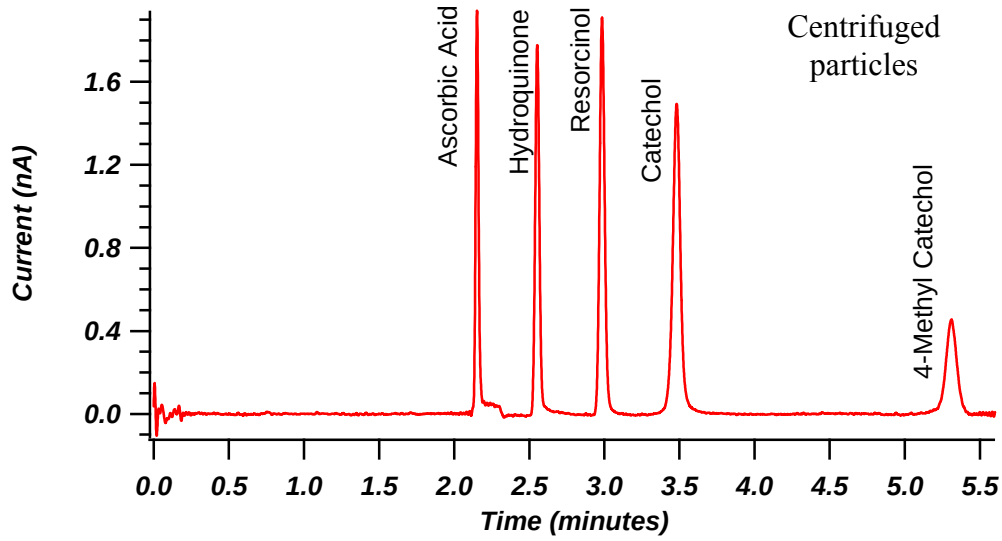

B

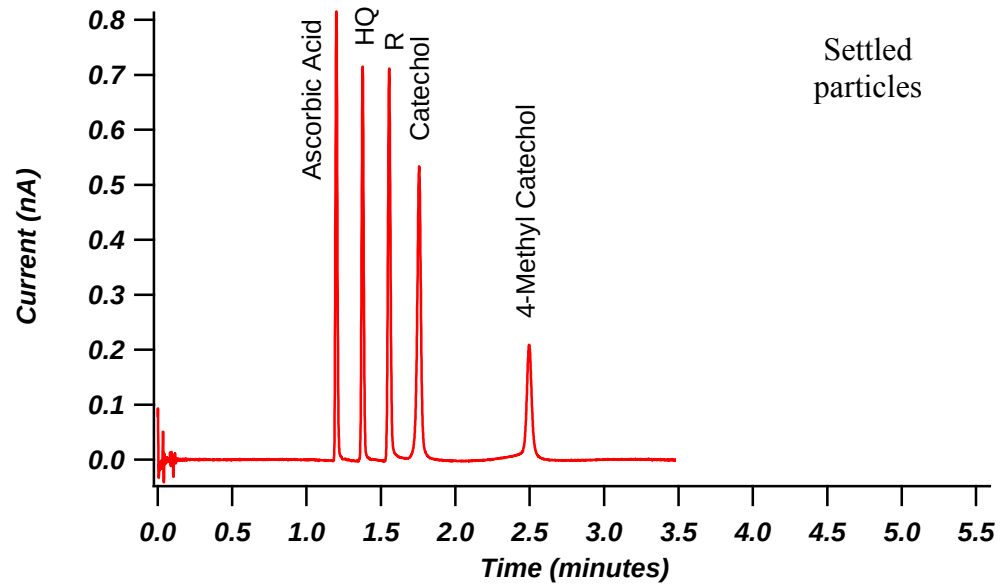

Figure 5-12: Example chromatograms for columns packed with centrifuge washed particles and settle washed 1.1 µm ($d_{p,n}$), 28 nm coated particles. A) Column LB7-33, LB7-23-3 particles, 30 µm x 12.8 cm, h_{min} (HQ) = 2.6, u_{opt} = 0.16 cm/sec (8700 psi), k'(4MC) = 1.3 B) Column LB7-49, LB7-114-3 particles, 30 µm x 12.6 cm, h_{min} (HQ) = 2.3, u_{opt} = 0.17 cm/sec (8300 psi), k'(4MC) = 1.0

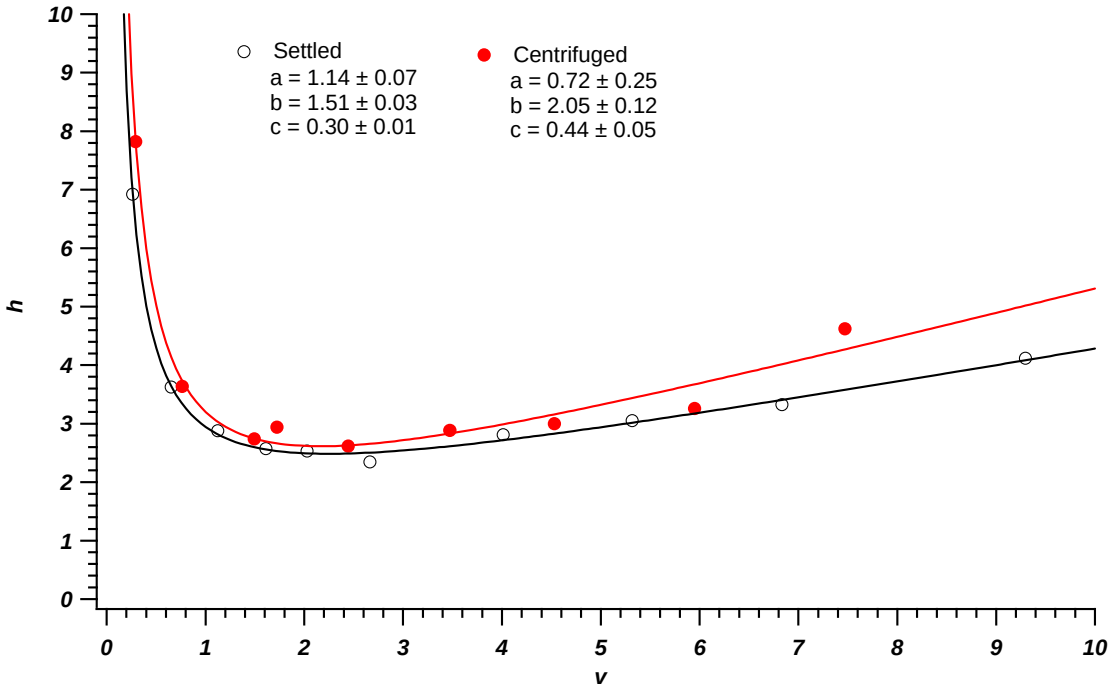

Figure 5-13: Reduced parameters plots for hydroquinone for columns packed with centrifuge washed particles and settle washed 1.1 μm ($d_{p,n}$), 28 nm coated particles fit to the van Deemter equation.

APPENDIX 1: Calculation of Amount of Carbon per Column Volume

1) Total particle volume

$$V = \frac{4}{3}\pi r^3$$

Example for 5 layer particles (1.7 μm): V = (4/3)*π*(0.85 μm)^3 = 2.57 μm^3

2) Total column volume

$$V_c = \pi r^2 L$$

Example for 5 layer particles (1.7 μm): V_c = π*(15 μm)^2 * 25 x 10^4 μm = 1.77 x 10^8 μm^3

3) Volume of particle in column

$$V_p = V_c - \varepsilon V_c$$

Example for 5 layer particles (1.7 μm): V_p = 1.77 x 10^8 μm^3 – 0.4 (1.77 x 10^8 μm^3) = 1.06 x 10^8 μm^3

4) Number of particle in column

$$N_p = \frac{V_p}{V}$$

Example for 5 layer particles (1.7 μm): N_p = 1.06 x 10^8 μm^3/2.57 μm^3) = 4.14 x 10^7

5) Weight of a particle

$$\%V_{porous} = \frac{V - V_{core}}{V} * 100$$

$$\%V_{core} = \frac{V_{core}}{V} * 100$$

$$\rho = \frac{\%V_{porous}\rho_{BEH}}{100} + \frac{\%V_{non-porous}\rho_{silica}}{100}$$

$$W_p = V\rho$$

Example for 5 layer particles (1.7 μm):

$\%V_{porous}$ = 2.57 μm^3-1.44 μm^3/2.57 μm^3 = 44 %

$\%V_{core}$ = 1.44 μm^3/2.57 μm^3 = 56 %

ρ= (44 * 2.01 g/cm^3)/100 + (56 * 2.20 g/cm^3)/100 = 2.12 g/cm^3

W_p = (2.57 μm^3 * 2.12 g/cm^3) * (1 cm^3/1 x 10^{12} μm^3) = 5.45 x 10^{-12} g

6) Weight of carbon per particle

$$W_{C,p} = \%C * W_p$$

Example for 5 layer particles (1.7 μm):

$W_{C,p}$ = (3.4/100)* 5.45 x 10-^{12} g = 1.85 x 10^{-13} g carbon

7) Weight of carbon per column volume

$$W_{C,v} = W_{C,p} * N_p$$

Example for 5 layer particles (1.7 μm):

$W_{C,v}$ = 1.85 x 10^{-13} g * 4.14 x 10^7= 7.66 x 10^{-6} g carbon/column volume

APPENDIX 2: Calculation of Surface Area per Column Volume

1) Surface Area of NPS Core

$$SA_{NPS} = 4\pi r^2$$

Example for 87 Å and 187 Å particles (1.1 μm): $SA_{NPS} = 4\pi(0.45\ \mu m)^2 = 2.54\ \mu m^2$

Example for 248 Å particles (1.6 μm): $SA_{NPS} = 4\pi(0.7\ \mu m)^2 = 6.16\ \mu m^2$

2) Footprint of Colloidal Silica

$$A = \pi r^2$$

Example for 87 Å particles (1.1 μm): $A = \pi * (6\ nm)^2 * (1\ \mu m/10^3\ nm)^2 = 1.13 \times 10^{-4}\ \mu m^2$

Example for 187 Å particles (1.1 μm): $A = \pi * (14\ nm)^2 * (1\ \mu m/10^3\ nm)^2 = 6.16 \times 10^{-4}\ \mu m^2$

Example for 248 Å particles (1.6 μm): $A = \pi * (33.5\ nm)^2 * (1\ \mu m/10^3\ nm)^2 = 3.53 \times 10^{-3}\ \mu m^2$

3) Number of Colloids per NPS Core

$$N_c = \frac{SA_{NPS} * F_{cs}}{A}$$

Example for 87 Å particles (1.1 μm): $N_c = (2.54\ \mu m^2 * (\pi/2\sqrt{3}))/1.13 \times 10^{-4}\ \mu m^2 = 2.05 \times 10^4$ colloids/layer

Example for 87 Å particles (1.1 μm): $N_c = (2.54\ \mu m^2 * (\pi/2\sqrt{3}))/ 6.16 \times 10^{-4}\ \mu m^2 = 3.75 \times 10^3$ colloids/layer

Example for 248 Å particles (1.6 μm): $N_c = (6.16\ \mu m^2 * (\pi/2\sqrt{3}))/3.53 \times 10^{-3}\ \mu m^2 = 1.59 \times 10^3$ colloids/layer

4) Surface Area of a Colloid

$$SA_{CS} = 4\pi r^2$$

Example for 87 Å particles (1.1 μm): $SA_{CS} = 4\pi(6 \times 10^{-3}\ \mu m)^2 = 4.52 \times 10^{-4}\ \mu m^2$
Example for 187 Å particles (1.1 μm): $SA_{CS} = 4\pi(14 \times 10^{-3}\ \mu m)^2 = 2.46 \times 10^{-3}\ \mu m^2$

Example for 248 Å particles (1.6 μm): $SA_{CS} = 4\pi(33.5 \times 10^{-3}\ \mu m)^2 = 1.41 \times 10^{-2}\ \mu m^2$

5) Surface Area of Porous Layer

$$SA_{porous} = SA_{CS} * N_C * N_L$$

Example for 87 Å particles (1.1 μm): SA_{porous} = 4.52 x 10^{-4} μm^2 * 2.05 x 10^4 colloids/layer * (4.5 layers) = 41.67 μm^2

Example for 187 Å particles (1.1 μm): SA_{porous} = 2.46 x 10^{-3} μm^2 * 3.75 x 10^3 colloids/layer * (4.5 layers) = 41.51 μm^2

Example for 248 Å particles (1.6 μm): SA_{porous} = 1.41 x 10^{-2} μm^2 * 1.59 x 10^3 colloids/layer * (1 layer) = 22.42 μm^2

6) Surface Area of Superficially Porous Particle

$$SA_{total} = SA_{NPS} + SA_{porous}$$

Example for 87 Å particles (1.1 μm): SA_{total} = 41.67 μm^2 + 2.54 μm^2 = 44.24 μm^2

Example for 187 Å particles (1.1 μm): SA_{total} = 41.51 μm^2 + 2.54 μm^2 = 44.05 μm^2

Example for 248 Å particles (1.6 μm): SA_{total} = 22.42 μm^2 + 6.16 μm^2 = 23.85 μm^2

7) Total Particle Volume

$$V = \frac{4}{3}\pi r^3$$

Example for 87 Å and 187 Å particles (1.1 μm): V = 4/3 * π * (0.55 μm)^2 = 0.70 μm^3

Example for 248 Å particles (1.6 μm): V = 4/3 * π * (0.80 μm)^2 = 2.14 μm^3

8) Total column volume

$$V_c = \pi r^2 L$$

Example for a 30 μm i.d. x 25 cm column: V_c = π*(15 μm)^2 * 25 x 10^4 μm = 1.77 x 10^8 μm^3

9) Volume of particle in column

$$V_p = V_c - \varepsilon V_c$$

Example for all particles: $V_p = 1.77 \times 10^8\ \mu m^3 - 0.4\ (1.77 \times 10^8\ \mu m^3) = 1.06 \times 10^8\ \mu m^3$

10) Number of particles in column

$$N_{p,c} = \frac{V_p}{V}$$

Example for 87 Å and 87 Å particles (1.1 μm): $N_p = 1.06 \times 10^8\ \mu m^3 / 0.70\ \mu m^3) = 1.51 \times 10^8$ particles/column

Example for 248Å particles (1.6 μm): $N_p = 1.06 \times 10^8\ \mu m^3 / 2.14\ \mu m^3) = 4.95 \times 10^7$ particles/column

11) Surface Area per Column Volume

$$SA_V = SA_{total} * N_{p,c}$$

Example for 87 Å particles (1.1 μm): $SA_v = 44.24\ \mu m^{2\,*}\ (1\ m/10^6\ \mu m)^2 * 1.51 \times 10^8$ particles/column $= 6.68 \times 10^{-3}\ m^2$/column

Example for 187 Å particles (1.1 μm): $SA_v = 44.05\ \mu m^{2\,*}\ (1\ m/10^6\ \mu m)^2 * 1.51 \times 10^8$ particles/column $= 6.65 \times 10^{-3}\ m^2$/column

Example for 248 Å particles (1.6 μm): $SA_v = 28.58\ \mu m^{2\,*}\ (1\ m/10^6\ \mu m)^2 * 4.95 \times 10^7$ particles/column $= 1.41 \times 10^{-3}\ m^2$/column

12) Pore volume per particle

$$V_{pore} = \frac{TPV}{N_p}$$

Example for 87 Å particles (1.1 μm): $V_{pore} = ((0.12\ cm^3/g) / 6.76 \times 10^{11}$ particles/g) * $(10^4\ \mu m/cm)^3 = 0.18\ \mu m^3$/particle

Example for 187 Å particles (1.1 μm): $V_{pore} = ((0.10\ cm^3/g) / 6.76 \times 10^{11}$ particles/g) * $(10^4\ \mu m/cm)^3 = 0.15\ \mu m^3$/particle

Example for 248 Å particles (1.6 μm): $V_{pore} = ((0.03\ cm^3/g) / 2.20 \times 10^{11}$ particles/g) * $(10^4\ \mu m/cm)^3 = 0.14\ \mu m^3$/particle

13) Porous fraction of a particle

$$\varepsilon_p = \frac{V_{pore}}{V}$$

Example for 87 Å particles (1.1 μm): ε_i = 0.18 μm^3/0.70 μm^3 = 0.26

Example for 187 Å particles (1.1 μm): ε_i = 0.15 μm^3/0.70 μm^3 = 0.21

Example for 248 Å particles (1.6 μm): ε_i = 0.14 μm^3/2.14 μm^3 = 0.07

14) Volume of mobile phase in the column

$$V_{MP} = \varepsilon V_c + \varepsilon_p N_{p,c} V$$

Example for 87 Å particles (1.1 μm): V_{MP} = (0.4 * 1.77 x 10^8 μm^3) + (0.26 * 1.51 x 10^8 particles * 0.70 μm^3/particle) = 9.83 x 10^7 μm^3

Example for 187 Å particles (1.1 μm): V_{MP} = (0.4 * 1.77 x 10^8 μm^3) + (0.21 * 1.51 x 10^8 particles * 0.70 μm^3/particle) = 9.30 x 10^7 μm^3

Example for 248 Å particles (1.6 μm): V_{MP} = (0.4 * 1.77 x 10^8 μm^3) + (0.07 * 4.95 x 10^7 particles * 2.14 μm^3/particle) = 7.82 x 10^7 μm^3

15) Volume of stationary phase in the column

$$V_{SP} = N_{p,c} * V * \rho * \frac{\%C}{100} * \frac{1}{\rho_{SP}}$$

Example for 87 Å particles (1.1 μm): V_{SP} = 1.51 x 10^8 particles/column * 0.70 μm^3/particle * 2.11 g/cm^3 * (1 cm/10^4 μm)^3 * (3.9/100) * (1 cm^3/0.795 g) * (10^4 μm/cm)^3 = 1.09 x 10^7 μm^3

Example for 187 Å particles (1.1 μm): V_{SP} = 1.51 x 10^8 particles/column * 0.70 μm^3/particle * 2.11 g/cm^3 * (1 cm/10^4 μm)^3 * (2.0/100) * (1 cm^3/0.795 g) * (10^4 μm/cm)^3 = 5.61 x 10^6 μm^3

Example for 248 Å particles (1.6 μm): V_{SP} = 4.95 x 10^7 particles/column * 2.14 μm^3/particle * 2.14 g/cm^3 * (1 cm/10^4 μm)^3 * (0.70/100) * (1 cm^3/0.795 g) * (10^4 μm/cm)^3 = 2.00 x 10^6 μm^3

16) Phase ratio

$$\beta = \frac{V_{SP}}{V_M}$$

Example for 87 Å particles (1.1 μm): $\beta = (1.09 \times 10^7\ \mu m^3)/(9.83 \times 10^7\ \mu m^3) = 0.11$

Example for 187 Å particles (1.1 μm): $\beta = (5.61 \times 10^6\ \mu m^3)/(9.30 \times 10^7\ \mu m^3) = 0.06$

Example for 248 Å particles (1.6 μm): $\beta = (2.00 \times 10^6\ \mu m^3)/(7.82 \times 10^7\ \mu m^3) = 0.03$

APPENDIX 3: Sedimentation Velocity Calculations

1) Total particle volume

$$V = \frac{4}{3}\pi r^3$$

Example for 12 nm coated particles (1.1 μm): $V = 4/3 * \pi * (0.55\ \mu m)^2 = 0.70\ \mu m^3$

2) Weight of a particle

$$\%V_{porous} = \frac{V - V_{core}}{V} * 100$$

$$\%V_{core} = \frac{V_{core}}{V} * 100$$

$$\rho = \frac{\%V_{porous}\rho_{BEH}}{100} + \frac{\%V_{non-porous}\rho_{silica}}{100}$$

$$W_p = V\rho$$

Example for 12 nm coated particles (1.1 μm):

$\%V_{porous}$ = 0.70 μm^3-0.38 μm^3/0.70 μm^3 = 46 %

$\%V_{core}$ = 0.38 μm^3/0.70 μm^3 = 54 %

ρ= (46 * 2.01 g/cm^3)/100 + (54 * 2.20 g/cm^3)/100 = 2.11 g/cm^3

W_p = (0.70 μm^3 * 2.11 g/cm^3) * (1 cm^3/1 x 10^{12} μm^3) = 1.47 x 10^{-12} g/particle

3) Number of particles per gram

$$N_p = \frac{1}{W_p}$$

Example for 12 nm coated particles (1.1 μm): N_p = 1 g/1.47 x 10^{-12} g/particle = 6.67 x 10^{11} particles

4) Pore volume per particle

$$V_{pore} = \frac{TPV}{N_p}$$

Example for 12 nm coated particles (1.1 μm): V_{pore} = ((0.12 cm^3/g)/ 6.67 x 10^{11} particles/g) * (10^4 μm/cm)^3 = 0.18 μm^3/particle

Example for 28 nm coated particles (1.1 μm): V_{pore} = ((0.10 cm^3/g)/ 6.67 x 10^{11} particles/g) * (10^4 μm/cm)^3 = 0.15 μm^3/particle

5) Volume fraction of pores per particle

$$\varepsilon_i = \frac{V_{pore}}{V}$$

Example for 12 nm coated particles (1.1 μm): $\varepsilon_i = 0.18\ \mu m^3/0.70\ \mu m^3 = 0.26$

Example for 28 nm coated particles (1.1 μm): $\varepsilon_i = 0.15\ \mu m^3/0.70\ \mu m^3 = 0.21$

6) Volume fraction of particles, ϕ

$$\phi = \frac{W_{p,slurry}}{W_p} * \frac{V}{V_{solvent}}$$

Example for 12 nm and 28 nm coated particles (1.1 μm): $\phi = (0.003\ g/\ 1.47 \times 10^{-12}\ g/particle) * (0.70\ \mu m^3/(\mu m/10^{-4}\ cm)^3 = 0.0014$

5.7 REFERENCES

[1] Broquaire, M. *J. Chromatogr.* 170 (1979) 43-52.

[2] Bruns, S.; Tallarek, U. *J. Chrom. A* 1218 (2011) 1849-1860.

[3] Shelly, D.C.; Antonucci, V.L.; Edkins, T.J.; Dalton, T.J. *J. Chromatogr*. 458 (1989) 267-279.

[4] Shelly, D.C.; Edkins, T.J. *J. Chromatogr*. 411 (1987) 185-199.

[5] Angus, P.D.A.; Demarest, C.W.; Catalano, T.; Stobaugh, J.F. *J. Chrom. A* 887 (2000) 347-365.

[6] Gluckman, J.C.; Hirose, A.; McGuffin, V.L.; Novotny, M. *Chromatographia* 17 (1983) 303-309.

[7] Bruns, S.; Grinias, J.P; Blue, L.E.; Jorgenson, J.W.; Tallarek, U. *Anal. Chem.* 84 (2012) 4496-4503.

[8] Cavazzini, A.; Gritti, F.; Kaczmarski, K.; Marchetti, N.; Guiochon, G. *Anal. Chem.* 79 (2007) 5972-5979.

[9] Gritti, F.; Guiochon, G. *J. Chrom. A* 1166 (2007) 30-46.

[10] Kirkland, J.J.; DeStafano, J.J. *J. Chrom. A* 1126 (2006) 50-57.

[11] Guiochon, G.; Farkas, T.; Guan-Sajonz, H.; Koh, J.-H.; Sarker, M.; Stanley, B.J.; Yun, T. *J. Chrom. A* 762 (1997) 83-88.

[12] Verzele, M.; Dewaele, C. *J. Chromatogr*. 391 (1987) 111-118.

[13] Vissers, J.P.C.; Hoeben, M.A.; Laven, J.; Claessens, H.A.; Cramers, C.A. *J. Chrom. A* 883 (2000) 11-25.

[14] Meyer, R.F.; Hartwick, R.A. *Anal. Chem.* 56 (1984) 2211-2214.

[15] Vissers, J.P.C.; Claessens, H.A.; Laven, J.; Cramers, C.A. *Anal. Chem.* 67 (1995) 2103-2109.

[16] Vissers, J.P.C.; Laven, J.; Claessens, H.A.; Cramers, C.A.; Agterrof, W.G.M. *Colloids Surf. A* 126 (1997) 33-44.

[17] Malvern Instruments, *Zetasizer Nano ZS Users Manual*.

[18] Lide, D.R. *CRC Handbook of Chemistry & Physics*, 92nd edition, electronic edition, 2011.

[19] Song, S.; Peng, C. *J. Disp. Sci. Tech.* 29 (2008) 1367-1372.

[20] Saksena, M.P.; Kumar, H.; Kumar, S. *J. Phys. C.:Solid State Phys.* 8 (1975) 2376-2381.

[21] Wohlfarth, C. *Viscosity of Pure Organic Liquids and Binary Liquid Mixtures*, Springer, New York, 2009.

[22] Neue, U.D. *HPLC Columns: Theory, Technology, and Practice*, Wiley-VCH, New York, 1997.

[23] Martin, M.; Blu, G.; Guiochon, G. J. Chrom. Science 11 (1973) 641-654.

[24] Mellors, J.S. *UNC Doctoral Dissertation* 2005.

[25] MacNair, J.E.; Patel, K.D.; Jorgenson, J.W. *Anal. Chem.* 71 (1999) 700 -708.

[26] Maiolica, A.; Borsotti, D.; Rappsibler, J. *Proteomics* 5 (2005) 3847-3850.

[27] MacNair, J.E.; Lewis, K.C.; Jorgenson, J.W. *Anal. Chem.* 69 (1997) 983-989.

[28] Bergna, H.E.; Kirkland, J.J. *US Patent 4,447,492* 1984.

[29] Reichardt, C. *Solvents and Solvent effects in Organic Chemistry*, Wiley-VCH Publishers, 3rd ed., New York, 2003.

[30] Symons, M.C.R.; Eaton, G. *J. Chem. Soc. Faraday Trans.* 81 (1985) 1963-1977.

[31] Snyder, L.; Kirkland, J. J.; Glajch, J.L. *Practical HPLC Method Development*, 2nd ed., Wiley, New York, 1997.

[32] Hsieh, S.; Jorgenson, J.W. *Anal. Chem.* 68 (1996) 1212-1217.